2021

Investigating the role of proteostasis pathways in regulating the intracellular inclusion formation of firefly luciferase: a model system to study protein aggregation in cells

Shannon McMahon

Investigating the role of proteostasis pathways in regulating the intracellular inclusion formation of firefly luciferase: a model system to study protein aggregation in cells

Shannon McMahon

This thesis is submitted in fulfilment of the requirements for the award of the degree

Doctor of Philosophy

from

University of Wollongong

School of Chemistry and Molecular Bioscience

Illawarra Health and Medical Research Institute

This research has been conducted with the support of an Australian Government

Research Training Program Scholarship

June, 2021

DECLARATION

This thesis is submitted in accordance with the regulations of the University of Wollongong in partial fulfilment of the degree of Doctor of Philosophy. It does not include any material published by another person unless otherwise referenced in the text. The experimental work described in this thesis is original work and has not been submitted for qualifications at any other university.

Shannon McMahon
11/06/2021

ACKNOWLEDGEMENTS

If there is one thing that I am unequivocally certain of, it is that I would not have gotten here without the support of my supervisor Prof Heath Ecroyd. Throughout my PhD, there have been many twists and turns, but we have stumbled our way through the world of DNAJs together. Thank you for your unwavering support and encouragement, for reading drafts, for providing me with the opportunity to conduct research overseas and for making a damn good baked cheesecake. I am extremely grateful for your mentorship, but also, for the partnership that we have formed throughout the course of my PhD.

Thank you to my co-supervisor Prof Justin Yerbury, whose passion for research and enduring determination is truly inspiring. Thanks also to my supervisory team in the Netherlands – Prof Harm Kampinga and Dr Steven Bergink – for saying yes to mentoring a first year PhD student from the other side of the world and for your expert guidance on my first published manuscript.

A massive thank you to amazing friends in the various lab groups that I have been lucky enough to be a part of. From the Yerbury lab, in particular Luke, Nat and Jeremy, thank you for adopting me and for sharing your microscopy, cell culture and Western blot wisdom. In the Kampinga group, Carolina, Maria, Mohsen, Abi, Els and Wouter – for making a scary move across the world feel a bit more like home. A huge thank you to the Ecroyd lab in its various forms over the years, but especially Meg, Dezerae, Bec, BJ, Anthea, Caitlin, Nick, Kristian and Lauren. A special thanks to Dezerae and Anthea who have been amazing (boss female) mentors, but also great and supportive friends. Thank you to Nick – my ride or die bestie who has been on this journey with me from the beginning. We have laughed, cried, drank, celebrated the small wins and commiserated in the losses together and I think it is safe to say that you are stuck with me for life.

Thank you to the amazing staff in both IHMRI and Molecular Horizons for their world-class technical support. Thanks to my PhD comrades, who are always up for ‘my experiment failed’ beers – you are all fantastic people who have made these four years incredibly enjoyable. A special thank you to my close pals, Ben, Amy, Maddy and Geraghty – I am so thankful for your friendship. To my Mum Leanne and Dad Stephen, who are the most supportive parents anyone could ask for – everything that I have accomplished has been a result of your support. Thank you to my grandparents for their love and encouragement. Finally, to my partner Jordan, I cannot express how grateful I am for your patience, for always making me laugh, for putting up with my Collingwood-induced rants and for helping me be the best version of myself. I am so proud of you and know that you will achieve such greatness in your post-PhD endeavours.

ABSTRACT

The maintenance of cellular protein homeostasis, or proteostasis, is dependent upon a complex network of molecular chaperones, degradation machinery and other regulatory factors, which together act to keep the proteome soluble and functional. Disturbances to proteostasis can lead to protein aggregation and inclusion formation, processes associated with a variety of neurodegenerative disorders. The heat shock proteins (Hsps) are a superfamily of molecular chaperones that are dramatically upregulated in response to cellular stress. The Hsps can bind aggregation-prone proteins and either refold or traffic them for degradation. One class of Hsps, the DNAJBs, act as co-factors of the Hsp70 machine and have been previously identified as potent suppressors of disease-related protein aggregation. This has raised the potential of targeting DNAJB chaperone action in the context of protein aggregation associated with disease.

In the work described in this thesis, a destabilised isoform of the protein firefly luciferase (R188Q/R261Q Fluc; Fluc^{DM}) was overexpressed in cells to assess how components of the proteostasis machinery engage with aggregation-prone proteins to prevent them from forming intracellular inclusions. In Chapter 3, Fluc^{DM} was used as a model aggregation-prone protein to screen for the generic capacity of the major human Hsps to suppress intracellular inclusion formation by destabilised proteins. This work marks the first use of the quantitative flow cytometric analysis of inclusions and trafficking (FloIT) technique to conduct an Hsp overexpression screen for modulators of inclusion formation in cells. Of the small Hsps, HspB4 HspB6, HspB7 and HspB9, reduced inclusion formation by Fluc^{DM} in cells. The major nucleotide exchange factors, including members of the Bcl-2-associated athanogene and Hsp110 families, did not modulate Fluc^{DM} aggregation. Of the HspA (Hsp70) family members tested, HspA1A and HspA2 reduced inclusion formation by Fluc^{DM}. Significantly, all of the DNAJBs tested were effective at reducing the aggregation of Fluc^{DM} into inclusions in cells, with DNAJB1, DNAJB5, DNAJB6 and DNAJB8 being the most potent suppressors.

Experiments investigating the exact molecular mechanism by which specific DNAJBs prevent inclusion formation by destabilised proteins in cells are described in Chapter 4. DNAJBs suppress inclusion formation by supporting the Hsp70-dependent degradation of $Fluc^{DM}$ via the proteasome. The serine-rich stretch in DNAJB6 and DNAJB8, essential for preventing fibrillar aggregation, is not involved in the suppression of $Fluc^{DM}$ inclusion formation. Conversely, deletion of the C-terminal TTK-LKS motif in DNAJB6 and DNAJB8, a region not required to suppress polyQ aggregation, abolished its ability to inhibit inclusion formation by $Fluc^{DM}$. Thus, DNAJB6 and DNAJB8 possess two distinct regions for binding substrates, one that is responsible for binding β-hairpins that form during amyloid formation and another that interacts with exposed hydrophobic patches in aggregation-prone clients.

Finally, the aggregation propensity of $Fluc^{DM}$ was exploited in order to measure the ability of mouse neuroblastoma (Neuro-2a) and mouse neuroblastoma × spinal cord (NSC-34) motor neuron hybrid cells to prevent inclusion formation. As part of the work presented in Chapter 5, a first step towards a robust and quantitative method to measure the proteostasis capacity of a cell was established. Using this method, it was demonstrated that NSC-34 cells were more susceptible to $Fluc^{DM}$ inclusion formation than Neuro-2a cells. Investigation into the major arms of the proteostasis network indicated that heat shock transcription factor 1 (HSF1) activation remains a valid therapeutic target for the treatment of neurodegenerative diseases, as overexpression of wild-type HSF1 reduced inclusion formation by $Fluc^{DM}$ in both Neuro-2a and NSC-34 cells. The mechanism by which HSF1 overexpression inhibits inclusion formation by $Fluc^{DM}$ is dependent upon proteostasis networks other than the Hsps and this likely involves presentation of destabilised proteins for processing by the degradation machinery.

This work highlights the dynamic nature of the proteostasis network. This study validates the use of $Fluc^{DM}$ as a destabilised model protein that can be used as a sensor to elucidate how components

of the protein quality control network act together to maintain the conformational stability of aggregation-prone proteins. The development of $Fluc^{DM}$ as a protein folding sensor, along with the diverse applications of flow cytometry described throughout this thesis provide a foundation towards measuring the proteostasis capacity of a cell. This work identified that the Hsps have unique client specificities and that DNAJBs possess distinct substrate binding regions for the suppression of amyloidogenesis versus amorphous inclusion formation in cells. Future work should investigate the potential of pharmacologically or genetically targeting molecular chaperones and arms of the proteostasis network to treat neurodegenerative diseases.

TABLE OF CONTENTS

LIST OF FIGURES

LIST OF TABLES

LIST OF ABBREVIATIONS

°C	degrees Celsius
3-MA	3-methyladenine
ACN	acetonitrile
AFU	arbitrary fluorescence units
AGC	automatic gain control
AI	aggregation index
ALS	amyotrophic lateral sclerosis
ANOVA	analysis of variance
AU	arbitrary units
ATP	adenosine triphosphate
Bag	Bcl-2 associated athanogene
BCA	bicinchoninic acid
BSA	bovine serum albumin
CASA	chaperone-assisted and selective autophagy
CHIP	C-terminus of the Hsc70-interacting protein
CTD	C-terminal domain
Da	dalton
DM	double mutant
DMEM/F-12	Dulbecco's Modified Eagle Medium/Ham's F-12 media
DMSO	dimethyl sulfoxide
DNA	deoxyribonucleic acid
EDTA	ethylenediaminetetraacetic acid
EGFP	enhanced green fluorescent protein
ER	endoplasmic reticulum
FCS	foetal calf serum
FloIT	flow cytometric analysis of inclusions and trafficking
Flp-In T-Rex	HEK293 cells stably expressing the tetracycline repressor
Fluc	firefly luciferase
$Fluc^{DM}$	double mutant firefly luciferase

$Fluc^{DM}$-EGFP	double mutant firefly luciferase with an N-terminal enhanced green fluorescent protein tag
$Fluc^{WT}$	wild-type firefly luciferase
$Fluc^{WT}$-EGFP	wild-type firefly luciferase with an N-terminal enhanced green fluorescent protein tag
FRT	Flippase recognition target
FSC	forward scatter
FT	Fourier transform
FUS	fused in sarcoma
g	gravity
g	grams
G/F	glycine/phenylalanine
GFP	green fluorescent protein
h	hour
HCD	higher C-trap dissociation
HCl	hydrochloride
HEK293	human embryonic kidney cells
HPD	histidine-proline-aspartate
H/Q	histidine replaced with a glutamine
HRP	horseradish peroxidase
HSF1	heat shock transcription factor 1
Hsc70	constitutive Hsp70
Hsp	heat shock protein
Htt25Q	huntingtin protein with 25 polyglutamine repeats
Htt46Q	huntingtin protein with 46 polyglutamine repeats
IgG	immunoglobulin G
IPOD	insoluble protein deposits
JUNQ	juxtanuclear quality control compartments
kDa	kilodalton
KEGG	Kyoto Encyclopedia of Genes and Genomes
kV	kilovolts
L	litre

LB	lysogeny broth
LC3I/II	microtubule-associated protein-light chain 3I/II
LC-MS	liquid chromatography-mass spectrometry
mCherry	monomeric cherry fluorescent protein
min	minute
mL	millilitre
mM	millimolar
mRFP	monomeric red fluorescent proteins
mRNA	messenger ribonucleic acid
NEF	nucleotide exchange factor
Neuro-2a	mouse neuroblastoma cells
ng	nanogram
nL	nanolitre
nm	nanometre
NP-40	Nonidet™ P-40
NSC-34	mouse neuroblastoma × spinal cord motor neuron hybrid cells
PANTHER	Protein Annotation through Evolutionary Relationship
PBS	phosphate buffered saline
PFA	paraformaldehyde
polyQ	polyglutamine
ppm	parts per million
PulSA	pulse-shape analysis
PVDF	polyvinyldiene difluoride
RLUs	relative light units
RNA	ribonucleic acid
rpm	revolutions per minute
SDS	sodium dodecyl sufate
SDS-PAGE	sodium dodecyl sufate polyacrylamide gel electrophoresis
sec	second
S.E.M.	standard error of the mean
sHsp	small heat shock protein

SOD1	superoxide dismutase 1
$SOD1^{G93A}$	glycine-to-alanine substitution at position 93 of superoxide dismutase 1
SSC	side scatter
S/T	serine/threonine
TBS	tris-buffered saline
TBS-T	TBS containing 0.05% (v/v) Tween-20
TDP-43	transactive response DNA-binding protein 43
TPE-MI	tetraphenylethene maleimide
v/v	volume/volume
V	volts
w/v	weight/volume
WT	wild-type
µg	microgram
µL	microliters
µm	micrometre
µM	micromolar
ZFLR	zinc-finger-like region

LIST OF PUBLICATIONS AND PRESENTATIONS

REFEREED PUBLICATIONS:

1. **McMahon, S.**, Bergink, S., Kampinga, H. H. and Ecroyd, H. (2021). DNAJB chaperones suppress destabilised protein aggregation via a region distinct from that used to inhibit amyloidogenesis. *Journal of Cell Science.*134, jcs255596. doi:10.1242/jcs.255596

CONFERENCE PRESENTATIONS:

1. "Investigating the role of Hsp40 and Hsp70 in regulating the intracellular aggregation of firefly luciferase"
   Lorne Protein Structure and Function Conference, Lorne, Australia. February 2020
   Poster Presentation, awarded student poster prize

2. "Investigating the role of heat shock proteins in preventing intracellular protein aggregation"
   Lorne Protein Structure and Function Conference, Lorne, Australia. February 2019
   Poster Presentation

3. "A heat shock protein overexpression screen for suppressors of mutant firefly luciferase aggregation"
   Lorne Protein Structure and Function Conference, Lorne, Australia. February 2018
   Poster Presentation

4. "A heat shock protein overexpression screen for suppressors of mutant firefly luciferase aggregation"
   The PhD 'Work in Progress' Seminar Series, University of Groningen, The Netherlands. October 2017
   Oral Presentation

Chapter 1: Introduction

Protein homeostasis, or proteostasis, refers to the maintenance of the conformational and functional integrity of the proteome. The term proteostasis therefore encompasses all of the pathways that regulate the synthesis, concentration, folding, trafficking and degradation of proteins. Molecular chaperones are a key component of proteostasis as they play a central role in facilitating the correct folding of nascent polypeptides and stabilising misfolded proteins to prevent aggregation. Heat shock proteins (Hsps) are a family of molecular chaperones; when cells are exposed to stress, the expression of some Hsps is dramatically upregulated. Hsps can bind aggregation-prone proteins and either refold them or traffic them for degradation. Disturbances to proteostasis are associated with many age-related diseases including neurodegenerative conditions, with studies linking age to a subsequent decline in cellular proteostasis capacity (Ben-Zvi et al., 2009). Consequently, the proteostasis network appears to be a promising therapeutic target for the treatment of neurodegenerative diseases (Balch et al., 2008, Powers et al., 2009). This literature review will discuss the association of cellular protein aggregation with disease before highlighting the emerging evidence to suggest that different cell types display a differential capacity to prevent protein aggregation. The role of Hsps in proteostasis will be discussed, due to their proposed roles in minimising protein aggregation. Finally, this review will highlight current methods used to investigate protein aggregation in cells and identify how these may be adapted for use as potential methods to measure the proteostasis capacity of a cell.

1.1 Protein folding

The ability of a protein to adopt its correct three-dimensional structure depends upon the linear sequence of amino acids of the polypeptide chain (Anfinsen, 1973). Following translation, most proteins fold into a biologically active or functional conformation, termed the native state (Broadley and Hartl, 2009). However, throughout their lifetime, certain factors may cause a protein to unfold, misfold or reside in an intermediate (partially-folded) state. Schubert et al. (2000) estimate that under physiological conditions, one third of all newly synthesised

polypeptides never reach their native state. This is due, at least in part, to random errors in translation and post-translational modifications that would normally aid in ensuring correct protein folding (Allan Drummond and Wilke, 2009).

A further hindrance to protein folding is macromolecular crowding. The intracellular environment is crowded by the presence of high concentrations of macromolecules throughout the cytosol. These macromolecular constituents, which include lipids, carbohydrates and proteins, are vital for cellular function. Generally, protein folding must occur under conditions in which macromolecules are present at concentrations of ~300–400 g/L (Hartl and Hayer-Hartl, 2009), which limits the space available for a protein to fold (Van Den Berg et al., 1999, Ellis and Minton, 2006). Under conditions of cellular stress, this crowded environment increases the probability of unfavourable associations between partially-folded protein intermediates (Ecroyd and Carver, 2008). Despite the many hurdles that proteins must overcome in order to fold correctly, most do so rapidly and without difficulty (Dobson, 2003). The processes that facilitate and regulate the folding of a polypeptide chain into its functional native conformation are described below.

1.1.1 The thermodynamics of protein folding

Anfinsen (1973) was the first to describe the underlying mechanisms of protein folding, often termed Anfinsen's dogma or the "thermodynamic hypothesis". Anfinsen postulated that all requirements for a protein to fold correctly (and become biologically active) are contained within the amino acid sequence of the polypeptide chain (Anfinsen, 1973). This led to the thermodynamic hypothesis of protein folding which states that the three-dimensional structure of a protein in its normal environment occurs when the Gibbs free energy of the entire system is at its lowest (Anfinsen, 1973). Theoretically, due to the freedom of rotation of the bonds that link individual amino acids in an unfolded polypeptide chain, even a short polypeptide can sample an almost infinite number of conformations. Thus, if a protein with 100 amino acid residues were to sample

every possible conformation before reaching its native state, the length of time taken for it to fold would be astronomical (Dobson, 2003). Despite this, most proteins fold into their native state within a matter of milliseconds.

The ability of a protein to fold so rapidly relies on the cooperation of many weak, non-covalent interactions between side chains (e.g. hydrogen bonds and hydrophobic forces). Hydrogen bonds between amino acid residues provide most of the directional and selective interactions that facilitate correct protein folding (Myers and Pace, 1996). At some stage during folding, most proteins undergo hydrophobic collapse (i.e. the burial of hydrophobic side chains inside the protein structure), resulting in the formation of compact molten globular intermediates (Brockwell and Radford, 2007, Hartl et al., 2011). The formation of these thermodynamically favourable globular intermediates is a key process in the folding of a protein towards its native, biologically active conformation. Proteins that form these partially-folded intermediates prior to reaching their native state must overcome energy barriers that dictate the kinetic and thermodynamic properties that allow the protein to fold correctly. This concept has led to the energy landscape model of protein folding, in which polypeptide chains explore funnel-shaped potential energy surfaces as they fold towards their native conformation (Figure 1.1) (Hartl et al., 2011). Under normal conditions, native proteins are in equilibrium with partially-folded intermediate states and completely unfolded (denatured) conformations, as part of the on-folding pathway (Hartl and Hayer-Hartl, 2002). However, under conditions of stress (e.g. increases in temperature or changes in pH), partially-folded intermediates can persist at higher than normal concentrations, leading to increased exposure of hydrophobic side chains (Wang et al., 2010).

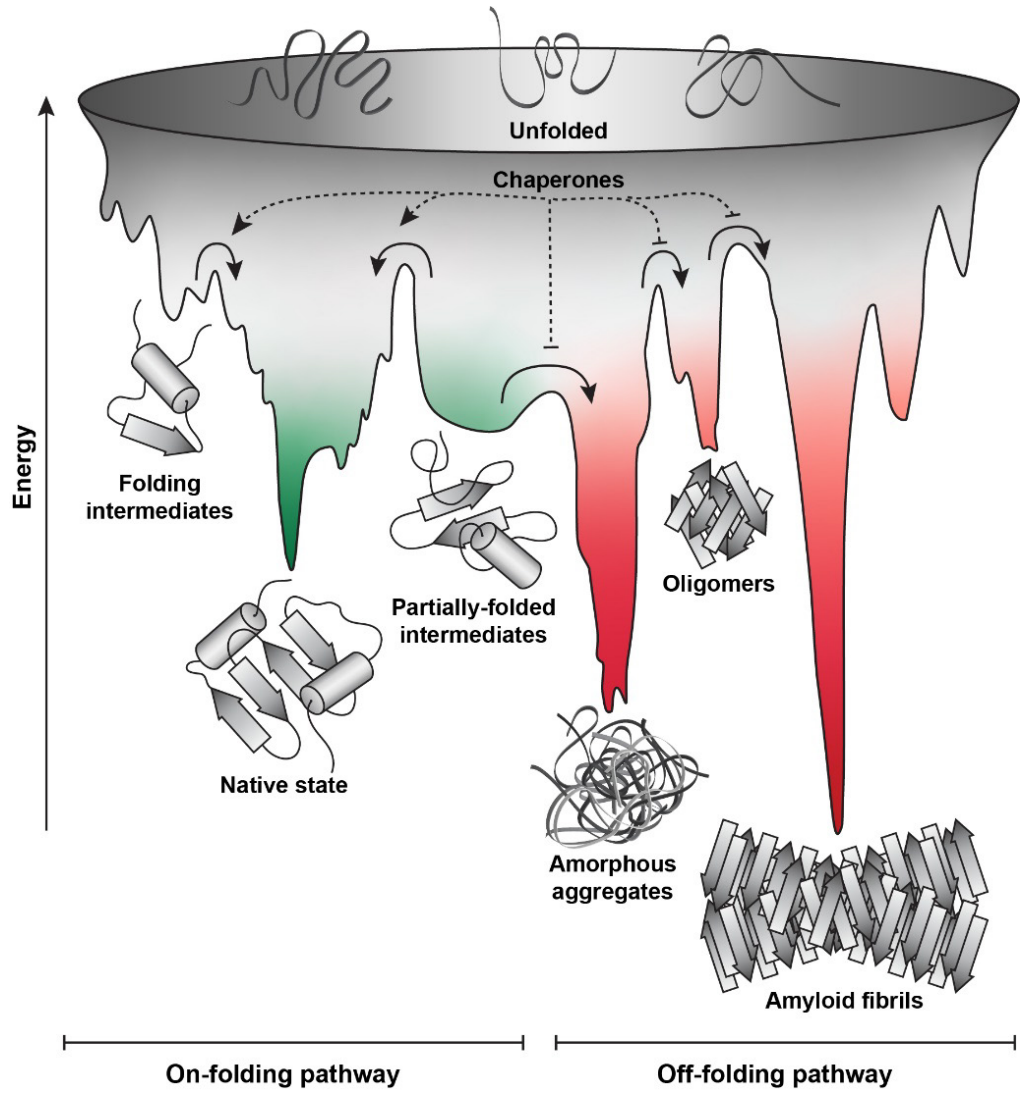

Figure 1.1. The funnel-shaped energy landscape model of protein folding. The model describes the funnel-shaped energy landscape that polypeptide sequences explore as they fold into their native state. The representative unfolded polypeptides first must progress through these potential energy surfaces (*green*) and are essentially funnelled towards a state of lower free energy, resulting in the formation of folding intermediates (transition states). The transition state represents the energy barrier which all intermediates must overcome in order to progress to the conformation in which the Gibbs free energy is lowest, termed the native state. This process of transitioning into the native state can occur via the assistance of chaperones. Alternatively, proteins unable to transition to the native state, either during *de novo* synthesis or unfolding following exposure to cell stress, can adopt partially-folded intermediate conformations. These partially-folded intermediates are prone to hydrophobically-driven self-association, causing them to leave the on-folding pathway and enter off-folding pathways (*red*). The two irreversible off-folding pathways result in the formation of either disordered amorphous aggregates or highly ordered amyloid fibrils. Chaperones are important in preventing these hydrophobically-driven, non-native interactions. Figure adapted from Hartl et al. (2011).

1.2 Protein misfolding

When a protein is subjected to conditions of cellular stress, such as oxidative stress (Papp et al., 2003), heat shock (Feder and Hofmann, 1999), exposure to heavy metals (Richter-Landsberg and Goldbaum, 2003) or endoplasmic reticulum (ER) stress (Kawahara et al., 1997), the bonds which maintain the native conformation may be disrupted. As a result, hydrogen bonds and hydrophobic

interactions between side chains are broken and proteins begin to partially unfold into intermediate conformations (Smith et al., 2007). Exposed hydrophobic regions are attracted to similar hydrophobic surfaces on neighbouring molecules and thus, these partially-folded intermediates are prone to self-association and aggregation (Fink, 1998, Ecroyd and Carver, 2008). This process results in proteins exiting the protein on-folding pathway and entering off-folding pathways (Shea and Brooks, 2001, Stefani, 2008), leading to the formation of amorphous (disordered) aggregates or amyloid fibrils (Dobson, 2004, Stranks et al., 2009, Greenwald and Riek, 2010).

The mechanism of disordered protein aggregation proceeds following the rapid unfolding and association of protein intermediates, whereby aggregation results from the addition of individual monomers that are randomly incorporated into growing clumps. This process is associated with the formation of amorphous aggregates that, when large enough, precipitate out of solution (Stranks et al., 2009). Alternatively, aggregation can occur via a slower but highly ordered process that starts with the formation of soluble, β-sheet rich oligomeric forms of the protein, which associate to form a stable nucleus. This nucleus creates a 'seed' which acts as a template to sequester other protein intermediates into the growing chain of aggregated protein, termed a protofibril. The growth and association of protofibrils eventually leads to the formation of highly ordered and insoluble protein deposits that are referred to as amyloid fibrils. Whether a protein proceeds to aggregate via an amorphous or fibrillar mechanism is thought to depend upon the structure and stability of the partially-folded intermediate. For example, protein intermediates which have little loss of secondary structure and a high degree of exposed hydrophobicity tend to rapidly form disordered amorphous precipitates (Uversky and Ptitsyn, 1994, Khurana et al., 2001, Cheung and Truskett, 2005, Stranks et al., 2009). Conversely, protein intermediates that are more significantly unfolded, and therefore have lost most of their secondary structure and have a low degree of exposed hydrophobicity, preferentially associate to form fibrils via a slow, but highly

ordered mechanism (Lai et al., 1996, Harper and Lansbury Jr, 1997, Chamberlain et al., 2000, Khurana et al., 2001, Quintas et al., 2001).

1.2.1 Protein aggregation and human disease

Amyloid fibrils have long been implicated in a variety of debilitating diseases, some of the most notable being neurodegenerative disorders, including Alzheimer's disease (Kidd, 1963), Parkinson's disease (Duffy and Tennyson, 1965), amyotrophic lateral sclerosis (ALS) (Abarbanel et al., 1986) and the prion diseases (Ishii et al., 1984). The common pathological hallmark of these and other neurodegenerative diseases is the presence of aggregated protein in the form of amyloid fibrils, which have self-assembled into large tangled deposits in the brain (Selkoe, 2004). Depending on the location of the aggregated protein, amyloid fibrils can deposit into intracellular protein inclusions or extracellular plaques (Westermark et al., 2005). Many age-related neurodegenerative diseases, including Alzheimer's disease, Huntington's disease and ALS, are associated with the expression of aggregation-prone proteins or polypeptide fragments that oligomerise and deposit into inclusions. For example, the deposition of the tau protein and amyloid-β peptide into intracellular and extracellular deposits, respectively, are pathological hallmarks of Alzheimer's disease (Bucciantini et al., 2002, Hardy and Selkoe, 2002, Haass and Selkoe, 2007, Iqbal et al., 2009). Proteins containing expanded polyglutamine (polyQ) repeats aggregate to form amyloid precursors and mature fibrils which have been linked to Huntington's disease and various ataxias (Zoghbi and Orr, 2000, Chiti and Dobson, 2006).

Although many diseases are characterised by the formation of amyloid fibrils, not all proteins aggregate through an ordered mechanism. For example, mutations in superoxide dismutase 1 (SOD1), which are causative of some familial forms of ALS, lead to the formation of highly disordered and hydrophobic amorphous precipitates (Banci et al., 2007, Prudencio et al., 2009). In addition, recent studies have demonstrated that almost all cases of sporadic ALS and

frontotemporal dementia share a common neuropathology of predominantly amorphous, intracellular deposits that contain transactive response DNA-binding protein 43 (TDP-43) (Neumann et al., 2006, Adachi et al., 2009, Scotter et al., 2015). Furthermore, some proteins are known to adopt intermediate conformations before forming amyloid fibres (Dobson, 2003, Stathopulos et al., 2003). Finally, amorphous aggregation is associated with protein misfolding that occurs during conditions of cellular stress (Chiti and Dobson, 2006, Ecroyd and Carver, 2008). Thus, protein aggregation can lead to amyloid-fibril and/or amorphous forms, each with their own unique characteristics (Kampinga and Bergink, 2016). Different mechanisms or protein quality control machinery is likely to be required to maintain each of these forms of aggregation-prone proteins in a soluble state.

The deposition of protein into aggregates is associated with progressive neuronal loss, reduced synaptic transmission and neuro-inflammation. The death of neurons has been suspected to occur by programmed cell death (apoptosis) (Mattson, 2000), however, the specific mechanism by which this occurs is still not completely understood. There have been at least three hypotheses proposed to describe how protein misfolding and aggregation cause neuronal loss and subsequent neurodegeneration. Cattaneo et al. (2001) proposed the 'loss-of-function' hypothesis, which states that neuronal loss is a result of reduced protein activity due to unfolding and aggregation. However, such a mechanism has been refuted by research into Huntington's disease, which demonstrates that patients that are either homozygous or heterozygous for mutations in the huntingtin protein both present with similar clinical features (Wexler et al., 1987). These results imply that mutant huntingtin is capable of performing the same function as non-mutated (wild-type) huntingtin, and thus, the loss-of-function hypothesis does not correctly describe the pathogenesis associated with Huntington's disease. Another strong argument against the loss-of-function hypothesis pertains to research into SOD1, the aggregation of which is associated with some familial forms of ALS (Turner and Talbot, 2008). Studies involving the knockout of SOD1

in mice have shown that this does not lead to degeneration of motor neurons (Reaume et al., 1996). In addition, there is no correlation between enzyme activity and disease severity with regard to disease-associated mutations of SOD1 (Borchelt et al., 1995).

The 'brain inflammation' hypothesis proposes that protein aggregates and deposits cause a chronic inflammatory response in the brain, leading to neuronal loss and synaptic decline (McGeer and McGeer, 1995). Several *in vitro* studies have demonstrated that protein aggregates can activate microglia and astrocytes, causing them to release pro-inflammatory proteins (e.g. cytokines and chemokines) (Peyrin et al., 1999, Yates et al., 2000). In addition, clinical trials in animal models and humans have shown that treatment with nonsteroidal anti-inflammatory drugs slows the progression of Alzheimer's disease (McGeer et al., 1996). Other studies have indicated a beneficial role for neuro-inflammation in these diseases (Wyss-Coray and Mucke, 2002). For example, immune-boosting vaccinations with amyloid-β resulted in a pronounced decrease in the prevalence of cerebral amyloid plaques (Schenk et al., 1999) and improved behavioural and cognitive function in mouse models of Alzheimer's disease (Janus et al., 2000, Morgan et al., 2000). However, when this vaccination was trialled in humans, cases of brain encephalopathies and subsequent increased inflammation were observed, including an elevated white blood cell count in the cerebrospinal fluid, indicative of a central inflammatory response (Schenk, 2002). These studies suggest that brain inflammation resulting from neurodegenerative conditions may have simultaneous positive and negative effects.

The final and most widely accepted hypothesis regarding the mechanism by which protein misfolding and aggregation lead to neurodegeneration is the 'gain-of-toxic-activity' hypothesis. This hypothesis is based on the concept that the presence of aggregates induces neuronal apoptosis. Seminal *in vitro* studies undertaken by Forloni et al. (1993), Loo et al. (1993) and Lunkes and Mandel (1998) demonstrated that increased aggregation directly promotes the neurotoxic effects

of misfolded proteins. Additional evidence to support this hypothesis is based on more recent experiments involving TDP-43, in which overexpression of both mutant and wild-type TDP-43 induces disease phenotypes in mouse models of ALS (Wils et al., 2010, Xu et al., 2010). These results suggest that TDP-43 gains toxic properties as the disease progresses. It has also been postulated that in some diseases, a combination of these hypothesised mechanisms may be involved in neurodegeneration (Soto, 2003).

1.2.2 Inclusion formation in cells

An evolutionarily conserved action of cells in response to stress is the localisation of misfolded or aggregated proteins into subcellular protein deposits, termed protein inclusions (Wigley et al., 1999, Kaganovich et al., 2008, Kirstein et al., 2008). Cells can develop different types of inclusions depending upon the nature of the misfolded protein. These inclusions include aggresomes (Johnston et al., 1998), juxtanuclear quality control compartments (JUNQ) and insoluble protein deposits (IPOD) (Figure 1.2) (Kaganovich et al., 2008). Aggresomes are a type of insoluble inclusion body generated in the cytoplasm of mammalian cells, the formation of which is initiated by small protein aggregates that form at the periphery of the cell (Tyedmers et al., 2010). The aggregates are then transported, in a dynein/dynactin-dependent manner, along the microtubule cytoskeleton until they are delivered to a juxtanuclear, pericentriolar site at the main microtubule organising centre (centrosome) (Johnston et al., 1998, Kopito, 2000).

Work undertaken by Kaganovich et al. (2008) identified two other inclusion structures in the cytoplasm of mammalian and yeast cells that have been proposed to act as quality control compartments, JUNQ and IPOD inclusions. JUNQ inclusions harbour misfolded (but soluble) proteins, which are still mobile and can readily exchange with proteins in the surrounding cytoplasm. The proteins in JUNQ compartments are ubiquitinated, indicative of them having been targeted for degradation by the proteasome (Kaganovich et al., 2008). The accumulation of

ubiquitinated protein in JUNQ inclusions perhaps suggests that when the capacity of the proteasome is limited (as observed in aged cells), ubiquitinated substrates can be reversibly held in JUNQ compartments (Bagola and Sommer, 2008). In contrast, proteins deposited in IPOD compartments typically cannot diffuse out of the inclusions and are terminally unfolded (aggregated), not ubiquitinated and therefore, presumably not intended for degradation by the proteasome (Kaganovich et al., 2008).

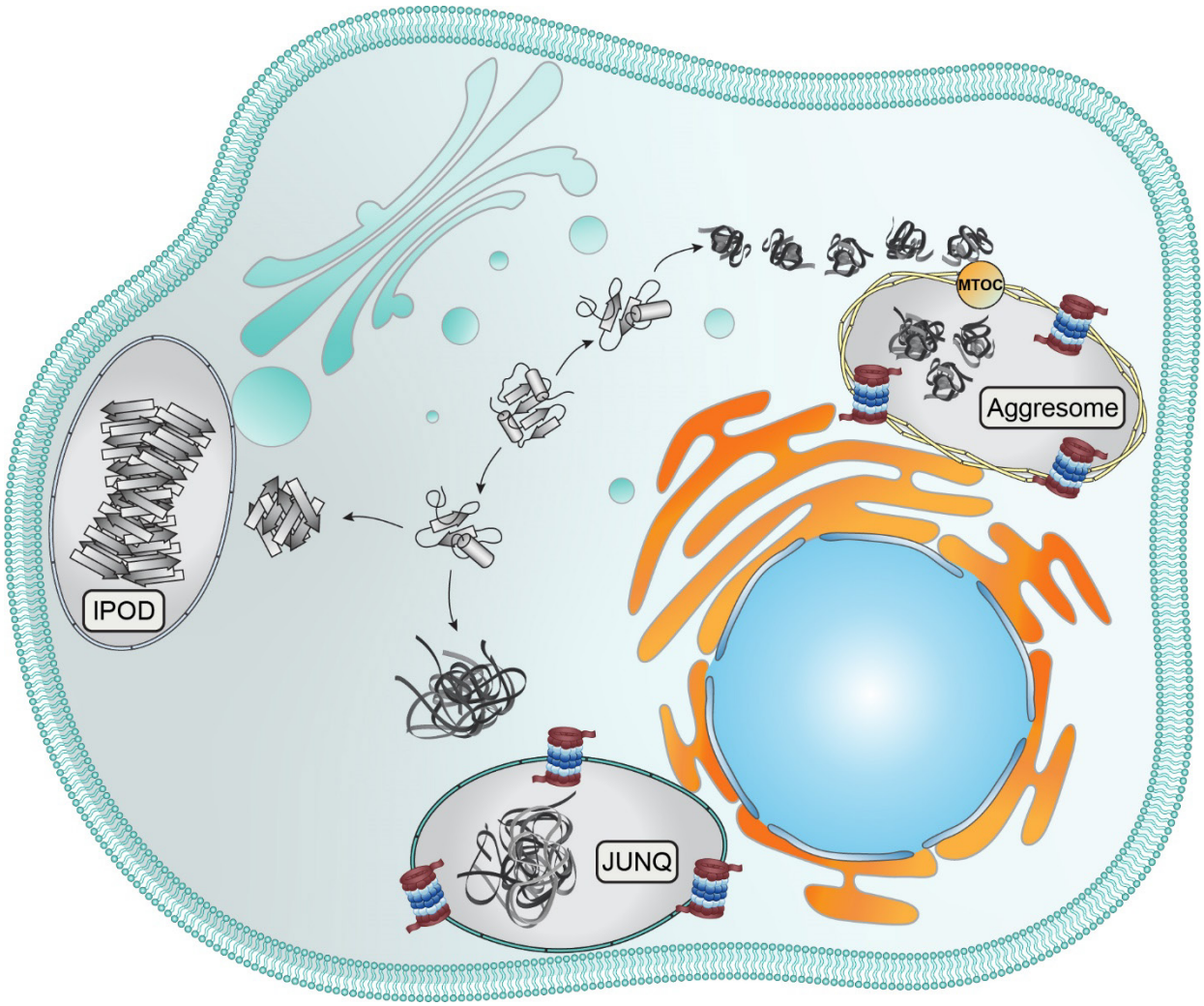

Figure 1.2. The distinct quality control compartments formed in cells when misfolded proteins are localised into inclusions. Cells can localise misfolded proteins into discrete cytosolic compartments depending on the features of the aggregating protein. There are currently three types of inclusions that have been identified in mammalian and yeast cells; aggresomes, and JUNQ and IPOD inclusions. Aggresome formation is initiated by small protein aggregates at the perimeter of the cell. The aggregates are transported along the microtubule cytoskeleton until they are delivered to the microtubule-organising centre (MTOC). JUNQ inclusions, which are found close to the nucleus, contain misfolded (but soluble) proteins that can still associate with proteins in the surrounding cytoplasm. Proteins in JUNQ compartments are ubiquitinated and are associated with proteasomes. IPOD compartments are usually located at the periphery of the cell and contain terminally unfolded (aggregated) proteins that are not ubiquitinated and cannot associate with proteins in the cytoplasm.

Whilst the intracellular and extracellular proteinaceous deposits found in patients who suffer from neurodegenerative diseases contain one dominant aggregated protein (Alexandrescu, 2005, Chiti and Dobson, 2006), other proteins and molecules, including chaperones and co-chaperones, are also found in these deposits (Sherman and Goldberg, 2001). The exact reason why these other proteins are associated with these deposits remains unclear, but it is assumed to be, at least in part, due to the functional roles these proteins have in the rescue of misfolded proteins found in inclusions (Bergemalm et al., 2010). Moreover, it has been postulated that inclusions may play a protective role in the cell by sequestering non-functional proteins into discrete entities (Bucciantini et al., 2002, Walsh et al., 2002, Tanaka et al., 2004, Miller et al., 2011). However, whilst inclusions appear to protect cells over short time periods, eventually cells with inclusions die as a result of the associated toxicity (Lang-Rollin et al., 2003, Ramdzan et al., 2017). This effect has been hypothesised to represent a failure of the systems in cells that act to maintain the solubility and function of aggregation-prone proteins. In any case, it is evident that neuronal degradation is related to protein aggregation and subsequent inclusion formation (Chiti and Dobson, 2006, Ticozzi et al., 2010, Ormsby et al., 2013). Thus, further research into the mechanisms by which proteins aggregate and factors that prevent inclusion formation is extremely important, as this will likely provide promising therapeutic targets for treating neurodegenerative conditions.

1.2.3 Are some cells more susceptible to the formation of inclusions than others?

It has been reported that different cell types have varying susceptibilities to inclusion formation (Wyttenbach et al., 2002, Cecchi et al., 2005). However, there remains a substantial gap in knowledge surrounding the molecular basis of resistance or susceptibility to inclusion formation between cell types. The innate ability of the cell to maintain aggregation-prone proteins in a soluble state is known to vary significantly among different cell types (Lim and Yue, 2015). For example, neurons appear to be particularly susceptible to inclusion formation since many debilitating neurodegenerative conditions are characterised by the accumulation of misfolded

proteins into inclusions in neurons. This raises the question as to why neurons are so susceptible to inclusion formation, given that many aggregation-prone proteins are also expressed (sometimes at higher concentrations) in other cells of the body? The reason why neurons are so vulnerable to inclusion formation is not well understood at the molecular level, but it has been proposed to be as a result of their limited capacity to divide (and therefore dilute toxic protein aggregates) and low turnover rate, stemming from their increased longevity compared to other cell types (Saxena and Caroni, 2011, Lim and Yue, 2015, Smith et al., 2015). It may also be that the cellular pathways that maintain an aggregation-prone protein in a soluble state are regulated differently in neurons compared to other cell types (Lim and Yue, 2015). Therefore, intrinsic differences in the pathways that regulate the intracellular environment and act to prevent protein aggregation may also explain the susceptibility of certain cell types to inclusion formation.

1.3 Protein homeostasis (proteostasis)

Anfinsen's (1973) dogma of protein folding, whilst significant, is limited as it mostly relates to the folding of small, single domain polypeptide chains *in vitro*. Thus, the *in vivo* folding of proteins, particularly large and/or multi-domain proteins, is not accurately described by Anfinsen's thermodynamic hypothesis. In addition, once a protein successfully folds into its native state, this does not signal the end of the folding events that it may endure during its lifetime. Proteins can partially unfold when subjected to cellular stress and then refold back into their biologically active states (Dobson, 2003), whilst other proteins must be unfolded and refolded as part of their normal trafficking within the cell, for example when being transported across intracellular membranes or undergoing cellular secretion (Schnell and Hebert, 2003). Moreover, protein folding *in vivo* is much more complex than in solution, primarily due to the effect of macromolecular crowding in cells. Therefore, cells possess regulatory networks that assist in folding proteins and maintaining protein homeostasis (proteostasis) in order to prevent protein aggregation and inclusion formation (Roth and Balch, 2011). For recent published reviews on the

systems involved in maintaining cellular proteostasis, see Kaushik and Cuervo (2015), Labbadia and Morimoto (2015), Yerbury et al. (2016), Dikic (2017), Gomez-Pastor et al. (2018), Klaips et al. (2018), Hipp et al. (2019), Hetz et al. (2020), Hetz (2021).

The proteostasis network refers to the pathways that help to maintain a stable and functional proteome. The integrity of the proteome is maintained by a network of approximately 800 proteins that are involved in processes that include the synthesis, folding, trafficking and degradation of proteins. Of these, 332 function as molecular chaperones or co-chaperones (Brehme et al., 2014, Balchin et al., 2016). This network of proteins act to maintain proteostasis in the intracellular and extracellular environments by responding and adapting to internal and external changes. Under normal physiological conditions, the proteostasis network can successfully maintain the proteome in a functional state. However, certain factors, such as gene mutations, epigenetic factors, aging and cell stress, can act to disrupt proteostasis and therefore reduce cell viability (Balch et al., 2008, Morimoto, 2008). When the cell is exposed to conditions that promote protein misfolding and aggregation, non-native or partially-folded proteins can self-associate to form aggregates (described above), be rescued by molecular chaperones or be directed for degradation by proteases.

1.4 Chaperone-mediated protein handling

A cell may be exposed to a variety of environmental conditions, including macromolecular crowding (Ellis and Minton, 2006), an increase in temperature (Feder and Hofmann, 1999) and suboptimal pH (Fink et al., 1994), which result in an increase in partially-folded or misfolded proteins. This is counterbalanced by the upregulation of some molecular chaperones that occur as a result of cellular stress (Hartl et al., 2011). Molecular chaperones are a ubiquitous family of extracellular and intracellular proteins that stabilise aberrantly folded polypeptides and target them for refolding or degradation, thereby minimising protein aggregation (Hartl, 1996, Broadley and

Hartl, 2009, Hartl et al., 2011, Wyatt et al., 2013). The term 'chaperone' encompasses many different families of proteins. The best described is the heat shock protein (Hsp) superfamily, which includes Hsp40, Hsp60, Hsp70, Hsp90, Hsp110 and the small Hsps (sHsps) (Bukau et al., 2006, Hartl et al., 2011).

1.4.1 The heat shock response

The heat shock response is a primary pathway that is activated in cells during periods of stress. The heat shock response was first identified in *Drosophila busckii* by Ritossa (1962). The accumulation of partially-folded protein intermediates that form following proteotoxic stress can activate transcription factors and induce the heat shock response, a response that acts to protect the cell and re-establish proteostasis. The human genome encodes four heat shock transcription factors (HSF), HSF1 – HSF4, with HSF1 identified as the 'master regulator' of transcriptional responses during cell stress (Åkerfelt et al., 2010). Under normal conditions, HSF1 resides as an inactive monomer in the cytoplasm via weak and transient interactions with chaperone proteins, Hsp90, Hsp40, Hsp70 or the chaperonin TriC/CCT (Shi et al., 1998, Bharadwaj et al., 1999, Guo et al., 2001, Gómez et al., 2008, Neef et al., 2014, Vihervaara and Sistonen, 2014). Under conditions of cellular stress, the chaperone-HSF1 equilibrium is altered due to the rapid formation of partially-folded proteins, which are substrates for the chaperones (Zuo et al., 1994, Zuo et al., 1995). Thus, HSF1 is released from chaperone-HSF1 complexes and undergoes self-association to form trimers that can then translocate into the nucleus. (Morimoto, 2011). Activated HSF1 trimers are then able to bind heat shock elements in the promotor region of heat shock genes, leading to the transcription and upregulation of these Hsps (Trinklein et al., 2004).

HSF1-mediated transcription is attenuated by a negatively regulated feedback mechanism, whereby elevated levels of HSF1-induced Hsps competitively inhibit HSF1 trimer activity in the nucleus to promote its inactive, monomeric form (Anckar and Sistonen, 2011, Zheng et al., 2016).

This negative feedback loop ensures that the concentration and expression of Hsps is proportional to the pool of non-native proteins present in the cell. Thus, modulation of HSF1 activity has been suggested as a potential therapeutic approach for the treatment of diseases associated with protein aggregation (Neef et al., 2010, Neef et al., 2011, Gomez-Pastor et al., 2018). Despite this, the majority of Hsps are not stress-inducible and instead are constitutively expressed, performing general 'house-keeping' functions for the maintenance of cell viability. The extensive roles of Hsps in proteostasis have been well documented in recent comprehensive reviews (Winkler et al., 2012, Priya et al., 2013, Kakkar et al., 2014, Tóth et al., 2015, Treweek et al., 2015, Kampinga and Bergink, 2016, Zarouchlioti et al., 2018, Rosenzweig et al., 2019) and are therefore only briefly summarised below.

1.4.2 Hsp70 chaperone machinery

Chaperones can be broadly categorised as adenosine triphosphate (ATP)-dependent 'foldase' or ATP-independent 'holdase' proteins, depending on the type of interaction they have with client proteins. ATP-dependent foldase chaperones can fold newly synthesised proteins and refold unfolded or misfolded proteins via a process known as kinetic partitioning. These foldases, which includes the Hsp70 family, bind to exposed hydrophobic regions in unfolded proteins to prevent aggregation, and exploit the energy of ATP to promote folding of the protein into the native state (Langer et al., 1992, Lin et al., 2008, Hartl et al., 2011). The functional diversity of Hsp70 members is rather striking considering Hsp70 chaperones are among the most evolutionarily conserved proteins in humans and participate in diverse functions within the cell (Kampinga and Craig, 2010, Hageman et al., 2011). The major members of the human Hsp70 family and their previously reported roles within the cell are outlined in Table 1.1.

Table 1.1. Human Hsp70 proteins, their reported stress inducibility, subcellular localisation and proposed roles within the cell.

Name	*Synonyms*	*Stress inducible*	*Subcellular localisation*	*Suggested cellular roles*	*References*
HspA1A	Hsp70 Hsp70-1 Hsp72 Hsp70-1A	Yes	Cytosol, nucleus, cell membrane, extracellular exosomes	Most widely studied and the major stress-inducible member of the Hsp70 family. Expression is upregulated upon HSF1 activation following a variety of cellular assaults, for protection against harmful protein aggregation. Known to participate in the refolding of denatured proteins. Can inhibit substrate accumulation, thereby removing the trigger of programmed cell death. Stabilises the lysosomal membrane to inhibit release of lysosomal hydrolases into the cytosol to prevent cell death via apoptosis. Participates cooperatively with Hsp110 and Hsp40 to form the disaggregase machinery to solubilise aggregated proteins. Participates in protein translocation across the ER and mitochondrial membranes. With the assistance of co-chaperones, can pass on misfolded proteins for degradation via autophagy or the proteasome.	(Chirico et al., 1988, Deshaies et al., 1988, Li et al., 1991, Jäättelä and Wissing, 1993, Mestril et al., 1994, Bellmann et al., 1996, Wissing and Jäättelä, 1996, Michels et al., 1997, Kwak et al., 1998, Nollen et al., 1999, Mosser et al., 2000, Leist and Jäättelä, 2001, Nylandsted et al., 2004, Kroemer and Jäättelä, 2005, Carra et al., 2008b, Gamerdinger et al., 2009, Rampelt et al., 2012, Nillegoda et al., 2015)
HspA1L	Hsp70-hom Hsp70-1L	No	Cytosol, nucleus	Lacks the heat shock binding element in its promoter region, and therefore is less heat-inducible than HspA1A. Expressed endogenously at low levels in most tissues, with high abundance in the testis. Evidence suggests that, under normal conditions, HspA1L acts to mitigate deleterious effects of mutant protein aggregation, thereby providing cells with basal protection against the continual assault of protein misfolding.	(Milner and Duncan Campbell, 1990, Warrick et al., 1999, Hageman et al., 2011)
HspA2	Heat shock	No	Cytosol, nucleus, cell	Primarily expressed in the testis. Within spermatocytes, it is the main chaperone for the CyclinB1/Cdk1 complex during	(Dix et al., 1997, Zhu et al., 1997, Rohde et al., 2005,

	70kD protein 2 Hsp70-2		membrane, extracellular exosomes	meiotic cell division. Involved in packaging DNA proteins for post-meiotic genome reorganisation. Essential for the proliferation and survival of human cancer cells.	Govin et al., 2006, Daugaard et al., 2007a)
HspA5	BiP GRP78 Mif2	No	ER	ER-resident Hsp70 member that possesses a C-terminal retention signal which prevents its secretion out of the ER lumen. Involved in the general folding of proteins and maintenance of proteostasis following stress in the ER. Is recruited in the post-translational translocation of substrates through the translocon into the cytosol.	(Munro and Pelham, 1987, Brodsky and Schekman, 1993, Matlack et al., 1997, Lee, 2005, Oka et al., 2013)
HspA6	Hsp70-6 Hsp70B	Yes	Cytosol, extracellular exosomes	Strictly only induced proceeding severe stress insults. Functions as a component of the general stress-response. Compared to related Hsp70 members, HspA6 has enhanced N-terminal ATPase activity and is believed to have evolved a distinct functional role in the maintenance of cell reproduction and viability under conditions of cellular stress.	(Parsian et al., 2000, Noonan et al., 2007, Hageman et al., 2011)
HspA8	Hsp70-8 Hsc70 Hsc71 Hsp71 Hsp73	No	Cytosol, nucleus, cell membrane, extracellular exosomes	Constitutively expressed housekeeping member of the Hsp70 family. Has been reported to participate in a plethora of cellular functions, including folding of nascent polypeptides, promoting correct protein translocation across membranes, chaperone-mediated degradation by the proteasome or autophagy, protection against protein aggregation under stress conditions, and disassembly of clathrin cages for recycling.	(Lindquist and Craig, 1988, Beckmann et al., 1990, Demand et al., 2001, Albanèse et al., 2006, Kettern et al., 2010, Morgan et al., 2013)
HspA14	Hsp70-14 Hsp70L1	Yes	Cytosol, membrane	Functions in the cell are currently unclear. Lacks the canonical substrate binding domain and instead participates in protein translation.	(Huang et al., 2005, Kampinga and Craig, 2010)

Despite the functional diversity of members of the Hsp70 family, they share a common molecular mechanism of action: a cycle of ATP-dependent client-binding and release that facilitates interaction with client proteins. The diverse roles that Hsp70s have in the cell is likely a result of them not acting in isolation; rather, Hsp70 'machines' are regulated by co-factors, such as other chaperones and nucleotide exchange factors (NEFs).

1.4.3 Hsp40 proteins – drivers of the Hsp70 machine

The activity of Hsp70 chaperones is driven by interactions with Hsp40 proteins (also known as DNAJs, J proteins, or J-domain proteins), whereby DNAJs deliver misfolded clients to the Hsp70 machinery and, in turn, stimulate Hsp70 ATPase activity (Bukau et al., 2006). The DNAJs are so named as they have a highly conserved J-domain which contains the histidine-proline-aspartate (HPD) motif for interaction with the Hsp70 machinery. The human genome encodes 53 DNAJ proteins that can be divided into three separate subfamilies, the DNAJA, DNAJB and DNAJC proteins, based upon intrinsic structural features (Figure 1.3A) (Cheetham and Caplan, 1998, Kampinga and Craig, 2010). The DNAJAs are comprised of an N-terminal J-domain, a glycine/phenylalanine (G/F)-rich linker region and two C-terminal domains (CTD-I and CTD-II), with a zinc-finger-like region (ZFLR) inserted into CTD-I. The two barrel topology contained in the C-terminal region forms a hydrophobic pocket with the ZFLR extruding from it to create a substrate binding domain (Linke et al., 2003, Kota et al., 2009). The ZFLR in DNAJAs is thought to contribute to client binding since mutation of the first of the two Zn^{2+} -binding sites renders the DNAJA-Hsp70 complex unable to prevent the aggregation of misfolded proteins in bacteria (Linke et al., 2003) and yeast (Lu and Cyr, 1998, Fan et al., 2005). The second Zn^{2+}-binding site is important for the transfer of DNAJA-bound clients to Hsp70 (Linke et al., 2003, Baaklini et al., 2012). There is some evidence to suggest that members of the mammalian DNAJA family have a differential capacity to bind client proteins. For example, a complex of DNAJA2-Hsp70, but not DNAJA4-Hsp70, can support refolding of denatured luciferase, despite both DNAJAs being able to stimulate Hsp70 ATPase activity (Hafizur et al., 2004).

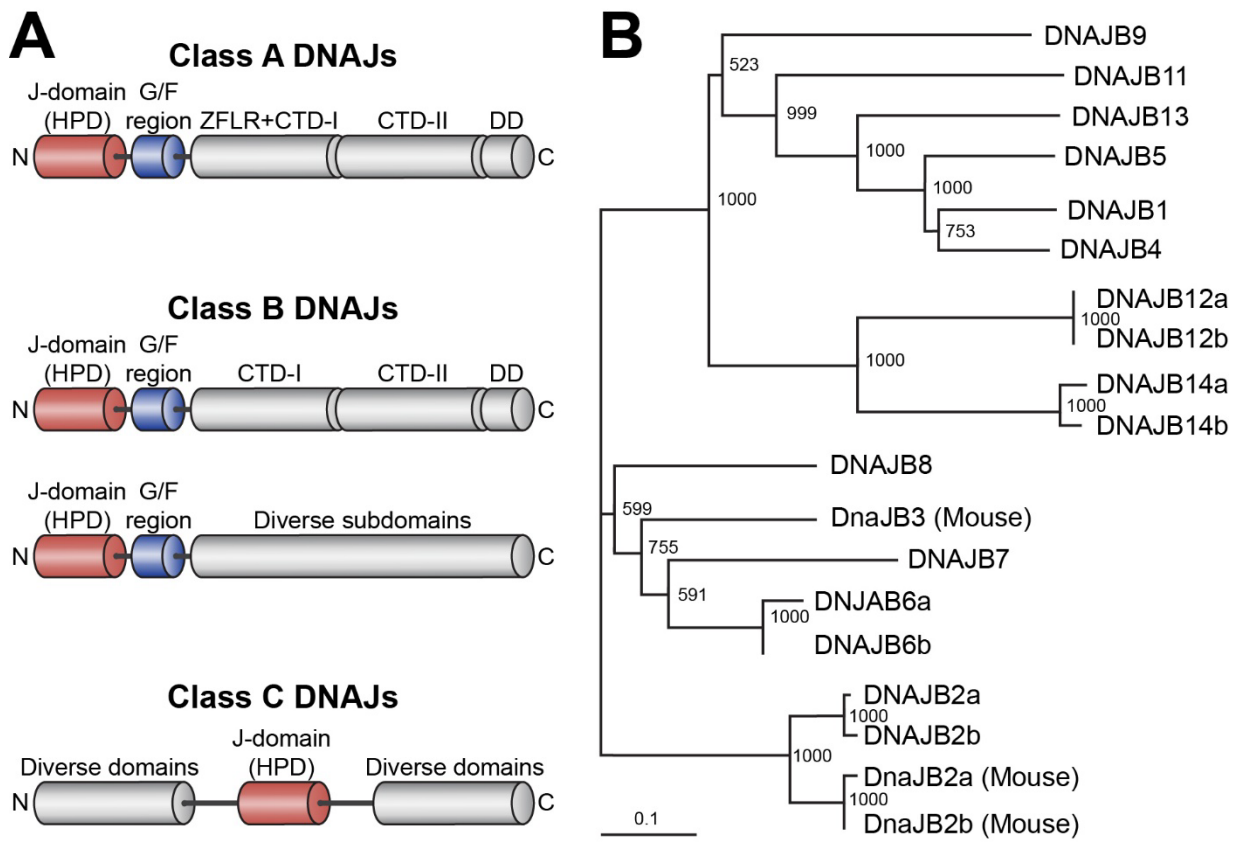

Figure 1.3. The divergence of DNAJ proteins based on their structural features. (A) Schematic representation of the domain organisation of class A (*top*), class B (*middle*) and class C (*bottom*) DNAJ proteins. The histidine-proline-aspartate (HPD) motif lies within the J-domain, which is highly conserved among the three classes of DNAJs. Class A DNAJs have an N-terminal J-domain, a glycine/phenylalanine (G/F)-rich linker region and two C-terminal domains (CTD-I and CTD-II), with a zinc-finger-like region (ZFLR) in CTD-I and a dimerisation domain (DD). Class B DNAJ proteins are comprised of an N-terminal J-domain, an internal G/F-rich linker region, diverse C-terminal domain(s) for binding clients and in some cases, a DD. Class C DNAJs contain a J-domain (which can be located anywhere within the protein) and are heterogeneous in terms of their C-terminal domains. **(B)** Combined phylogenetic distribution of aligned DNAJB primary amino acid sequences using the neighbour-joining algorithm and Blosum matrixes. Scale bar represents phylogenetic distance of 0.1 amino acids substitutions per position. Numbers on the branch-points indicate bootstrap values of 1000 trials.

Structurally, DNAJB proteins are defined by an N-terminal J-domain, an internal G/F-rich linker region and a C-terminal domain that is thought to bind clients (Cheetham and Caplan, 1998, Kampinga and Craig, 2010). The DNAJB proteins can be further divided into two subfamilies, based on their C-terminal structure (Hageman and Kampinga, 2009, Kampinga and Craig, 2010, Rosenzweig et al., 2019) and phylogenetic classification following sequence analysis (Figure 1.3B) (Hageman et al., 2010, Hageman et al., 2011). The first subclass (termed DNAJB1-like) includes DNAJB1, DNAJB4 and DNAJB5, whereas the second (termed DNAJB6-like) includes DNAJB2, DNAJB6, DNAJB7 and DNAJB8. In contrast to DNAJB6-like proteins, which possess

one (albeit diverse) C-terminal domain, DNAJB1-like proteins have two distinct C-terminal regions for binding clients. Of the DNAJs, the DNAJB proteins are the most extensively studied due to them being previously identified as potent suppressors of aggregation associated with many disease-related proteins, including polyQ, amyloid-β and SOD1 proteins (Howarth et al., 2007, Hageman et al., 2010, Labbadia et al., 2012, Gillis et al., 2013, Månsson et al., 2014a, Kakkar et al., 2016b, Serlidaki et al., 2020). The proposed cellular roles of the major human DNAJB members and their previously reported capacity to prevent the aggregation of a variety of aggregation-prone proteins is outlined below (Table 1.2).

Table 1.2. Human DNAJBs, their reported stress inducibility, subcellular localisation, reported capacity to suppress the aggregation of client proteins and proposed roles within the cell.

Name	*Synonyms*	*Stress inducible*	*Subcellular localisation*	*Reported chaperone activity*	*Suggested cellular roles*	*References*
DNAJB1	Hsp40 Hdj-1	Yes	Cytosol	Acts with Hsp70 to reduce amyloid-β aggregation *in vitro*. Prevents the nucleation of polyQ-expanded huntingtin tracts to reduce the formation of mature toxic fibrils *in vitro*. Decreases the rate of assembly of α-synuclein fibrils and increases the capacity of Hsp70 to bind α-synuclein *in vitro*. Suppresses tau aggregation in a dose-dependent manner *in vitro*. Cooperates *in vitro* with Hsp110 and Hsp70 to solubilise amorphous aggregates formed by both denatured firefly luciferase and α-synuclein as part of the disaggregase machinery. Has mild suppressive activity against inclusion formation by polyQ-expanded huntingtin, but does not suppress toxicity in cells. When expressed in combination with Hsp70 can increase cellular proliferation and reduce the cytotoxicity associated with polyQ-expanded huntingtin inclusion formation. Reduces the misfolding and aggregation of mutant Parkin in cells. Increases the solubility of polyQ-expanded androgen receptor and enhances its	Participates in downstream stages in the folding of proteins directly off the ribosome. Interacts alongside Hsc70, Hsp90 and the co-chaperones Bag1, HIP and HOP to traffic substrates for degradation via chaperone-mediated autophagy. Expression is upregulated upon HSF1 activation following cell stress to protect against accumulation of misfolded proteins.	(Jana et al., 2000, Kazemi-Esfarjani and Benzer, 2000, Kobayashi et al., 2000, Muchowski et al., 2000, Agarraberes and Dice, 2001, Bailey et al., 2002, McLean et al., 2002, Takeuchi et al., 2002, Evans et al., 2006, Hageman et al., 2010, Kampinga and Craig, 2010, Pemberton et al., 2011, Shorter, 2011, Rampelt et al., 2012, Kuo et al., 2013, Ormsby et al., 2013, Vihervaara and Sistonen, 2014, Nillegoda et al.,

				proteasomal degradation in a cellular model of spinal and bulbar muscular atrophy. Overexpression decreases intracellular inclusion formation in α-synuclein cell culture model of disease. Reduces cytoplasmic inclusion formation by mutant SOD1 to improve neurite outgrowth in cells. Suppresses toxicity of aggregation and reduces eye degeneration in *Drosophila melanogaster* models of polyQ-expanded disease.		2015, Kakkar et al., 2016a, Nillegoda et al., 2017, Serlidaki et al., 2020, Tittelmeier et al., 2020)
DNAJB2a/b	Hsjla Hsj1b	Yes	Cytosol, nucleus, ER	Regulates proteasomal degradation to reduce the aggregation associated with a polyQ-expanded form of ataxin-3 in cells. Reduces polyQ-expanded huntingtin aggregation *in vitro*, in cells, in mice and rats. Inhibits the misfolding of mutant Parkin in cells to reduce protein aggregation and promote functional refolding. Prevents mutant SOD1 aggregation in cells. Inhibits the aggregation of SOD1 in mice and, in turn, increases muscle function, motor neuron survival and body weight. Overexpression reduces TDP-43 aggregation in cells. Inhibits polyQ-expanded huntingtin-induced death of striatal neurons and promotes neuronal function in *Caenorhabditis elegans*.	Contains ubiquitin-interacting motifs (UIMs) that bind ubiquitinated proteins and shuttles them for degradation via the proteasome.	(Chapple and Cheetham, 2003, Chapple et al., 2004, Westhoff et al., 2005, Borrell-Pagès et al., 2006, Howarth et al., 2007, Hageman et al., 2010, Kampinga and Craig, 2010, Gao et al., 2011, Hageman et al., 2011, Rose et al., 2011, Blumen et al., 2012, Labbadia et al.,

						2012, Novoselov et al., 2013, Chen et al., 2016, Kakkar et al., 2016a, Serlidaki et al., 2020)
DNAJB3	HCG3 Hsj3 Msj1	No	Cytosol, nucleus	None reported	Marker for risk of obesity and insulin resistance as its expression is reduced at the mRNA and protein levels in both blood and adipose tissue of obese individuals. May play a role in insulin signalling and glucose uptake by modulating the c-Jun NH2-terminal kinase (JNK).	(Abubaker et al., 2013, Abu-Farha et al., 2015)
DNAJB4	Hlj1 Hsc40	Yes	Cytosol	Suppresses intracellular inclusion formation of mutant Parkin.	Has close homology to DNAJB1 and is the non-heat inducible and constitutively expressed member of the DNAJ family. Proposed to act as a housekeeping Hsp40	(Chen et al., 1999, Kakkar et al., 2016a)

					member, much like HspA8 (Hsc70) of the Hsp70 family.	
DNAJB5	Hsc40 Hsp40-3	Yes	Cytosol	Inhibits polyQ aggregation in certain cell types.	Structurally is near identical to DNAJB4. Associates with class II histone deacetylases (HDACs) in a redox-dependent manner in response to hypertrophic stimuli, suggesting it may participate as a redox-regulated chaperone.	(Ago et al., 2008, Oka et al., 2009, Hageman et al., 2011)
DNAJB6a/b	Hsj2a Mrja Hsj2b Mrjb	Yes	Cytosol, nucleus	Prevents the primary nucleation of amyloid-β and polyQ-expanded huntingtin peptides into mature fibrils *in vitro*. Suppresses the aggregation of many disease-related polyQ-expanded proteins, including huntingtin, ataxin-3 and the androgen receptor in cells. Inhibits mutant Parkin inclusion formation in cells. Reduces intracellular amyloid-β aggregation, but this activity is dependent upon interaction with Hsp70. Suppresses prion-like aggregation of a nuclear TDP-43 mutant protein in cells.	Mediates keratin turnover in placental development and participates in stem cell self-renewal. Mutations in the protein have been implicated in severe forms of inheritable myopathies that are distinguished by myofibrillar disintegration along	(Chan et al., 2000, Hanai and Mashima, 2003, Fayazi et al., 2006, Watson et al., 2007, Watson et al., 2009, Hageman et al., 2010, Hageman et al., 2011, Sarparanta et al., 2012, Gillis et al., 2013, Månsson et al., 2014a, Månsson et al.,

				Restores eye structure in a mutant ataxin-3 *Drosophila melanogaster* model. Overexpression significantly reduces inclusion formation of polyQ-expanded huntingtin and alleviates associated toxicity in transgenic *Xenopus laevis* tadpole and *Drosophila melanogaster* models of disease. Overexpression of human DNAJB6 in transgenic mice reduces polyQ aggregation in the brain, increases neurological performance and lifespan and slows overall rate of disease progression.	with DNAJB6 accumulation. This may suggest a role for DNAJB6 in the maintenance of muscle structure and/or as a chaperone which normally functions to prevent the accumulation of misfolded sarcomeric proteins in the muscle. However, the role of DNAJB6 in muscle and these inheritable diseases is yet to be determined.	2014b, Udan-Johns et al., 2014, Hussein et al., 2015, Kakkar et al., 2016a, Kakkar et al., 2016b)
DNAJB7	DJ-5 Hsc3	No	Cytosol, nucleus	Prevents intracellular inclusion formation by mutant SOD1 and Parkin.	Cellular function not well understood. May participate in intermediate filament organisation.	(Kakkar et al., 2016a, Chiarelli et al., 2019, Serlidaki et al., 2020)
DNAJB8	mDj6	No	Cytosol, nucleus	Delays the fibrillation of polyQ expanded huntingtin *in vitro*. Inhibits the intracellular aggregation of disease-related polyQ-expanded proteins, such as huntingtin, ataxin-3 and the androgen receptor. Inhibits	Functional homologue of DNAJB6. Required for the survival of cancer stem cells and controls tumour-initiating processes.	(Hageman et al., 2010, Hageman et al., 2011, Nishizawa et al., 2012, Gillis et al., 2013, Månsson et

				intracellular inclusion formation of mutant Parkin in an Hsp70-dependent manner. Reduces inclusion formation of polyQ-expanded huntingtin and attenuates toxicity in a transgenic *Xenopus laevis* tadpole model.	Identified as a cancer/testis antigen.	al., 2014b, Kakkar et al., 2016a)
DNAJB9	ERdj4 Mdg1	Yes	ER	Mediates the clearance of the mutant transmembrane-conductance regulator membrane protein, implicated in cystic fibrosis, via ER-associated degradation in cells and mice. Promotes the turnover of misfolded surfactant protein C (associated with interstitial lung disease in humans) via ER-associated degradation in cells.	The ER-resident member of the DNAJ family. Plays a primary role in binding client proteins throughout the ER and transfers them to Hsp70/BiP for ER-associated degradation.	(Dong et al., 2008, Lai et al., 2012, Behnke et al., 2016, Huang et al., 2019)

The DNAJC family is highly diverse and includes any DNAJs that do not fit within the specifications outlined for DNAJA and DNAJB proteins, instead only sharing the conserved J-domain. In contrast to DNAJA and DNAJB members, in which the J-domain is always located at the N-terminus, DNAJCs contain a J-domain that can be located anywhere within the protein. The DNAJC members are heterogeneous in terms of their C-terminal domain structure and no mode of action has currently been defined for their interaction with substrates. These proteins differ drastically in length (from ~100 amino acids in DNAJC19 to ~4,600 amino acids in DNAJC29) and contain variable structural domains/motifs (e.g. thioredoxin boxes, GTP binding sites, transmembrane helices, tetratricopeptide repeat domains, coiled coils, ISU-1 binding domains, clathrin-binding regions and protein kinase domains) (Kampinga and Craig, 2010). The intracellular roles of the DNAJC members are currently not well understood (Kampinga et al., 2019); those that have been studied have been shown to participate in diverse cellular functions, including protein translocation into the mitochondria and ER (Craig, 2018), ER-associated degradation (Ushioda et al., 2016) translation (Sahi et al., 2010) and endocytosis and exocytosis (Ungewickell et al., 1995, Rapoport et al., 2008, Vos et al., 2008).

1.4.4 The Hsp70/Hsp40-mediated protein folding cycle

Molecular chaperones of the Hsp70 family have a 40 kDa N-terminal nucleotide binding (ATPase) domain and a 25 kDa C-terminal domain for the binding of unfolded clients. Hsp70 members also contain a short, flexible hydrophobic linker region, which separates the N- from the C-terminal, as well as a far C-terminal helical ‘lid’ that closes over the substrate binding domain to capture client proteins (Figure 1.4A). Hsp70 chaperone activity is defined by the rapid association and release of client proteins to prevent subsequent protein aggregation and to promote protein folding. The Hsp70 cycle begins when DNAJs bind client proteins via the C-terminal substrate binding region to then interact with the Hsp70 ATPase domain via the conserved HPD motif located in the J-domain (Figure 1.4B). The client protein rapidly, but transiently, interacts with the ‘open’

conformation of the Hsp70 substrate binding region. The J-domain and client protein stimulate ATP hydrolysis to cause a conformational change in Hsp70, which in turn closes its lid over the substrate binding domain to stabilise the interaction with the client protein. The DNAJ then dissociates from the complex (Kampinga and Craig, 2010). Following ATP hydrolysis, Hsp70 in the ADP-bound state has high affinity for substrate (Rosenzweig et al., 2019). A NEF (outlined briefly below), which has higher affinity for the ADP-bound state than the ATP-bound conformation, binds to Hsp70, inducing ADP to dissociate from Hsp70. This allows ATP to re-bind, reverting Hsp70 back to its low-affinity substrate binding state, which triggers substrate release. The released substrate can then fold into its native state or, if it is unable to do so, DNAJs can re-bind exposed regions of hydrophobicity in the substrate such that it re-enters the Hsp70 cycle.

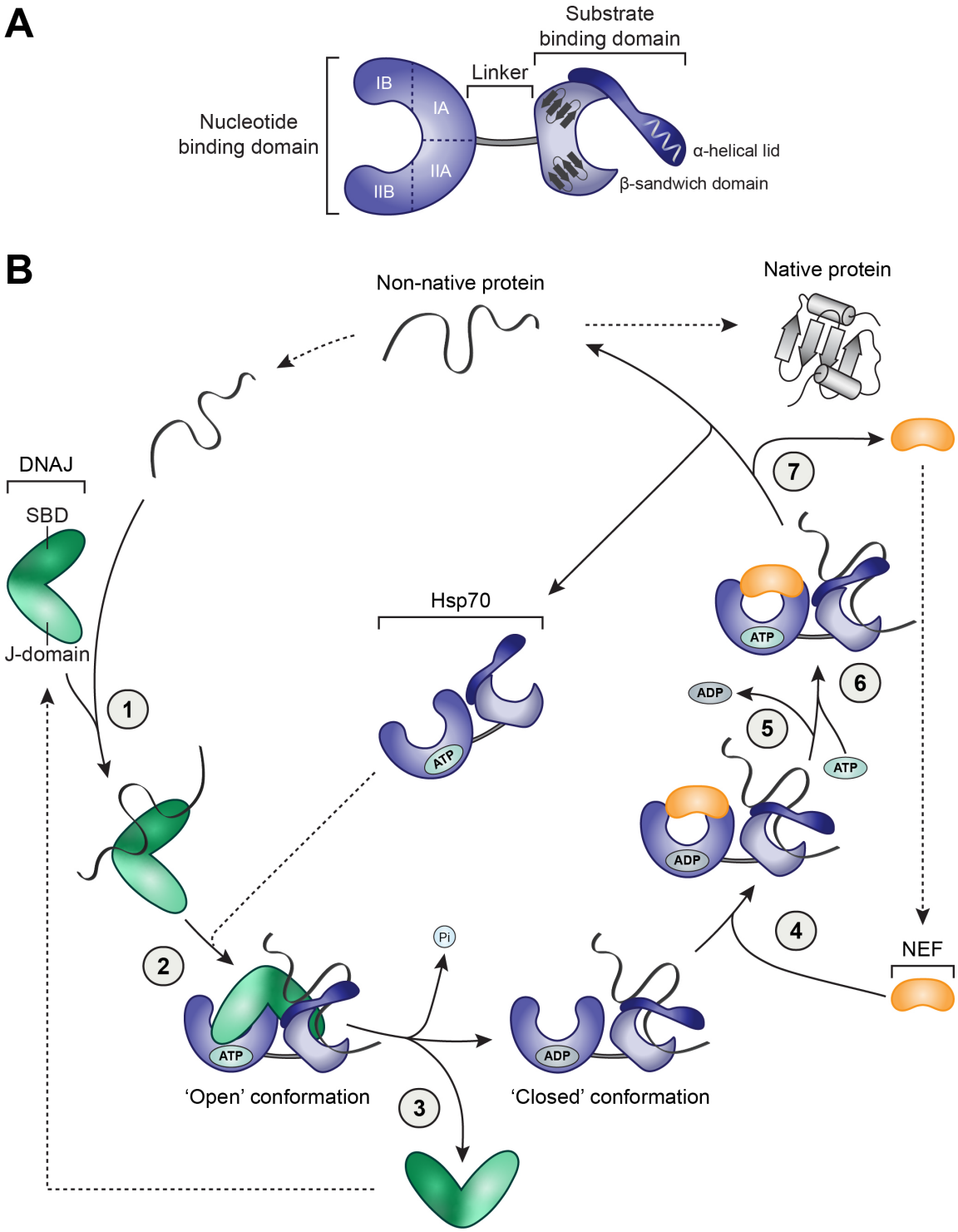

Figure 1.4. The Hsp70/Hsp40 chaperone cycle. (A) Cartoon representation of Hsp70 with the subdomains (IA/B and IIA/B) of the nucleotide binding (ATPase) domain indicated. The flexible linker region separates the N- and C-terminal domains. The C-terminal substrate binding domain is split into a β-sandwich-containing region for the binding of misfolded client proteins. Once substrate is bound, the C-terminal α-helical 'lid' closes over the substrate binding domain to capture and stabilise client proteins. **(B)** Canonical model of the handling of client proteins by the Hsp70 machinery. (1) DNAJs bind client proteins via the C-terminal substrate binding domain and then (2) interact with the Hsp70 nucleotide binding domain via the conserved HPD motif in the J-domain. (3) The client protein interacts with the 'open' conformation of the Hsp70 substrate binding domain. A conformational change induced by the J-domain and client protein stimulates ATP hydrolysis and the α-helical lid in the Hsp70 substrate binding domain closes over the substrate. The DNAJ dissociates from the complex and the Hsp70 substrate binding domain is left in the 'closed' conformation. (4) A NEF then binds the ADP-bound form of Hsp70, (5) inducing ADP to dissociate. (6) This allows ATP to re-bind, triggering substrate release. (7) The NEF is released from the complex and the client protein can fold into its native state. Alternatively, if the native state is not reached, DNAJs can re-bind non-native proteins and the cycle begins again.

1.4.5 Small heat shock proteins (sHsps)

The sHsps are ATP-independent holdase chaperones. Similar to DNAJs, the sHsps bind solvent-exposed hydrophobic rich regions in partially-folded states of proteins. The sHsps act to stabilise these partially-folded protein intermediates by forming soluble, high molecular weight complexes with them, thus preventing their aggregation (Frydman et al., 1994, Eyles and Gierasch, 2010, Johnston et al., 2021). This process creates a pool of protein intermediates which, once conditions are favourable, are released and allowed to spontaneously refold, passed on to foldase chaperones for ATP-dependent chaperone-mediated refolding, or targeted for degradation (Hartl et al., 2011). The sHsp molecular chaperones possess a conserved α-crystallin domain, which is flanked by variable N- and C-terminal regions. The human genome encodes ten sHsps (HspB1 - HspB10) (Kappé et al., 2003, Kampinga et al., 2009) and whilst the monomeric subunits of sHsps are of low molecular mass (12 to 43 kDa), some of these sHsps form large polydisperse oligomers in solution (Aquilina et al., 2013). The sHsps play a primary role in minimising protein aggregation in cells and their proposed roles within the cell are described below (Table 1.3).

Table 1.3. Human sHsps, their reported binding partners, subcellular localisation and proposed roles within cells.

Name	*Synonyms*	*Reported binding partners*	*Subcellular localisation*	*Suggested cellular roles*	*References*
HspB1	Hsp27 Hsp25 (mouse)	HspB5; HspB8; HspB4; CRYBB2; CRYGC; Rif1; TP53; AKT1; CYCS; MED31; ILK; Daxx; MAGED1; TGFB1I1; MGC15730; SERPINH1	Cytosol, cell membrane	Participates in cytoskeletal stabilisation and acts as an antioxidant by regulating intracellular redox homeostasis. Has chaperone and pro-refolding functions. Confers anti-apoptotic function.	(Jakob et al., 1993, Lavoie et al., 1993, Lavoie et al., 1995, Charette et al., 2000, Lee and Vierling, 2000, Pandey et al., 2000, Arrigo et al., 2005, Outeiro et al., 2006, Bryantsev et al., 2007, Minoia et al., 2014b, Cox and Ecroyd, 2017)
HspB2	MKBP	DMPK; HspB2; HspB8; HspB3; HspB5; Ubl5;	Cytosol, nucleus, mitochondria	Acts in concert with HspB3 to function in muscle cell differentiation and myofibrillar integrity. Inhibits the extrinsic apoptotic pathway. Activates, chaperones and enhances kinase activity of the myotonic dystrophy protein kinase (DMPK).	(Suzuki et al., 1998, Sugiyama et al., 2000, Nakagawa et al., 2001, Vos et al., 2009, Oshita et al., 2010)
HspB3	HspL27	ANP32A; MED31; OLFML3; MED8; MRPL38; NELF; Ramp3; BBOX1; Rif1; SETDB1;	Cytosol, nucleus	Forms complexes with HspB2 to participate in muscle cell differentiation.	(Sugiyama et al., 2000, Vos et al., 2009)

		ZZEF1; UNC119; HspB2			
HspB4	αA-crystallin	HspB1; CRYZ; MIP; ALB; HspB4; HspB5	Cytosol	Maintains the proper refractive index in the eye lens. Has chaperone activity and acts with ATP-dependent chaperones to assist in protein refolding.	(Jakob et al., 1993, Andley et al., 1998, Mackay et al., 2003, Bhagyalaxmi et al., 2009)
HspB5	αB-crystallin	HspB1; PSMA3; CS; HspB2; HspB5; BMPR2; HspB4	Cytosol, nucleus, cell membrane, mitochondria	Maintains the proper refractive index in the eye lens. Plays a role in cytoskeleton stabilisation. Effective anti-aggregation chaperone and acts with ATP-dependent chaperones to assist in refolding.	(Jakob et al., 1993, Iwaki et al., 1994, Nicholl and Quinlan, 1994, Morrison et al., 2003, van Rijk et al., 2003, Jin et al., 2008, Noh et al., 2008, Vos et al., 2008, Vos et al., 2010, Cox and Ecroyd, 2017)
HspB6	Hsp20 p20	Bag3	Cytosol, nucleus	Acts in cytoskeletal stabilisation. Has some anti-aggregation capacity. Evidence suggests it plays a role in autophagy regulation. Has cardio-protective properties and functions in smooth muscle relaxation.	(Fan et al., 2004, Dreiza et al., 2005, Zhu et al., 2005, Islamovic et al., 2007, Qian et al., 2009, Fuchs et al., 2010, Vos et al., 2010, Ke et al., 2011)
HspB7	cvHsp	HspB8	Cytosol, nucleus, cytoskeleton, mitochondria	Maintains myofibrillar integrity. Can protect against protein aggregation and associated toxicity. Involved in dynamic, stress-induced translocation to SC35 splicing speckles.	(Krief et al., 1999, Golenhofen et al., 2000, Vos et al., 2009, Carra et al., 2010, Vos et al., 2010)
HspB8	Hsp22 H11 E2IG1	HspB1; HspB8; HspB7; HspB2; Bag3	Cytosol, nucleus	Can inhibit protein synthesis and is an effective anti-aggregation chaperone. Targets Hsp-loaded substrates for degradation via macroautophagy.	(Chowdary et al., 2004, Irobi et al., 2004, Carra et al., 2005, Carra et al., 2008a, Carra et al., 2008b, Carra, 2009, Carra et

					al., 2009, Crippa et al., 2010, Fuchs et al., 2010, Gamerdinger et al., 2011, Crippa et al., 2016)
HspB9	CT51	-	Cytosol, nucleus	Expressed exclusively in the testis. Involved in cytoskeletal stabilisation. Has chaperone activity. Has been identified as a cancer/testis antigen.	(de Wit et al., 2004, Vos et al., 2010)
HspB10	ODFP ODF1	SPAG4; SPAG5; TRIP6; ODF1	Cytosol	Expressed exclusively in the testis. Role in the cell currently not well understood. May participate in cytoskeletal stabilisation.	(Fontaine et al., 2003, Vos et al., 2009)

Most work that has been conducted to study the chaperone function of the sHsps has involved recombinant proteins tested in solution-based assays. Thus, the precise molecular mechanism(s) by which sHsps prevent protein aggregation in cells is still not understood (Hilton et al., 2013).

1.4.6 Bcl-2 associated athanogene (Bag) proteins

The actions of maintaining, refolding and repairing damaged proteins by molecular chaperones are thought to be essential for maintaining cell viability. In addition, it requires far less energy to refold proteins than it does to degrade them and synthesise new ones (Richter et al., 2010). However, when proteins become severely or irreversibly damaged, thus making refolding impossible, the proteostasis mechanisms which manage these proteins switch and chaperones present unfolded substrates for degradation (Spiess et al., 1999). Co-chaperones play a central role in determining the route through which Hsp-loaded substrates are degraded (Gamerdinger et al., 2011). The Bcl-2 associated athanogene (Bag) proteins (Bag1–6) are a ubiquitous family of co-chaperones and function as NEFs. Bag proteins are so named because they share an evolutionarily conserved region of ~50 amino acids, known as the BAG domain. The BAG domain facilitates their interaction with Hsp70. Bag proteins bind to the ATPase domain of Hsp70 with high affinity (Doong et al., 2002) and, as such, modulate interactions of the Hsp70 C-terminal substrate binding domain with unfolded polypeptides. Thus, by binding to Hsp70, Bag proteins regulate substrate binding and release (Takayama and Reed, 2001, Gamerdinger et al., 2011). Their proposed contribution to the maintenance of proteostasis has sparked recent interest into the interactions that dictate their cellular function (Fuchs et al., 2010). However, the precise role(s) of the Bag isoforms within the cell are still relatively unclear. The suggested roles of Bag proteins in the cell are summarised below (Table 1.4).

Table 1.4. Human Bag proteins, their reported binding partners, subcellular localisation and proposed roles within cells.

Name	*Synonyms*	*Reported binding partners*	*Subcellular localisation*	*Suggested cellular roles*	*References*
Bag1	RAP46 HAP46 HAP50	Bcl-2; Raf1, Siah1, HGFR; PDGFR; steroid receptors; RAR; Hsc70/Hsp70	Cytosol	Accelerates ATP-triggered substrate release by Hsc70/ Hsp70. Plays a role in trafficking Hsp-loaded substrates to the proteasome.	(Wang et al., 1996, Takayama et al., 1997, Zeiner et al., 1997, Takayama et al., 1998, Knee et al., 2001, Takayama and Reed, 2001, Lilienbaum, 2013)
Bag2	-	-	Nucleus	Inhibits the ubiquitin ligase activity of CHIP (C-terminus of the Hsc70-interacting protein) and regulates the Hsc70/Hsp70 complex.	(Arndt et al., 2005)
Bag3	CAIR-1 Bis	PLCγ; Bcl-2; HspB5; HspB6; HspB8; Hsc70/Hsp70	Cytosol	Prevents the accumulation of unfolded polypeptides by trafficking Hsp-loaded substrates for degradation by macroautophagy.	(Doong et al., 2000, Carra et al., 2008b, Gamerdinger et al., 2009, Fuchs et al., 2010, Shemetov and Gusev, 2011)
Bag4	SODD	TNFR1; DR3; Hsc70/Hsp70	Cytosol, nucleus	Recruits Hsc70/Hsp70 to receptors which participate in the initiation of apoptosis.	(Jiang et al., 1999, Antoku et al., 2001, Briknarová et al., 2002, Takada et al., 2003)
Bag5	-	-	Vesicles	May regulate the Hsc70/Hsp70 complex in a similar manner to Bag1.	(Kalia et al., 2011)
Bag6	Scythe BAT3	Hsc70/Hsp70	Cytosol, nucleus	Nuclear apoptosis regulator.	(Thress et al., 2001)

1.4.7 Hsp110 proteins

Another group of proteins which participate as NEFs in the Hsp70 substrate binding and release cycle are the Hsp110 (HspH) family (Dragovic et al., 2006, Raviol et al., 2006). In humans, there are four known Hsp110 proteins and they belong to the eukaryotic Hsp70 superfamily. The nucleotide-binding domains of Hsp110 and Hsp70 members share high sequence similarity, with Hsp110 proteins differing mainly through having a more divergent substrate binding (ATPase) domain. The structure of the Hsp110s is similar to that of the 'open' conformation of Hsp70s, with the addition of a β-stranded sandwich of variable length inserted into the C-terminal helical lid of the Hsp110 substrate binding domain (Schuermann et al., 2008, Rosenzweig et al., 2019). Hsp110s modulate nucleotide release from Hsp70s in a manner that is distinct from the Bag proteins; Hsp110s first bind ATP, which induces a conformational change that allows them to interact with Hsp70 (Shaner et al., 2006). Hsp110s can then catalyse nucleotide exchange through a direct interaction of the Hsp110 and Hsp70 nucleotide-binding domains. This facilitates the formation of a stable Hsp110-Hsp70 complex which, in turn, dissociates when ATP binds to Hsp70 (Andréasson et al., 2008). Whilst Hsp110 proteins do not participate directly in substrate refolding (Polier et al., 2008), they have been reported previously to bind aggregation-prone proteins, such as amyloid-β, tau and mutant SOD1 and, in some cases, suppress their aggregation (Oh et al., 1999, Yamashita et al., 2007, Wang et al., 2009, Eroglu et al., 2010, Polier et al., 2010, Olzscha et al., 2011, Serlidaki et al., 2020). However, unlike Hsp70s, the interaction of Hsp110s with client proteins is not modulated by a nucleotide-dependent, substrate binding release cycle. It is therefore believed that Hsp110s can only act as holdases that pass client proteins onto the Hsp70 chaperone machinery for processing (Hideyuki et al., 1993, Dragovic et al., 2006, Raviol et al., 2006, Polier et al., 2008, Schuermann et al., 2008). The suggested roles of the four human Hsp110 members within the cell are outlined briefly below (Table 1.5).

Table 1.5. Human Hsp110 proteins, their reported binding partners, expression patterns and proposed roles within cells.

Name	*Synonyms*	*Reported binding partners*	*Subcellular localisation*	*Suggested cellular roles*	*References*
HspH1	Hsp105	Hsc70/Hsp70; HspA2; HspA4; DNAJA1; HspA9; DNAJB1; DNAJB4; HspA12a; GrpEL1; HspA5/BiP	Cytosol, nucleus, vesicles	Implicated in cancer signalling. Protects against stress-induced apoptosis. Participates as a NEF and has holdase activity.	(Yu et al., 2015, Zappasodi et al., 2015, Kimura et al., 2016, Zuo et al., 2016)
HspH2	Apg-2, Hsp110, HspA4	Hsc70/Hsp70; DNAJB1; Hsp90AA1; Bag3; Bag1; Stip1; Stub1; HspH1; HspA9; DNAJB4	Cytosol, nucleus, extracellular exosomes	Implicated in spermatogenesis.	(Held et al., 2011)
HspH3	Apg-1, HspA4L	Hsc70/Hsp70; DNAJB1; HspA9; HspA12a; DNAJC2; DNAJB6; HspA5/BiP; DNAJC7; HspA12b	Cytosol, nucleus	Participates as a NEF and has putative holdase activity. Implicated in leukaemia.	(Matsumori et al., 2002, Held et al., 2006, Takahashi et al., 2007)
HspH4	HYOUI, Grp170	Hsp90B1; DNAJC10; DNAJB11; DNAJC3; SEC63; CALR; P4HB; DNAJB11; HspA5/BiP; PDIA4; ERP29; SIL1	ER	Participates as a NEF and has holdase activity.	(Tsukamoto et al., 1998, Behnke et al., 2016)

1.5 Protein degradation pathways

1.5.1 Ubiquitin-proteasome system

If chaperones are unable to refold a protein substrate, they can maintain the folding intermediate in a soluble state for recognition by degradation machinery (Esser et al., 2004). There are two major pathways for the degradation of aggregation-prone proteins in eukaryotic cells; the ubiquitin-proteasome system and autophagy (Lilienbaum, 2013). Under normal cellular conditions, the ubiquitin-proteasome system is thought to degrade up to 90% of aberrant, short-lived, denatured or damaged proteins (Rock et al., 1994, Hershko and Ciechanover, 1998,

Glickman and Ciechanover, 2002, Luo and Le, 2010). Once Hsps present substrates to the ubiquitin-proteasome system, degradation proceeds via recognition of exposed hydrophobicity in non-native proteins by cytosolic enzymes called ubiquitin ligases. Non-native proteins are then covalently tagged with ubiquitin, a structurally conserved polypeptide made up of 76 amino acids. Ubiquitin possesses free lysine residues which can become ligated to another ubiquitin molecule to form polyubiquitin chains (Xu et al., 2009). Typically, polyubiquitin chains direct the misfolded protein to the proteasome, a multi-subunit barrel-shaped structure containing several proteolytic enzymes to ensure specificity to a diverse range of proteins. Proteolysis of the misfolded substrate results in the release of small peptides or single amino acids from the proteasome back into the cytosol to be recycled. Free ubiquitin polypeptides are also released and are then able to bind nearby unfolded substrates (Nassif et al., 2014).

1.5.2 Autophagy

Autophagy also facilitates the degradation of partially-folded protein intermediates or protein aggregates. There are three forms of autophagy; microautophagy, macroautophagy and chaperone-mediated autophagy. Macroautophagy is the major inducible autophagic pathway for the degradation of aggregated proteins and cytoplasmic components (Klionsky and Emr, 2000, Lilienbaum, 2013). Chaperone-assisted selective autophagy (CASA) is a specialised form of macroautophagy in which non-native proteins bound to chaperones are targeted for degradation by co-chaperones. Mammalian macroautophagy (including CASA) occurs via an integrated and regulated set of processes (Lilienbaum, 2013). Upon presentation of unfolded polypeptides by Hsps, macroautophagy is initiated via nucleation of the phagophore, a small membranous vesicle which elongates and closes in on itself to form the autophagosome. The autophagosome selectively engulfs non-native proteins and other cytoplasmic organelles and then fuses with lysosomes to form autophagolysosomes (Johansen and Lamark, 2011). The acidic environment inside the autophagolysosome activates lysosomal enzymes called hydrolases, which degrade non-

native proteins and other macromolecules (Klionsky and Emr, 2000, Rubinsztein, 2006, Lilienbaum, 2013). The proteostasis mechanisms outlined above, including protein folding and aggregation, degradation by the ubiquitin-proteasome system or autophagy, and the heat shock response, are summarised in Figure 1.5.

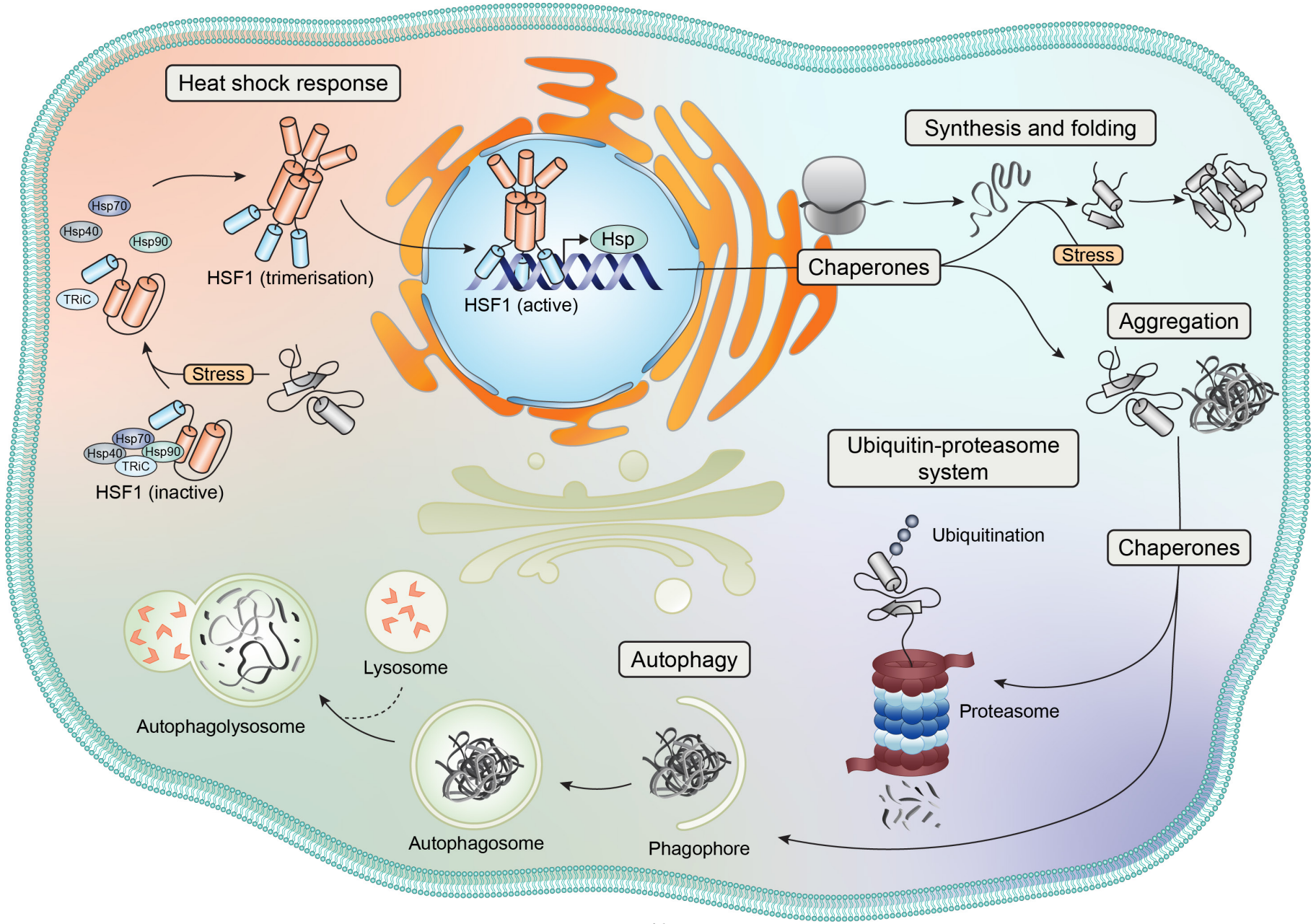
Heat shock response
Hsp70
Hsp40
Hsp90
TRiC
HSF1 (trimerisation)
Hsp
HSF1 (active)
Chaperones
Synthesis and folding
Stress
Aggregation
Stress
Hsp70
Hsp40
Hsp90
TRiC
HSF1 (inactive)
Ubiquitin-proteasome system
Ubiquitination
Chaperones
Proteasome
Lysosome
Autophagy
Autophagolysosome
Autophagosome
Phagophore

Figure 1.5. The proteostasis network in cells. The proteostasis network is responsible for maintaining proteins in their native conformation, in the correct location and concentration. In most cases, nascent protein synthesis and folding requires attention from molecular chaperones. Under conditions of cell stress, partially-folded intermediates can accumulate and potentially self-associate (aggregate). Cytosolic misfolded proteins and aggregates can be bound by molecular chaperones (such as the Hsps) and shuttled for refolding (not shown) or degradation. There are two major pathways that exist in the cell for the degradation of terminally misfolded and aggregated proteins; the ubiquitin-proteasome system and autophagy. Degradation via the ubiquitin-proteasome system proceeds once partially-folded or misfolded proteins are covalently tagged with ubiquitin molecules, which in turn form a polyubiquitin chain. The polyubiquitin chain directs the complex through the proteasome where proteolysis occurs and the broken down peptides are released back into the cytosol to be recycled. Autophagy is initiated by the nucleation of the phagophore, which in turn elongates and closes in on itself, engulfing aggregated or misfolded proteins. The autophagosome fuses with the lysosome to form the autophagolysosome and the internal environment activates lysosomal enzymes to mediate degradation. Under normal conditions, HSF1 resides as an inactive monomer in the cytoplasm via interactions with the molecular chaperones Hsp90, Hsp40, Hsp70 and TriC/CCT. Under conditions of cellular stress, partially-folded intermediates accumulate and the chaperones dissociate from chaperone-HSF1 complexes. HSF1 undergoes trimerisation and can then translocate into the nucleus. Activated HSF1 trimers bind heat shock elements in the promotor region of heat shock genes for the transcription and upregulation of inducible target genes, which include the Hsp molecular chaperones.

1.6 Investigating proteostasis in cells

Uncovering the roles that the heat shock response, autophagy and the ubiquitin-proteasome system have in the proteostasis network is essential, as these may be therapeutic targets to treat diseases associated with protein misfolding and aggregation. Unfortunately, the methods available for monitoring pathways that affect proteostasis in cells are still somewhat limited. Whilst many studies have utilised genetic or pharmacological approaches to reveal the mechanisms involved in protein folding and misfolding in cells (Seglen and Gordon, 1982, Lee and Goldberg, 1998, Yamamoto et al., 1998, Taylor et al., 2007, Lee et al., 2010, Oslowski and Urano, 2011, Hou et al., 2012, Wang et al., 2017), it remains to be determined which (if any) pathway(s) of the protein quality control network is/are responsible for one cell type being more susceptible to protein aggregation compared to another. Thus, there is a need to further characterise the role of proteostasis-related pathways in preventing protein aggregation in the context of neurodegenerative disease phenotypes. Drugs that target important components of the proteostasis network may assist in uncovering the mechanisms by which proteins aggregate and/or the pathways that prevent protein aggregation in response to cellular stress (Kampinga and Bergink, 2016). The currently available bioanalytical and chemical methods to investigate proteostasis pathways in cells have been reviewed recently (Sebastian and Shoulders, 2020, Zhang et al., 2021).

Understanding the status, function and regulation of the proteostasis network within cells is extremely important and requires the use of various biological tools. In this respect, the protein firefly luciferase (Fluc) has been used extensively to assess chaperone activity *in vitro* (Schröder et al., 1993, Heyrovská et al., 1998, Naylor, 1999, Hageman et al., 2007). Moreover, destabilised (i.e. aggregation-prone) forms of Fluc have been exploited to study proteostasis in cells and to detect proteostasis imbalance or dysfunction (Gupta et al., 2011). By tagging Fluc with a fluorescent protein, such as green fluorescent protein (GFP), its aggregation state can be monitored in cells and organisms (Gupta et al., 2011). In this way, destabilised mutants of Fluc serve as protein folding sensors that can be used to assess the capacity of cells (or organisms) to maintain an aggregation-prone protein in a soluble state. Another advantage of using Fluc to study protein aggregation in cells is that the protein has no biological function in commonly used mammalian cell and animal models. This makes it an ideal model to study generic aspects of protein aggregation in cells since its misfolding and aggregation is not due to endogenous interactions that could confound analyses. Moreover, inhibition of aggregation of Fluc-based proteostasis sensors relies on engagement of the aggregation-prone protein with components of the cellular protein quality control network that generically act to solubilise or degrade aggregated proteins.

Whilst previous studies have employed Fluc as a model aggregation-prone protein to study protein aggregation in cells (Gupta et al., 2011, Whiten et al., 2016, San Gil et al., 2017, San Gil et al., 2020), the role the protein quality control network has in preventing the aggregation of mutant Fluc into inclusions is yet to be definitely characterised. Furthermore, the aggregation propensity of Fluc is yet to be exploited in order to comparatively ascertain the relative capacity of different cell types to inhibit inclusion formation by aggregation-prone proteins. Doing so would be a first step towards delineating why some cells are more susceptible to the formation of protein inclusions than others.

1.6.1 Analysis of inclusion formation in cells using flow cytometry

Cellular models of protein aggregation have previously been used to investigate the role(s) of chaperones and other proteostasis-related pathways in preventing the accumulation of misfolded proteins into inclusions (Ramdzan et al., 2012). Earlier approaches to detect the formation of inclusions in cells primarily involved microscopy-based techniques; however, even with the advancement of automated microscopy systems, these techniques are limited in their ability to provide high-throughput and quantitative analyses. Another common method used to assess the formation of inclusions in cells is the fractionation of lysates into insoluble and soluble material for analysis by traditional bulk-based biochemical analyses, such as the filter trap assay (Hageman et al., 2010, Kakkar et al., 2016a, Serlidaki et al., 2020). However, when screening many different samples, these types of assays can be time consuming, laborious and, when it comes to counting inclusions in individual cells, subjective. More recently, two flow cytometry-based approaches for the detection of inclusions in cells have been described, both of which afford high-throughput and quantitative analysis of cells with inclusions.

Pulse-shape analysis (PulSA) is a flow cytometry-based technique that can detect inclusions formed by some aggregation-prone proteins in intact cells (Ramdzan et al., 2012). PulSA relies on the aggregation-prone protein to be fluorescently tagged so that its localisation into inclusions can be observed (and quantified) in cells. For example, this technique can differentiate diffuse non-aggregated huntingtin from aggregated forms of huntingtin in protein inclusions due to differences in the fluorescent pulse shapes as a cell passes through the laser of the flow cytometer (Figure 1.6A). Ramdzan et al. (2012) reported that cells containing huntingtin inclusions exhibit a reduced pulse width and an increased pulse height compared to cells containing non-aggregated huntingtin (Figure 1.6B). Thus, cells with inclusions can be identified and quantified in a plot of fluorescent pulse width versus pulse height. PulSA has been used to assess the impact of chaperones on huntingtin aggregation in cells (Ramdzan et al., 2012) and may therefore provide a valuable tool

to characterise chaperone function and the regulation of degradation pathways in other cell-based models of protein aggregation.

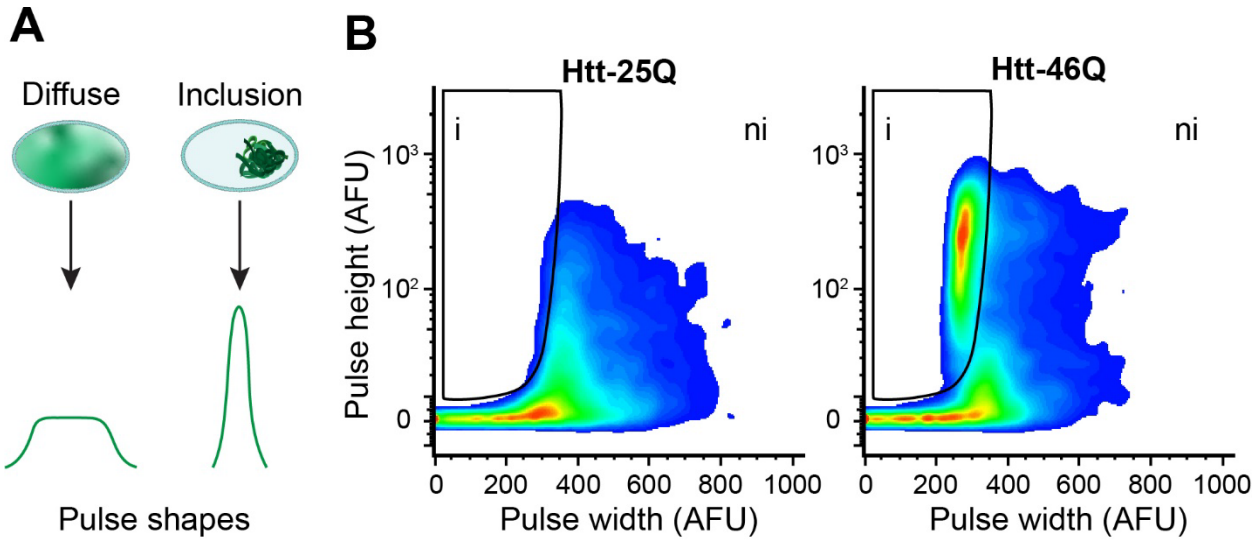

Figure 1.6. The flow cytometric technique pulse-shape analysis (PulSA) used to monitor the aggregation of proteins into inclusions in cells. (A) The principle behind PulSA. Cells in which the fluorescently-tagged protein is in inclusions have increased pulse heights and narrower pulse widths compared to cells in which the protein remains soluble and diffuse throughout the cytoplasm, a phenomenon which can be monitored by flow cytometry. **(B)** Flow cytometric analysis, in arbitrary fluorescence units (AFU), of inclusion formation by non-aggregating (25Q) and aggregation-prone (46Q) forms of mCherry-tagged huntingtin (i.e. polyglutamine (polyQ) stretches of 25 and 46 glutamines; here referred to as 25Q and 46Q) expressed in mouse neuroblastoma cells following transfection. Htt-25Q is diffusely distributed throughout the cell and Htt-46Q aggregates into inclusions. Two distinct populations can be identified by PulSA, cells with no inclusions (ni) and cells with inclusions (i). The cells with inclusions have a narrower pulse width and higher pulse height than cells without inclusions.

Whilst PulSA is effective at identifying cells with large inclusions, the technique cannot be reliably used to identify cells that contain smaller punctate inclusions, such as those formed by SOD1 (Whiten et al., 2016). To address this, a technique known as flow cytometric analysis of inclusions and trafficking (FloIT) was developed (Whiten et al., 2016). FloIT can identify intracellular inclusions of various sizes in cell lysates, including those less than 200 nm in diameter (Whiten et al., 2016). The FloIT technique is based on an earlier study in which yeast were mechanically lysed in order to analyse fluorescently-tagged protein aggregates by quantitative flow cytometry (Shiber et al., 2014). Whilst the basic principle behind methods such as the filter trap assay and FloIT are the same (Figure 1.7A) (i.e. analysis of insoluble protein in a cell lysate), FloIT is advantageous due to the high-throughput and quantitative capacity of flow cytometry. In FloIT, the nuclei within a cell lysate are stained and enumerated using a nuclear marker (e.g. RedDot1) and quantified based upon forward scatter (FSC) and RedDot1 fluorescence signals in the flow

cytometer (Figure 1.7B), before being excluded from further analyses. Inclusions produced by fluorescently-tagged (e.g. enhanced green fluorescent protein; EGFP) aggregation-prone proteins within a cell lysate are detected and enumerated using signals from the FSC and EGFP fluorescence (Figure 1.7C). Finally, the number of inclusions is normalised against the number of nuclei present to enable a quantitative analysis between samples.

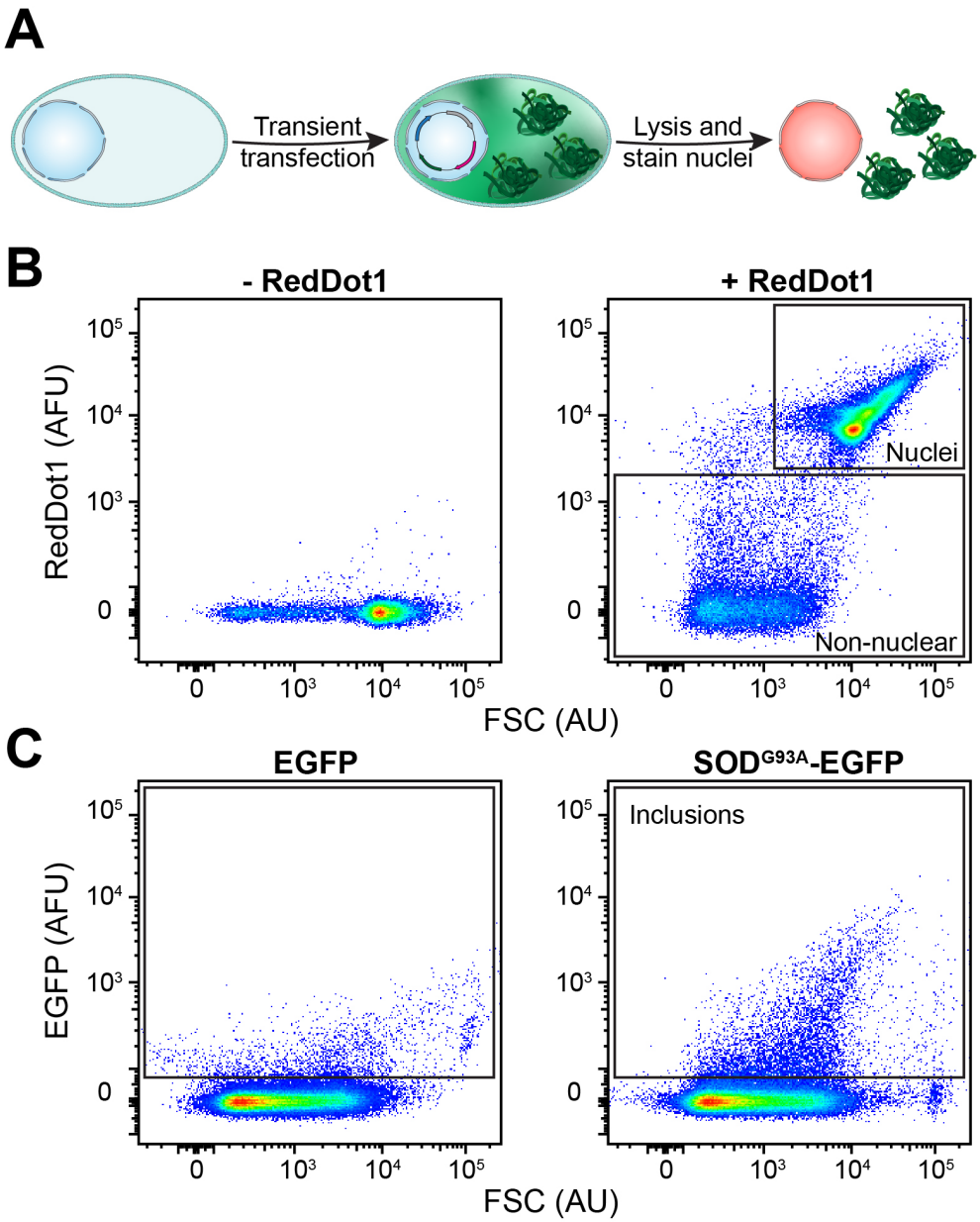

Figure 1.7. Flow cytometric analysis of inclusions and trafficking (FloIT) used to quantify the number of inclusions in a cell lysate. (A) Schematic representation depicting the preparation of cells for FloIT. Following transient transfection with the fluorescently-tagged aggregation-prone protein of interest, the cells are lysed and nuclei stained prior to analysis by flow cytometry. **(B)** Two parameter, pseudo-colour flow cytometry plots gating nuclei and non-nuclear particles (indicated) from lysates prepared from mouse neuroblastoma × spinal cord motor neuron hybrid cells transiently transfected to express EGFP-tagged aggregation-prone $SOD1^{G93A}$ ($SOD1^{G93A}$-EGFP; glycine substituted to alanine at position 93). Nuclei and non-nuclear particles are identified based on FSC (in arbitrary units; AU) and RedDot1 fluorescence (in arbitrary fluorescence units; AFU) (*left*: unstained, *right*: stained with RedDot1). **(C)** Non-nuclear particles (gated in (A)) analysed for the presence of inclusions based on EGFP fluorescence (in AFU) and FSC of lysates prepared from cells transiently expressing EGFP (*left*) or $SOD1^{G93A}$-EGFP (*right*). Inclusions formed by $SOD1^{G93A}$-EGFP have been indicated.

FloIT can be used to count and characterise the inclusions within a given cell population and, by exploiting fluorescence-activated cell sorting methods, can even be used to facilitate the physical recovery of protein inclusions from a cell lysate. FloIT can be used to detect inclusions formed by a range of aggregation-prone proteins that differ in size and granularity (Whiten et al., 2016), making FloIT broadly applicable to most (if not all) model systems of protein aggregation .

1.7 Measuring the proteostasis capacity of cells

The proteostasis capacity of a cell can be defined as the ability to prevent protein accumulation and aggregation through the regulation of its protein quality control network. The ability to quantitatively measure the proteostasis capacity of a cell is an important step towards deciphering why some cell types are more susceptible to the formation of inclusions than others. This is especially true given that the proteostasis capacity of a cell is known to influence the rate at which misfolded proteins accumulate (Gidalevitz et al., 2006, Hutt et al., 2009, Powers et al., 2009, Gidalevitz et al., 2010). Thus, a decline in proteostasis capacity is linked to an impaired ability of a cell to prevent protein aggregation, which can lead to the onset and progression of toxicity associated with disease (Brehme et al., 2014, Hipp et al., 2014). At present there is no definitive method to quantitatively measure the proteostasis capacity of cells.

One major challenge in the field is determining the baseline efficiency with which different cell types can maintain proteostasis. There have been recent publications describing potential methods which could be used to measure the proteostasis capacity of different cell types. Liu et al. (2015) utilised a conformationally metastable retroaldolase protein with thermo-labile properties as a marker for the decline of proteostasis. The protein was labelled with a small-molecule fluorogenic probe as a folding sensor to monitor the proteostasis network capacity proceeding stress. However, the system was only used to assess the effects of heat stress and it is unclear whether it has the capacity to report on protein “foldedness” after other types of cellular insults or following

interactions with proteins such as chaperones. Ebbinghaus et al. (2010) described a method which examined the biomolecular dynamics and folding rates of a probe-labelled phosphoglycerate kinase protein in human cells following rapid temperature-induced jumps and tracked the re-establishment of equilibrium. However, this technique does not quantitatively report on the capacity of cells to re-establish proteostasis or define the ability of the protein quality machinery to engage with these client proteins.

Wood et al. (2018) described a biosensor system that utilises metastable barnase isoforms as bait proteins that then report on foldedness and aggregation state in cells via fluorescence resonance energy transfer (FRET) and quantitative flow cytometry methods. Briefly, this method involves flanking the barnase moiety with two fluorescent proteins, such that both the folded state of barnase and chaperone-unfolded client complexes can be monitored simultaneously. However, this method assumes that the holdase activity of the protein quality control network is an overall indicator of proteostasis health. A method described by Chen et al. (2017), which utilises a cell-permeable fluorogenic dye called tetraphenylethene maleimide (TPE-MI), was used to measure the levels of unfolded protein in cells. Fluorescence from the TPE-MI occurs when it reacts with free cysteine thiols in proteins that become exposed during protein unfolding. This technique demonstrated that TPE-MI fluorescence is enhanced upon reaction with cellular proteomes under conditions that promote the accumulation of unfolded proteins (Chen et al., 2017). However, it is yet to be determined whether this method can be used to decipher the ability of cells to prevent protein aggregation. A molecular rotor-based fluorophore technique developed by Fares et al. (2018) aimed to detect changes in the conformation of a protein in live cells, including misfolded or unfolded states of monomers, as well as the formation of soluble oligomers that occurs during the early stages of proteome stress (prior to the formation of insoluble aggregates). This work highlights the ability of molecular rotor-based Halo tags to be used to visualise the aggregation of proteins in live cells and may enable the real-time analysis of cellular proteostasis capacity in

different cell types. However, further characterisation of the method is required to test its suitability, for example, upon exposure to different types of cellular stress.

1.8 Summary and aims

There is now overwhelming evidence demonstrating the important role that the protein quality control network plays in preventing inclusion formation by aggregation-prone proteins. However, fundamental questions remain as to the role(s) specific components of this network have in this process. For example, whilst it is well known that some DNAJBs are potent inhibitors of amyloidogenesis (Hageman et al., 2010, Hageman et al., 2011, Månsson et al., 2014a, Månsson et al., 2014b, Kakkar et al., 2016b, Månsson et al., 2018), it remains to be determined whether DNAJs have a generic capacity to engage destabilised amorphously aggregating client proteins, and, if so, whether this occurs via the same mechanism. Moreover, the relative importance of the ubiquitin-proteasome system, autophagy and chaperone network in maintaining proteostasis in cells remains to be established. Identification of pathways important in preventing protein aggregation, along with approaches to assess the susceptibility of cell types to inclusion formation, would provide a basis for the development of effective therapies against diseases associated with protein aggregation.

The work described in this thesis primarily involved the investigation of the role of proteostasis pathways, and in particular molecular chaperones, in preventing intracellular inclusion formation of destabilised proteins. To do so, a double mutant (DM; R188Q, R261Q) form of Fluc ($Fluc^{DM}$) was exploited in this work as it readily aggregates in cells and has been previously identified to be an effective proteostasis sensor (Gupta et al., 2011). In addition, as Fluc is not endogenously expressed in mammalian cells, it has no natural binding partners, so cellular components only interact with it as a result of its aggregation-prone state and to prevent it forming inclusions in the cell (Gupta et al., 2011).

The specific aims of the work described in this thesis were to:

i. Perform a comprehensive Hsp overexpression screen to identify modulators of $Fluc^{DM}$ inclusion formation in mammalian cells.

ii. Characterise the mechanism by which DNAJBs inhibit the aggregation of destabilised client proteins into intracellular inclusions.

iii. Exploit the aggregation propensity of $Fluc^{DM}$ in order to quantitatively assess the relative proteostasis capacity of two mammalian neuronal cell lines.

iv. Modulate pathways in the protein quality control network to identify those that play a key role in inhibiting the formation of inclusions in cells.

Chapter 2: Materials and Methods

Methods used in multiple chapters of this thesis are outlined in this chapter. Methods specifically pertaining to work presented in Chapters 3 – 5 are provided in the relevant chapters.

2.1 Materials

All common laboratory chemicals and materials used in this work were purchased from Sigma-Aldrich (St. Louis, MO, USA) or Amresco (Solon, OH, USA), unless otherwise indicated. Dulbecco's Modified Eagle Medium/Ham's F-12 (DMEM/F-12), foetal calf serum (FCS), L-glutamine and 0.05% trypsin/EDTA were obtained from Gibco (Carlsbad, CA, USA). The transfection reagents Lipofectamine® LTX/PLUS™ or Lipofectamine™ 3000 were purchased from Life Technologies (Carlsbad, CA, USA) and linear (MW 25,000) polyethylenimine was obtained from BioScientific (Gymea, Australia). The PureYield™ Plasmid Midiprep System was purchased from Promega (Madison, WI, USA). Tetracycline, poly-L-lysine, dimethyl sulfoxide (DMSO), paraformaldehyde (PFA), thapsigargin and azoramide were purchased from Sigma-Aldrich and RedDot1 was obtained from Biotium (Hayward, CA, USA). The bicinchoninic acid (BCA) protein assay kit, Halt™ Protease and Phosphatase Inhibitor Cocktail, Nonidet™ P-40 (NP-40) and Triton X-100 were purchased from Thermo Fisher Scientific (Glen Burnie, MD, USA). Zeocin and blasticidin were purchased from InvivoGen (San Diego, CA, USA). MG132 was obtained from SelleckChem (Boston, MA, USA) and 3-methyladenine (3-MA) was purchased from AdipoGen (San Diego, CA, USA). Bafilomycin A1 and rapamycin were obtained from Sapphire Bioscience (Sydney, Australia). Precision Plus Protein™ dual colour standards and ImmunoBlot™ polyvinylidene difluoride (PVDF) membrane used for immunoblotting were purchased from Bio-Rad (Hercules, CA, USA).

Human embryonic kidney (HEK293) cells and mouse neuroblastoma (Neuro-2a) cells were purchased from the American Type Culture Collection (Manassas, VA, USA). HEK293 cells stably expressing the tetracycline (tet) repressor (Flp-In T-REx) were obtained from Invitrogen

(Carlsbad, CA, USA). Mouse neuroblastoma × spinal cord (NSC-34) motor neuron hybrid cells, originally described by Cashman et al. (1992), were generously donated by Professor Justin Yerbury (University of Wollongong, Australia). The heat shocked HeLa cell lysate was prepared and donated by Dr Rebecca San Gil (University of Wollongong, Australia). Cell lines were routinely tested for mycoplasma contamination (~ every 6 months) and the identity of the human-derived cell lines were verified via short tandem repeat profiling (Garvan Institute of Medical Research, Australia).

2.2 Antibodies

Antibodies were sourced from Abcam (Cambridge, MA, USA), unless otherwise indicated, and their specifications, including the dilutions used for immunoblotting, are outlined in Table 2.1.

Table 2.1. Primary and secondary antibodies used for immunoblotting

Primary antibodies				
Product name	***Description***	***Supplier***	***Product #***	***Dilution***
Anti-GFP antibody	Rabbit polyclonal	Abcam	ab290	1:2500
Anti-GRP78 antibody	Rabbit polyclonal	Abcam	ab21685	1:1000
Anti-Hsc70 antibody	Mouse monoclonal	Abcam	ab2788	1:1000
Anti-HSF1 antibody	Rat monoclonal	Abcam	ab81279	1:1000
Anti-Hsp40 antibody	Mouse monoclonal	Abcam	ab78437	1:5000
Anti-Hsp70 antibody	Mouse monoclonal	Abcam	ab47455	1:1000
Anti-Hsp90 antibody	Mouse monoclonal	Abcam	ab13492	1:1000
Anti-LC3II antibody	Rabbit polyclonal	Cell Signalling Technology (Danvers, MA, USA)	2775	1:1000
Anti-SQSTM1/p62	Mouse monoclonal	Abcam	ab56416	1:2000
Anti-Ubiquitin antibody	Mouse monoclonal	Santa Cruz Biotechnology (Dallas, TX, USA)	sc-8017	1:1000
Anti-V5 antibody	Mouse monoclonal	Thermo Fisher Scientific	46-0705	1:5000
Secondary antibodies				
Goat anti-rabbit IgG horse radish peroxidase (HRP)-conjugated antibody	Goat polyclonal	Thermo Fisher Scientific	31466	1:5000
Rabbit anti-mouse IgG HRP-conjugated antibody	Rabbit polyclonal	Sigma-Aldrich	A9044	1:5000
Rabbit anti-rat IgG HRP-conjugated antibody	Rabbit polyclonal	Abcam	ab6734	1:5000

2.3 Preparation of mammalian expression constructs

2.3.1 Plasmid constructs

The pN3-enhanced green fluorescent protein (EGFP) plasmid was kindly donated by Dr Darren Saunders (University of New South Wales, Australia). Plasmids encoding wild-type (WT) and double mutant (DM; R188Q, R261Q) Fluc with an N-terminal EGFP tag ($Fluc^{WT}$-EGFP and $Fluc^{DM}$-EGFP) (Gupta et al., 2011) were kindly gifted by Professor Ulrich Hartl (Max Planck Institute of Biochemistry, Munich, Germany) and were cloned into pcDNA4/TO/myc/hisA for mammalian expression by GenScript (Piscataway, NJ, USA). The pCDNA5/FRT/TO-monomeric red fluorescent protein (mRFP) and pCDNA5/FRT/TO/V5-tagged heat shock protein (Hsp) plasmid library, including all mutational variants, were generously donated by Professor Harm Kampinga (University of Groningen, The Netherlands) and are outlined in more detail in the relevant chapters of this thesis.

2.3.2 Preparation of chemically competent *Escherichia coli (E. coli)*

Chemically competent DH5α *E. coli* were prepared by inoculating 10 mL of lysogeny broth (LB; 5% (w/v) yeast, 10% (w/v) NaCl, 10% (w/v) tryptone, pH 7.4) with a single colony. The culture was incubated overnight at 37°C with shaking at 180 rpm. Cells were centrifuged at 5,000 × *g* for 5 min at room temperature, washed in ice-cold 100 mM $CaCl_2$ and incubated on ice for 30 min. The cells were centrifuged again (5,000 × *g* for 5 min at 4°C) and washed in ice-cold 100 mM $CaCl_2$ containing 15% (v/v) glycerol and snap frozen in liquid nitrogen for storage at -80°C.

2.3.3 Transformation of chemically competent *E. coli*

To transform cells, 100 ng/µL of plasmid DNA was mixed gently with an aliquot (100 µL) of chemically competent DH5α *E. coli* and incubated on ice for 30 min. Cells were then heat shocked at 42°C for 30 sec and immediately returned to ice. Cells were diluted 1:7 in LB broth and the transformation mixture was incubated at 37°C for 1 h on an orbital shaker (180 rpm).

Transformation cultures were then plated onto selective LB agar media (LB with 15% (w/v) agar) supplemented with ampicillin (100 μg/mL) or kanamycin (50 μg/mL) as required, and incubated at 37°C overnight. A single colony was then used to inoculate LB media containing the appropriate antibiotic, which was incubated overnight at 37°C. This culture was then mixed 1:1 with sterile 30% (v/v) glycerol and stored in sterile cryovials at -80°C until required.

2.3.4 Bacterial culture and preparation of plasmid DNA

Single colonies of chemically competent DH5α *E. coli*, containing the plasmid sequence of interest, were used to inoculate cultures consisting of 100 mL LB supplemented with the appropriate antibiotic, i.e. either ampicillin (100 μg/mL) or kanamycin (50 μg/mL). The cultures were incubated at 37°C overnight with shaking at 180 rpm. Cultures were pelleted by centrifugation at 5,000 × *g* for 10 min at room temperature and the supernatant discarded. Transfection-quality plasmid DNA was purified from the bacterial cell pellets by centrifugation using the PureYield™ Plasmid Midiprep System, as per the manufacturer's instructions. Concentrations and purity of plasmid DNA were determined using a NanoDrop 2000c spectrophotometer (Thermo Fisher Scientific) by measuring the absorbance at 260 and 280 nm.

2.4 Mammalian cell culture

2.4.1 Passaging and plating

HEK293, Neuro-2a and NSC-34 cells were cultured in DMEM/F-12 supplemented with L-glutamine (2.5 mM) and 10% FCS (v/v) at 37°C under 5% CO_2/95% air in a Heracell 150i CO_2 incubator (Thermo Fisher Scientific). Stably transfected Flp-In T-REx HEK293 cells were cultured as above with the addition of zeocin (50 μg/mL) and blasticidin (5 μg/mL) to the culture medium weekly to ensure maintenance of the tet-repressor. Flp-In T-REx HEK293 cells contain a single stably integrated flippase recognition target (FRT) site at a transcriptionally active genomic locus for homogenous expression from a tetracycline-inducible expression vector, such

as the pCDNA5/FRT/TO/V5-tagged constructs used in this work. Following transient transfection of Flp-In T-REx HEK293 cells, the expression of the gene of interest from a FRT-tagged plasmid can be induced using tetracycline. A major benefit of using this system is that, if required, the expression of a protein of interest can be induced in a time-dependent manner.

Cells were sub-cultured into fresh CELLSTAR® culture flasks or plates (Greiner Bio-One, Frickenhausen, Germany) every three days or when they were deemed to be ~80% confluent. Briefly, culture media was removed and replaced with sterile phosphate buffered saline (PBS; 135 mM NaCl, 2.7 mM KCl, 1.75 mM KH_2PO_4, 10 mM Na_2HPO_4, pH 7.4) to remove excess serum. The PBS was pipetted off and a sufficient volume of 0.05% (v/v) trypsin/EDTA was added to cover the bottom of the flask. Cells were incubated at 37°C for 5 min and the flask was gently tapped to dislodge cells. An aliquot of DMEM/F-12 containing 1% (v/v) FCS was used to wash the bottom of the flask (~20 times) in order to collect cells. For passaging purposes, ~15% of the cells were collected and centrifuged at 300 × *g* for 5 min at room temperature. The supernatant was discarded and cells were resuspended in the appropriate volume of culture medium before being transferred to a fresh culture flask. For plating purposes, the remaining cell suspension was collected and centrifuged as above prior to being resuspended in DMEM/F-12 containing 10% (v/v) FCS for counting. A sample of the cell suspension was combined 1:1 with trypan-blue (Sigma-Aldrich) and the cell density determined using a BLAUBRAND® Neubauer-improved counting chamber (Marienfeld 50 Superior, Lauda-Königshofen, Germany). Cells were then diluted with culture medium and seeded in the appropriate plate at the desired cellular density.

2.4.2 Storage

Cell lines were maintained in liquid nitrogen for long-term storage. To generate stocks for storage, cells were harvested as above before being resuspended in DMEM/F-12 supplemented with 40% (v/v) FCS and 10% (v/v) DMSO. The suspension was then aliquoted (1 mL) into sterile cryovials

and placed in a pre-cooled Nalgene® Mr. Frosty Freezing Container (Thermo Fisher Scientific) containing isopropanol. Cells were stored at -80°C overnight prior to transfer to liquid nitrogen. When removing stocks from liquid nitrogen for use, cells were thawed slowly in 70% ethanol and then immediately diluted 1:10 into DMEM/F-12 containing 10% (v/v) FCS. Cells were centrifuged at 300 × *g* for 5 min at room temperature and resuspended in full culture medium before being transferred to a flask. After 24 h, the culture medium was discarded and replaced with fresh media and the cells were allowed to reach 80% confluency prior to being passaged. Thawed cells were allowed to grow as normal with regular passaging for a minimum of two weeks prior to use in subsequent experiments. Details regarding the transient transfection, co-transfection or treatment of established cells lines are outlined in the relevant chapters of this thesis.

2.5 Immunocytochemistry and confocal microscopy

In some experiments, HEK293, Neuro-2a or NSC-34 cells were grown to 60-70% confluency in 8-well chamber µ-Slides (Ibidi, Martinsried, Germany) and were transfected as outlined in the relevant chapters of this thesis. At 48 h post-transfection, cells were pre-fixed with warmed (37°C) 2% (v/v) PFA for 5 min, prior to fixing with 4% (v/v) PFA for 15 min at room temperature. Cells were washed twice with 100 mM Tris-HCl (pH 8.0) for 10 min with gentle rocking to quench residual PFA. Cells were then permeabilised with 0.1% (v/v) Triton X-100 in PBS for 10 min and blocked for 1 h at room temperature in blocking buffer (1% (v/v) FCS, 1% (w/v) bovine serum albumin (BSA), 0.1% (v/v) Triton X-100 in PBS, pH 7.4). Cells were incubated with the primary antibody of interest diluted (dilutions specified in relevant chapters) in blocking buffer for 1 h at 37°C and then washed 3 times (each for 10 min) with gentle rocking in 0.1% (v/v) Triton X-100 in PBS. Cells were then incubated with the appropriate secondary antibody diluted in blocking buffer for 30 min at 37°C in the dark, prior to 3 washes (each for 10 min) in 0.1% (v/v) Triton X-100 in PBS with rocking. Finally, cells were stained with 0.1 µg/mL Hoechst 33342 nucleic acid stain (Thermo Fisher Scientific) for 5 min at room temperature, washed twice in PBS, and imaged

in ~150 µL PBS/well using a SP8 TCS confocal microscope (Leica Microsystems, Wetzlar, Germany), the 20× objective lens or the 63× oil objective lens and, where required, the 4× zoom function in the Leica Application Suite (LAS)-X software (Leica Microsystems). To eliminate spectral overlap, fluorescent images were acquired by sequential scanning, where Hoechst 33482 was excited with a 405 nm laser, EGFP was excited with a 488 nm laser, mRFP or Dylight® 550 were excited with a 552 nm laser and Alexa Fluor 647 was excited with a 638 nm laser. Images were prepared using the LAS-X Version 3 software.

2.6 Flow cytometry

In some experiments, 48 h post-transfection, cells were prepared for flow cytometric analysis. Cells were harvested with 0.05% (v/v) trypsin/EDTA, then diluted with DMEM/F-12 containing 1% (v/v) FCS and centrifuged at 300 × *g* for 5 min at room temperature. Cells were then washed twice in PBS and resuspended in 500 µL PBS. Cells were kept on ice throughout this process to minimise cell death. In all experiments, flow cytometry was performed using a BD LSRFortessa X-20 or BD LSR-II analytical flow cytometer (BD Biosciences, San Jose, CA, USA) and FCS files were analysed using FlowJo version 10 (Tree Star, Ashland, OR, USA).

2.6.1 Pulse-shape analysis (PulSA)

An aliquot of the cell suspension (250 µL) was taken and analysed by flow cytometry. The percentage of cells containing inclusions was identified by the previously described technique known as PulSA (Ramdzan et al., 2012), using the excitation wavelength and emission collection window for EGFP (488 nm, 525/50 nm, respectively). In all experiments a minimum of 50,000 events were acquired, unless otherwise specified. Briefly, in addition to fluorescence area, the width and height parameters of the EGFP fluorescence signal of each event were recorded and used to determine the number of cells with inclusions. The PulSA technique facilitates (in some cases) the identification of cells with inclusions as a result of a shift in their EGFP fluorescence

profile, such that they have a narrower EGFP fluorescence pulse width and increased EGFP fluorescence pulse height compared to cells expressing EGFP alone. The transfection efficiency of cells was also quantified by flow cytometry in these experiments for use in later analyses.

2.6.2 Flow cytometric analysis of inclusions and trafficking (FloIT)

The remaining 250 µL of cells were centrifuged as above (section 2.6) and analysed by FloIT as previously described (Whiten et al., 2016). To do so, cells were resuspended in PBS containing 0.5% (v/v) Triton X-100 to facilitate cell lysis. Except in control samples used to set gates, RedDot1 was diluted (1:1000) into PBS and then diluted further (1:500) upon addition to cell lysates. Following a 2 min incubation on ice to stain nuclei, flow cytometry was performed as previously described (Whiten et al., 2016). Forward scatter (FSC) and side scatter (SSC), together with RedDot1 fluorescence (640 nm excitation, 670/30 nm collection) and EGFP fluorescence (section 2.6.1) of particles present in cell lysates were measured. The FSC threshold was set to 200 (minimum possible) in order to include small inclusions in analyses. In all experiments, axes were set to $\log_{10}$ and a minimum of 100,000 events were acquired. Nuclei were identified based on FSC and RedDot1 fluorescence and were excluded from further analyses. Inclusions were counted based on their FSC and EGFP fluorescence, in comparison to untransfected or EGFP-only expressing cells. Unless otherwise stated, voltages of 300 (FSC), 200 (SSC), 300, (EGFP), 290 (mRFP; 561 nm excitation, 586/15 nm collection) and 520 (RedDot1) were used in all experiments. The number of inclusions identified within the population was normalised against the number of nuclei present and values are reported as the number of inclusions/100 cells according to the equation:

$$i = 100\left(\frac{n_i}{\gamma . n_{nuc}}\right) \qquad \text{Equation 2.1}$$

Where n_i is the number of inclusions present, n_{nuc} is the number of nuclei, and γ is the transfection efficiency.

2.7 Immunoblotting

2.7.1 Cellular protein extraction and quantification by the bicinchoninic acid (BCA) assay

In some experiments, transfected cells were trypsinised, harvested, washed twice in PBS (300 × *g* for 5 min at room temperature) and cellular protein was extracted by lysis with NP-40 lysis buffer (50 mM Tris-HCl, 150 mM NaCl, 1 mM EDTA, 1% (v/v) NP-40 supplemented with 0.5% (v/v) Halt™ Protease and Phosphatase Inhibitor Cocktail, pH 8.0). Cell lysates were then sonicated using the Sonifer® 250 Digital cell disruptor and a double step micro-tip (Branson Ultrasonics, CT, USA) at 50% amplitude for 5 sec. The total protein concentration for each sample was then determined using a BCA assay. The assay was carried out using a standard 96-well plate format, as described previously (Redinbaugh and Turley, 1986), and BSA was used as a standard for determining protein concentrations in cell lysates. The concentration in each sample was adjusted with NP-40 lysis buffer to generate cell lysates with a total protein concentration of 1 mg/mL to ensure equal loading onto SDS polyacrylamide gel electrophoresis (SDS-PAGE) gels for subsequent immunoblotting.

2.7.2 Cellular fractionation by centrifugation

A 45 µL aliquot of total protein (total fraction) was taken and kept on ice until use. The remaining 155 µL lysate was centrifuged at 20,000 × *g* for 30 mins at 4°C and the supernatant (soluble fraction) carefully collected and placed on ice. The pellet was washed in ice-cold TNE buffer (50 mM Tris-HCl, 150 mM NaCl, 1 mM EDTA, pH 8.0) and centrifuged again at 20,000 × *g* for 30 mins at 4°C. The supernatant was carefully removed and discarded and the pellet resuspended in 50 µL NP-40 lysis buffer. The insoluble pellet was vortexed to dislodge it from the tube and the fraction was sonicated at 50% amplitude for 5 sec (insoluble fraction) and remained on ice until required.

2.7.3 SDS-PAGE

SDS-PAGE loading buffer (final concentrations: 500 mM Tris-HCl, 2% (w/v) SDS, 25% (v/v) glycerol, 0.01% (w/v) bromophenol blue, 15% (v/v) β-mercaptoethanol, pH 6.8) was added to cell lysate samples and they were then heated at 95°C for 5 min before being loaded onto an SDS-PAGE gel. SDS-PAGE was undertaken using polyacrylamide resolving gels (12% (w/v) acrylamide/bis, 375 mM Tris (pH 8.8), 0.1% (w/v) SDS, 0.25% (v/v) tetramethylethylenediamine, 0.02% (w/v) ammonium persulfate) with polyacrylamide stacking gels (4% (w/v) acrylamide/bis, 330 mM Tris (pH 6.8), 0.1% (w/v) SDS, 0.4% (v/v) tetramethylethylenediamine, 0.04% (w/v) ammonium persulfate) following standard procedures (Laemmli, 1970). The gels were run in a Mini-Protean® Tetra Cell system (Bio-Rad) filled with SDS-PAGE running buffer (25 mM Tris base, 192 mM glycine, 0.5% (w/v) SDS, pH 8.3). Samples were electrophoresed for 15 min at 100 V until proteins had migrated through the stacking gel, at which point, the voltage was increased to 150 V and was allowed to run until the bromophenol blue dye front had migrated off the end of the gel (~1 h). When required, gels were stained with Coomassie Blue staining solution (40% (v/v) methanol, 10% (v/v) acetic acid, 0.02% (w/v) Coomassie Brilliant Blue R-250) and de-stained in de-staining solution (40% (v/v) methanol, 10% (v/v) acetic acid), otherwise gels were used for immunoblotting.

2.7.4 Immunoblotting and detection

Samples were separated by SDS-PAGE as described above prior to transfer onto a PVDF membrane using a standard technique (Towbin et al., 1979). Briefly, proteins were transferred onto a PVDF membrane at 100 V for 1 h in ice-cold transfer buffer (25 mM Tris base, 192 mM glycine, 20% (v/v) methanol, pH 8.3). The membrane was blocked at 4°C overnight with 5% (w/v) skim milk powder in Tris-buffered saline (TBS; 50 mM Tris base, 150 mM NaCl, pH 7.6). Membranes were incubated with primary antibodies of interest (refer to Table 2.1 above for the dilutions used for specific antibodies) in 5% (w/v) skim milk powder in TBS containing 0.05%

(v/v) Tween 20 (TBS-T) for 2 h at room temperature. The membrane was washed four times (each for 10 min) in TBS-T before being incubated with the appropriate HRP-conjugated secondary antibody, diluted 1:5000 into 5% (w/v) skim milk powder in TBS-T (see Table 2.1). The membrane was rocked at room temperature for 1 h before being washed four times (each for 10 min) in TBS-T. Proteins of interest were detected with SuperSignal® West Pico Chemiluminescent Substrate or SuperSignal® West Dura Extended Duration Chemiluminescent Substrate (Thermo Fisher Scientific) using an Amersham Imager 600RGB (GE Healthcare Life Sciences, Little Chalfont, UK) or ChemiDoc™ Imaging System (Bio-Rad), with exposure times ranging from 1–15 min.

2.8 Statistical analyses

Histograms were generated and statistical analyses were performed using GraphPad Prism v8 (GraphPad Software, La Jolla, CA, USA). Unless otherwise stated, results are reported as the mean ± standard error of the mean (S.E.M) and the number of independent (biological) replicates (n) of each experiment is specified. Data were analysed by one-way (or two-way) analysis of variance (ANOVA) and Tukey's, Bonferroni's or Dunnett's post-hoc test or, where appropriate, assessed assuming unequal variance using the unpaired two-tailed Student's t-test. In all analyses, $P < 0.05$ was considered statistically significant.

Chapter 3: A Hsp overexpression screen for suppressors of Fluc^{DM} inclusion formation

The research in this chapter was conducted as part of a 3 month research exchange at the University Medical Center Groningen, University of Groningen, in collaboration with the Kampinga Laboratory. To conduct this work, the candidate was supported by a New Holland Scholarship presented by Nuffic. Portions of this chapter have been previously published in the following work:

McMahon, S., Bergink, S., Kampinga, H. H. and Ecroyd, H. (2021). DNAJB chaperones suppress destabilised protein aggregation via a region distinct from that used to inhibit amyloidogenesis. Journal of Cell Science.134, jcs255596.

Author contributions: S.M., H.E., S.B. and H.H.K conceptualised the project and the experimental approach. S.M. performed the experiments, analysed the data, constructed the figures and wrote the initial manuscript. All authors edited the manuscript for submission.

3.1 Introduction

Cell-based and *in vivo* studies investigating the role and function of the Hsps have demonstrated their remarkable ability to prevent the aggregation of disease-associated proteins. For example, overexpression of Hsp70 has been shown to reduce α-synuclein aggregation and the associated toxicity in a cell culture and transgenic mouse model of Parkinson's disease (Klucken et al., 2004). Overexpression of Hsp70 in a transgenic mouse model of spinocerebellar ataxia type 1 reduced neurodegeneration and repaired motor function (Cummings et al., 2001). In addition, overexpression of Hsp70 can reduce the toxicity associated with mutant α-synuclein aggregation in *Drosophila melanogaster* models of Parkinson's disease (Auluck et al., 2002), whilst its interaction with aggregation-prone huntingtin *in vitro* has been shown to supress the formation of amyloid-like fibrillar aggregates (Muchowski et al., 2000). Furthermore, the upregulation of Hsp70, Hsp40 and Hsp60 in combination, protects neurons against the toxicity associated with amyloid-β aggregation both *in vitro* and *in vivo* (Evans et al., 2006). Previous work has demonstrated that overexpression of Hsp27 (HspB1) inhibits the aggregation of SOD1 *in vitro* (Yerbury et al., 2013) and α-synuclein in cell culture models (Outeiro et al., 2006, Cox and Ecroyd, 2017). Similarly, αB-crystallin (HspB5) can suppress the aggregation of SOD1 (Yerbury et al., 2013) and α-synuclein (Cox and Ecroyd, 2017) *in vitro* and has been identified to be important in maintaining the solubility of misfolded proteins (Ghosh et al., 2006, Eyles and Gierasch, 2010, Kampinga and Garrido, 2012, Treweek et al., 2015). The identification of mutations in molecular chaperones linked to familial cases of neurodegenerative disease further demonstrates their importance in the maintenance of proteostasis (Hansen et al., 2002, Irobi et al., 2004, De Mena et al., 2009, Selcen et al., 2009).

Interestingly, in some cases different Hsps appear to be required to impede the aggregation of disease-associated proteins, suggesting a degree of specificity in the interaction of chaperones with these client proteins (Kampinga and Bergink, 2016). For example, HspA1A was the only member

of the Hsp70 family capable of preventing intracellular inclusion formation by a disease-related SOD1 mutant (Serlidaki et al., 2020). To-date, the majority of cell-based screens of the capacity of chaperones to prevent protein aggregation have involved proteins whose aggregation is disease related (Hageman et al., 2010, Vos et al., 2010, Hageman et al., 2011, Minoia et al., 2014b, Kakkar et al., 2016a, Serlidaki et al., 2020). However, since these proteins are endogenously expressed in cells, their misfolding and aggregation may be associated with disruptions to functional interactions. To avoid this, in this work a previously described mutant isoform of Fluc, $Fluc^{R188Q/R261Q}$ (herein referred to double mutant Fluc, $Fluc^{DM}$) (Gupta et al., 2011) was chosen in order to assess the generic capacity of Hsp molecular chaperones and co-chaperones to engage with a highly destabilised, aggregation-prone protein in cells to prevent its aggregation into inclusions. This $Fluc^{DM}$ isoform therefore acts as a proteostasis sensor by reporting on the capacity of Hsps to maintain aggregation-prone proteins in a soluble state. Fluc has no biological role in the human cell model used in this study; thus, its aggregation is not influenced by interaction with endogenous ligands or binding partners. Moreover, since Fluc forms amorphous-type aggregates (Schröder et al., 1993, Buchberger et al., 1996, Rampelt et al., 2012) this work sought to test whether Hsps previously identified to suppress the fibrillar aggregation of proteins (Vos et al., 2010, Månsson et al., 2014a, Kakkar et al., 2016b) also inhibit the amorphous aggregation of destabilised proteins in cells.

3.2 Methods

3.2.1 Plasmid constructs

Construction of the V5-tagged Hsp (HspA, HspB, DNAJ and HspH) plasmid library used in this study was previously described by Hageman and Kampinga (2009). Plasmids encoding HA-Bag1, FLAG-Bag2, FLAG-Bag3, pcDNA5/FRT/TO-V5-Bag4 and FLAG-Bag5 were donated by Professor Harm Kampinga (University of Groningen, The Netherlands).

3.2.2 Cell culture and transfection of HEK293 and Flp-In T-REx HEK293 cells

HEK293 and Flp-In T-Rex HEK293 cells were cultured as described in section 2.4.1. For transient transfections, cells were grown to 60-70% confluence in CELLSTAR® 6-well plates (Greiner Bio-One) coated with 0.001% poly-L-lysine. Cells were co-transfected 24 h post-plating with linear polyethylenimine according to the manufacturer's instructions, using 0.2 µg of plasmid encoding for $Fluc^{DM}$ and 0.8 µg of plasmid DNA encoding for either mRFP (as a negative control) or a Hsp isoform. For transfection of Flp-In T-REx HEK293 cells, 1 µg/mL tetracycline was added to the culture medium 4 h post-transfection to induce expression. To test the luciferase activity of cells expressing $Fluc^{WT}$ or $Fluc^{DM}$, Flp-In T-REx HEK293 cells were transfected with $Fluc^{WT}$-EGFP or $Fluc^{DM}$-EGFP DNA at amounts of 0.1, 0.2 or 0.3 µg, with linear polyethylenimine as stated above.

3.2.3 Epifluorescence microscopy

The formation of inclusions following expression of $Fluc^{WT}$-EGFP or $Fluc^{DM}$-EGFP was assessed directly in 6-well plates 48 h post-transfection by epifluorescence microscopy. Green fluorescence was detected by excitation at 488 nm. All images were taken at 20× magnification using a Leica DMi8 fluorescence microscope (Leica Microsystems). Images were prepared with the LAS-Advanced Fluorescence (LAS-AF) Version 3 software (Leica Microsystems).

3.2.4 Cellular protein fractionation and subsequent immunoblotting

Cells were fractionated and protein was extracted and quantified as outlined in section 2.7.2. Subsequent SDS-PAGE and immunoblotting was undertaken as described in sections 2.7.3 and 2.7.4, respectively.

3.2.5 Antibodies

See Table 2.1 in section 2.2 for antibodies and dilutions used for immunoblotting.

3.2.6 Flow cytometry assays to assess inclusion formation

See section 2.6 for methods pertaining to standard flow cytometry, PulSA and FloIT analyses of cells.

3.2.7 Flow cytometry to assess relative Fluc^{DM}-EGFP levels in cells

To account for any differences in the level of Fluc^{DM}-EGFP being expressed between treatment groups and for use in the luciferase assays (see section 3.2.8), the EGFP geometric mean was determined for live cells transfected as described above and analysed by flow cytometry. Data in Figure 3.9 and Figure 8.1 in Appendix I are presented as the raw EGFP geometric means of each treatment group. The average EGFP geometric mean was taken from three independent experiments and used to calculate the relative EGFP fluorescence. In some experiments, the data was analysed using the following equation:

$$\text{Relative EGFP fluorescence} = \frac{\text{Average EGFP geometric mean of Hsp sample}}{\text{Average EGFP geometric mean of mRFP}} \qquad \text{Equation 3.1}$$

The relative EGFP fluorescence was then used to normalise between treatment groups for the relative amount of Fluc^{DM} in the luciferase assay (see section 3.2.8).

3.2.8 Luciferase activity measurements

The ability of the chaperones to maintain $Fluc^{DM}$-EGFP in a functional state was assessed using a luciferase activity assay. Cells were transfected in a 6-well plate as per section 3.2.2 and cell lysis and luciferase assays were performed 48 h post-transfection as described previously (Michels et al., 1995). Briefly, cells were lysed on ice in 1.0 mL Triton X-100 lysis buffer (25 mM Tris/H_3PO_4, 10 mM $MgCl_2$, 1% (v/v) Triton X-100, 15% glycerol, 1 mM EDTA, pH 7.8) prior to being transferred to -80°C overnight to facilitate total cell lysis. Samples were thawed on ice and 100 µL was added to a cuvette. Luciferase activity was measured for 10 sec following injection of 100 µL substrate (1.25 mM ATP, 0.087 mg/mL D-luciferin) using a Sirius Luminometer (Berthold Technologies, Baden-Württemberg, Germany). Untransfected cells were plated and treated as above and the average relative light units (RLUs) of these cells was subtracted (as a baseline activity) from other treatment groups. Measurements from three separate wells (technical replicates) of each sample were performed and data are presented as the mean ± S.E.M of these technical replicates. In addition, the RLUs of each sample was normalised to the relative levels of $Fluc^{DM}$-EGFP as per the following equation:

$$\text{RLUs/Fluc}^{\text{DM}}\text{ levels} = \frac{\text{Luciferase activity in RLUs}}{\text{Relative EGFP fluorescence}} \qquad \text{Equation 3.2}$$

3.2.9 Sequence alignment and structural modelling

Sequence alignment of HspA1A and HspA1L were performed with the Clustal Omega (EMBL-EBI, Cambridgeshire, UK) Needle (EMBOSS) pairwise sequence alignment tool and the Needleman-Wunsch algorithm. Structural modelling of the HspA1A nucleotide binding domain was undertaken using PyMOL version 2 (PyMOL Molecular Graphics System, Schrödinger, Inc., NY, USA). The nucleotide binding domains of HspA1A (PDB ID: 3JXU) and HspA1L (PDB ID: 3GDQ) were first aligned in PyMOL using the alignment command and then non-conserved regions in HspA1L were identified manually using the above sequence alignment. Non-conserved

regions in HspA1L were mapped onto the HspA1A structure and were chosen to be presented as main chain spheres.

3.2.10 Statistics

Statistical tests were performed as described in section 3.2.10.

3.3 Results

3.3.1 Characterisation of mutant Fluc as a suitable client protein to screen for Hsp chaperone activity

Prior to conducting an Hsp overexpression screen to identify modulators of Fluc^{DM} aggregation in cells, the intracellular aggregation propensity of Fluc^{DM} into inclusions in HEK293 cells was first confirmed by transfecting cells so they expressed Fluc^{DM}-EGFP or the less aggregation-prone Fluc^{WT}-EGFP (Figure 3.1A). Some cells expressing Fluc^{DM}-EGFP contained green fluorescent puncta throughout the cytoplasm (~15% of transfected cells), corresponding to the aggregation and formation of inclusions by this protein. Whilst inclusions were occasionally observed in cells expressing Fluc^{WT}-EGFP (less than 5%), most of these cells exhibited diffuse green fluorescence throughout the cytoplasm and the nucleus. The significantly enhanced aggregation propensity of Fluc^{DM}-EGFP compared to Fluc^{WT}-EGFP was confirmed by examining the distribution of detergent soluble and insoluble protein between cells expressing either of these two Fluc isoforms (Figure 3.1B). There was approximately triple the amount of insoluble protein detected in cells expressing Fluc^{DM} compared to those expressing Fluc^{WT}, whilst the soluble protein formed by cells expressing Fluc^{DM} was two-fold higher than that observed in cells expressing Fluc^{WT}.

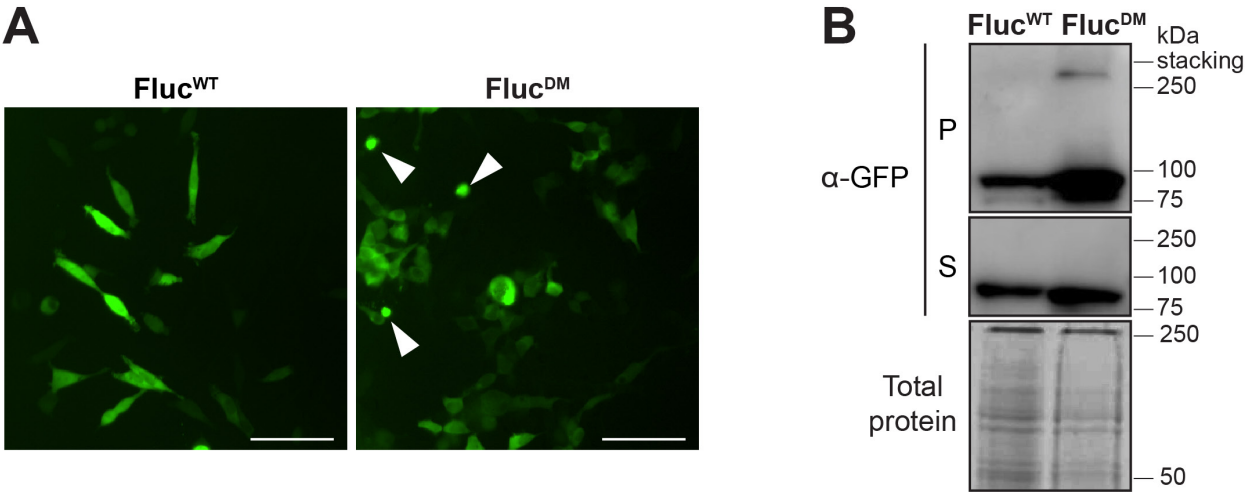

Figure 3.1. Fluc^{DM} readily aggregates to form inclusions in cells, which can be assessed using traditional analyses. HEK293 cells were transfected with Fluc^{WT}-EGFP or Fluc^{DM}-EGFP and analysed 48 h post-transfection by **(A)** epifluorescence microscopy or **(B)** NP-40 cell fractionation followed by immunoblotting. In (A) green fluorescence was detected by excitation at 488 nm. Examples of cells containing inclusions are denoted by the arrows. All images were taken at 20× magnification using a Leica DMi8 fluorescence microscope and scale bars represent 60 µm. Images are representative of three experiments. In (B) an anti-GFP antibody was used to detect Fluc^{WT} or Fluc^{DM} in the soluble (S) or insoluble pellet (P) fraction. A section of the gel showing the total protein was used as a loading control. The blots shown are representative of three experiments.

The percentage of HEK293 cells with inclusions was then analysed by the previously described flow cytometric, pulse shape analysis (PulSA) technique (Ramdzan et al., 2012). First, polygonal gating of the forward scatter (FSC) and side scatter (SSC) signals was used to identify viable, live cells and to remove dead cells, cellular debris and cell doublets from subsequent analyses (Figure 3.2A). Transfected cells were selected based upon EGFP fluorescence, using untransfected cells as a control; cells that did not fluoresce were excluded from further analyses (Figure 3.2B). Finally, live, single, EGFP-positive cells were analysed, plotting the pulse width (W) versus height (H) of the EGFP fluorescence signal (Ramdzan et al., 2012). Cells expressing EGFP, which rarely contain inclusions (Figure 3.2C; *left*), were used to set the gate to identify cells with inclusions formed by $Fluc^{DM}$-EGFP (Figure 3.2C; *right*). PulSA demonstrated that there was a significantly higher percentage of $Fluc^{DM}$-expressing cells with inclusions (9.0 ± 1.1%) compared to cells expressing $Fluc^{WT}$ (2.1 ± 0.2%) (Figure 3.2D).

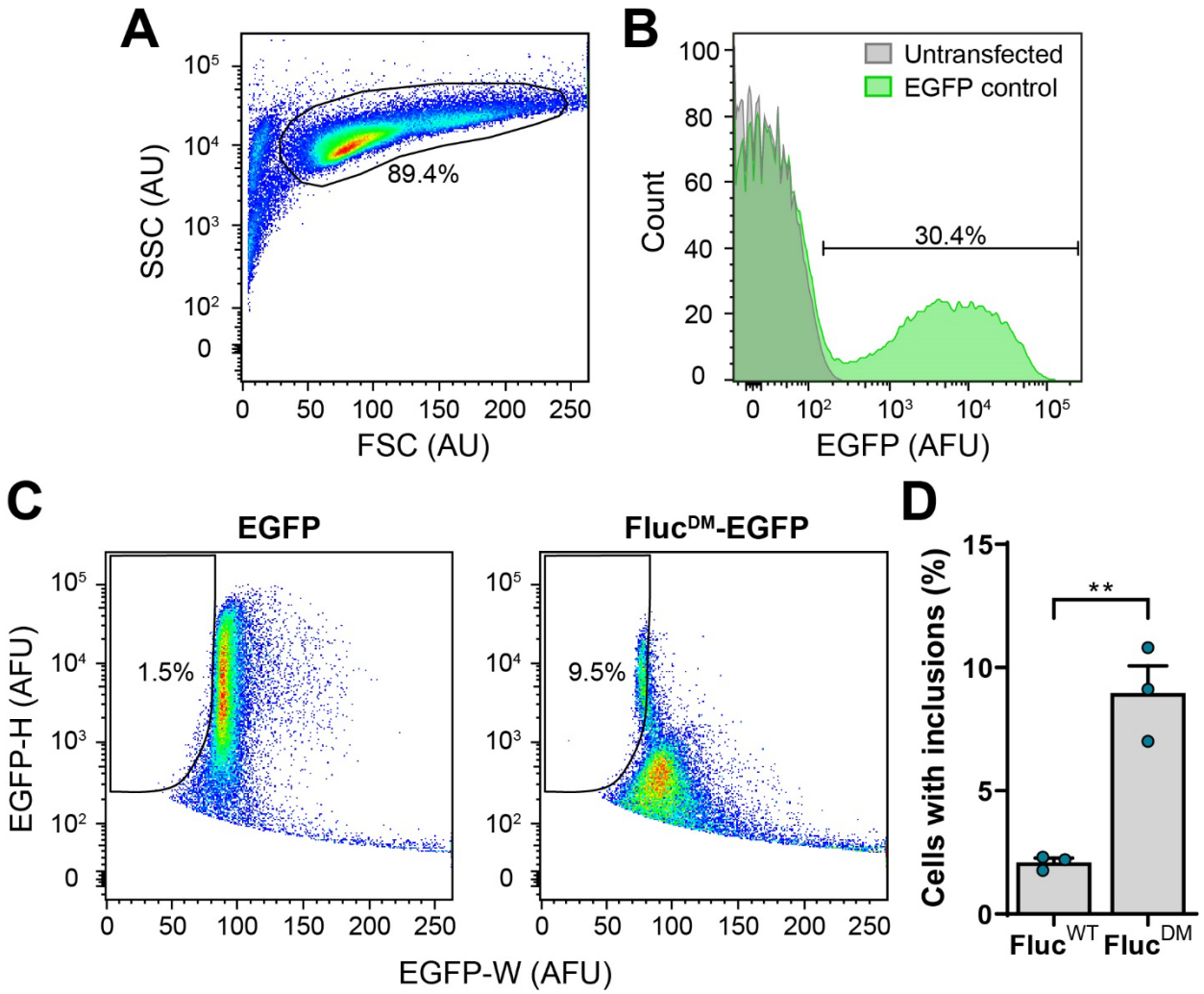

Figure 3.2. The formation of inclusions by Fluc in HEK293 cells can be assessed by PulSA. HEK293 cells were transiently transfected to express Fluc^{WT}-EGFP or Fluc^{DM}-EGFP (or EGFP as a control) and were analysed by PulSA 48 h post-transfection. EGFP fluorescence was detected using a 488 nm laser and 525/50 nm emission filter and 100,000 events were collected for each cell population. Values within plots represent the percentage of cells within each gate. **(A)** Forward scatter (FSC) and side scatter (SSC) pseudo-colour plot of untransfected cells. The polygonal gate encompasses the viable, live cells in the population which were selected for subsequent analyses. **(B)** Frequency histogram of the relative EGFP fluorescence of untransfected (*grey*) and transiently transfected cells expressing EGFP (*green*). Cells expressing EGFP (gate shown) were selected for subsequent analyses. **(C)** Pulse-shape analysis (PulSA) of cells transiently transfected with EGFP (*left*) or Fluc^{DM}-EGFP (*right*) used to identify cells with inclusions based upon the EGFP pulse width (W) and pulse height (H) signals. **(D)** The proportion of HEK293 cells expressing Fluc^{WT}-EGFP or Fluc^{DM}-EGFP with inclusions. Data in (D) are presented as the mean ± S.E.M (n=3) of the percentage of cells containing inclusions. Significant differences between group means were determined using an unpaired two-tailed Student's t-test (** = $P < 0.01$).

Cells expressing EGFP-tagged Fluc were also analysed by the FloIT assay, a technique that readily enumerates the number of inclusions formed in cells (Whiten et al., 2016). Thus, cells were lysed in PBS containing 0.5% (v/v) Triton X-100 and analysed by flow cytometry. Nuclei and non-nuclear particles were identified (and quantified) based on the FSC signal and RedDot1 fluorescence (*left:* unstained, *right:* stained with RedDot1) (Figure 3.3A) and nuclei were excluded from subsequent analyses. The EGFP fluorescence of cells expressing Fluc was exploited to

identify cytoplasmic inclusions containing Fluc based on their FSC and EGFP fluorescence signals (untransfected or EGFP-expressing cells were used as a negative control) (Figure 3.3B). The number of inclusions measured by FloIT was significantly higher (~3 fold) in cells expressing $Fluc^{DM}$ compared to those expressing $Fluc^{WT}$ (Figure 3.3C), in accordance with the results from the fluorescence microscopy, detergent insolubility analyses and PulSA of these proteins. Taken together, these data show that $Fluc^{DM}$ readily aggregates in cells and that FloIT can be used as a rapid and non-subjective method to assess this aggregation into inclusions.

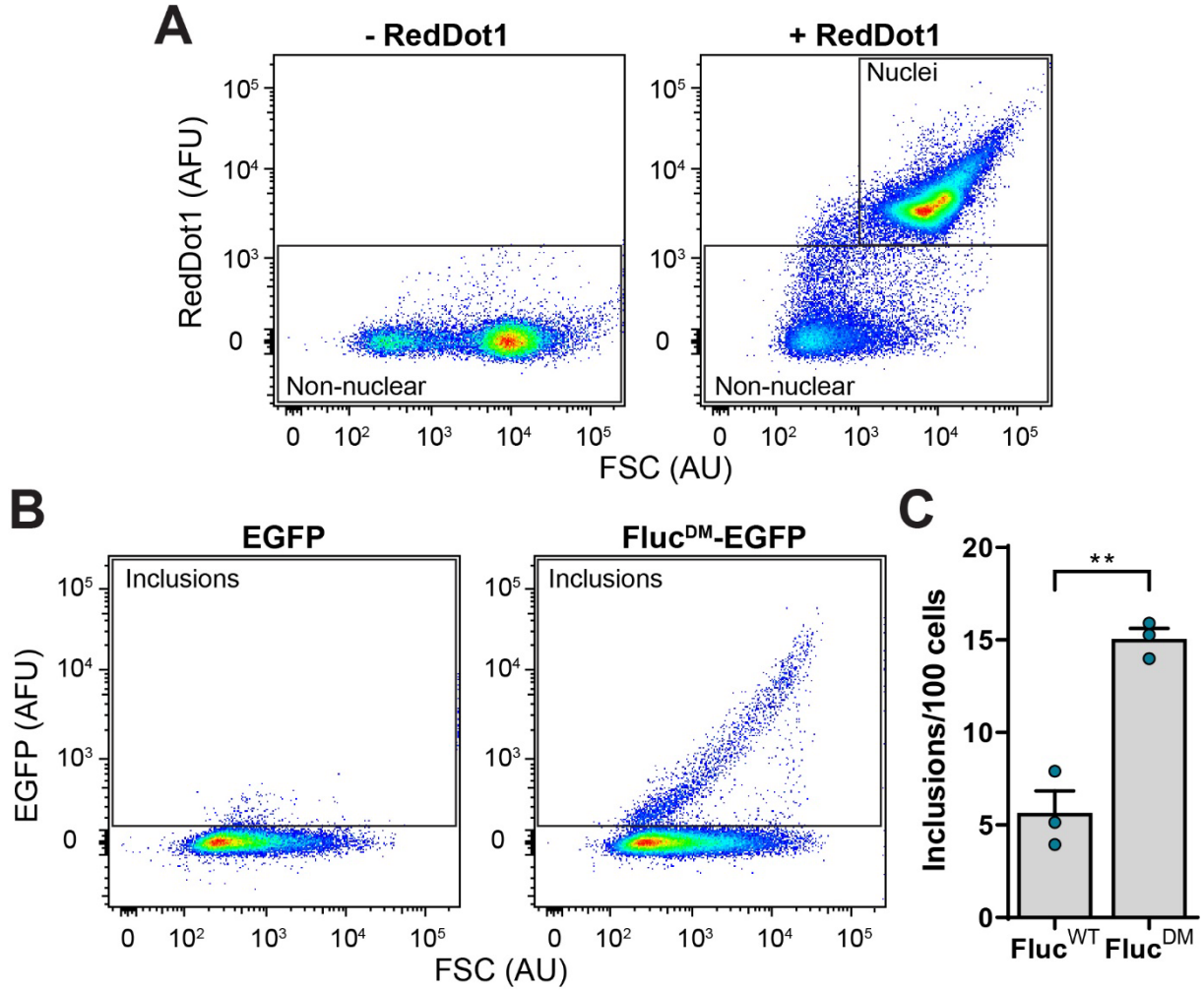

Figure 3.3. The formation of inclusions by Fluc in HEK293 cells can be assessed by FloIT. HEK293 cells were transiently transfected to express EGFP, $Fluc^{WT}$-EGFP or $Fluc^{DM}$-EGFP and were analysed by FloIT 48 h post-transfection. Prior to analysis, cells were lysed in PBS with 0.5% (v/v) Triton X-100. RedDot1 was added (1:1500 dilution) to cell lysates immediately prior to performing flow cytometry and 100,000 events collected for each population. RedDot1 fluorescence was analysed using a 640 nm laser and 670/30 nm collection window. EGFP fluorescence was detected using a 488 nm laser and 525/50 nm emission filter. **(A)** Two parameter, pseudo-colour plots identifying nuclei and non-nuclear particles (indicated) in cells based on the FSC and RedDot1 fluorescence signals (*left:* unstained, *right:* stained with RedDot1). **(B)** Non-nuclear particles were then analysed for the presence of inclusions based on the FSC versus EGFP fluorescence signals in cells transiently transfected to express EGFP (*left*) or $Fluc^{DM}$-EGFP (*right*). Fluc inclusions (indicated) are identified based on increased EGFP fluorescence. **(C)** The number of inclusions measured in HEK293 cells transiently transfected to express $Fluc^{WT}$-EGFP or $Fluc^{DM}$-EGFP. Data in (C) are presented as the mean ± S.E.M (n=3). Significant differences between group means were determined using a two-tailed unpaired Student's t-test (** = $P < 0.01$).

Next, to establish whether Fluc^{DM} expressed in cells is enzymatically active, a luciferase assay was performed to quantify the luminescence-based activity of Fluc^{DM} compared to the wild-type protein. Cells were transfected (or not) to express increasing amounts (0.1, 0.2 or 0.3 µg) of Fluc^{WT}-EGFP or Fluc^{DM}-EGFP and were incubated for 48 h prior to being lysed and analysed for luciferase activity using a luminometer. The luciferase activity of untransfected cells, which was very low (~500 relative light units; RLUs) compared to the other samples, was subtracted from all other treatment groups. The absolute RLUs was significantly higher for cells expressing Fluc^{WT} compared to those expressing Fluc^{DM} at each amount of DNA tested (Figure 3.4A). At 0.1, 0.2 and 0.3 µg of DNA, cells expressing Fluc^{DM} exhibited 11.6, 9.4 and 14.6% respectively of the luciferase activity of cells expressing Fluc^{WT} (Figure 3.4B). This is in accordance with previous work which indicated that Fluc^{DM} retained ~20% of the luciferase activity compared to Fluc^{WT} (Gupta et al., 2011). Nevertheless, this work shows that Fluc^{DM} has measurable luciferase activity and therefore is a suitable client protein to screen for Hsps that modulate unfolding and/or inclusion formation of aggregation-prone proteins in the cell.

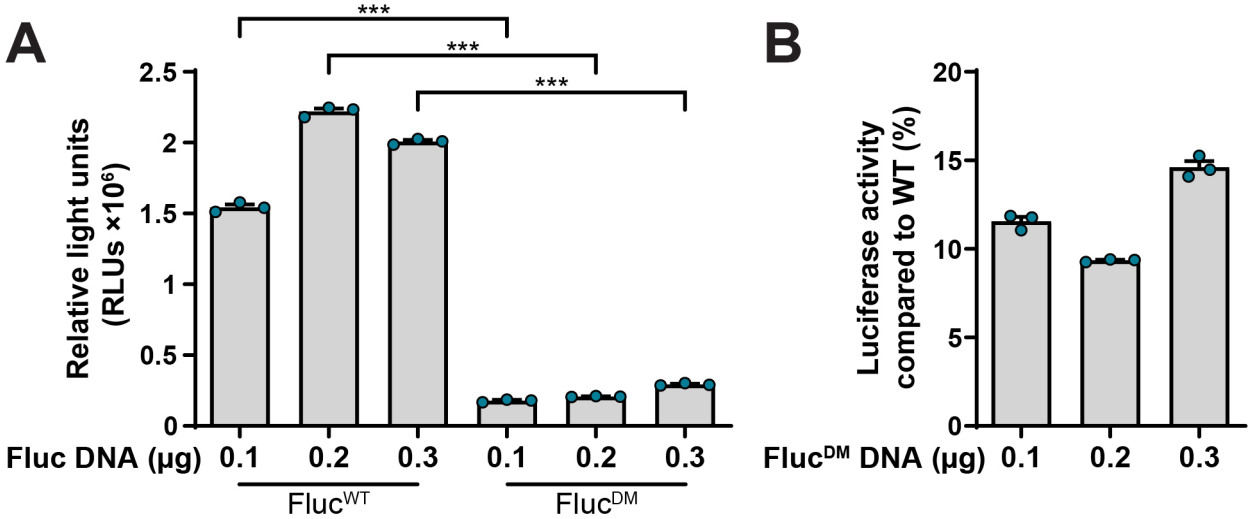

Figure 3.4. Fluc^{DM} retains measureable luciferase activity. Flp-In T-REx HEK293 cells were transfected to express increasing amounts of Fluc^{WT}-EGFP or Fluc^{DM}-EGFP by using 0.1, 0.2 or 0.3 µg of plasmid DNA and incubated for 48 h prior to analysis for luciferase activity. Luciferase activity is presented in (A) as the mean ± S.E.M (of 3 technical replicates) (relative light units; RLUs). Data in (B) are presented as the mean ± S.E.M (of 3 technical replicates) of Fluc^{DM} luciferase activity as a percentage of the Fluc^{WT} control at the same concentration. Significant differences between group means were determined using a one-way ANOVA ($P < 0.05$) followed by a Tukey's post-hoc test. Group means determined to be statistically different from each other are indicated (***$P < 0.001$).

3.3.2 The effect of sHsps on Fluc^{DM} inclusion formation

Following the validation of Fluc^{DM} as a model system to monitor inclusion formation by aggregation-prone proteins in cells, a comprehensive overexpression screen of the major human Hsps was conducted using quantitative flow cytometry in order to identify those molecular chaperones that modulate the aggregation of Fluc^{DM}. This experimental approach can elicit positive results of those chaperones which i) work singly or ii) are bottle-necks, whereby their amount is limiting for all the other chaperones in the network. In addition, cells co-expressing mRFP were used as a negative control throughout this work as mRFP is a protein with no intrinsic chaperone activity and is expressed from the same vector backbone as the other constructs screened from the V5-tagged Hsp library.

The sHsps (HspBs) have been previously identified as highly dynamic species which play a primary role in minimising disease-related protein aggregation in cells (Outeiro et al., 2006, Vos et al., 2010, Carra et al., 2013, Minoia et al., 2014b, Cox and Ecroyd, 2017). To compare the relative efficacies of the HspB family to inhibit Fluc^{DM} inclusion formation, all ten members (HspB1 - HspB10) were individually co-expressed with Fluc^{DM} in Flp-In T-REx HEK293 cells. PulSA was used to determine the proportion of cells with Fluc^{DM} inclusions. HspB2 and HspB3 significantly increased the percentage of cells with inclusions compared to the mRFP control (Figure 3.5A), whilst the remaining HspBs had no significant effect on the proportion of cells with Fluc^{DM} inclusions.

As an alternate and complementary approach, FloIT was used to assess the number of inclusions formed in the transfected cell population. As determined by FloIT, and when compared to cells expressing mRFP, HspB2, HspB3 and HspB10 increased the number of Fluc^{DM} inclusions per 100 cells (Figure 3.5B), whereas HspB4, HspB6, HspB7 and HspB9 significantly inhibited the number of Fluc^{DM} inclusions per 100 cells. HspB1, HspB5 and HspB8 had no significant effect on the

number of Fluc^{DM} inclusions per 100 cells. Interestingly, HspB10 has no significant effect on the percentage of cells with inclusions as assessed by PulSA; however, when the cells were lysed, the FloIT assay demonstrated that HspB10 significantly increased the number of inclusions per 100 cells. This most likely reflects an increased sensitivity of the FloIT technique compared to PulSA to detect inclusions in cells or that expression of HspB10 increases the number of inclusions formed in a cell, but not the proportion of cells with inclusions.

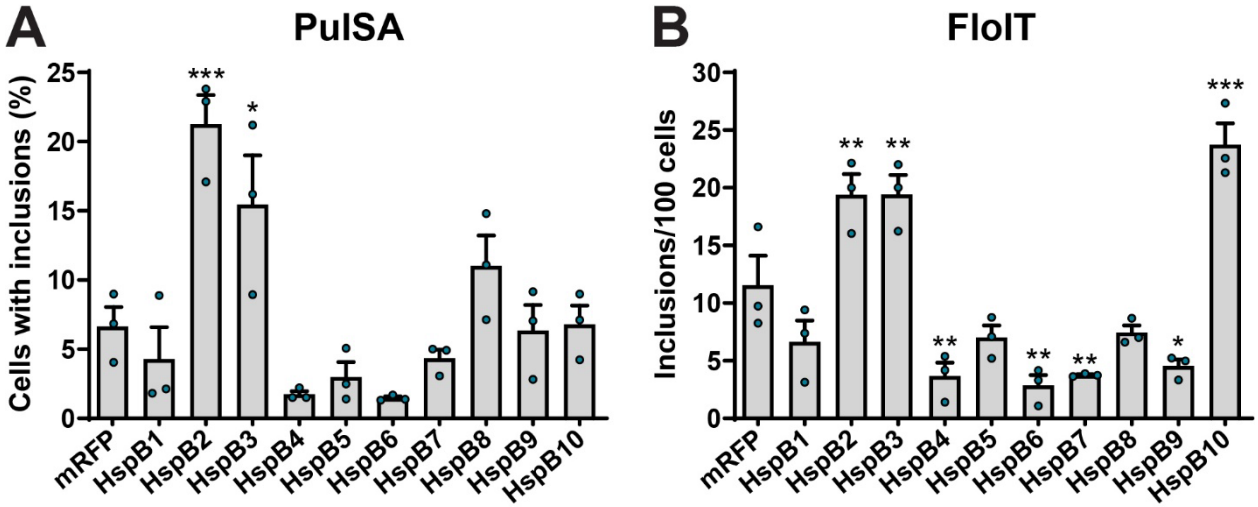

Figure 3.5. The effect of sHsp (HspB) family members on intracellular inclusion formation by Fluc^{DM} is variable. Flp-In T-REx HEK293 cells were co-transfected with V5-tagged HspBs (or mRFP as a negative control) and Fluc^{DM}-EGFP. Expression of HspBs was induced by addition of tetracycline and cells were analysed by **(A)** PulSA or **(B)** FloIT 48 h post-transfection. Data in (A) are presented as the mean ± S.E.M (n=3) of the percentage of cells containing inclusions and data in (B) are presented as the mean ± S.E.M (n=3) of the number of inclusions per 100 cells. Significant differences between group means in the data were determined using a one-way ANOVA ($P < 0.05$) followed by a Dunnett's post-hoc test, comparing group means to the mRFP control. Group means determined to be statistically different to the mRFP control are indicated (*$P < 0.05$, **$P < 0.01$ and ***$P < 0.001$).

3.3.3 Investigating the role of nucleotide exchange factors (NEFs) on intracellular Fluc^{DM} aggregation

Previous studies have suggested that co-chaperones, such as NEFs, play a central role in determining the fate of Hsp-loaded substrates (Takayama et al., 1997, Gamerdinger et al., 2011, Winkler et al., 2012, Serlidaki et al., 2020). To identify whether NEFs are capable of modulating the intracellular aggregation of Fluc^{DM} into inclusions, members of the Bag family (Bag1-5) and two HspH (Hsp110) family members (HspH1 and HspH3) were tested in the overexpression screen. None of these NEFs were capable of significantly inhibiting inclusion formation by

Fluc^{DM}, as determined by either PulSA (Figure 3.6A) or FloIT (Figure 3.6B). Whilst there were trends towards Bag1, Bag4 and Bag5 increasing Fluc^{DM} inclusion formation compared to the mRFP-expressing control, these were not statistically significant.

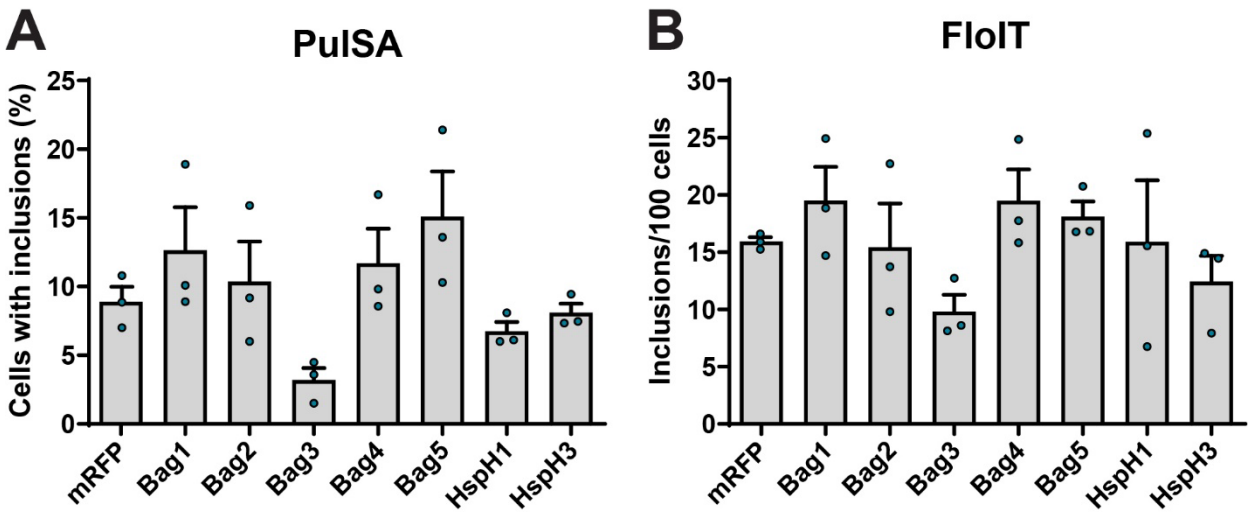

Figure 3.6. Overexpression of individual NEFs has no effect on intracellular inclusion formation by Fluc^{DM}. Flp-In T-REx HEK293 cells were co-transfected with NEFs (or mRFP as a negative control) and Fluc^{DM}-EGFP. Expression of V5-tagged NEFs were induced by addition of tetracycline and cells were analysed by **(A)** PulSA or **(B)** FloIT 48 h post-transfection. Data in (A) are presented as the mean ± S.E.M (n=3) of the percentage of cells containing inclusions and data in (B) are presented as the mean ± S.E.M (n=3) of the number of inclusions per 100 cells. Significant differences between group means were tested using a one-way ANOVA ($P > 0.05$).

3.3.4 Assessing the chaperone activity of the Hsp70 family on Fluc^{DM} inclusion formation

Various members of the Hsp70 (HspA) family have previously been identified as suppressors of protein aggregation (Kampinga and Craig, 2010, Hageman et al., 2011, Serlidaki et al., 2020) and were therefore screened for their capacity to modulate the aggregation of Fluc^{DM} into inclusions. Of the 13 members of the Hsp70 family, the major nuclear/cytosolic Hsp70s were chosen for testing, including HspA1A (stress-inducible Hsp70), HspA1L (Hsp70-like), HspA2, HspA6, HspA8 (constitutive Hsp70; Hsc70), HspA9 (also present in mitochondria) and HspA14. Only HspA1A and HspA2 significantly inhibited inclusion formation by Fluc^{DM} compared to the mRFP-expressing control, as assessed by both PulSA (Figure 3.7A) and FloIT (Figure 3.7B). The remaining Hsp70 members tested had no significant effect on inclusion formation by Fluc^{DM}.

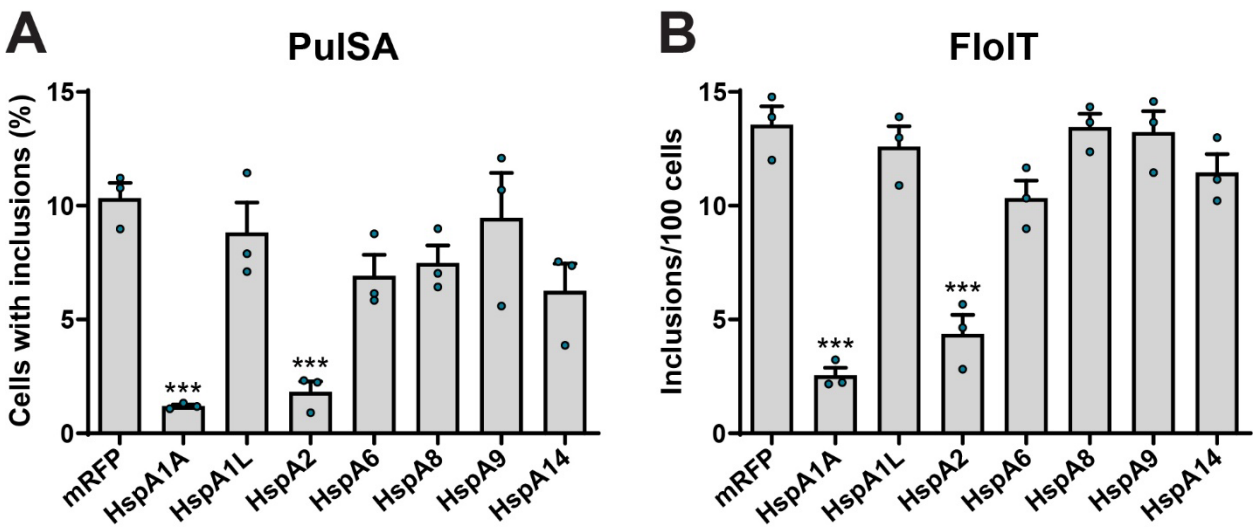

Figure 3.7. Hsp70 members have diverse effects on intracellular Fluc^{DM} aggregation. Flp-In T-REx HEK293 cells were co-transfected with V5-tagged Hsp70s (or mRFP as a negative control) and Fluc^{DM}-EGFP. Expression of Hsp70s was induced by addition of tetracycline and cells were analysed by **(A)** PulSA or **(B)** FloIT 48 h post-transfection. Data in (A) are presented as the mean ± S.E.M (n=3) of the percentage of cells containing inclusions and data in (B) are presented as the mean ± S.E.M (n=3) of the number of inclusions per 100 cells. Significant differences between group means in the data were determined using a one-way ANOVA ($P < 0.05$) followed by a Dunnett's post-hoc test, comparing group means to the mRFP control. Group means determined to be statistically different compared to the mRFP control are indicated (***$P < 0.001$).

Strikingly, despite sharing 89% sequence identity, HspA1A was capable of significantly suppressing the aggregation of Fluc^{DM}, whilst HspA1L was ineffective under these experimental conditions. To investigate this further, the two protein sequences were aligned: the majority of the amino acid variations occur in the C-terminal domain, whilst the nucleotide binding domain and the substrate binding domain share 91% and 97% sequence identity, respectively (Figure 3.8A). However, previous studies have reported that the nucleotide binding domain is responsible for the observed functional differences between members of the Hsp70 family (James et al., 1997, Hageman et al., 2011, Serlidaki et al., 2020). An alignment of the nucleotide binding domains of HspA1A and HspA1L using previously published crystal structures (Wisniewska et al., 2010) revealed that the non-conserved regions are found throughout the entire domain and display slightly different degrees of surface exposure (Figure 3.8B), with the exception of the ATP/ADP-binding pocket (located in the middle of the nucleotide binding domain), which is fully conserved between HspA1A and HspA1L (Figure 3.8B). Thus, these slight differences in surface-exposed residues between the nucleotide binding domains may account for the differences in the abilities of HspA1A and HspA1L to inhibit Fluc^{DM} inclusion formation. This finding is consistent with

work that suggests that differences in the nucleotide binding domain of Hsp70s may be important for recognition by specific co-chaperones and NEFs (Serlidaki et al., 2020).

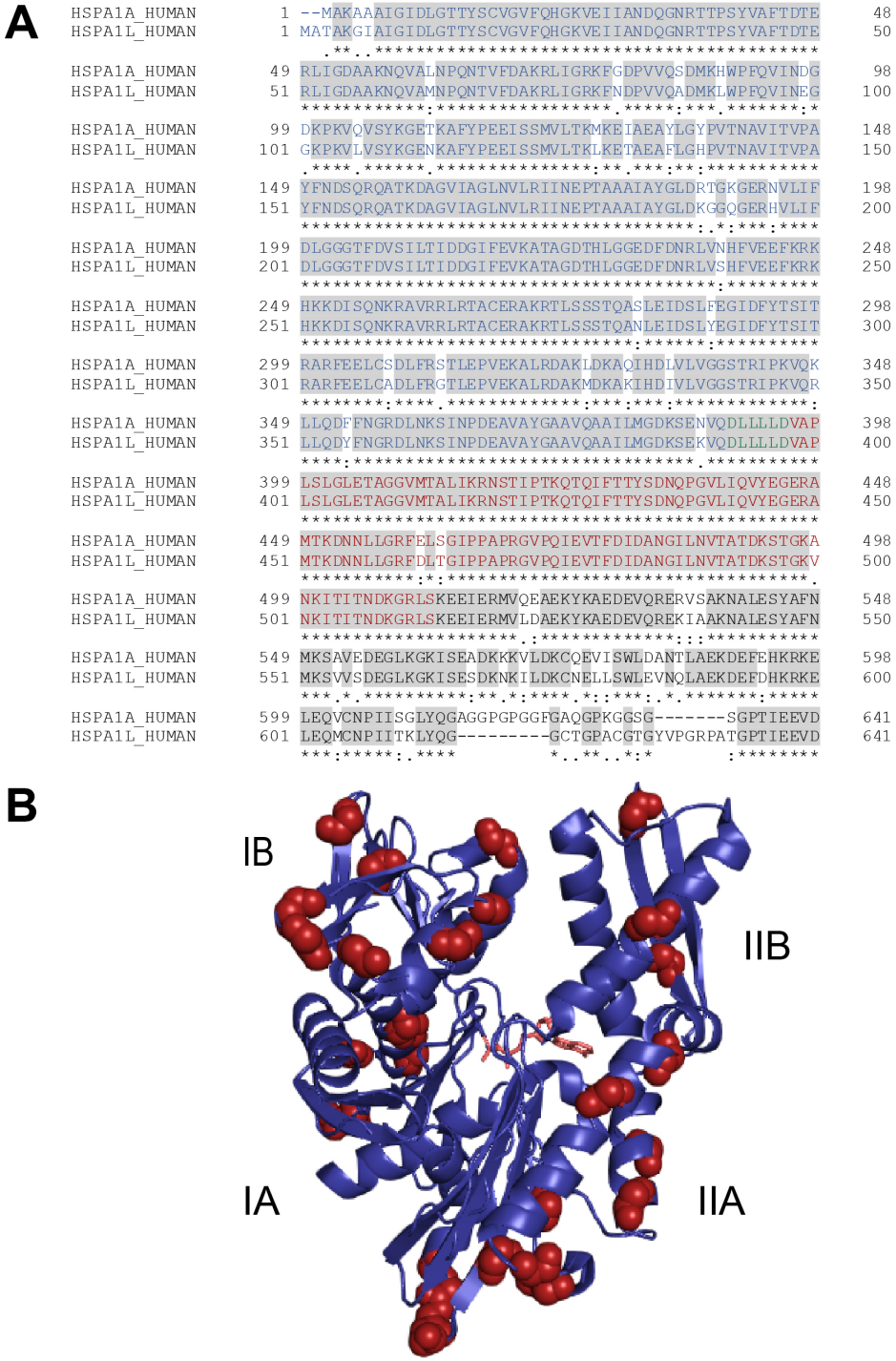

Figure 3.8. The nucleotide binding domain appears to be responsible for opposing chaperone effects of HspA1A and HspA1L, despite being 91% homologous. (A) Pairwise sequence alignment of human HspA1A and HspA1L. Identical residues are highlighted in grey and are denoted by (*), chemically similar amino acids are represented by (:), amino acids denoted by (.) share weak chemical similarity and mismatches or gaps are marked by a space. The nucleotide binding domain (blue), substrate binding domain (red), C-terminal domain (black) and flexible linker (green) region are indicated by different coloured text. Alignment was created using the Clustal Omega (EMBL-EBI) Needle (EMBOSS) pairwise sequence alignment tool and the Needleman-Wunsch algorithm. **(B)** Non-conserved regions between the nucleotide binding domains of HspA1A and HspA1L. Ribbon structure of HspA1A (blue; PDB ID: 3JXU) in complex with ADP (pink). Residues that are not conserved with HspA1L (PDB ID: 3GDQ) are highlighted with main chain spheres (red). Subdomains (IA/B and IIA/B) are indicated for orientation purposes. Structure of the HspA1A nucleotide binding domain was built in PyMOL.

To further investigate these apparent differences in the capacity of HspA1A and HspA1L to inhibit inclusion formation by Fluc^{DM} in cells, Flp-In T-REx HEK293 cells were transiently co-transfected with a selection of the V5-tagged HspAs (HspA1A, HspA1L, HspA2 and HspA6) and EGFP-tagged Fluc^{DM} and an NP-40 fractionation of cell lysates was performed. Overall, the data obtained using this approach mirrored the results of the flow cytometry-based screen. Thus, upon lysis with NP-40 most of the Fluc^{DM} was found in the insoluble (pellet) fraction (Figure 3.9A). Co-expression of HspA1A decreased Fluc^{DM} aggregation, as measured by a substantial decrease in the amount of Fluc^{DM} in the insoluble fraction and a corresponding increase in the amount in the soluble fraction. The decrease in the total amount of Fluc^{DM} in the lysate of cells co-transfected with Fluc^{DM} and HspA1A may be due to HspA1A promoting the degradation of this aggregation-prone protein. Interestingly, co-expression of Fluc^{DM} with HspA2 reduced Fluc^{DM} in the total and soluble fractions of the cell lysate, but had little effect on the amount in the insoluble fraction. In addition, HspA1L and HspA6 did not reduce the amount of Fluc^{DM} in the total or insoluble fractions of the cell lysate. These data confirm that HspA1A and HspA1L, despite sharing nearly 90% sequence identity, differ in their capacity to inhibit inclusion formation by Fluc^{DM}. The expression of V5-tagged HspAs did differ slightly among treatment groups, which may be due to differences in the capacity of HspA members to inhibit inclusions formed by Fluc^{DM}. However, quantification of the levels of the V5-tagged HspAs was not performed in this work.

The mechanism by which HspA1A suppresses Fluc^{DM} aggregation was investigated by measuring the luciferase activity (in RLUs) in cell lysates from Flp-In T-REx HEK293 cells co-transfected to express Fluc^{DM} and one of the aforementioned HspAs (Figure 3.9B). To account for potential differences in the levels of Fluc^{DM} expression between treatment groups, the EGFP geometric mean of live, transfected cells was assessed using flow cytometry. There was no significant difference between the amount of Fluc^{DM}-EGFP expressed in transfected cells from each treatment (Figure 3.9C). When the luciferase activity was normalised to the corresponding level of Fluc^{DM}-

EGFP expressed in the cells it was determined that luciferase activity was significantly reduced in cells expressing the Hsp70 isoforms compared to those expressing mRFP (Figure 3.9D). Co-expression of HspA1A or HspA2 reduced the luminescence-based activity of $Fluc^{DM}$ to 40% and 33%, respectively compared to the mRFP (non-chaperone) control, whilst cells co-expressing either HspA1L or HspA6 retained 87% of the luciferase activity relative to the mRFP control. Together with the immunoblotting data, these results show that co-expression of HspA1A or HspA2 with $Fluc^{DM}$ reduces luciferase activity and the overall amount of $Fluc^{DM}$ in the total protein fraction. Moreover, HspA2 decreases the amount of $Fluc^{DM}$ found in the soluble fraction and its luciferase activity, but has little impact on the amount of protein found in the insoluble pellet. This suggests that whilst co-expression of either HspA1A or HspA2 results in a decrease in the amount of $Fluc^{DM}$ in cells, these chaperones play different roles in the processing of this destabilised protein. Given that expression of HspA1A, but not HspA1L, leads to a reduction in the aggregation of $Fluc^{DM}$ as well as the amount of $Fluc^{DM}$ in both the total and insoluble fractions of the cell lysate, this suggests that HspA1A mediates the degradation of $Fluc^{DM}$ in these cells.

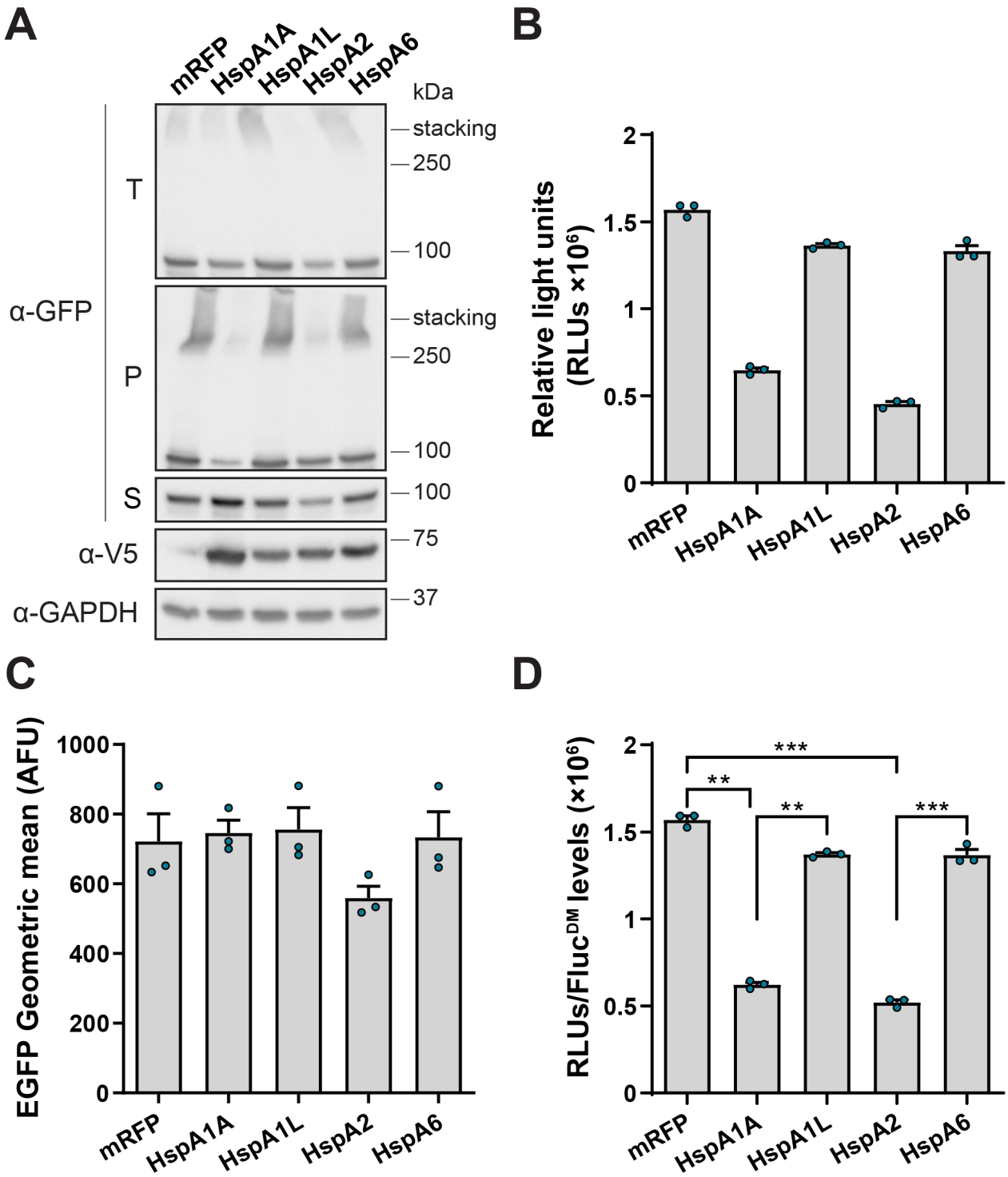

Figure 3.9. HspA1A, but not HspA1L, reduces Fluc^{DM} aggregation by facilitating its degradation. Flp-In T-Rex HEK293 cells were co-transfected with V5-tagged HspA1A, HspA1L, HspA2, HspA6 or mRFP (as a negative control) and Fluc^{DM}-EGFP and analysed 48 h post-transfection by **(A)** NP-40 fractionation and subsequent immunoblotting or **(B – D)** luciferase activity assay. In (A) an anti-GFP antibody was used to detect Fluc^{DM} in the total (T), insoluble pellet (P) and soluble (S) fractions. In the total protein fraction, the expression of HspAs were detected with an anti-V5 antibody and GAPDH was used as a loading control. The blots shown are representative of two experiments. Data in (B) are presented as mean ± S.E.M (of 3 technical replicates) RLUs of Fluc^{DM} luciferase activity following co-expression of HspA members. Data in (C) are the mean S.E.M (n=3) EGFP geometric mean (arbitrary fluorescence units; AFU) of live, transfected cells co-expressing Fluc^{DM}-EGFP and an HspA member (or mRFP as a negative control), measured by flow cytometry. Data in (D) are the mean ± S.E.M (of 3 technical replicates) Fluc^{DM} luciferase activity in cells co-expressing a member of the HspA family, normalised for the levels of Fluc^{DM}-EGFP expression. Significant differences between group means in the data were determined using a one-way ANOVA ($P < 0.01$) followed by a Tukey's post-hoc test. Group means determined to be statistically different are indicated (** $P < 0.01$ and *** $P < 0.001$).

3.3.5 Comparing the ability of DNAJB family members to suppress Fluc^{DM} aggregation

The Hsp70 chaperone system is a highly complex integrative machine which often requires co-factors to mediate its functions. Ongoing evidence has suggested that the DNAJs (J proteins; Hsp40s) are the drivers of the Hsp70 chaperone cycle and govern Hsp70-client interaction (Kampinga and Craig, 2010). Of the DNAJs, the DNAJB proteins are the most extensively studied due to some of them (namely DNAJB6b and DNAJB8) being previously identified as potent suppressors of amyloid aggregation associated with many disease-related proteins, including polyQ-expanded proteins (Hageman et al., 2010). To test the ability of DNAJBs to engage destabilised proteins at risk of forming amorphous aggregates in cells, V5-tagged DNAJBs were transiently co-expressed with Fluc^{DM} in Flp-In T-REx HEK293 cells. The PulSA (Figure 3.10A) and FloIT (Figure 3.10B) assays demonstrated that Fluc^{DM} inclusion formation was significantly reduced by all the DNAJB isoforms tested, with DNAJB1, DNAJB5, DNAJB6b and DNAJB8 being the most potent suppressors.

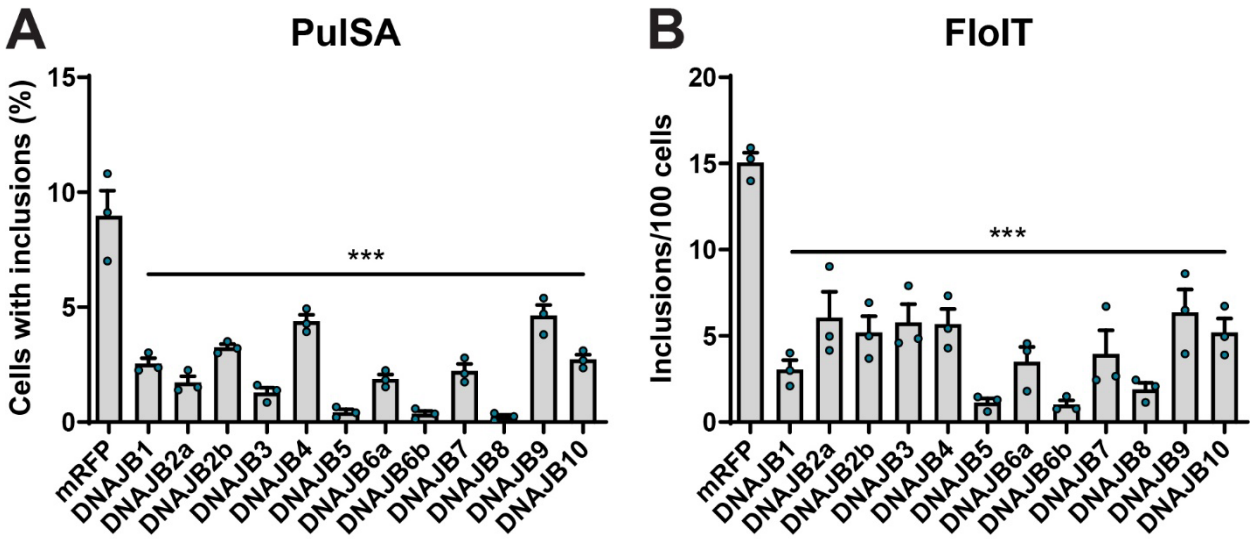

Figure 3.10. DNAJBs prevent the intracellular aggregation of Fluc^{DM} into inclusions. Flp-In T-REx HEK293 cells were co-transfected with V5-tagged DNAJBs (or mRFP as a negative control) and Fluc^{DM}-EGFP. Expression of DNAJBs was induced by addition of tetracycline and cells were analysed by **(A)** PulSA or **(B)** FloIT 48 h post-transfection. Data in (A) are presented as the mean ± S.E.M (n=3) of the percentage of cells containing inclusions and data in (B) are presented as the mean ± S.E.M (n=3) of the number of inclusions per 100 cells. Significant differences between group means were determined using a one-way ANOVA ($P < 0.05$) followed by a Dunnett's post-hoc test, comparing group means to the mRFP control. Group means determined to be statistically different to the mRFP control are indicated (***$P < 0.001$).

The EGFP geometric mean of live, transfected cells was assessed using flow cytometry to determine whether there were any differences in $Fluc^{DM}$ expression across the Hsp overexpression screen. There were no significant differences in the amount of $Fluc^{DM}$-EGFP expressed following co-transfection with members of the HspB (Figure 8.1A), NEF (Figure 8.1B), HspA (Figure 8.1C) or DNAJB (Figure 8.1D) families compared to the corresponding mRFP control (Appendix I). Some small inter-assay variability was observed for the mean number of inclusions formed in cells expressing the mRFP control between the Hsp families screened. The R188Q and R261Q mutations in the N-terminus of Fluc influences its thermostability and hence, aggregation propensity. As such, the levels of inclusions formed by $Fluc^{DM}$ are influenced by temperature (San Gil et al., 2017). Therefore, the observed inter-assay variability is likely an effect of fluctuations in ambient temperature across replicates.

3.4 Discussion

In this work, Fluc^{DM} was used as a model aggregation-prone protein to screen for the generic capacity of the major human Hsps to suppress intracellular inclusion formation by a destabilised protein. The work outlined in this chapter represents the first use of quantitative flow cytometry to conduct an Hsp overexpression screen for modifiers of inclusion formation in cells. Expression of the destabilised aggregation-prone Fluc^{DM} protein in HEK293 cells results in the formation of intracellular inclusions, a process which is able to be quantified by PulSA and FloIT. In addition, Fluc^{DM}-EGFP retains measurable enzyme activity and thus its levels in the cell, as well as its folded (native) and aggregation states can be assessed. This makes it an ideal model to screen for Hsps that modulate the folding, unfolding and/or processing of aggregation-prone proteins in cells. The major findings of the Hsp overexpression screen conducted as part of this work are as follows: (i) of the sHsps, HspB4 HspB6, HspB7 and HspB9, reduce the aggregation of Fluc^{DM} in cells; (ii) the major NEFs, including members of the Bag and Hsp110 families, do not modulate Fluc^{DM} aggregation; (iii) of the Hsp70 family members tested, HspA1A and HspA2 significantly reduce inclusion formation by Fluc^{DM}. Following further investigation into the mechanism by which Hsp70 members reduce protein aggregation, it was identified that HspA1A, and not HspA1L (despite sharing 89% sequence identity at the amino acid level), likely facilitates the degradation of Fluc^{DM} in these cells; and (iv) all of the DNAJBs tested were effective at reducing the aggregation of Fluc^{DM} into inclusions in cells.

3.4.1 sHsps have variable effects on Fluc^{DM} inclusion formation

The sHsps are some of the first and most upregulated molecular chaperones in response to conditions of cellular stress (Haslbeck et al., 2005, Garrido et al., 2012, Hilton et al., 2013), which makes them interesting potential therapeutic targets for disease intervention. This study examined the effect of overexpression of the ten mammalian sHsps on the intracellular aggregation of Fluc^{DM} in order to assess their relative capacity to inhibit Fluc^{DM} from forming intracellular inclusions.

Hsp27 (HspB1) and αB-crystallin (HspB5) are the most widely-studied sHsps, in part because they have been found to co-localise with astrocytic inclusions in patients with familial ALS (Kato et al., 1997). In addition, both Hsp27 and αB-crystallin have been previously reported to prevent the aggregation of a range of model client proteins (Ito et al., 2001, Lee et al., 2006, Outeiro et al., 2006, Ecroyd et al., 2007, Vos et al., 2009, Kulig and Ecroyd, 2012, Cox and Ecroyd, 2017). HspB8 (Hsp22) is another well-characterised sHsp that plays a key role in recognising misfolded clients and, in doing so, forms a complex with Bag3 in order to shuttle the aggregation-prone client protein for degradation via macroautophagy (Carra et al., 2008b, Fuchs et al., 2010). Furthermore, when overexpressed in cells, HspB8 can reduce the aggregation of many disease-related clients, including proteins containing a polyQ-expanded tract (Carra et al., 2008a), amyloid-β (Wilhelmus et al., 2006), TDP-43 (Carra et al., 2013) and SOD1 (Crippa et al., 2010). However, in this current work none of these three sHsps (i.e. neither Hsp27, αB-crystallin nor HspB8) had a significant impact on the formation of Fluc-based inclusions. These results could be attributed to $Fluc^{DM}$ forming insoluble inclusions too rapidly to facilitate the interaction of these chaperones with the protein.

Previous work has shown that the rate of aggregation is a significant factor in determining how effectively the sHsps can prevent protein aggregation. For example, the sHsp αB-crystallin prevents amorphous aggregation by forming stable high molecular mass complexes with the client protein, but inhibits ordered fibril formation via weak and transient interactions (Kulig and Ecroyd, 2012). This suggests that the conformation of the aggregation-prone intermediate dictates the mechanism by which αB-crystallin prevents the aggregation of client proteins (Kulig and Ecroyd, 2012). Cox et al. (2016) identified that the rate of α-synuclein aggregation has a significant effect on the chaperone efficacy of αB-crystallin and Hsp27, whereby an increase in the rate of α-synuclein aggregation resulted in a reduced capacity of these sHsps to prevent protein aggregation.

Thus, the chaperone capacity of Hsp27, αB-crystallin and HspB8 may be overwhelmed in the context of $Fluc^{DM}$ aggregating to form inclusions.

3.4.1.1 sHsps have distinct client protein specificities and mechanisms of action

An analysis of purified recombinant *Drosophila melanogaster* sHsps demonstrated that HspB8 and Hsp27 can inhibit the heat-induced aggregation of Fluc at a 1:1 molar ratio (Morrow et al., 2006); however, this is the first work undertaken to assess the capacity of the human sHsps to prevent the aggregation of Fluc into inclusions within the highly dynamic intracellular environment. An alternate explanation as to why these sHsps do not prevent inclusion formation by $Fluc^{DM}$ is that Hsp27, αB-crystallin and HspB8 simply do not interact with $Fluc^{DM}$ within the cellular environment. Previous research has demonstrated that the sHsps do have some specificity with regard to their interactions with client proteins. Overexpression of Hsp27 significantly reduced the intracellular aggregation of α-synuclein (Outeiro et al., 2006, Cox and Ecroyd, 2017) and a Parkinson's disease-associated mutant form of Parkin (Minoia et al., 2014b), but did not inhibit the intracellular oligomerisation of the amyloid-β peptide (Ojha et al., 2011) or inclusion formation by polyQ-expanded proteins, including mutant huntingtin exon 1 or a fragment of ataxin-3 (associated with spinocerebellar ataxia type 3) (Wyttenbach et al., 2002, Vos et al., 2010).

A comparative analysis of the capacity of the eight major human sHsps (HspB1-HspB8) to inhibit the *in vitro* aggregation of various model proteins revealed that the sHsps do display distinct client specificities (Mymrikov et al., 2017). It was discovered that the canonical sHsps, which form large polydisperse oligomers (e.g. Hsp27, αA-crystallin, and αB-crystallin), are fairly promiscuous, whereas the chaperone activity of the remaining sHsps is more client-dependent (Mymrikov et al., 2017). For example, Hsp27, αA-crystallin, and αB-crystallin could prevent malate dehydrogenase aggregation, whereas HspB6 (Hsp20) and HspB3 had no effect, and HspB2, HspB7, and HspB8 increased malate dehydrogenase aggregation. A similar result was observed in this work, whereby

overexpression of HspB2 or HspB3 resulted in a significant increase in the number of Fluc^{DM} inclusions, which could be due to these sHsps co-aggregating with the client protein. In addition to displaying varying degrees of client specificity with regard to their chaperone action, the mechanism by which members of the sHsp family interact with clients can also differ substantially. For example, unlike HspB7, Hsp27 and αB-crystallin form high-molecular mass oligomers with client proteins in cells, thereby preventing their aggregation by holding them in a folding-competent state for Hsp70-assisted refolding (Vos et al., 2009, Vos et al., 2010). Furthermore, unlike HspB9, the anti-aggregation activity of HspB7 against polyQ-expanded proteins is not dependent upon degradation via the proteasome (Carra et al., 2013). In contrast to HspB8, HspB7 does not stimulate autophaghic clearance, but does require an active autophagy pathway for anti-aggregation activity (Vos et al., 2010, Minoia et al., 2014b). HspB7 is instead thought to prevent the primary nucleation of fibrillar intermediates prior to them forming mature (toxic) fibrils, mediating their clearance via autophagy (Vos et al., 2010). Moreover, HspB8 and its co-chaperone Bag3, traffic misfolded client proteins for degradation via a specific arm of macroautophagy, called CASA, an action that is mediated only by HspB8 (Carra et al., 2008a, Carra et al., 2008b, Behl, 2011).

This work identified HspB4, HspB6, HspB7 and HspB9 as potent inhibitors of Fluc^{DM} inclusion formation. These results are consistent with previous studies that have examined the capacity of one or more of these sHsps to inhibit the aggregation of client proteins. For example, HspB9 can efficiently inhibit the aggregation of polyQ-containing proteins by lowering the level of soluble protein present in the cell and keeping clients in a degradation-competent state, thereby facilitating their disposal via the proteasome before they form large, insoluble species (Carra et al., 2013). αA-crystallin (HspB4) has been previously identified as a proteasome-dependent inhibitor of inclusion formation by a mutant isoform of Parkin (Minoia et al., 2014b); however, it is not capable of inhibiting the aggregation of proteins containing polyQ-expansions (Vos et al., 2010).

Of the ten sHsps members, HspB6 and HspB7 were found to be the most potent inhibitors of $Fluc^{DM}$ inclusion formation in this work. Overexpression of HspB6 and HspB7 significantly decreases the intracellular inclusion formation of polyQ-expanded proteins (Vos et al., 2010), with HspB7 being the most potent inhibitor. Overexpression of HspB6 or HspB7 in cardiomyocytes protects against cytoskeletal injury during stress to prevent tachycardia remodelling (Ke et al., 2011). However, whilst overexpression of HspB7 can suppress the formation of intracellular inclusions by misfolded Parkin, HspB6 is ineffective at doing so (Minoia et al., 2014b). This again highlights that whilst there is some degree of overlap with regard to client protein specificity of some sHsps, this needs to be empirically tested since the mechanisms that drive client specificity remain to be established.

Co-expression of HspB10 did not affect the proportion of cells containing $Fluc^{DM}$ inclusions (as assessed by PulSA), however, it did result in a significant increase in the number of inclusions formed by $Fluc^{DM}$ (as determined via FloIT). HspB10 is the largest and most structurally diverse sHsp (in terms of its amino acid sequence and in comparison to the other nine sHsp members) and has been hypothesised to participate in cytoskeletal stabilisation (Fontaine et al., 2003, Kappé et al., 2003). There is little currently known about the capacity of HspB10 to act as a molecular chaperone. Based on the data obtained in this study, overexpression of HspB10 may result in an imbalance within the cell, such that the ability of other chaperones to facilitate the degradation of inclusions formed by $Fluc^{DM}$ becomes limited. Hence, this results in more inclusions being formed in the cell but does not change the number of cells containing inclusions. In any case, since HspB10 expression is localised only to the testis, HspB10 upregulation as a means of treating neurodegenerative diseases is not likely to be a viable approach. However, these results do highlight the differences between the two flow cytometry methods used to assess inclusion formation in this work. The inability of PulSA to identify cells with small inclusions is a disadvantage of the technique (Whiten et al., 2016). FloIT is therefore advantageous as the

technique can enumerate small inclusions and, since the cells are lysed, can facilitate the release of multiple inclusions from the same cell for analysis. Thus, this work highlights that PulSA and FloIT are highly complementary techniques to study intracellular inclusion formation in cells.

Overall, the data obtained in this study suggests that the human sHsps have distinct client protein specificities (albeit with some overlap) as has been suggested by previous work (Vos et al., 2010, Boncoraglio et al., 2012, Carra et al., 2013, Kakkar et al., 2014, Minoia et al., 2014b, Mymrikov et al., 2017). Moreover, the sHsp members can hold clients in a refolding-competent state following acute stress and facilitate degradation. Thus, upregulation of certain sHsps may offer a novel therapeutic strategy to reduce the accumulation of misfolded proteins in cells that arise from disease states or those which have been exposed to cellular stress, including aging.

3.4.2 NEFs do not inhibit Fluc^{DM} aggregation

The NEFs encompass families of co-chaperone proteins which have diverse roles in the cell. These include participation in Hsp70-mediated folding by facilitating substrate binding and release, and in the targeting of Hsp-loaded substrates for proteolytic degradation (Bukau et al., 2006). In this study, two members of the human Hsp110 family and most of the Bag family members were screened for their ability to inhibit inclusion formation by Fluc^{DM} in cells. None of the NEFs tested had a significant effect on inclusion formation by Fluc^{DM}; however, there was a trend whereby overexpression of Bag3 did reduce intracellular aggregation. Previous cell-based studies have described the ability of Bag3 to clear aggregation-prone huntingtin (Fuchs et al., 2010) and SOD1 (Crippa et al., 2010). When cells age or become exposed to acute stress, misfolded and aggregated proteins can accumulate such that they exceed the degradative capacity of the proteasome. It has been shown that this leads to an increase in Bag3 expression, which subsequently switches the degradation of polyubiquitinated Hsp70 client proteins and facilitates, along with HspB8, the degradation of these misfolded proteins by trafficking them for degradation via macroautophagy

(Behl, 2011). In this work, overexpression of Bag1, Bag4 and Bag5 resulted in a trend towards an increase in the number of $Fluc^{DM}$ inclusions present in cells. Given that this is an overexpression system, these results are not unexpected as previous studies have reported that high stoichiometric ratios of NEFs to Hsp70 can have inhibitory effects on Hsp70-mediated folding and regulation (Nollen et al., 2000, Gässler et al., 2001, Rampelt et al., 2012, Rauch and Gestwicki, 2014, Serlidaki et al., 2020).

Previous research has indicated that targeting of the Hsp110 members may be a viable therapeutic approach to treat protein misfolding diseases. For example, overexpression of Hsp110s in a mutant SOD1 mouse model of ALS has been reported to enhance overall survival (Nagy et al., 2016) and also decrease inclusion formation in a SOD1 cell culture model of disease (Serlidaki et al., 2020). However, in this current work, expression of the Hsp110s had no effect on intracellular aggregation of $Fluc^{DM}$ into inclusions. This is likely due to the chaperone action of Hsp110s requiring interaction with HspA1A (the major stress-inducible Hsp70), which is likely not sufficiently expressed under the conditions used in these cell-based assays. For example, the interaction of Hsp110s with HspA1A is essential for the chaperone action of this disaggregation machinery (Shorter, 2011, Rampelt et al., 2012). The identification of a role of Hsp110s in the targeting of Hsp70-loaded substrates for degradation in yeast (Kandasamy and Andréasson, 2018) further supports the claim that the Hsp110-Hsp70 interaction is crucial for the chaperone function of Hsp110. Future studies investigating the function of NEFs in the context of protein aggregation should therefore consider co-expressing relevant Hsp70s that are required for NEF chaperone activity. Alternatively, the knockdown of specific NEFs to elucidate chaperone function could be more advantageous than an overexpression-based screen, as this would eliminate the need to increase the expression of other members of the Hsp machinery.

3.4.3 Fluc^{DM} inclusion formation is significantly reduced by HspA1A, but not HspA1L, despite it being 89% identical

The Hsp70 family of chaperones are among some of the most highly conserved proteins throughout evolution (Gribaldo et al., 1999). The Hsp70 machinery plays a central role in many branches of cellular protein quality control, including protein refolding, degradation, disaggregation and suppression of aggregation. This work tested the capacity of seven major cytosolic members of the Hsp70 family to inhibit Fluc^{DM} inclusion formation. HspA1A is the most extensively studied and well-characterised Hsp70 member, however, there is currently little known about HspA1L and its role in maintaining proteostasis. In this work, Fluc^{DM} inclusion formation was significantly reduced by HspA1A, but not HspA1L. This result is in accord with previous work that has reported a similar effect against the intracellular inclusion formation by other amorphous clients, including SOD1 (Serlidaki et al., 2020), a Parkin mutant associated with familial Parkinson's disease (Kakkar et al., 2016a), and heat-denatured Fluc (Hageman et al., 2011). Moreover, the overexpression of HspA1A resulted in an increase in the amount of soluble Fluc^{DM} present in these cells and a reduction in the luciferase activity, pointing to a holdase-type function of HspA1A. The majority of the amino acid differences between HspA1A and HspA1L exist within the substrate binding (C-terminal) domains - the nucleotide binding domains share high sequence identity. As such, this has prompted analysis into the C-terminal substrate binding region in an attempt to identify residues in HspA1A that interact with amorphous clients (Serlidaki et al., 2020). Surprisingly, this work showed (via co-immunoprecipitation) that both HspA1A and HspA1L efficiently bind SOD1. In addition, the ATPase activities of HspA1A and HspA1L were found not to be significantly different, which suggests that differences in ATP-dependent (re)folding are not responsible for the opposing anti-aggregation effects (Serlidaki et al., 2020).

The alignment of the nucleotide binding domains of HspA1A and Hspa1L revealed that the non-conserved residues differ in terms of their surface exposure, suggesting that this may account for

the capacity of HspA1A, but not HspA1L, to inhibit Fluc^{DM} inclusion formation. This finding is consistent with previous studies using yeast (James et al., 1997) and cell culture models (Hageman et al., 2011, Serlidaki et al., 2020), which have identified that the nucleotide binding domain is responsible for conferring functional differences between Hsp70 members. More specifically, the differential function of HspA1A compared to HspA1L in cells is thought to be due to the interaction of HspA1A with the Hsp110 co-chaperone HspH2, which results in HspA1A-mediated degradation of SOD1 via the proteasome (Serlidaki et al., 2020). Since HspA1A (i) suppressed Fluc^{DM} inclusion formation, (ii) decreased the overall amount of Fluc^{DM} in the total protein and insoluble fraction of the cell lysate, and (iii) reduced luciferase activity in the cell lysate, it is likely that a mechanism of HspA1A-driven degradation following interaction with NEFs in exposed regions of the nucleotide binding domain also mediates chaperone activity against Fluc^{DM}.

3.4.4 Conserved HspA members, HspA8, HspA6 and HspA2, have unique chaperone activities

HspA8, otherwise known as the constitutively expressed Hsp70 (Hsc70), is ubiquitously expressed at high basal levels in normal (non-stressed) cells and its expression is not heat-inducible (Hageman et al., 2011). Analysis of the human chaperome revealed that the gene encoding for HspA8 is significantly repressed in both Alzheimer's disease and Huntingtin's disease (Brehme et al., 2014). In addition, targeted knockdown of HspA8 in cells leads to toxicity and eventual cell death (Hageman et al., 2010, Vos et al., 2010). Whilst it is clear that functional expression of HspA8 is vital for maintaining proteostasis, overexpression of HspA8 in this work did not significantly reduce the intracellular aggregation of Fluc^{DM} into inclusions. This was similar to the results obtained following the overexpression of HspA8 in cells models of polyQ (Hageman et al., 2010, Hageman et al., 2011) and SOD1 (Serlidaki et al., 2020) aggregation, whereby the levels of insoluble protein in cells was unaffected by increased levels of HspA8. Previous studies have suggested that a complex of HspA8, Hsp110, and a DNAJ can solubilise

fibrils resulting from polyQ-expanded protein fragments, suggesting that DNAJs (most notably DNAJB1, DNAJB6b and DNAJB8) are the rate-limiting factor in reducing intracellular polyQ aggregation (Scior et al., 2018). Thus, the overexpression of HspA8 alone may not have been sufficient to suppress Fluc^{DM} inclusion formation. Despite this, it appears that when the 'housekeeping' function of HspA8 is reduced, as observed in patients with neurodegenerative diseases (Brehme et al., 2014), the capacity of the cell to maintain proteostasis in response to inclusion formation becomes compromised. As such, a decline in the expression of HspA8 could be used as an early marker to help in identifying those most at risk of developing neurodegenerative diseases in the future.

HspA6 is a heat-inducible member of the Hsp70 family, with 85% sequence similarity to the well-characterised HspA1A (Daugaard et al., 2007b); however, in this work HspA6 had no significant effect on Fluc^{DM} inclusion formation. This result was similar to previous work which identified that HspA6 is unable to assist in the refolding of heat-unfolded Fluc in cells or in solution *in vitro*, nor can it prevent the *in vitro* aggregation of the model protein citrate synthase (Hageman et al., 2011). Following mutational studies, it was concluded that HspA6 contains an irregular N-terminal ATPase domain (compared to related Hsp70 members) and this accounts for its inability to interact with and refold heat-inactivated Fluc (Hageman et al., 2011). This same study demonstrated that the basal ATPase activity of HspA6 is significantly higher than that of HspA1A, supporting the notion that the functional differences between these two Hsp70s are intrinsic to the ATPase domain and, subsequently, the nucleotide exchange cycle (Hageman et al., 2011). Thus, it has been postulated that HspA6 has evolved a distinct functional role in the maintenance of cell reproduction and viability under conditions of cellular stress (Noonan et al., 2007). Overall, the inability of HspA6 to interact with Fluc in solution *in vitro* explains why HspA6 did not affect intracellular Fluc^{DM} inclusion formation in this work.

HspA2 is a constitutively expressed member of the Hsp70 family, ubiquitously expressed at low levels in most tissues but highly expressed in the testis and brain (Bonnycastle et al., 1994, Son et al., 2000). Interestingly, it was found in this work that overexpression of HspA2 potently reduces inclusion formation by Fluc^{DM} as determined by flow cytometry and immunoblotting. Moreover, there was a decrease in the amount of total and soluble Fluc^{DM} in cell lysates and a reduction in luciferase activity in these cells, suggesting that HspA2 may inhibit Fluc^{DM} inclusion formation by promoting its degradation. Previous work has shown that the aggregation of heat-denatured Fluc (Hageman et al., 2011) and SOD1 (Serlidaki et al., 2020) are also significantly reduced following overexpression of HspA2, however, the mechanism by which HspA2 prevents the aggregation of these amorphous clients has not been defined. Given that low expression of HspA2 is associated with abnormal spermatogenesis (Son et al., 2000) and sterility (Dix et al., 1996), HspA2 is gaining interest as a potentially useful clinical marker of sperm quality in fertility-related conditions (Nixon et al., 2015). Overexpression of HspA14 had no anti-aggregation effect against Fluc^{DM}; this was not unexpected as this member lacks the canonical substrate binding domain and instead participates in protein translation (Kampinga and Craig, 2010). Similarly, the role of HspA9 in the cell (along with select DNAJs and NEFs) involves translocating polypeptides from the cytosol into the inner mitochondrial matrix (Chacinska et al., 2009) and this likely accounts for why its overexpression has no effect on inclusion formation in this study.

3.4.5 DNAJB family members are potent suppressors of Fluc^{DM} inclusion formation

The Hsp70 chaperone activities require the regulatory and substrate targeting function of various DNAJs (Bukau et al., 2006, Kampinga and Craig, 2010, Rosenzweig et al., 2019). In this work, Fluc^{DM} inclusion formation was significantly reduced by all DNAJBs tested, with DNAJB1, DNAJB5, DNAJB6b and DNAJB8 being the most potent suppressors. The finding that all of the DNAJBs tested significantly suppressed Fluc^{DM} inclusion formation contrasts to the ability of only a few specific DNAJB isoforms, namely DNAJB2a, DNAJB6 and DNAJB8, to strongly inhibit

polyQ aggregation, with DNAJB1 having an intermediate effect (Hageman et al., 2010). However, unlike what was observed for suppression of inclusion formation by Fluc^{DM}, DNAJB4, DNAJB5, DNAJB9 were significantly less active against polyQ aggregation, with DNAJB2b having no effect at all (Hageman et al., 2010). This suggests that the mechanism by which DNAJBs act to suppress the amorphous aggregation of Fluc^{DM} is not the same as that used to suppress the fibrillar aggregation of proteins.

The mechanistic interaction of DNAJBs with aggregation-prone proteins that form amyloid, such as polyQ and the amyloid-β peptide, have been investigated previously (and will be discussed in the next chapter) (Månsson et al., 2014a, Kakkar et al., 2016b), however, whether DNAJBs handle amorphously aggregated clients, such as disordered Fluc, via the same or a distinct route remains unclear. Since DNAJB1 (weak polyQ aggregation inhibitor), DNAJB6b (herein referred to as DNAJB6) and DNAJB8 (strong polyQ aggregation inhibitors) were among the most effective DNAJBs at suppressing Fluc^{DM} aggregation, these isoforms formed the basis of the work in the following chapter of this thesis aimed at further interrogating the mechanism by which DNAJBs and Hsp70 together act to suppress inclusion formation by Fluc^{DM} in cells.

3.4.6 Summary

In summary, the results of this work demonstrate that not all Hsps are equal in their capacity to suppress the intracellular inclusion formation of the model destabilised aggregation-prone protein Fluc^{DM}. This study is unique in that it used Fluc^{DM} as a model protein to provide insights into the Hsps that are important for suppressing amorphous inclusion formation by destabilised client proteins in cells. The results of the Hsp overexpression screen performed in this study confirm that sHsps possess unique specificities for substrates, some of which overlap with other chaperones. This work identified that the handling of Fluc^{DM} by HspA1A is likely mediated by NEFs which, in turn, hold amorphous client proteins in a soluble state for their subsequent degradation by the

proteolytic machinery. Significantly, DNAJBs are potent suppressors of destabilised protein aggregation in cells, however, the mechanism by which DNAJBs act to suppress the amorphous aggregation of $Fluc^{DM}$ is distinct from that used to suppress the fibrillar aggregation of proteins. This screening approach has prompted further investigation into the exact mechanism by which specific DNAJBs prevent inclusion formation by destabilised client proteins in cells. Overall, this work highlights that chaperones are viable targets for the development of drugs aimed at reducing proteinopathies that are associated with neurodegenerative conditions; however, it will be essential to consider chaperone specificity in such work.

Chapter 4: DNAJB chaperones suppress destabilised protein aggregation via a region distinct from that used to inhibit amyloidogenesis

The majority of this chapter has been previously published in the following work:

McMahon, S., Bergink, S., Kampinga, H. H. and Ecroyd, H. (2021). DNAJB chaperones suppress destabilised protein aggregation via a region distinct from that used to inhibit amyloidogenesis. *Journal of Cell Science.*134, jcs255596.

Author contributions: S.M., H.E., S.B. and H.H.K conceptualised the project and the experimental approach. S.M. performed the experiments, analysed the data, constructed the figures and wrote the initial manuscript. All authors edited the manuscript for submission.

4.1 Introduction

The DNAJs are a diverse class of multifunctional molecular chaperones that act as cofactors for the Hsp70 chaperone machine. Ongoing research into the chaperone action of the DNAJB family has identified that they are extremely potent suppressors of disease-related protein aggregation. For example, previous work has shown that DNAJB2a and the closely related members DNAJB6 and DNAJB8 potently suppress the aggregation of a polyQ-expanded protein in a cell culture model of disease (Howarth et al., 2007, Hageman et al., 2010, Gillis et al., 2013). Increasing the expression of DNAJB2a or DNAJB6 in a mouse model of Huntington's disease delays polyQ aggregation, alleviates symptoms and prolongs lifespan (Labbadia et al., 2012, Kakkar et al., 2016b). Moreover, DNAJB6, both *in vitro* and in cells, prevents the nucleation of the amyloid-β peptides into mature fibrils (Månsson et al., 2014a). More recently, mutant SOD1 aggregation was reported to be significantly suppressed by DNAJB1, DNAJB2b and DNAJB7, whilst other DNAJBs were found to have little or no effect (Serlidaki et al., 2020).

Broadly, DNAJB proteins contain the highly conserved N-terminal J-domain shared by all DNAJ proteins, as well as an internal G/F-rich linker region and a C-terminal domain (Figure 4.1A, B) (Cheetham and Caplan, 1998) The J-domain contains the conserved HPD motif for interaction with the Hsp70 machinery, whilst the C-terminal region is thought to bind substrates (Kampinga and Craig, 2010). Specialised members of the DNAJB6-like family (DNAJB6 and DNAJB8) contain a serine/threonine (S/T)-rich motif in between the G/F-rich region and C-terminal domain. The hydroxyl groups within the side chains of this S/T-rich region participate in intramolecular hydrogen bonding with β-hairpin structures in amyloid-β and polyQ peptides to prevent their primary nucleation into mature (disease causing) toxic amyloid fibres (Hageman et al., 2010, Månsson et al., 2014a, Kakkar et al., 2016b). The role of the G/F-rich region is currently not well understood; however, mutations in this region have been linked to a reduced capacity to bind substrates (Perales-Calvo et al., 2010) and have been implicated in inheritable forms of limb-girdle

muscular dystrophy (Harms et al., 2012, Sarparanta et al., 2012). It has therefore been hypothesised that the G/F-rich region may also be directly involved in substrate binding, as well as participate as a flexible linker region for inter-domain stabilisation.

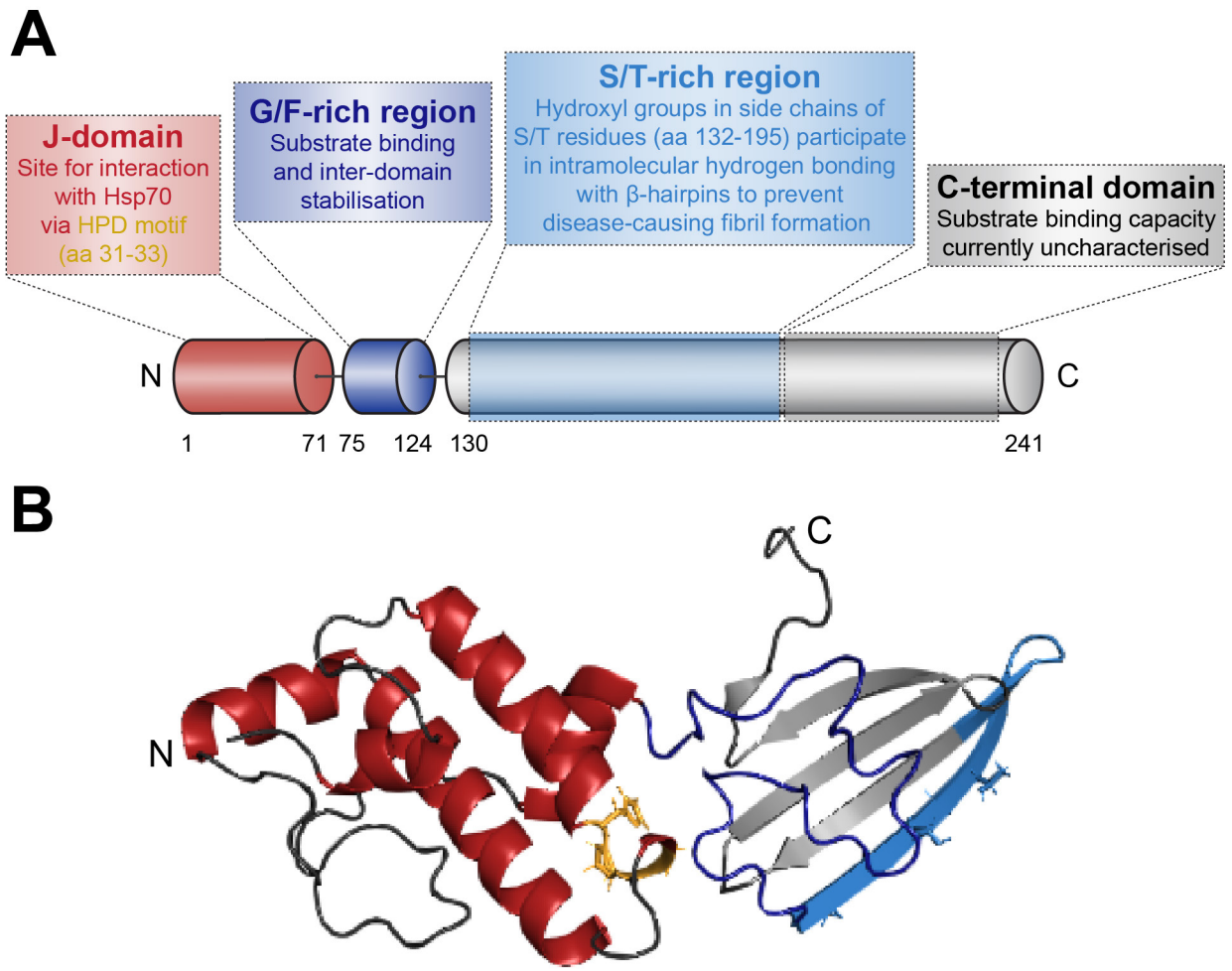

Figure 4.1. The structure of DNAJB6-like proteins and proposed substrate binding regions. (A) Schematic representation of DNAJB6b. The conserved N-terminal J-domain of DNAJB6b is depicted in red and contains the HPD motif; the site for interaction with Hsp70. The G/F-rich linker region is indicated in dark blue and is proposed to participate in substrate binding and inter-domain stabilisation. The C-terminal substrate binding domain contains the S/T-rich region (shown in light blue), which is known to prevent the nucleation of amyloid precursors into mature fibrils. The capacity of the remaining substrate binding domain (highlighted in grey) to bind client proteins is currently unknown. **(B)** Ribbon structure of a DNJAB6b monomer (PDB ID: 6U3R) with regions colour-coded as outlined in (A). The HPD motif in the J-domain is highlighted in yellow using the side chain stick representation. The surface exposed S/T residues within the β-sheet-containing C-terminal domain are indicated with side chain sticks. The structure of the DNAJB6b monomer was built in PyMOL using previously published structural data (Karamanos et al., 2019).

Based on the Hsp overexpression screen conducted as part of the work described in Chapter 3 of this thesis, it was found that all DNAJBs tested significantly supressed $Fluc^{DM}$ inclusion formation, a result that contrasts to what has been reported previously regarding the capacity of

DNAJBs to inhibit amyloidogenesis (Hageman et al., 2010). This suggests that the mechanism by which DNAJBs suppress the nucleation of amyloid precursors into toxic fibrils is different to that required for the suppression of amorphous aggregation by destabilised client proteins. Thus, the intrinsic properties of an aggregation-prone client may dictate the mechanism by which these specialised DNAJBs interact with client proteins Whilst the mechanism for how specific DNAJBs inhibit amyloidogenesis has been investigated previously (Hageman et al., 2010, Månsson et al., 2014b, Kakkar et al., 2016b), their interaction with client proteins that aggregate in a disordered manner remains to be elucidated. This work aimed to exploit the aggregation propensity of $Fluc^{DM}$ to first investigate whether an interaction with Hsp70 is required for the DNAJB-mediated suppression of $Fluc^{DM}$ inclusion formation. This work then went on to assess whether the anti-aggregation activity by DNAJBs is dependent upon the activity of the ubiquitin-proteasome system or autophagy. The role of the S/T-rich domain in DNAJB6 and DNAJB8, which is essential for inhibiting nucleation of polyQ amyloid fibrils (Hageman et al., 2010, Kakkar et al., 2016b), was also investigated with regard to its role in the suppression of $Fluc^{DM}$ aggregation. Finally, the role of the C-terminal of DNAJB6 and DNAJB8, a region not required for the suppression of polyQ aggregation (Hageman et al., 2010), was analysed for its anti-aggregation activity against $Fluc^{DM}$.

4.2 Methods

4.2.1 Plasmid constructs

Plasmids expressing mutations in DNAJBs in which a histidine residue is replaced with a glutamine (H/Q) within the J-domain and C-terminal deletions in DNAJB8 (ΔSSF-SST and ΔTTK-LKS) are outlined in Hageman et al. (2010). Plasmids encoding mutations in the S/T-rich region of DNAJB6 have previously been described by Kakkar et al. (2016b) and similarly referred to herein as M1–4. Constructs expressing disease-related missense mutations (F93L and P96R) in the G/F-rich region have previously been described by Thiruvalluvan et al. (2020). The plasmid encoding deletion of the TTK-LKS region in DNAJB6 was cloned by Dr Jurre Hageman (Hanze University of Applied Sciences, Groningen, The Netherlands).

4.2.2 Cell culture, transient transfections and treatment

HEK293 and Flp-In T-Rex HEK293 cells were cultured, plated and transfected as per section 3.2.2. For co-transfections, 0.2 µg of plasmid encoding for $Fluc^{DM}$ and 0.8 µg of plasmid DNA encoding for either mRFP (as a negative control) or a DNAJB isoform (wild-type or mutational variant) was used. For inhibition of the proteasome, 10 µM MG132 was added to cells 24 h post-transfection and cells were incubated for a further 18 or 24 h. Autophagy was inhibited 24 h post-transfection using a combination of 1 µM bafilomycin A1 and 5 mM 3-methyladenine and then the cells were incubated for a further 24 h. Since MG132, bafilomycin A1 and 3-methyladenine were dissolved in dimethyl sulfoxide, an equivalent volume of DMSO was added to control samples. In some experiments, HEK293 cells were grown as above and at 48 h post-plating were heat-shocked at 42°C for 1 h, before being allowed to recover at 37°C for 2 h prior to harvesting. The concentrations of MG132 (Tanaka et al., 2004), bafilomycin A1 (Yoshimori et al., 1991) and 3-methyladenine (Li et al., 2010) used in these experiments were chosen based on previous work.

4.2.3 Cellular protein extraction, quantification and fractionation

Cells were fractionated and protein was extracted and quantified as outlined in section 2.7.2. Subsequent SDS-PAGE and immunoblotting was undertaken as described in sections 2.7.3 and 2.7.4, respectively.

4.2.4 Antibodies

See Table 2.1 in section 2.2 for antibodies and dilutions used for immunoblotting.

4.2.5 Flow cytometry assay to assess inclusion formation

See sections 2.6 and 2.6.2 for methods pertaining to standard flow cytometry and FloIT analyses of cells, respectively.

4.2.6 Immunocytochemistry and confocal microscopy

Immunocytochemistry and confocal microscopy was performed to detect the co-expression of $Fluc^{DM}$-EGFP and V5-tagged DNAJBs or mutational variants (or mRFP). HEK293 cells were grown to 60-70% confluency in 8-well chamber µ-slides and transfected as above (section 4.2.2). Immunocytochemistry and confocal microscopy were then performed as outlined previously (section 2.5) with the following modifications. Cells were incubated with an anti-V5 antibody (1:200; 46-0705, Thermo Fisher Scientific) diluted in blocking buffer for 1 h at 37°C and then washed 3 times (each for 10 min) with gentle rocking in 0.1% (v/v) Triton X-100 in PBS. Cells were then incubated with the goat anti-mouse IgG H&L Dylight® 550 secondary antibody (1:250; ab96872, Abcam) diluted in blocking buffer for 30 min at 37°C in the dark. Cells were then washed, stained with the Hoechst 33342 nucleic acid stain and imaged using a SP8 TCS confocal microscope and the 63× objective lens and the 4× zoom function in the LAS-X Version 3 software as described in section 2.5.

4.2.7 Statistics

Statistical tests were performed as described in section 3.2.10.

4.3 Results

4.3.1 DNAJBs promote the degradation of Fluc^{DM}, primarily via the proteasome

We first sought to determine whether the inhibition of Fluc^{DM} aggregation into inclusions by DNAJBs requires the degradative activity of the proteasome or autophagy. To do so, HEK293 cells were co-transfected to express Fluc^{DM} and DNAJB1 or DNAJB6 (or mRFP as a control) and, 24 h post-transfection, were treated with proteasome (MG132) or autophagy (3-methyladenine + bafilomycin A1) inhibitors and analysed at 48 h. Treatment of cells with inhibitors of autophagy had no significant effect on the level of inclusion formation and little effect on the insolubility of Fluc^{DM} in cells co-expressing a DNAJB (Figure 4.2A, B). Inhibition of autophagy was confirmed in cells treated with 3-methyladenine + bafilomycin A1 by the increased levels of SQSTM1/p62 (a commonly used marker of autophagy). An increase in SQSTM1/p62 was also observed in cells treated with MG132, an effect which has been reported previously whereby inhibition of the proteasome leads to upregulation of p62 transcription (Myeku and Figueiredo-Pereira, 2011), suggesting a crosstalk between these two pathways (Liu et al., 2016). As there was no substantial increase in the level of insoluble Fluc^{DM} in cells treated with the autophagy inhibitors, these data suggest that Fluc^{DM} is primarily degraded by the proteasome.

Upon treatment with MG132, the number of Fluc^{DM} inclusions as assessed by FloIT significantly increased in cells co-expressing the mRFP non-chaperone control (Figure 4.2A) and this corresponded to an increase in the proportion of Fluc^{DM} found in the NP-40 insoluble fraction (Figure 4.2B). Inhibition of the proteasome following treatment with MG132 was evidenced by large smears of polyubiquitinated protein in these samples. Proteasome inhibition also led to a significant increase in inclusion formation in cells overexpressing DNAJBs compared to DMSO-treated cells, such that the capacity of the co-expressed DNAJBs to reduce the amount of insoluble Fluc^{DM} was significantly reduced when cells were treated with MG132. Additionally, the amount of soluble Fluc^{DM} also decreased in cells expressing DNAJBs that were treated with MG132

compared to the DMSO-treated controls. This was despite aggregation still being significantly reduced in MG132-treated cells that overexpressed a DNAJB compared to those expressing mRFP. Furthermore, treatment with MG132 also likely impairs the capacity of endogenous DNAJBs (primarily DNAJB1 and DNAJB6) to process $Fluc^{DM}$ for degradation via the proteasome, hence why we observed a significant increase in inclusions formed by cells expressing the mRFP control. These data suggest that DNAJBs can keep destabilised $Fluc^{DM}$ in a non-aggregated soluble form (proteasome independent) such that, with time, the proteasome can facilitate its degradation. Furthermore, $Fluc^{DM}$ aggregation is dependent upon proteasomal degradation and the inhibition of $Fluc^{DM}$ aggregation into inclusions by DNAJBs requires the activity of the proteasome.

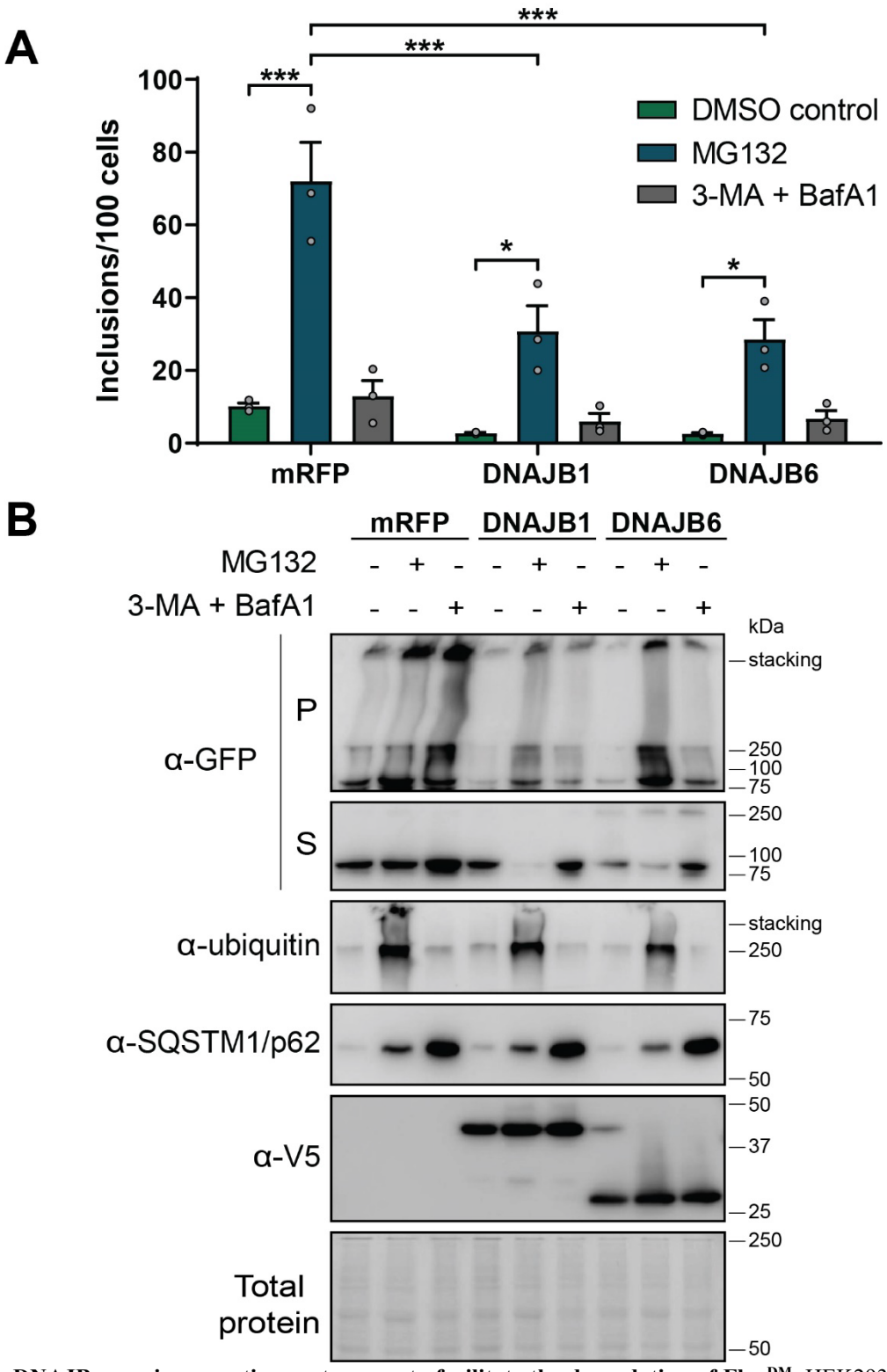

Figure 4.2. DNAJBs require an active proteasome to facilitate the degradation of Fluc^{DM}. HEK293 cells were co-transfected to express Fluc^{DM}-EGFP and mRFP (as a negative control), DNAJB1 or DNAJB6 and 24 h post-transfection, cells were treated with the proteasome inhibitor MG132 (10 μM) or autophagy inhibitors 3-methyladenine (3-MA; 5 mM) and bafilomycin A1 (Baf A1; 1 μM), or a DMSO-treated control. Cells were incubated for a further 24 h and then analysed by **(A)** quantitative flow cytometry or **(B)** NP-40 fractionation and subsequent immunoblotting. Data in (A) are presented as the mean ± S.E.M (n=3) of the number of inclusions per 100 cells. Significant differences between group means were determined using a one-way ANOVA ($P < 0.05$) followed by a Tukey's post-hoc test. Group means determined to be statistically different from each other are indicated (*$P < 0.05$ and ***$P < 0.001$). In (B) an anti-GFP antibody was used to detect Fluc^{DM} in the insoluble pellet (P) and soluble (S) fractions. In the total protein fraction, the expression of DNAJBs were detected with an anti-V5 antibody, an anti-ubiquitin antibody was used to detect ubiquitinated proteins and an anti-SQSTM1/p62 antibody was used to assess autophagy inhibition. Total protein was used as a loading control. The blots shown are from a single experiment.

4.3.2 The J-domain is crucial for DNAJBs to protect against Fluc^{DM} aggregation

We next examined whether DNAJBs require an interaction with Hsp70 in order to suppress the aggregation of Fluc^{DM} into inclusions. To do so, we employed mutant forms of the DNAJBs in which a histidine residue is replaced with a glutamine (H/Q) within the highly conserved HPD motif of the J-domain (Hageman et al., 2010) (Figure 4.3A). The HPD motif plays a critical role in the regulation of Hsp70 activity; the H/Q mutation in this motif blocks the ability of the DNAJB to interact with Hsp70 (Cheetham and Caplan, 1998), thereby abrogating its ability to stimulate Hsp70 ATPase activity (Tsai and Douglas, 1996) and recruit Hsp70 to clients. The H/Q mutation abolished the capacity of each of the three DNAJBs to inhibit the aggregation of Fluc^{DM}, as evidenced by FloIT and assessment of the aggregation of Fluc^{DM} by NP-40 cell fractionation (Figure 4.3B, C). Thus, co-expression of the wild-type DNAJBs reduced the amount of insoluble protein whereas cells expressing the H/Q mutant isoforms contained an equivalent or increased amount of insoluble Fluc^{DM} compared to the mRFP control. The amount of soluble Fluc^{DM} in cells expressing a wild-type DNAJB decreased compared to cells expressing the mRFP control. This effect is likely due to there being less total Fluc^{DM} in cells expressing wild-type DNAJBs due to them promoting its degradation. The expression of the DNAJB H/Q variants were slightly higher than the corresponding wild-type protein and this could be due to the mutant becoming trapped with their substrates within inclusions, such that their own normal turnover is delayed. Strikingly, the relative loss in activity of the H/Q variants was highest for DNAJB1 (i.e. largest increase in insoluble protein compared to wild-type variant) and the ratio of insoluble to soluble Fluc^{DM} was different to that of cells expressing DNAJB6 H/Q or DNAJB8 H/Q. This effect could be, at least in part, due to an increased dependence of DNAJB1 upon interaction with Hsp70 for chaperone activity compared to DNAJB6 and DNAJB8. DNAJB1 may require more immediate interaction with Hsp70 in order to suppress inclusion formation by Fluc^{DM}, whereas DNAJB6 and DNAJB8 may be more capable of acting in an ATP-independent manner to hold this destabilised client protein, before requiring interaction with Hsp70 for subsequent proteasomal degradation.

We next investigated whether increased activation of HSF1 activity may account for the observed effect whereby DNAJB overexpression led to decreased $Fluc^{DM}$ inclusion formation, for example by increasing levels of Hsp70. Thus, the expression of Hsp70 was also assessed following overexpression of these DNAJB isoforms, because levels of some Hsp70s increase when HSF1 is activated (Lindquist, 1986, Lindquist and Craig, 1988). As expected, there was an increase in the expression of Hsp70 in heat-shocked cells as a result of HSF1 activation (~2 fold); however, the expression of Hsp70 was not increased in cells overexpressing DNAJBs compared to cells expressing mRFP as a control (Figure 4.3C). Thus, these data indicate that increased activity of HSF1 does not account for the decrease in $Fluc^{DM}$ inclusion formation in cells overexpressing DNAJBs. Moreover, given the expression of Hsp70 was not affected by DNAJB overexpression, these data imply that whilst DNAJBs prevent the aggregation of $Fluc^{DM}$ by interacting with Hsp70, their mode of action and relative dependence on Hsp70 may be dissimilar.

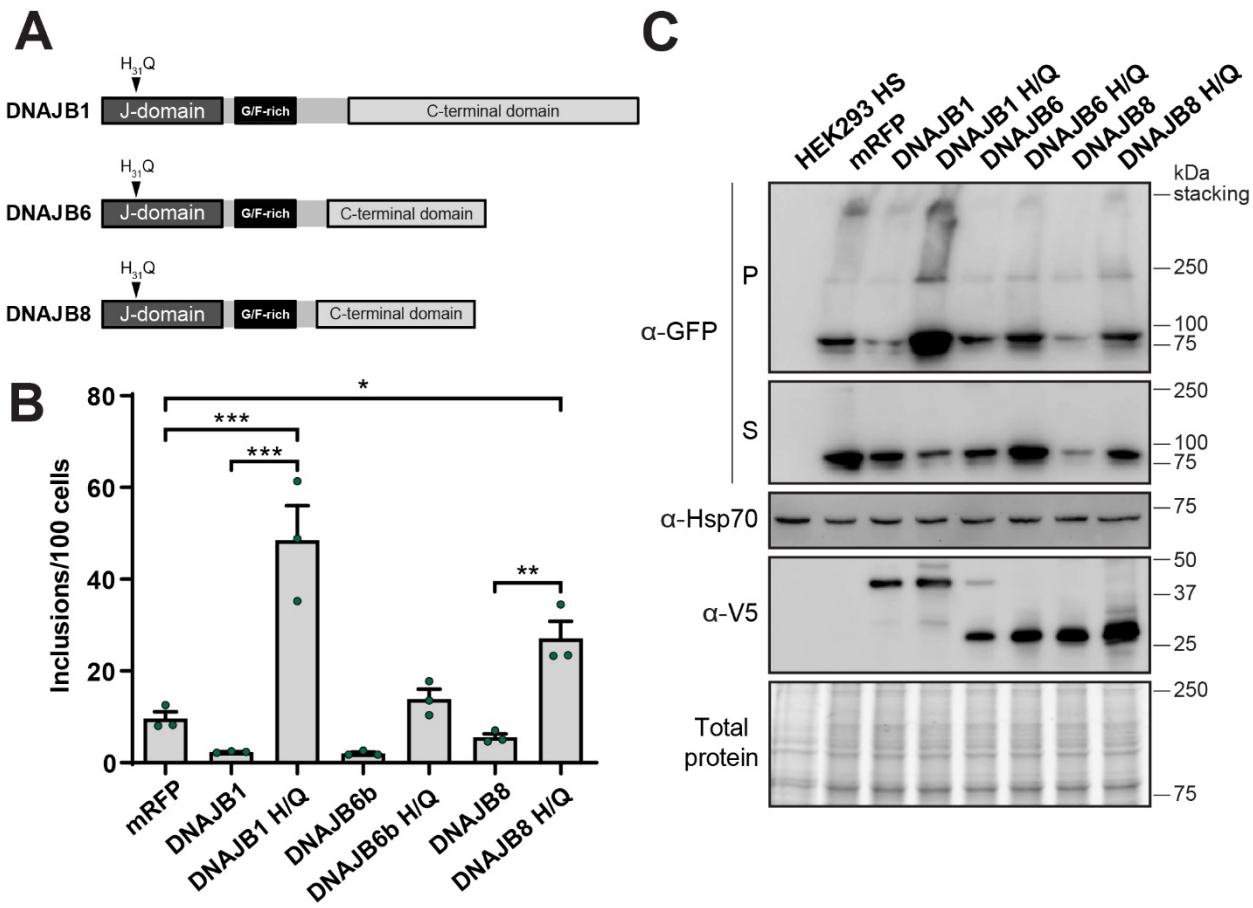

Figure 4.3. Interaction with Hsp70 is required for DNAJBs to suppress Fluc^{DM} aggregation. Schematic overview of DNAJB proteins identifying location of mutation within the J-domain, in which the histidine residue has been substituted for a glutamine (termed H/Q) at amino acid position 31 within the HPD (Hsp70-interacting) motif. HEK293 cells were co-transfected to express Fluc^{DM}-EGFP and mRFP (as a negative control), DNAJB1, DNAJB6, DNAJB8 or their H/Q variants. Cells were analysed 48 h post-transfection by **(B)** quantitative flow cytometry or **(C)** NP-40 cell fractionation followed by immunoblotting. Data in (B) are presented as the mean ± S.E.M (n=3) of the number of inclusions per 100 cells. Significant differences between group means were determined using a one-way ANOVA ($P < 0.05$) followed by a Tukey's post-hoc test. Group means determined to be statistically different from each other are indicated (*$P < 0.05$, **$P < 0.01$ and ***$P < 0.001$). In (C) an anti-GFP antibody was used to detect Fluc^{DM} in the insoluble pellet (P) and soluble (S) fractions. In the total protein fraction the expression of DNAJBs was detected with an anti-V5 antibody and an anti-Hsp70 antibody was used to detect endogenous Hsp70 or expression of Hsp70 following a 1 h heat shock (HEK293 HS) at 42°C with 2 h recovery at 37°C. Total protein was used as a loading control. The blots shown are from a single experiment.

4.3.3 DNAJBs facilitate interaction with Hsp70 and Fluc^{DM} for proteasomal degradation

In order to examine whether DNAJBs mediate Fluc^{DM} degradation by the proteasome via interaction with Hsp70, we co-expressed Fluc^{DM} and the DNAJB H/Q variants in cells and then treated with MG132. We surmised that if Hsp70 was the driver of proteasomal degradation of Fluc^{DM}, the H/Q variants, which are unable to interact with Hsp70, should not further increase the levels of inclusions formed in MG132-treated cells. Inhibition of the proteasome in these experiments was again confirmed by an increase in polyubiquitinated species, observed as large,

high molecular weight smears by immunoblotting with an anti-ubiquitin antibody. As before, there was a significant increase in the number of inclusions in cells expressing either the DNAJB1 H/Q or DNAJB8 H/Q variant compared to the mRFP expressing control (Figure 4.4A). However, inclusion formation did not further increase in cells expressing an H/Q variant and treated with MG132. Again, the result was different for DNAJB1 compared to DNAJB6 and DNAJB8, whereby treatment of cells expressing DNAJB1 with MG132 lead to a decline in the number of inclusions compared to the DMSO-treated control. Since MG132 is a substrate analogue (Lee and Goldberg, 1998), this effect could be attributed to the drug interfering with $Fluc^{DM}$-DNAJB1 H/Q complex formation. The C-terminus of DNAJB1, which is thought to be responsible for substrate binding, is structurally diverse from DNAJB6 and DNAJB8 (Kampinga and Craig, 2010) and this may explain why the effect is specific for DNAJB1 H/Q. There was no difference in the amount of insoluble protein detected between cells expressing the H/Q variants treated with MG132 compared to DMSO-treated controls (Figure 4.4B). We did note some inter-assay variability for cells expressing mRFP treated with MG132 compared to previous experiments (Figure 4.2A); we attribute this to differences in the time cells were treated with MG132 (i.e. cells were treated with MG132 for 24 h in the experiments presented in Figure 4.2 and 18 h in the experiments presented in Figure 4.4). Taken together, these data provide further evidence that DNAJBs antagonise $Fluc^{DM}$ aggregation by keeping it competent for proteasomal degradation, which requires interaction with Hsp70 to be effective.

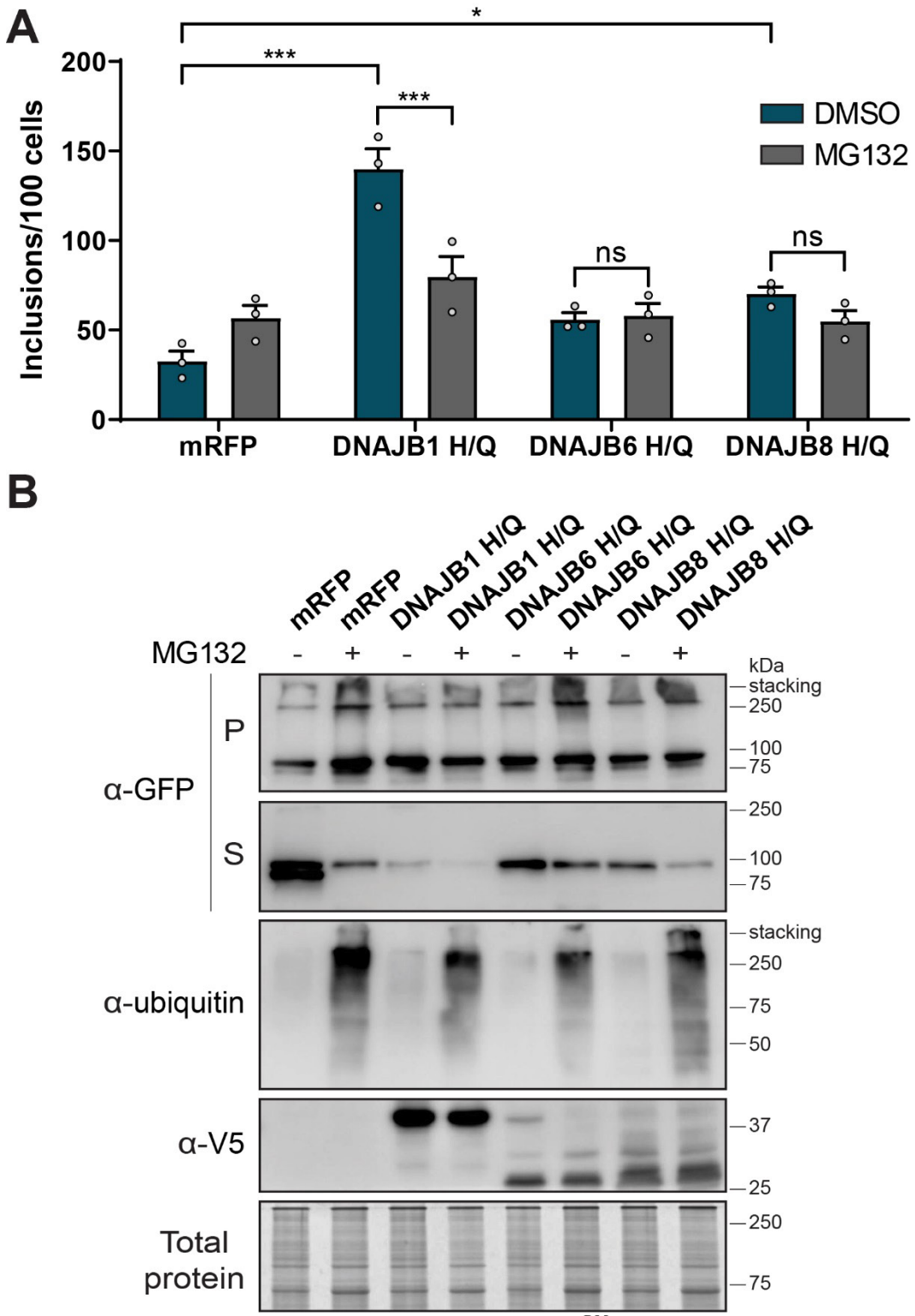

Figure 4.4. DNAJBs rely upon interaction with Hsp70 to deliver Fluc^{DM} for the degradation via the proteasome. HEK293 cells co-transfected with Fluc^{DM}-EGFP and mRFP (as a negative control), DNAJB1, DNAJB6 or DNAJB8 H/Q variants. Cells were treated with a proteasome inhibitor MG132 (10 μM) or a DMSO-treated control 24 h post-transfection. Cells were incubated for a further 18 h and analysed 42 h post-transfection by **(A)** quantitative flow cytometry or **(B)** NP-40 fractionation and subsequent immunoblotting. Data in (A) are presented as the mean ± S.E.M (n=3) of the number of inclusions per 100 cells. Significant differences between group means were determined using a one-way ANOVA ($P < 0.05$) followed by a Tukey's post-hoc test. Group means that are significantly different from one another are indicated (ns represent non-significant groups, $*P < 0.05$ and $***P < 0.001$). In (B) an anti-GFP antibody was used to detect Fluc^{DM} in the insoluble pellet (P) and soluble (S) fractions. In the total protein fraction, expression of DNAJBs was detected with an anti-V5 antibody and an anti-ubiquitin antibody was used to observe inhibition of the proteasome. Total protein was used as a loading control. The blots shown are from a single experiment.

4.3.4 Disease-related mutations in the G/F-rich region of DNAJB6 do not impact the capacity to prevent the aggregation of Fluc^{DM} into inclusions

To probe for other regions within DNAJBs that are required to suppress Fluc^{DM} aggregation, the impact of two disease-related missense mutations within the G/F-rich region of DNAJB6 (F93L and P96R) were assessed (Figure 4.5A). The F93L and P96R mutations have been associated with limb-girdle muscular dystrophy and it has been suggested that these mutations lead to disruption of the J to G/F-inter-domain interaction and minor loss of function in their capacity to suppress polyQ aggregation (Sarparanta et al., 2012, Thiruvalluvan et al., 2020). However, we found that both the F93L and P96R mutational variants of DNAJB6 fully retained the ability to inhibit the aggregation of destabilised Fluc^{DM} into inclusions (Figure 4.5B, C).

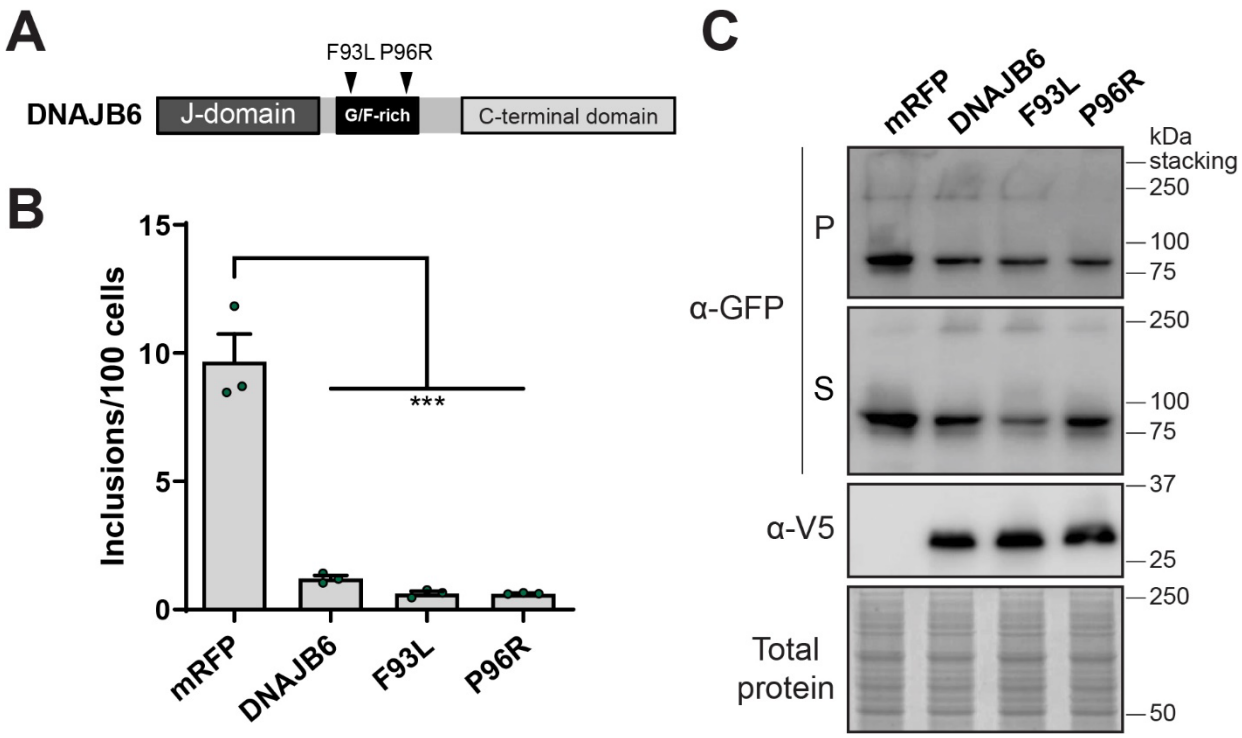

Figure 4.5. Disease-related mutations in the G/F-rich domain of DNAJB6 do not affect its capacity to inhibit Fluc^{DM} inclusions formation. (A) Schematic overview of DNAJB6 disease-related missense mutations at amino acid positions 93 and 96 in the G/F-rich region. HEK293 cells were co-transfected with Fluc^{DM}-EGFP and mRFP (as a negative control) or DNAJB6 wild-type or G/F-domain disease-related mutational variants. Cells were analysed 48 h post-transfection by **(B)** quantitative flow cytometry or **(C)** NP-40 fractionation and immunoblotting. Data in (B) are presented as the mean ± S.E.M (n=3) of the number of inclusions per 100 cells. Significant differences between group means were determined using a one-way ANOVA ($P < 0.05$) followed by a Tukey's post-hoc test. Group means determined to be statistically different from each other are indicated (***$P < 0.001$). In (C) an anti-GFP antibody was used to detect Fluc^{DM} in the insoluble pellet (P) and soluble (S) fractions. The expression of DNAJBs was detected with an anti-V5 antibody in the total protein fraction. Total protein was used as a loading control. The blots shown are from a single experiment.

4.3.5 The C-terminus, and not the serine-rich region of DNAJBs, is required for DNAJBs to suppress Fluc^{DM} inclusion formation in cells

Previous work has suggested that the hydroxyl groups of S/T side chains in the C-terminal domain of DNAJB6 participate in intramolecular hydrogen bonding with polyQ peptides and that this likely mediates inhibition of amyloid formation. For example, increasing the number of S/T residues substituted with alanine (A) residues (from 6, to 13 and to 18 substitutions; variants referred to as M1, M2 or M3, respectively: Figure 4.6A), leads to a progressive loss in the ability of DNAJB6 to inhibit polyQ or amyloid-β aggregation, with the M3 variant being functionally inactive in these assays (Kakkar et al., 2016b, Månsson et al., 2018). Interestingly, we found that the DNAJB6 M1, M2 and M3 variants fully retain their ability to suppress intracellular inclusion formation by Fluc^{DM} (Figure 4.6B, C), indicating that the hydroxyl groups of the S/T-rich domain of DNAJB6 are not required for interaction between DNAJB6 and Fluc^{DM}. Deletion of almost the entire S/T-rich region of the C-terminus of DNAJB6 (M4) did result in abrogation of DNAJB6-mediated suppression of Fluc^{DM} aggregation; however, this is likely due to the structural destabilisation of this DNAJB6 mutant which results in it being readily degraded (Kakkar et al., 2016b), as evidenced by its very low levels in the lysate from transfected cells (Figure 4.6C). Together, these data imply that the residues in DNAJB6 responsible for the inhibition of the amorphous aggregation of Fluc^{DM} into inclusions differ from those used to suppress amyloid fibril-type aggregation of proteins.

To further define the functional regions within the C-terminal domain responsible for the anti-aggregation activity of DNAJBs, the DNAJB6 ΔTTK-LKS deletion construct was co-expressed with Fluc^{DM} in cells (Figure 4.6A). Deletion of the short C-terminal TTK-LKS motif, which in DNAJB8 is dispensable for inhibiting polyQ aggregation (Hageman et al., 2010), does abrogate the capacity of DNAJB6 to inhibit Fluc^{DM} inclusion formation (Figure 4.6D, E). Consistent with the data obtained for DNAJB6, deletion of the TTK-LKS motif in DNAJB8 also abrogated this

activity (Figure 4.6F, G), further indicating different requirements for dealing with amorphous $Fluc^{DM}$ aggregation compared to polyQ aggregation. In line with the results following expression of the M3 isoform of DNAJB6, deletion of the S/T-rich region (ΔSSF-SST) in DNAJB8 had no effect on the ability to suppress the aggregation of $Fluc^{DM}$.

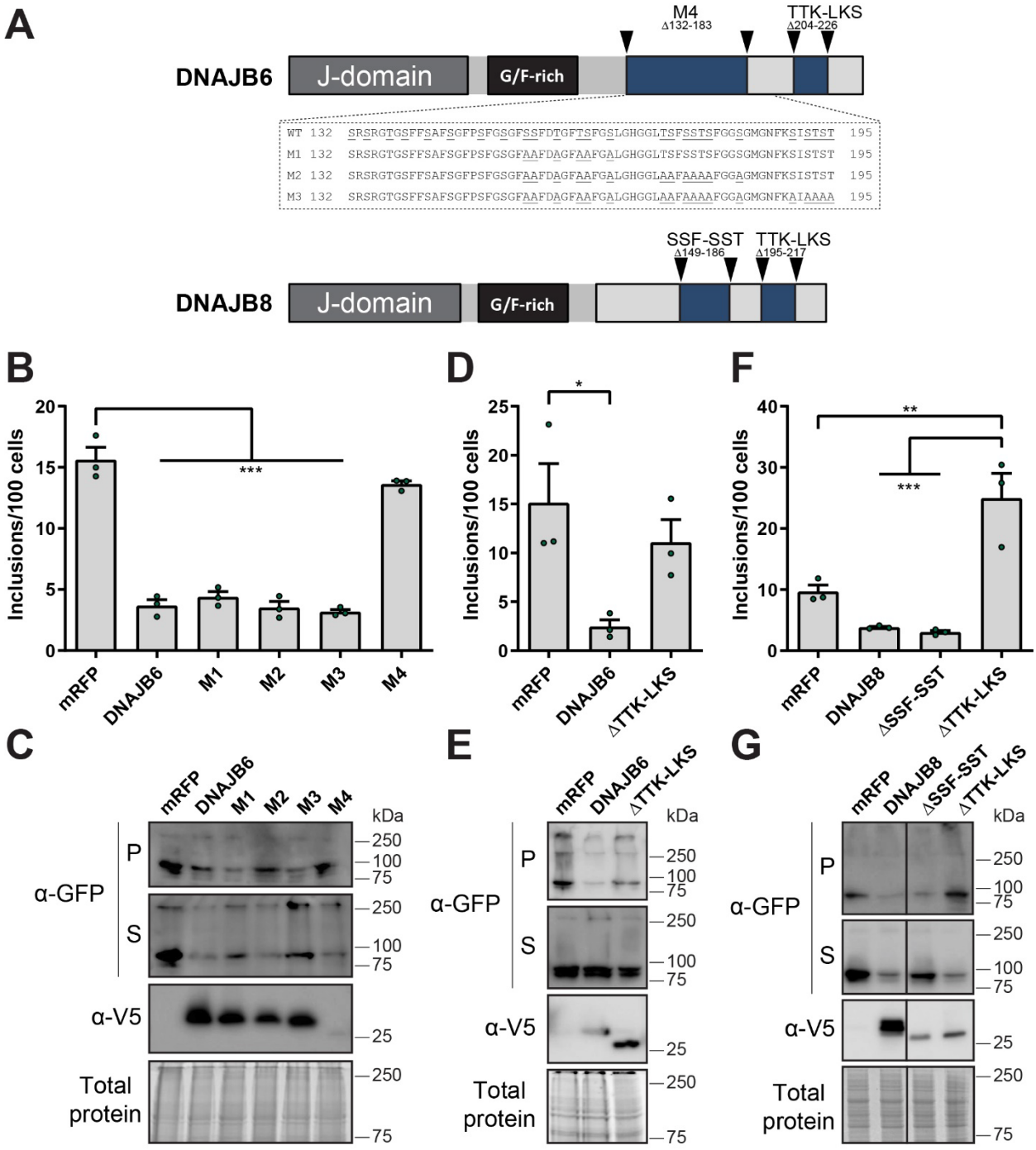

Figure 4.6. The TTK-LKS region in the C-terminus of DNAJB6 and DNAJB8 is required to suppress the aggregation of Fluc^{DM} into inclusions. (A) Schematic overview of DNAJB6 and DNAJB8 C-terminal mutational variants used in this work. Regions identified between sets of arrows indicate deletion mutations. M1, M2 and M3 are mutations in the S/T-rich region of DNAJB6 in which underlined amino acids represent 6, 13 and 18 S/T-to-A substitutions, respectively. HEK293 cells were co-transfected with Fluc^{DM}-EGFP and the indicated V5-tagged DNAJB6 **(B – E)** or DNAJB8 **(F, G)** wild-type or C-terminal mutational variants (or mRFP as a negative control). Cells were analysed 48 h post-transfection by quantitative flow cytometry **(B, D and F)** or NP-40 fractionation and subsequent immunoblotting **(C, E and G)**. Data in (B), (D) and (F) are presented as the mean ± S.E.M (n=3) of the number of inclusions per 100 cells. Significant differences between group means were determined using a one-way ANOVA *(P* < 0.05) followed by a Tukey's post-hoc test. Group means determined to be statistically different from each other are indicated (**P* < 0.05, ***P* < 0.01 and ****P* < 0.001). In (C), (E) and (G) an anti-GFP antibody was used to detect Fluc^{DM} in the insoluble pellet (P) and soluble (S) fractions. The expression of DNAJBs was detected with an anti-V5 antibody in the total protein fraction. Total protein was used as a loading control. The blots shown are from a single experiment.

Immunostaining and confocal microscopy was undertaken on HEK293 cells co-expressing $Fluc^{DM}$ and V5-tagged wild-type DNAJB6/8 or various mutational variants (or mRFP). Cells expressing $Fluc^{DM}$ together with the mRFP (non-chaperone) control contained many punctate $Fluc^{DM}$ inclusions located throughout the cytoplasm whilst mRFP remained diffuse and was expressed in both the cytoplasm and nucleus (Figure 4.7). Overexpression of DNAJB6 or DNAJB8 resulted in fewer cells with $Fluc^{DM}$ inclusions. In those cells with $Fluc^{DM}$ inclusions, the wild-type DNAJBs were co-localised with the inclusions. More cells expressing the DNAJB6 H/Q variant contained $Fluc^{DM}$ inclusions and the H/Q variant also co-localised with the inclusions. As expected, fewer cells that expressed the DNAJB6 M3 variant contained $Fluc^{DM}$ inclusions and co-localisation of $Fluc^{DM}$ inclusions with DNAJB6 M3 was also observed. Conversely, deletion of the TTK-LKS region in DNAJB8 resulted in increased $Fluc^{DM}$ inclusion formation compared to cells expressing wild-type DNAJB8 and DNAJB8 ΔTTK-LKS was not found to co-localise with $Fluc^{DM}$ in inclusions. Together these data suggest that DNAJB6 and DNAJB8 may have at least two regions involved in substrate handling, one that is responsible for proteins that form β-hairpins during amyloid formation (Kakkar et al., 2016b) and another that is required for the handling of destabilised aggregation-prone proteins, such as those represented here by $Fluc^{DM}$.

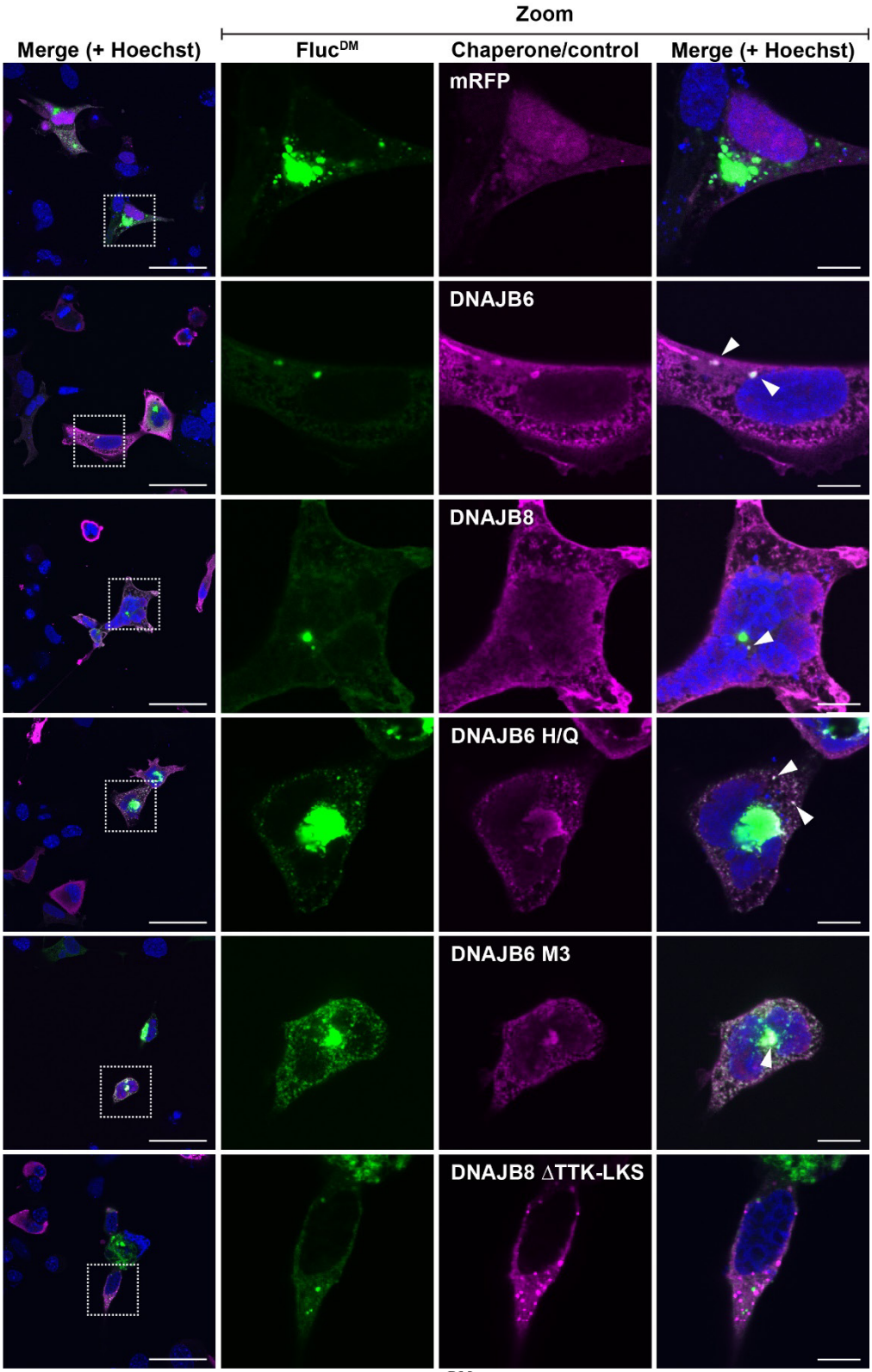

Figure 4.7. DNAJB6 and DNAJB8 co-localise with Fluc^{DM} inclusions and deletion of the TTK-LKS region in the C-terminus abrogates this effect. HEK293 cells were co-transfected with Fluc^{DM}-EGFP and wild-type DNAJB6/DNAJB8 or mutational variants (or mRFP as a negative control) and at 48 h post-transfection were fixed, permeabilised and analysed following immunostaining by confocal microscopy. Expression of Fluc^{DM}-EGFP (*green*) fluorescence was detected by excitation at 488 nm. Expression of the V5-tagged chaperones or mRFP (*magenta*) was detected following excitation at 552 nm and nuclei stained with Hoechst 33482 (*blue*) were excited at 405 nm. All images were taken using the Leica SP8 confocal microscope. Images on the left were taken at 63× magnification and scale bars represent 50 µm. The right-hand panels represent the zoomed-in area indicated by dotted squares in the left panel. Zoomed images were taken at 63× magnification with an additional 4× zoom and scale bars represent 10 µm. Representative cells containing Fluc^{DM}-EGFP inclusions co-localised with V5-tagged wild-type DNAJBs or mutational variants are denoted by the arrows. Images shown are representative of two experiments.

4.4 Discussion

In this work, we demonstrate that the DNAJB molecular chaperones are potent suppressors of the aggregation of Fluc^{DM} into inclusions in cells. This contrasts with what has been observed previously, whereby only specific DNAJB isoforms suppress the aggregation of polyQ-expanded proteins (Hageman et al., 2010). For DNAJB1, DNAJB6 and DNAJB8, we show that they inhibit Fluc^{DM} aggregation in a manner that depends on their ability to interact with Hsp70 and is associated with the cellular capacity to degrade Fluc^{DM} via the proteasome, thereby alleviating protein aggregation. For DNAJB6 and DNAJB8, the suppression of Fluc^{DM} aggregation not only appears mechanistically different from DNAJB1, but is also distinct from what has been reported previously for the handling of amyloid-fibril forming proteins, such as polyQ-expanded proteins and the amyloid-β peptide (Hageman et al., 2010, Kakkar et al., 2016b, Månsson et al., 2018). Whilst the S/T-rich region and, to some extent, the G/F-rich region (Sarparanta et al., 2012, Thiruvalluvan et al., 2020) in DNAJB6 and DNAJB8 are essential for amyloid suppression, these regions are not required to inhibit Fluc^{DM} inclusion formation. Finally, we identified a short, 23 amino acid (TTK-LKS) sequence in the C-terminus of DNAJB6 and DNAJB8 that is required to inhibit Fluc^{DM} inclusion formation: this region in these proteins is dispensable for suppression of polyQ aggregation (Hageman et al., 2010). Thus, whilst DNAJB6 and DNAJB8 are both potent inhibitors of polyQ and Fluc^{DM} aggregation, the mechanism by which they interact with these aggregation-prone proteins is different. Our data suggests that DNAJB6-like proteins possess distinct regions for interacting with clients and that this is likely dictated by the structure or composition of the aggregation-prone protein.

The S/T-rich stretch in DNAJB6 (amino acids 155-195) and DNAJB8 (amino acids 149-186) is highly conserved between these proteins. It has been proposed that interaction with hydroxyl groups in side chains of these S/T residues inhibits primary nucleation by outcompeting for hydrogen bonding essential for β-hairpin and mature amyloid fibril formation, thereby suppressing

aggregation (Kakkar et al., 2016b). DNAJB2 also contains a partial serine-rich stretch and, although it is not confirmed to be involved in polyQ handling, is also more effective than DNAJB1 and DNAJB5 (which lack this region) at suppressing polyQ aggregation (Hageman et al., 2010). DNAJB5 shares close homology to DNAJB1 (Chen et al., 1999) and has been shown to interact with Hsp70 (Hageman et al., 2011). Moreover, since DNAJB5 was also identified as a potent suppressor of $Fluc^{DM}$ inclusion formation, it is likely that DNAJB1 and DNAJB5 inhibit $Fluc^{DM}$ aggregation into inclusions via a similar mechanism. Mutation or deletion of the S/T-rich region did not result in loss of the ability of DNAJB6 or DNAJB8 to suppress the aggregation of $Fluc^{DM}$ into inclusions, indicating that a different region of the protein is involved in this process. Interestingly, DNAJB1 and the other DNAJBs we tested were all capable of suppressing $Fluc^{DM}$ aggregation. Whilst our data does not provide insight into the domains required by these other DNAJBs to prevent $Fluc^{DM}$ aggregation, our work has identified a short TTK-LKS (TTKRIVENGQERVEVEEDGQLKS) fragment conserved between DNAJB6 (amino acids 204-226) and DNAJB8 (amino acids 195-217) that is crucial for the handling of $Fluc^{DM}$. Since this TTK-LKS domain in DNAJB8 is dispensable for its capacity to inhibit polyQ aggregation (Hageman et al., 2010), our findings are the first to demonstrate that DNAJB6 and DNAJB8 have two distinct regions for handling client proteins. Little is currently known regarding the functional role of this conserved TTK-LKS motif in DNAJB6 and DNAJB8. However, based on our current data, we hypothesise that it is either directly or indirectly involved in binding hydrophobic patches in destabilised aggregation-prone proteins.

Recent structural homology modelling of the DNAJB6 dimer/oligomer revealed four β-strands within the C-terminal domain of DNAJB6 (Söderberg et al., 2018). Dimerisation of each DNAJB6 monomer likely occurs via same-to-same-residue crosslinks at lysine residues K189 and K232 within the first and fourth β-strands, respectively. When cross-linked to form a dimer, the symmetrically positioned β-strands within DNAJB6 monomers form a peptide-binding pocket that

is surface exposed and lined with the S/T residues responsible for binding fibrillar proteins. Based on these structural data, the TTK-LKS region (which lies downstream of the S/T-rich region) is contained within the fourth β-strand of DNAJB6/8, which is surface-exposed in the monomeric and dimeric form of DNAJB6. Thus, this region has the potential to be a second substrate binding region in DNAJB6/8, responsible for binding hydrophobic aggregation-prone client proteins.

One possible reason why DNAJB6 and DNAJB8-like proteins possess distinct mechanisms to interact with aggregation-prone client proteins is due to intrinsic structural differences in the misfolded states of proteins that lead to the formation of amorphous aggregates as opposed to amyloid fibrils. PolyQ-expanded proteins form large, tightly aggregated structures that are extremely insoluble and typical of amyloidogenic deposits (Hageman et al., 2010, Kubota et al., 2011). The R188Q and R261Q mutations in the N-terminus of Fluc used in this study conformationally destabilises the protein (Gupta et al., 2011), thereby inducing protein misfolding and increased regions of exposed hydrophobicity. This causes the protein to form aggregates that are SDS-soluble and localise into diffuse cytosolic inclusions (Gupta et al., 2011), distinct from the amyloid-like aggregates formed by polyQ-expanded proteins. Indeed, when both polyQ-expanded huntingtin and $Fluc^{DM}$ are expressed together in human cell lines, the two proteins deposit into distinct aggregated structures (Gupta et al., 2011), reaffirming that they aggregate via different mechanisms. Importantly, our data highlight that it may be possible to design therapeutics that boost the ability of DNAJB6/8 to prevent amyloid fibril formation associated with disease, whilst not impacting its capacity to interact with highly destabilised aggregation-prone proteins destined for degradation by the proteasome.

A major finding of this work is that all of the DNAJBs tested significantly inhibited $Fluc^{DM}$ inclusion formation, a result which contrasts with previous observations regarding the suppression of polyQ-expanded protein aggregation, whereby only a subset of DNAJB isoforms were effective

(Hageman et al., 2010). Whilst we identified that the TTK-LKS motif in DNAJB6 and DNAJB8 is essential for these proteins to prevent the intracellular aggregation of destabilised client proteins, such as Fluc^{DM}, this does not account for the capacity of other DNAJBs (that lack this region) to suppress inclusion formation by Fluc^{DM}. Our data are nevertheless largely consistent with findings on mutant Parkin in which the overexpression of most DNAJ proteins tested reduced its propensity to form amorphous aggregates (Kakkar et al., 2016a). Also, in the case of an ALS-causing mutant SOD1 protein, overexpression of multiple DNAJs (albeit not all) supressed its aggregation (Serlidaki et al., 2020). In all these cases, including our current data, the effects coincided with a reduction in steady state levels of the mutant protein. Whilst we cannot formally exclude effects of quality control during co-translational folding, we favour the hypothesis that the various DNAJs recognise and bind to these (partially) misfolded substrates post-translationally to support their proteasomal degradation (Kakkar et al., 2016a; this report). This mechanism is distinct from that seen for polyQ proteins which aggregate in a precise and ordered manner that can be chaperoned by distinct binding regions present only in the DNAJB6-like proteins (i.e. DNAJB2, DNAJB6, DNAJB7 and DNAJB8). The global unfolding of the other more structurally destabilised proteins may expose many hydrophobic surfaces that can be recognised by the multiple different substrate binding sites in DNAJB1-like proteins and by other regions of the DNAJB6-like chaperones. Future studies to elucidate the specific region(s) within DNAJB1-like proteins that act to suppress the aggregation of destabilised client proteins could utilise a similar approach to that undertaken in this work, by encompassing a range of deletion mutations located throughout the C-terminal substrate binding domain(s).

In conclusion, we have utilised the proteostasis sensor Fluc^{DM} to demonstrate that overexpression of the DNAJB molecular chaperones acts to boost the protein quality control capacity of cells. We demonstrate that the ability of DNAJBs to inhibit the aggregation of Fluc^{DM} into inclusions relies on interaction with Hsp70 and this facilitates degradation of Fluc^{DM} by the proteasome.

Significantly, we show that the TTK-LKS region in the C-terminal domain of DNAJB6 and DNAJB8 is essential for engaging this destabilised client protein to prevent its aggregation. Moreover, we show that the S/T-rich region of DNAJB6-like proteins that mediates interactions with amyloid-forming client proteins is not involved in suppressing $Fluc^{DM}$ aggregation. Overall, our data emphasises the important role of DNAJB molecular chaperones in preventing all forms of protein aggregation in cells and highlights the potential of targeting them for the amelioration of diseases associated with protein aggregation.

Chapter 5: A method to quantitatively measure the proteostasis capacity of cells

5.1 Introduction

The proteostasis capacity of a cell can be defined as the ability to prevent protein accumulation and aggregation into intracellular inclusions. Thus, proteostasis capacity is highly dependent on the protein quality control network. The ability to quantitatively measure the proteostasis capacity of a cell is an important step towards deciphering why some cell types are more susceptible to the formation of inclusions than others. This is especially true given that the proteostasis capacity of a cell is known to influence the rate at which misfolded proteins accumulate (Gidalevitz et al., 2006, Hutt et al., 2009, Powers et al., 2009, Gidalevitz et al., 2010). Thus, a decline in proteostasis capacity is linked to an impaired ability of a cell to prevent protein aggregation, which can lead to the onset and progression of toxicity associated with disease (Brehme et al., 2014, Hipp et al., 2014). Work towards characterising the proteostasis capacity of cells is an important first step in understanding why this varies between cell types.

The innate ability of a cell to prevent protein aggregation is known to vary significantly among different cell types (Lim and Yue, 2015). For example, it has been proposed that neurons have a reduced capacity to prevent the formation of inclusions (Saxena and Caroni, 2011), as neuronal loss and neurodegeneration are often characterised by the accumulation of misfolded proteins into inclusions (Soto and Pritzkow, 2018). However, it remains to be definitively established why neurons in particular are so vulnerable to inclusion formation. Since neurons are long-lived cells, it is likely a result of their post-mitotic inability to dilute toxic protein species through cell-division and/or due to an age-related failure in the mechanisms that act to degrade and clear aggregation-prone proteins (Balch et al., 2008, Powers et al., 2009, Liu et al., 2011, Proctor and Lorimer, 2011, Taylor and Dillin, 2011). Neuron-specific degeneration in the context of disease occurs despite many aggregation-prone proteins being ubiquitously expressed (sometimes at higher concentrations) in other cells of the body. It has been hypothesised that the relative susceptibility of some cells to inclusion formation is due to intrinsic differences in the cellular protein quality

control systems that maintain proteostasis (Finkbeiner et al., 2006, Komatsu et al., 2006, Malhotra and Kaufman, 2007, Rutkowski and Kaufman, 2007, Morimoto, 2008, Matus et al., 2011).

Few studies have used quantitative cell-based experiments to elucidate the precise roles each of these protein quality control systems have on proteostasis. The protein quality control network comprises the systems that act to prevent protein aggregation, for example, through proper guidance of protein folding or assisting in protein degradation (Kampinga and Bergink, 2016). These systems encompass all of the responses in the cell that are activated by proteotoxic stress and include the ER-unfolded protein response, the HSF1-mediated heat-shock response and proteolytic processing by the degradation machinery (i.e. autophagy or the ubiquitin-proteasome system). Whilst many studies have utilised genetic or pharmacological approaches to probe the molecular mechanisms involved in protein folding and misfolding in cells (Seglen and Gordon, 1982, Lee and Goldberg, 1998, Yamamoto et al., 1998, Taylor et al., 2007, Lee et al., 2010, Oslowski and Urano, 2011, Hou et al., 2012, Wang et al., 2017), no work has been done to systematically assess the impact that modulation of the protein quality control network has on the capacity of neuronal-like cells to prevent the formation of inclusions by an aggregation-prone protein.

In order to better understand the molecular mechanisms that underpin diseases associated with protein aggregation, and to advance the development of therapeutic strategies, methods to quantitatively measure the proteostasis capacity of a cell are essential. To address this, aggregation-prone $Fluc^{DM}$ was exploited to quantitatively compare the ability of two neuronal cells lines (mouse neuroblastoma cells [Neuro-2a] cells and mouse neuroblastoma × motor neuron hybrid [NSC-34] cells) to prevent the formation of inclusions. The impact of specific protein quality control pathways on the capacity of each cell line to prevent the formation of inclusions was also assessed. Previous work conducted to delineate differences in the proteomes of Neuro-

2a and NSC-34 cells revealed that these cell types are highly similar with regard to their global proteomes (Hornburg et al., 2014). However, the work presented in this chapter demonstrates that $Fluc^{DM}$ forms inclusions more readily in NSC-34 cells compared to Neuro-2a cells. The inclusions formed by $Fluc^{DM}$ in both Neuro-2a and NSC-34 cells were purified in order to identify differences in the types of proteins that engage with aggregation-prone proteins in these cells. The impact that protein quality control systems have on inclusion formation in these neuronal-like cells was also investigated. Overall, the work presented in this chapter is a step towards using a model aggregation-prone protein to quantitatively measure the proteostasis capacity of cells, and thus understanding why some cells are vulnerable to proteome dysfunction, leading to the formation of inclusions.

5.2 Methods

5.2.1 Plasmid constructs

The pcDNA3.1 constructs encoding wild-type HSF1 ($HSF1^{WT}$), a constitutively active form of HSF1 ($HSF1^{+}$) that has a deletion of the sequence encoding amino acids 203-315 (i.e. Δ203-315) of the regulatory domain, and an inactive variant of HSF1 ($HSF1^{-}$) that has a deletion of amino acids 453-523 (i.e. Δ453-523) located in the transcription activation domain, previously described by Taylor et al. (2007), were generously donated by Professor Heather Durham (McGill University, Canada). The $Ub^{[9]}$-mRFP plasmid originally described by Salomons et al. (2009) was gifted by Dr Luke McAlary and Professor Justin Yerbury (both of the University of Wollongong, Australia).

5.2.2 Cell culture, transfection and treatment of Neuro-2a and NSC-34 cells

Neuro-2a and NSC-34 cells were cultured as described in section 2.4.1. Unless otherwise specified, 1.3×10^5 cells/mL were seeded into 6-well or 12-well plates, or 8-well chamber µ-Slides and cultured in DMEM/F-12 with L-glutamine and 10% (v/v) FCS by incubation overnight at 37°C. In a 6-well plate, cells were transiently transfected with 2 µg/well of plasmid DNA using Lipofectamine® LTX/PLUS™ (6 µL/well of Lipofectamine® LTX and 2 µL/well PLUS™ reagent) or Lipofectamine™ 3000 (3 µL/well of Lipofectamine™ 3000 and 4 µL/well P3000 reagent) reagents, according to the manufacturer's instructions. For experiments involving co-transfections, complexes at a ratio of 4:1 of $Fluc^{DM}$-EGFP to chaperone, $Ub^{[9]}$-$mRFP^{[1]}$, HSF1 (or one of its mutational variants) or mRFP plasmid DNA were mixed together prior to the addition of the transfection reagent. DNA/reagent complexes were added in a dropwise manner to cells. Untransfected controls received equivalent volumes of Lipofectamine® LTX/PLUS™ or Lipofectamine™ 3000 reagents, but did not receive any plasmid DNA.

In some experiments, Neuro-2a and NSC-34 cells expressing $Fluc^{DM}$-EGFP were treated with various compounds known to modulate protein quality control pathways, namely the ER network, autophagy and the ubiquitin-proteasome system. To modulate the ER network, 24 h post-transfection cells were treated with 3 μM thapsigargin (to induce ER stress) or 20 μM azoramide (to upregulate ER resident chaperones for improved ER protein folding) and cells were incubated for a further 16 h prior to analysis. To modulate autophagy, 32 h post-transfection cells were treated with 1 μM bafilomycin A1 (inhibits late-stage autophagy) or rapamycin (binds mTOR to upregulate autophagy) and were incubated for a further 16 h before analysis. To inhibit the proteasome, 42 h post-transfection cells were treated with 10 μM MG132 and incubated for an additional 6 h. In each of these experiments an equivalent volume of DMSO was added to control samples. The concentrations of thapsigargin (Oslowski and Urano, 2011, Cox and Ecroyd, 2017), azoramide (Fu et al., 2015), bafilomycin A1 (Yoshimori et al., 1991), rapamycin (Ravikumar et al., 2004) and MG132 (Tanaka et al., 2004, Li et al., 2010) used in these experiments were chosen based on previous work.

5.2.3 Confocal microscopy to assess inclusion formation

Neuro-2a and NSC-34 cells were plated and transfected as above (section 5.2.2) and inclusions formed following expression of $Fluc^{WT}$-EGFP, $Fluc^{DM}$-EGFP or EGFP (as a control) were analysed directly in 8-well chamber μ-Slides. Cells were incubated for 37°C for 48 h prior to being analysed by confocal microscopy. Live cells were analysed using a Leica TCS SP5 confocal microscope and the 63× oil-immersion objective lens (Leica Microsystems), controlled by the LAS-AF Version 3 software. EGFP fluorescence was detected by excitation at 488 nm.

5.2.4 Flow cytometry assays to assess inclusion formation

Standard flow cytometry, including PulSA and FloIT analyses of cells, was conducted as per sections 2.6, 2.6.1 and 2.6.2, with slight modifications. To account for differences in protein

expression between the Neuro-2a and NSC-34 cell lines, PulSA analysis was only conducted on an equivalent subset of EGFP-positive events expressed by both cell types.

5.2.5 Flow cytometry to measure the relative proteostasis capacity of Neuro-2a and NSC-34 cells

Neuro-2a and NSC-34 cells were plated as described above in a 6-well plate and incubated at 37°C for 24 h. Both cell lines were then transfected (or not) to express EGFP, Fluc^{WT}-EGFP or Fluc^{DM}-EGFP using 2 μg of plasmid DNA/well. Following a 48 h incubation, cells were trypsinised, harvested and washed before being analysed by flow cytometry (section 2.6). In order to compare the relative propensity of Fluc to form aggregates in Neuro-2a and NSC-34 cells (and hence the capacity of cells to prevent aggregation), three different strategies were employed. Two of these strategies involved the use of PulSA. First, live, EGFP-positive cells were identified and selected (using the untransfected cells as a negative control), and the geometric mean of the EGFP fluorescence in EGFP-positive cells was determined (indicating the level of Fluc expression in the cell). The percentage of cells identified to contain inclusions, as assessed by PulSA, along with the EGFP geometric mean (of cells expressing Fluc^{WT}-EGFP or Fluc^{DM}-EGFP) were used to generate a PulSA aggregation index (PulSA$_{AI}$):

$$\text{PulSA}_{AI} = \frac{\text{Cells with inclusions (\%)}}{\text{EGFP Geometric mean}} \times 100 \qquad \text{(Equation 5.1)}$$

A second approach using PulSA was employed to determine the proportion of cells with inclusions as the levels of Fluc increased in the cells. To do so, EGFP-positive cells were identified and binned into groups based on their levels of EGFP fluorescence: On a $\log_{10}$-based scale, 16 gates (bins) of equal size were used to subdivide the EGFP-positive cells. PulSA was then performed on cells within each of these bins to determine the proportion of cells with inclusions in each bin (only bins with >100 cells were analysed). Data are presented as a plot of the bin number versus the proportion of cells with inclusions in that bin.

The third approach used to ascertain the relative propensity of Fluc to form inclusions in Neuro-2a and NSC-34 cells involved the use of FloIT analysis on these same cells. The number of inclusions/100 cells was determined using the gating strategies specified above (section 5.2.4) and equation 2.1. An aggregation-index based on FloIT analysis ($FloIT_{AI}$) was calculated using the following equation:

$$\text{FloIT}_{AI} = \frac{\text{Inclusions/100 cells}}{\text{EGFP Geometric mean}} \times 100 \qquad \text{(Equation 5.2)}$$

5.2.6 Time-resolved fluorescent imaging and image analysis to track inclusion formation

Fluorescence imaging of live cells was conducted on Neuro-2a and NSC-34 cells to assess the effects of inclusion formation by $Fluc^{WT}$ or $Fluc^{DM}$ (or EGFP as a control) on cell survival in real-time, using the IncuCyte® automated fluorescence microscope (Essen BioScience, Ann Arbor, MI, USA). Immediately following transfection (see section 5.2.2), cells were placed into the microscope. At least 4 images were acquired per well at 3 h time points over 192 h using the 10× objective in the phase (bright field) and green channel. A standard exposure time of 400 milliseconds was chosen to capture fluorescence in the green channel. The processing definition generated to analyse images acquired in the phase channel utilised segmentation adjustment (0.5 towards background) and clean-up (hole fill = 0 μm^2, pixel size = - 2). The processing definition produced to quantify fluorescence in the green channel used Top-Hat subtraction (radius = 25 µm, threshold = 0.8 GCU), edge split (edge sensitivity = 4) and clean-up (hole fill = 0 μm^2, pixel size = - 1).

The following equations used for analysis and data presentation were performed as described by McAlary et al. (2016) with modifications. The number of green objects (i.e. $EGFP_{+ve}$ cells) at each time point ($EGFP_{tx}$), was normalised to the value determined in the first scan immediately after plating ($EGFP_{t0}$):

$$\text{Normalised EGFP}_{tx} = \frac{\text{EGFP}_{tx}}{\text{EGFP}_{t0}} \qquad \text{(Equation 5.3)}$$

The number of $EGFP_{tx}$ of cells was then normalised to the total number of cells (phase object count) at the corresponding time point:

$$EGFP_{+ve} \text{ cells relative to total number of cells} = \frac{\text{Normalised sample } EGFP_{tx}}{\text{Sample phase object count}} \quad \text{(Equation 5.4)}$$

The normalised values at each time point taken from equation 5.4 ($EGFP_{+ve}$ cells relative to total number of cells) were divided by the normalised EGFP data at the same time point to determine the proportion of EGFP-positive cells for each transfection, relative to those cells expressing EGFP alone.

5.2.7 Purification of $Fluc^{DM}$ inclusions from SDS-PAGE

In order to purify $Fluc^{DM}$-EGFP inclusions from Neuro-2a and NSC-24 cells to identify proteins contained within these inclusions, cells were harvested, fractionated and the insoluble protein was extracted and quantified for loading onto SDS-PAGE gels as outlined in section 2.7.2. SDS-PAGE was undertaken as per section 2.7.3, with the following modifications. Native loading buffer without reducing agents (final concentrations: 200 mM Tris-HCl, 40% (v/v) glycerol, 0.01% (w/v), pH 8.6), was added to insoluble cell lysates and the samples were heated at 45°C for 5 min prior to loading onto SDS-PAGE gels, which were then run as previously described (section 2.7.3). Gels were placed into Milli-Q water and immediately imaged using the ChemiDoc™ Imaging System and the Pro-Q Emerald 488 exposure setting (exposure time ~ 5 sec) to visualise EGFP fluorescence from $Fluc^{DM}$-EGFP. Proteins were then fixed in Coomassie Blue staining solution and de-stained using de-staining solution as previously described (section 2.7.3). Regions of the stacking gel identified to contain aggregated $Fluc^{DM}$-EGFP (based on the in-gel fluorescence) were cut out using a clean razor blade and fixed in 10% (v/v) acetic acid for proteomic mass spectrometry. Untransfected Neuro-2a and NSC-34 cells were used as controls and treated as above in order to identify endogenous proteins or protein complexes that are found in the same region of the stacking gel. The subsequent in-gel trypsin digest and proteomic mass spectrometry

of the $Fluc^{DM}$ inclusions were performed by Dr Albert Lee and Ms Flora Cheng (Macquarie University, Sydney, Australia) as described below.

5.2.8 In-gel trypsin digestion

Excised protein gel bands were further de-stained in 50% (v/v) acetonitrile (ACN) and 50 mM ammonium bicarbonate (pH 8.0) and dehydrated in 100% ACN. The gel pieces were dried by vacuum centrifugation, reduced with 10 mM dithiothreitol at 55°C for 30 min and alkylated with 20 mM iodoacetamide at room temperature for 30 min. The gel pieces were then rehydrated with trypsin (12.5 ng/µL; Promega) and resuspended in 50 mM ammonium bicarbonate (pH 8.0), where the proteins were then digested overnight at 37°C. The digestion was inactivated by the addition of 2 µL of formic acid. Tryptic peptides were extracted twice with 50% (v/v) ACN and 2% (v/v) formic acid and dried under vacuum centrifugation. The peptides were resuspended in 0.1% (v/v) formic acid and desalted on a pre-equilibrated C_{18} Omix Tip (Agilent, Santa Clara, CA, USA) and eluted in 50 % (v/v) ACN, 0.1% (v/v) formic acid, and dried under vacuum centrifugation.

5.2.9 Reverse phase C_{18} liquid chromatography mass spectrometry (RP-LC-MS/MS)

Lyophilised peptides were resuspended in 0.1% (v/v) formic acid and sonicated for 20 min in a sonication bath (Branson Ultrasonics). The resuspended peptides were then centrifuged at 14,000 × *g* for 15 min to remove any insoluble debris, and the clarified peptides were analysed by LC-MS/MS. The peptides were separated on an UltiMate™ 3000 RSLCnano system (Thermo Fisher Scientific) fitted with an Acclaim PepMap RSLC column (Thermo Fisher Scientific), making use of a 60 min gradient (2-95% (v/v) ACN, 0.1% (v/v) formic acid) running at a flow rate of 300 nL/min. Peptides eluted from the nano-LC column were subsequently ionised into the Q Exactive™ Plus Hybrid Quadrupole-Orbitrap™ Mass Spectrometer (Thermo Fisher Scientific). The electrospray source was fitted with a 10 µm emitter tip (New Objective, Woburn, MA, USA) and maintained at 1.6 kV electrospray voltage. The temperature of the capillary was set to 250°C.

Precursor ions were selected for MS/MS fragmentation using a data-dependent "Top 10" method operating in Fourier transform (FT) acquisition mode with Higher C-trap Dissociation (HCD) fragmentation. FT-MS analysis on the Q Exactive™ Plus was carried out at 70,000 resolution and an automatic gain control (AGC) target of 1×10^6 ions in full MS. MS/MS scans were carried out at 17,500 resolution with an AGC target of 2×10^4 ions. Maximum injection times were set to 30 and 50 milliseconds, respectively. The ion selection threshold for triggering MS/MS fragmentation was set to 25,000 counts and an isolation width of 2.0 Da was used to perform HCD fragmentation with normalised collision energy of 27.

Raw spectra files were processed using the Proteome Discoverer software 2.4 (Thermo Fisher Scientific) incorporating the Sequest search algorithm. Peptide identifications were determined using a 20 ppm precursor ion tolerance and a 0.1 Da MS/MS fragment ion tolerance for FT-MS and HCD fragmentation. Carbamidomethylation modification of cysteines was considered a static modification while oxidation of methionine, deamidation of asparagine and glutamine, and acetyl modification on N-terminal residues were set as variable modifications allowing for a maximum of two missed cleavages. The data were processed through Percolator for estimation of false discovery rates. Protein identifications were validated employing a q-value of 0.01. The relative abundance of proteins within each sample was calculated by the Proteome Discoverer 2.4 software using the cumulative intensities of unique peptides. Only proteins identified with an abundance ≥ 2-fold higher than in the untransfected control, and which appeared in all three biological replicates of each sample were considered for further analyses.

5.2.10 Functional pathway enrichment analysis of proteins identified within Fluc^{DM} inclusions

Venn diagrams constructed to show the overlap of proteins identified in Fluc^{DM} inclusions in Neuro-2a and NSC-34 cells were produced using the Ven de Peer lab's Bioinformatics and

Evolutionary Genomics online tool (http://bioinformatics.psb.ugent.be/webtools/Venn). The functional enrichment analysis of the Kyoto Encyclopedia of Genes and Genomes (KEGG) biological pathways represented by proteins identified to co-interact with $Fluc^{DM}$ inclusions in Neuro-2a and NSC-34 cells was conducted using g:Profiler (Raudvere et al., 2019) with the following parameters: organism: *Mus Musculus*, statistical domain scope: only annotated genes, multiple testing significance threshold: g:Profiler tailor made g:SCS, user threshold: $P \leq 0.05$ and data sources: biological pathways – KEGG. To identify the classes of proteins enriched in these samples, Protein Annotation through Evolutionary Relationship (PANTHER) analysis was conducted using the following settings: organism: *Mus Musculus*, analysis: functional classification viewed as pie chart, ontology: protein class. Pie charts were constructed whereby the number of genes was expressed as a percentage of the total number of protein class hits. Dr Albert Lee performed the STRING analysis (Szklarczyk et al., 2017) of overlapping proteins identified with $Fluc^{DM}$ inclusions in both Neuro-2a and NSC-34 cells using Cytoscape (Shannon et al., 2003) and data are presented to show how the proteins identified were clustered based on protein class using the Reactome database (Croft et al., 2014).

5.2.11 Cellular protein fractionation and subsequent immunoblotting

Cells were fractionated and protein was extracted and quantified as outlined in sections 2.7.1 and 2.7.2. Subsequent SDS-PAGE and immunoblotting was undertaken as described in sections 2.7.3 and 2.7.4.

5.2.12 Antibodies

Refer to Table 2.1 in section 2.2 for antibodies and dilutions used for immunoblotting.

5.2.13 Immunocytochemistry, tUi staining and confocal microscopy

Free ubiquitin levels were measured in Neuro-2a and NSC-34 cells co-expressing Fluc^{DM}-EGFP and Ub$^{[9]}$-mRFP (or mRFP) using the high-affinity free ubiquitin sensor tUi-HA, described previously by Choi et al. (2019), and expressed and purified as outlined by Farrawell et al. (2020). Neuro-2a and NSC-34 cells were grown and transfected in 8-well chamber µ-slides as above (section 5.2.2). Immunocytochemistry and confocal microscopy were then performed as outlined in section 2.5, with the following modifications. Briefly, following blocking overnight, cells were incubated with the tUi-HA probe, diluted to a final concentration of 7.5 µg/mL in blocking buffer, for 30 min at room temperature followed by 3 washes with rocking (each for 10 min) in 0.1% (v/v) Triton X-100 in PBS. Cells were incubated with an anti-HA antibody (1:1000; ab9110, Abcam) diluted in blocking buffer for 1 h at room temperature and then washed 3 times (each for 10 min) with gentle rocking in 0.1% (v/v) Triton X-100 in PBS. Cells were incubated with the Alexa Fluor 647-conjugated anti-rabbit-IgG secondary antibody (1:1000; ab150079, Abcam) diluted in blocking buffer for 1 h at room temperature in the dark. Cells were then washed, stained with the Hoechst 33342 nucleic acid stain and imaged using the SP8 TCS confocal microscope and 20× objective lens as described in section 2.5.

5.2.14 Epifluorescence microscopy

Inclusions formed in Neuro-2a and NSC-34 cells following the co-expression of Fluc^{DM}-EGFP and either HSF1^{WT}, HSF1^{+} or HSF1^{-} were analysed directly in 6-well plates 48 h post-transfection by epifluorescence microscopy. Fluorescence from EGFP was detected following excitation at 488 nm. All images were taken at 20× magnification using a Leica DMi8 fluorescence microscope. Images were prepared with the LAS-AF Version 3 software.

5.2.15 Statistics

Statistical analyses were performed as described in section 5.2.15.

5.3 Results

5.3.1 Measuring the relative capacity of Neuro-2a and NSC-34 cells to prevent the aggregation of Fluc^{DM} into inclusions

The aggregation propensity of Fluc^{DM} was exploited in order to measure and compare the relative capacities of Neuro-2a and NSC-34 cells to prevent inclusion formation by aggregation-prone proteins. First, the presence and localisation of Fluc-based inclusions formed in Neuro-2a (*top*) and NSC-34 (*bottom*) cells was analysed 48 h post-transfection by confocal microscopy (Figure 5.1). Neuro-2a and NSC-34 cells expressing EGFP (*left*) exhibited soluble and diffuse green fluorescence throughout the cytoplasm and the nucleus. Punctate inclusions formed by Fluc^{WT}-EGFP (*centre*) were occasionally observed in transfected Neuro-2a and NSC-34 cells (< 3% of transfected cells). Both Neuro-2a and NSC-34 cells expressing Fluc^{DM}-EGFP (*right*) had a greater population of transfected cells containing inclusions (~ 15%) compared to cells expressing EGFP or Fluc^{WT}-EGFP. Overall, it was concluded that Fluc^{DM}-EGFP forms inclusion in both Neuro-2a and NSC-34 cells under these experimental conditions.

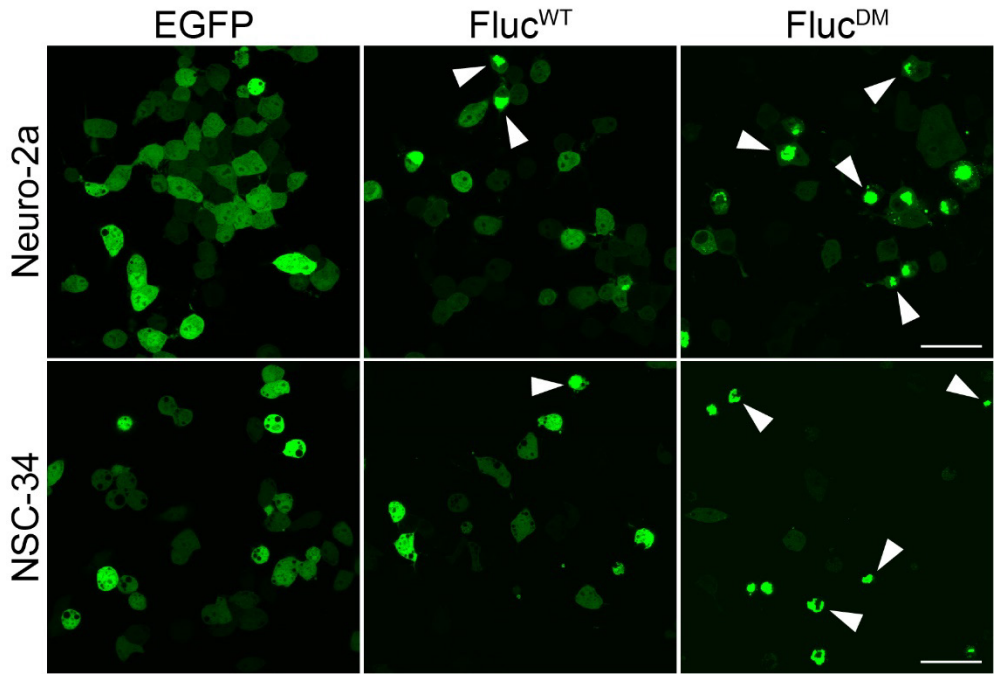

Figure 5.1. Characterisation of the formation of inclusions by Fluc in Neuro-2a and NSC-34 cells, as assessed by confocal microscopy. Neuro-2a and NSC-34 cells were transiently transfected to express EGFP, Fluc^{WT}-EGFP or Fluc^{DM}-EGFP and live cells were analysed 48 h post-transfection by confocal microscopy to examine the formation of inclusions. Images are representative of three experiments and show confocal micrographs of Neuro-2a (*top*) and NSC-34 (*bottom*) cells transfected with EGFP (*left*), Fluc^{WT}-EGFP (*centre*) or Fluc^{DM}-EGFP (*right*). EGFP fluorescence was detected by excitation at 488 nm. Arrowheads indicate cells with inclusions. All images were taken using a Leica SP5 confocal microscope and the 63× oil-immersion objective lens. Scale bar represents 50 µm.

Next, to determine the relative capacity of Neuro-2a and NSC-34 cells to maintain $Fluc^{DM}$-EGFP in a non-aggregated state, cells were transiently transfected with EGFP, $Fluc^{WT}$-EGFP or $Fluc^{DM}$-EGFP for 48 h and then analysed via the flow cytometric method PulSA. In Neuro-2a cells expressing $Fluc^{WT}$-EGFP or $Fluc^{DM}$-EGFP, the proportion of cells with inclusions was identified to be 2.0 ± 0.4% and 3.7 ± 0.2% respectively, whilst for NSC-34 cells the proportion of cells containing inclusions was 2.1 ± 0.6% and 8.3 ± 0.8% (Figure 5.2A). To further assess and compare the capacity of Neuro-2a and NSC-34 cells to prevent aggregation of Fluc, an aggregation index (AI) was calculated based upon the data obtained from PulSA ($PulSA_{AI}$). This aggregation index provides a first step towards establishing a quantitative evaluation of the susceptibility of a particular cell type to the formation of inclusions by Fluc. In order to take into account the amount of Fluc expressed in the different cell populations, the geometric mean of the EGFP-positive cells was determined (Figure 5.2B). There was no difference in the amount of $Fluc^{WT}$ or $Fluc^{DM}$ expressed between cell types. The $PulSA_{AI}$ was calculated as the ratio of the percentage of cells identified to contain inclusions (as determined by PulSA) to the EGFP geometric mean of transfected cells. Based on these analyses, NSC-34 cells expressing $Fluc^{DM}$ have a significantly higher $PulSA_{AI}$ than Neuro-2a cells expressing $Fluc^{DM}$ suggesting that NSC-34 cells have less capacity to prevent the aggregation of $Fluc^{DM}$ into inclusions (Figure 5.2C).

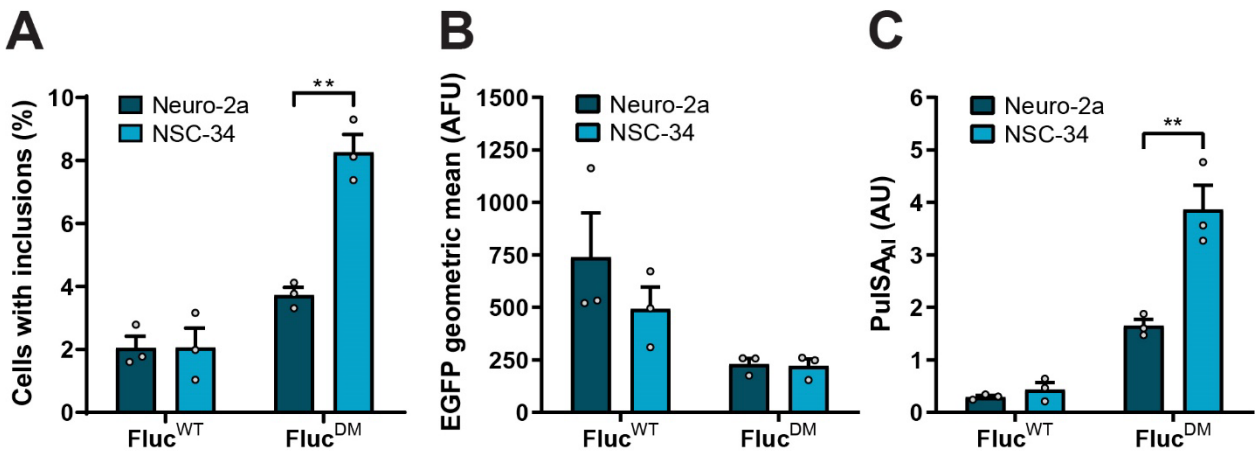

Figure 5.2. The formation of inclusions by Fluc in Neuro-2a and NSC-34 cells, as assessed by PulSA. Neuro-2a and NSC-34 cells were transiently transfected to express EGFP, Fluc^{WT}-EGFP or Fluc^{DM}-EGFP and were analysed by PulSA 48 h post-transfection. **(A)** The proportion of Neuro-2a and NSC-34 cells expressing Fluc^{WT}-EGFP or Fluc^{DM}-EGFP with inclusions. Data are presented as the mean ± S.E.M (n=3) of the percentage of cells containing inclusions. **(B)** The EGFP geometric mean, which corresponds to the average amount of Fluc expressed in transfected cells within each cell population. Data are presented as the EGFP geometric mean (arbitrary fluorescence units; AFU) of live, transfected cells. **(C)** PulSA aggregation index (PulSA$_{AI}$) calculated for Neuro-2a and NSC-34 cells transfected with Fluc constructs. The PulSA$_{AI}$ was calculated as the ratio of the percentage of cells identified to contain inclusions, divided by the EGFP geometric mean of EGFP-positive cells. Data in (A), (B) and (C) are presented as the mean ± S.E.M. (n=3). Significant differences between group means were determined using an unpaired two-tailed Student's t-test (** = $P < 0.01$).

As an alternative approach to compare the relative capacity of Neuro-2a and NSC-34 cells to maintain Fluc^{DM}-EGFP in a non-aggregated state, how the proportion of cells with inclusions change as the amount of Fluc in the cell increases was investigated. To do so, cells with equivalent levels of EGFP fluorescence were identified from the flow cytometry data and binned based upon the EGFP fluorescence intensity. Overall, 16 bins of equal size (based on a log scale) were used to subdivide the EGFP-positive cells (Figure 5.3A). The proportion of cells with inclusions was then determined by PulSA for cells in each of these bins (i.e. with increasing amounts of Fluc). In all samples, cells in bins 1–10 did not contain inclusions. From bin 11 onwards, there was a clear trend whereby as the amount of Fluc expressed in cells increased, there was an increase in the proportion of cells with inclusions (Figure 5.3B). Neuro-2a cells expressing Fluc^{DM}-EGFP were found to be less susceptible to inclusion formation by Fluc^{DM} than NSC-34 cells. This is observed as a significant shift to the right when bin number (e.g. bins 12 and 13) is plotted against the proportion of cells with inclusions for Neuro-2a cells compared to NSC-34 cells. There was little difference in the proportion of cells containing inclusions in both cell lines when they expressed

Fluc^{WT}, which remained below 40% even in cells expressing high amounts of Fluc^{WT}-EGFP (i.e. bins 14 – 16).

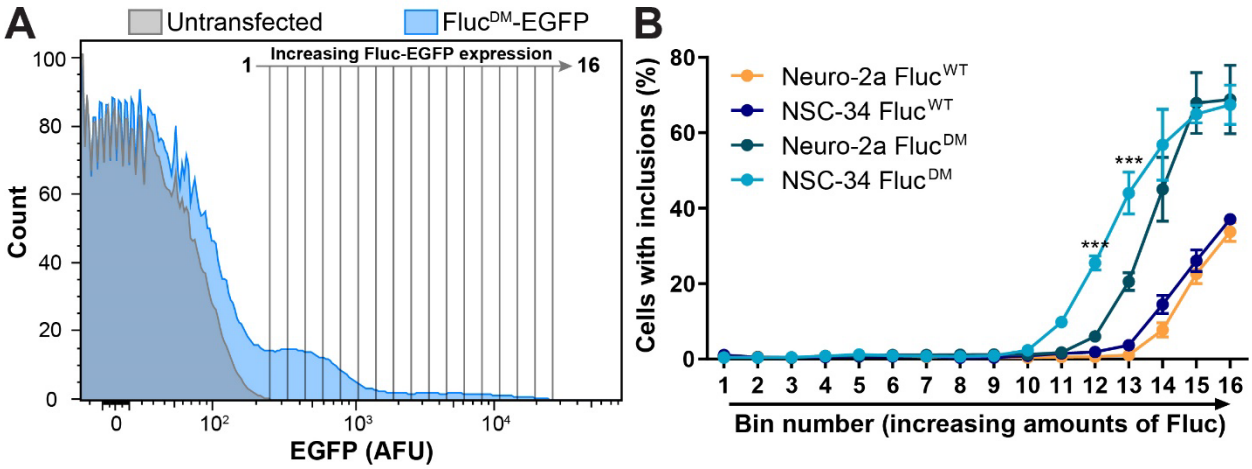

Figure 5.3. The relative susceptibility of Neuro-2a and NSC-34 cells to the formation of Fluc-based inclusions. Neuro-2a and NSC-34 cells were transiently transfected to express Fluc^{WT}-EGFP or Fluc^{DM}-EGFP and analysed by PulSA 48 h post-transfection. **(A)** Gating strategy used to determine the fraction of live cells with inclusions as a function of Fluc-EGFP expression. Overlay histograms of untransfected (*grey*) and Fluc^{DM}-EGFP (*blue*) transfected cells were generated to identify transfected cells for subsequent analyses. The frequency histogram of EGFP fluorescence was then subdivided into 16 bins of equal size (based on a log scale), whereby bin 1 represents the lowest, and bin 16 the highest level of Fluc-EGFP expression (indicated). PulSA was then applied to obtain **(B)** the proportion of Neuro-2a and NSC-34 cells with Fluc-based inclusions with increasing amounts of Fluc. Data are presented as the bin number plotted against the mean ± S.E.M. (n=3) percentage of cells containing inclusions. Significant differences between group means were determined using a two-way ANOVA ($P < 0.05$) followed by a Bonferroni's post-hoc test. Sample group means determined to be statistically different from each other within the same bin number are indicated (***$P < 0.001$).

As a third approach to measure the relative capacities of NSC-34 and Neuro-2a cells to maintain aggregation-prone Fluc in a soluble state, FloIT was performed as previously described (Whiten et al., 2016). In Neuro-2a cells expressing Fluc^{WT}-EGFP or Fluc^{DM}-EGFP, the number of inclusions/100 cells was 5 ± 1 and 9 ± 1, respectively (Figure 5.4A). In NSC-34 cells transfected to express Fluc^{WT}-EGFP or Fluc^{DM}-EGFP, the number of inclusions/100 cells was 4 ± 1 and 15 ± 2, respectively. The FloIT-derived aggregation-index (FloIT$_{AI}$) again indicated that NSC-34 cells are more susceptible to inclusion formation by Fluc^{DM} since these cells were found to have a FloIT$_{AI}$ that was significantly higher than Neuro-2a cells (Figure 5.4B).

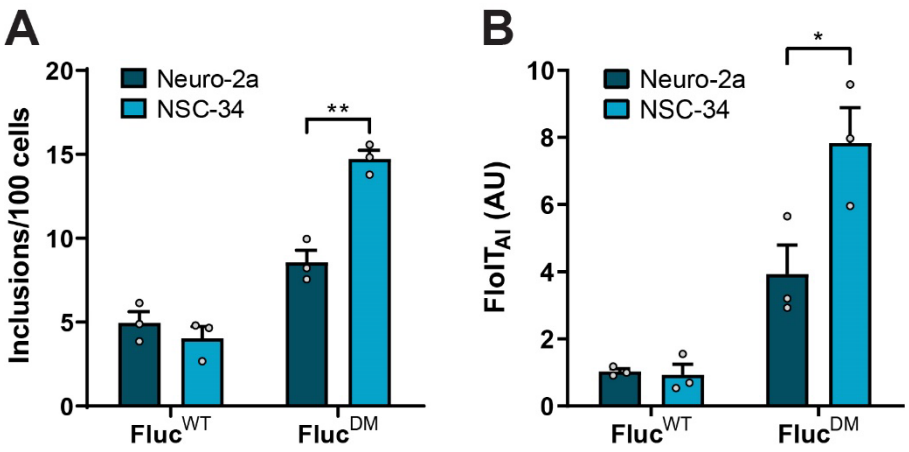

Figure 5.4. The formation of inclusions by Fluc in Neuro-2a and NSC-34 cells, as assessed by FloIT. Neuro-2a and NSC-34 cells were transiently transfected to express EGFP, Fluc^{WT}-EGFP or Fluc^{DM}-EGFP and were analysed by FloIT 48 h post-transfection. **(A)** The number of inclusions measured in Neuro-2a and NSC-34 cells transiently transfected to express Fluc^{WT}-EGFP or Fluc^{DM}-EGFP. **(B)** FloIT$_{AI}$ calculated for Neuro-2a and NSC-34 cells transfected with Fluc constructs. The FloIT$_{AI}$ was calculated as the ratio of the number of inclusions per 100 cells, divided by the EGFP geometric mean of EGFP-positive cells. Data in (A) and (B) are presented as the mean ± S.E.M (n=3). Significant differences between group means were determined using an unpaired two-tailed Student's t-test (*$P < 0.05$ and ** = $P < 0.01$).

5.3.2 The relative toxicity of Fluc^{DM} inclusion formation in Neuro-2a and NSC-34 cells

The localisation of misfolded proteins into inclusions in cells is associated with cytotoxicity (Lang-Rollin et al., 2003). To assess whether there were cell-type dependent differences in the toxicity associated with inclusion formation by an aggregation-prone protein, the cytotoxicity of Fluc expression in Neuro-2a and NSC-34 cells was also assessed using real-time imaging, as described previously (McAlary et al., 2016). Interestingly, Neuro-2a cells expressing Fluc^{WT} had increased survival compared to cells expressing EGFP alone at most points throughout the incubation; however, NSC-34 cells transfected to express Fluc^{WT} had lower overall survival relative to those expressing EGFP alone (Figure 5.5A). After 192 h, NSC-34 cells expressing Fluc^{WT} had significantly reduced survival compared to Neuro-2a cells expressing the same protein. For both cell lines, the survival of cells transfected with Fluc^{DM} was lower, relative to those cells expressing EGFP alone (Figure 5.5B). Moreover, the survival of NSC-34 cells expressing Fluc^{DM} was markedly lower than that of Neuro-2a cells expressing this same protein. Thus, this data demonstrates that aggregation-prone Fluc is more cytotoxic to NSC-34 cells than Neuro-2a cells.

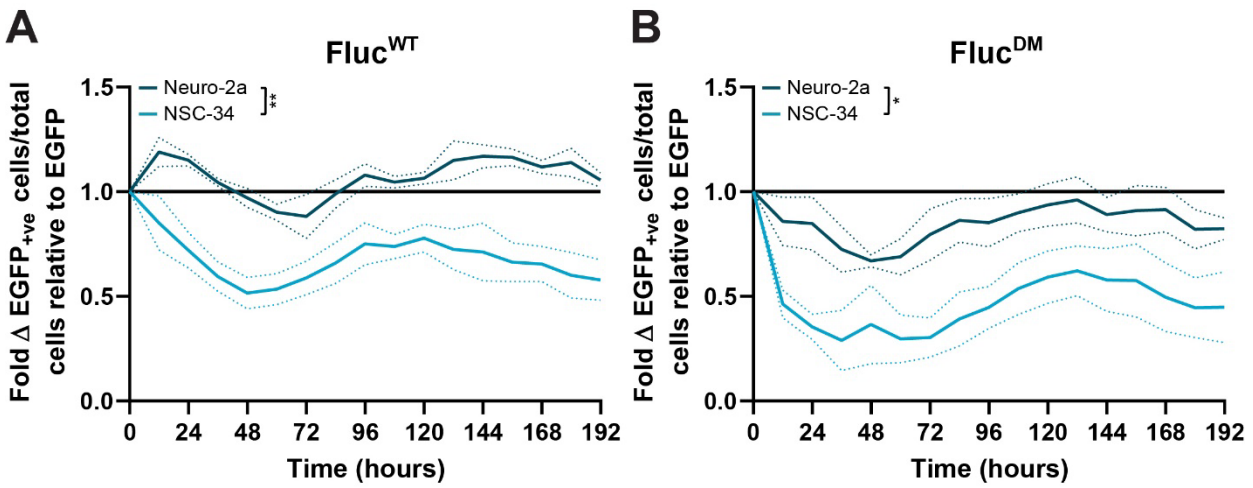

Figure 5.5. The relative toxicity of Fluc-EGFP expression compared to EGFP expression alone over time. Neuro-2a and NSC-34 cells were transiently transfected to express EGFP, Fluc^{WT}-EGFP or Fluc^{DM}-EGFP and were analysed over a 192 h time-course to examine the toxicity of cells expressing Fluc-EGFP constructs in real-time relative to cells expressing EGFP alone, using the IncuCyte® automated fluorescence microscope. Neuro-2a or NSC-34 cells expressing **(A)** Fluc^{WT}-EGFP or **(B)** Fluc^{DM}-EGFP. Data are presented as the mean ± S.E.M (n=3) of the fold change in EGFP-positive cells/total number of cells, relative to cells expressing EGFP. Significant differences between group means at the 192 h end-point were determined using a two-tailed Student's t-test (*$P < 0.05$ and ** = $P < 0.01$).

5.3.3 Identification of proteins associated with Fluc^{DM} inclusions in Neuro-2a and NSC-34 cells

The data presented above indicates that Fluc is more susceptible to protein aggregation into inclusions when expressed in NSC-34 cells compared to Neuro-2a cells. To further investigate potential reasons for this, the proteins that associate with Fluc^{DM} inclusions when they are formed in these two cell lines was established. As a result of their large molecular mass, Fluc^{DM} inclusions become trapped in the stacking gel during the migration of proteins as a result of SDS-PAGE (Shevchenko et al., 2007). This was exploited in order to purify Fluc^{DM} inclusions and identify the other proteins associated with them. Thus, Neuro-2a and NSC-34 cells expressing Fluc^{DM}-EGFP were harvested, lysed and the insoluble proteins extracted for loading onto an SDS-PAGE gel.

Cell lysates from Neuro-2a and NSC-34 cells that were transfected to express Fluc^{DM} contained a fluorescent band in the well of the stacking gel, indicative of EGFP-tagged Fluc^{DM} (Figure 5.6A). The fluorescence detected in the wells of the Neuro-2a samples was higher than that of the NSC-34 cells and is likely due to differences in transfection efficiency. Very low levels of fluorescence

were also observed in the stacking gel of the untransfected Neuro-2a and NSC-34 cell lysates. This likely arises due to autofluorescence from proteins such as collagen or elastin, cellular organelles such as mitochondria or lysosomes, or cyclic ring containing molecules, including NADPH or aromatic amino acids (Blomfield and Farrar, 1969, Fujimoto et al., 1977, Andersson et al., 1998). There were no discernible differences between the samples with regard to the profile of proteins that migrated within the resolving gel following SDS-PAGE (Figure 5.6B). Proteins trapped in the stacking gel that contained Fluc^{DM} were isolated for proteomic mass spectrometry. The corresponding region of the stacking gel from samples containing cell lysate from untransfected cells was used as controls in the mass spectrometry analyses (regions indicated by the arrow).

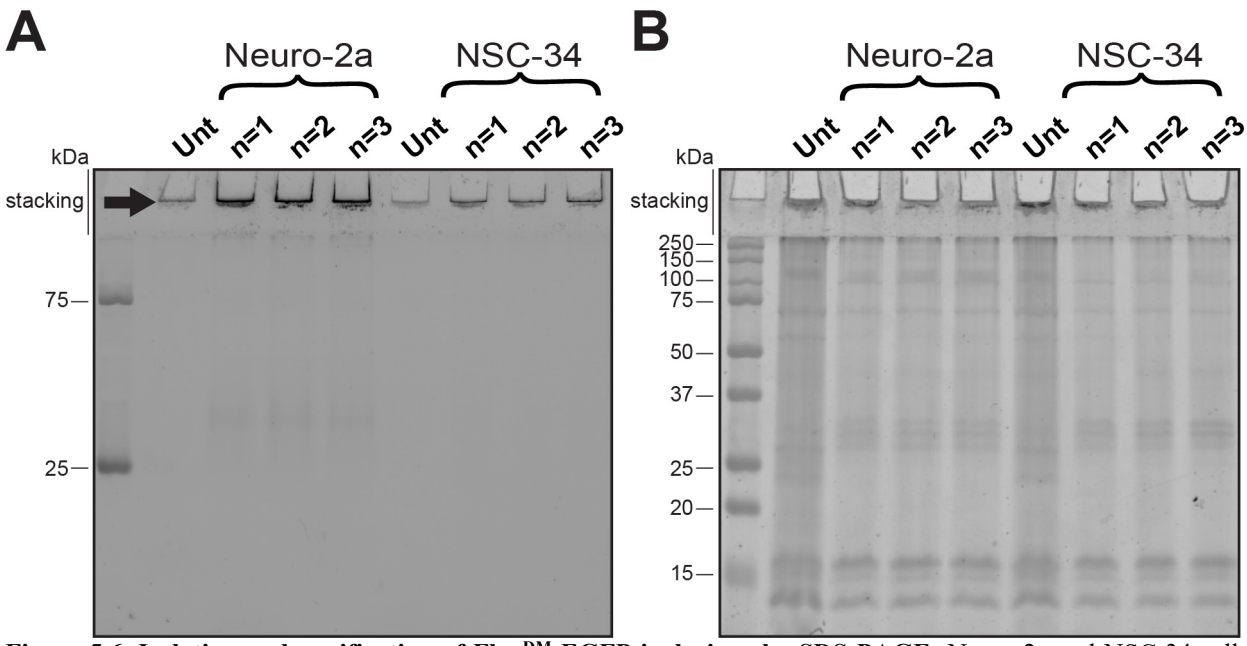

Figure 5.6. Isolation and purification of Fluc^{DM}-EGFP inclusions by SDS-PAGE. Neuro-2a and NSC-34 cells were transfected (or not) to express Fluc^{DM}-EGFP and 48 h post-transfection were harvested, fractionated and the insoluble protein from each sample was quantified and placed into native loading buffer (non-denaturing, non-reducing conditions) for loading prior to being subjected to electrophoretic separation by SDS-PAGE. **(A)** SDS-PAGE gel imaged following exposure to 488 nm light to detect fluorescence from EGFP-tagged Fluc^{DM}. High molecular mass proteins which are excited at 488 nm and are trapped in the stacking gel are indicated by the arrow. **(B)** SDS-PAGE gel stained with Coomassie Blue showing total protein in the lysates from these cells. Biological triplicates of cells transfected with Fluc^{DM}-EGFP are shown, along with insoluble protein from cell lysates of untransfected Neuro-2a and NSC-34 cells (Unt). Molecular masses of the protein standards are shown to the left of the gel (in kDa).

Of the 676 proteins identified in the mass spectrometric analysis of proteins associated with Fluc^{DM} inclusions, 259 (38.3%) were only detected in Neuro-2a cells and 176 (26%) were only

detected in NSC-34 cells (Figure 5.7A) (see Table 8.1 in Appendix II for the full list of proteins identified). Proteins implicated in neurodegenerative diseases, such as Alzheimer's disease, Parkinson's disease, Huntington's disease, spinocerebellar ataxia, ALS and prion-related diseases, were found to be enriched within the $Fluc^{DM}$ inclusions in both Neuro-2a and NSC-34 cells (Figure 5.7B). Other highly enriched KEGG pathways identified include those involved in cellular functions such as transcription, translation, cell cycle control and cellular respiration and metabolism. The remaining proteins identified corresponded to KEGG pathways that represent major arms of the proteostasis network, including proteasomal degradation and protein processing in the ER. In both Neuro-2a and NSC-34 cells, the most highly represented classes of proteins identified associated with $Fluc^{DM}$ inclusions by PANTHER analysis were metabolic enzymes, RNA binding proteins (i.e. translational machinery), cytoskeletal proteins, proteins involved in transport and chaperones (Figure 5.7C). Overall, the classes of proteins identified to be associated with $Fluc^{DM}$ inclusions and the relative distribution of these protein classes was nearly identical in the two cell lines.

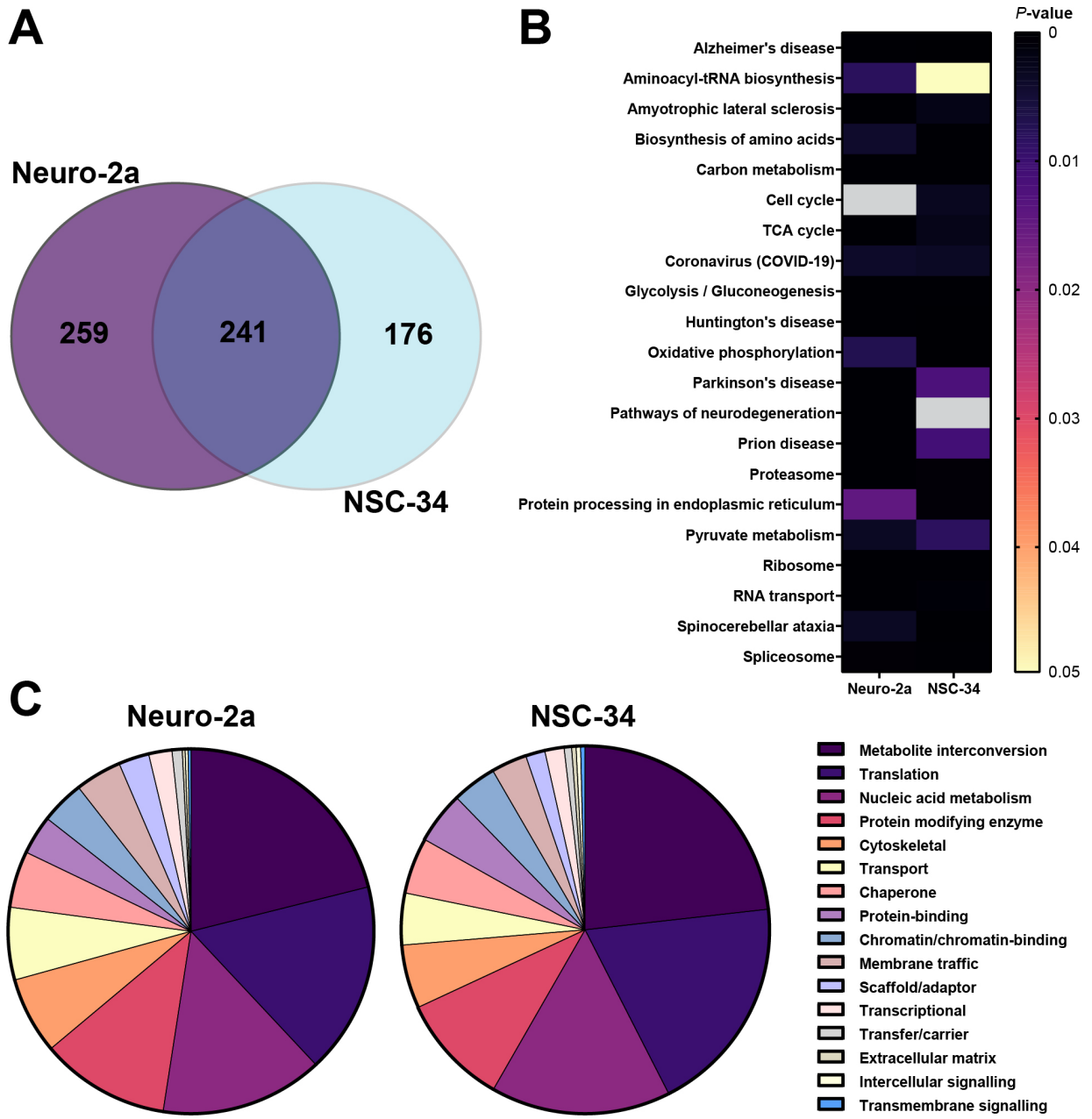

Figure 5.7. Distribution and enrichment of the KEGG pathways and classes of proteins identified within Fluc^{DM} inclusions by proteomic mass spectrometry. Proteins associated with Fluc^{DM} inclusions from Neuro-2a and NSC-34 cells were identified by mass spectrometry. **(A)** The total number of proteins identified within Fluc^{DM} inclusions from Neuro-2a (*purple*) and NSC-34 (*blue*) cells. **(B)** The functional enrichment of KEGG pathways represented by proteins identified within Fluc^{DM} inclusions in Neuro-2a and NSC-34 cells. Only KEGG pathways that were significantly enriched are shown (threshold set to $P \leq 0.05$). Colours represent *P*-values, whereby the lowest values (highest enrichment) are in *black* ($P < 0.001$), and the highest values (lowest enrichment) are in *yellow* ($P \leq 0.05$) and greyed-out boxes represent a pathway not enriched in that cell type. **(C)** PANTHER analysis of protein classes most enriched within Fluc^{DM} inclusions in Neuro-2a (*left*) and NSC-34 (*right*) cells.

Finally, STRING analysis was conducted on the 241 proteins found within Fluc^{DM} inclusions in both Neuro-2a and NSC-34 cells. The most highly represented protein classes were ribosomal proteins, translational machinery, proteasome components and chaperone proteins (Figure 5.8). These protein classes, all of which are components of the proteostasis network, act as interaction hubs, linking all the proteins found to associate with Fluc^{DM} inclusions in both cell lines.

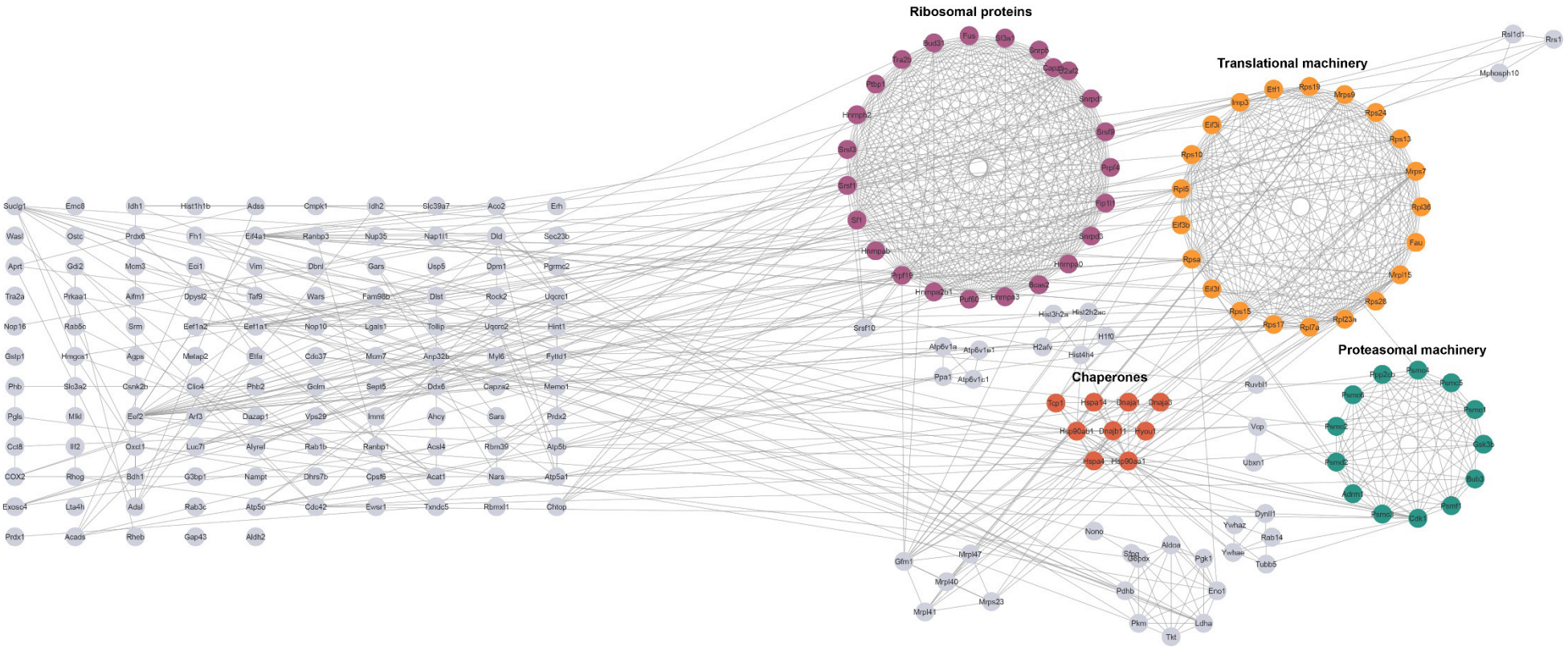

Figure 5.8. STRING network analysis of proteins identified within Fluc^{DM} inclusions in both Neuro-2a and NSC-34 cells. The reactome network was constructed using the STRING application in Cytoscape. Proteins within the most highly represented protein classes include ribosomal proteins (*purple*), proteins involved in translation (*orange*), proteasomal machinery (*teal*) and chaperone proteins (*red*). Nodes denoted in *grey* represent proteins not clustered based on protein class. Grey lines connecting nodes represent protein-protein associations.

5.3.4 The effect of modulating key arms of the proteostasis network on Fluc^{DM} inclusion formation in Neuro-2a and NSC-34 cells

5.3.4.1 The heat shock response

The relative susceptibility to inclusion formation between cell types may be dependent upon intrinsic differences in the cellular pathways that act to maintain proteostasis. Thus, this work sought to modulate key pathways involved in protein quality control, to identify those that are most critical in preventing the formation of inclusions by aggregation-prone proteins in Neuro-2a and NSC-34 cells. HSF1 is the master regulator of the heat shock response, a major arm of the protein quality control network, which is activated under conditions of cellular stress (Vihervaara and Sistonen, 2014). The activation of HSF1 leads to increased stress-induced gene transcription leading to chaperone induction, refolding of protein aggregates, and the re-establishment of proteostasis (Morimoto, 2011). Thus, to characterise the effect of increased HSF1 expression on Fluc^{DM} inclusion formation, HSF1 variants were co-expressed with Fluc^{DM}-EGFP in Neuro-2a and NSC-34 cells. These HSF1 isoforms have been previously described (Taylor et al., 2007) and include wild-type HSF1 (HSF1^{WT}), a constitutively active form of HSF1 (HSF1^{+}) which has a deletion of the sequence encoding amino acids (Δ203-315) of the regulatory domain, and an inactive variant of HSF1 (HSF1^{-}) that has a deletion of amino acids (453-523) located in the transcription activation domain (Figure 5.9A). As assessed by FloIT, the number of Fluc^{DM} inclusions was significantly reduced in both Neuro-2a and NSC-34 cells upon co-expression of HSF1^{WT} compared to cells co-expressing HSF1^{-}, the transcriptionally inactive HSF1 isoform (Figure 5.9B). In Neuro-2a cells, co-expression of the constitutively active HSF1^{+} isoform did not significantly reduce inclusion formation by Fluc^{DM}; however, Fluc^{DM} inclusion formation was significantly reduced by co-expression of HSF1^{+} in NSC-34 cells.

Whole cell fractionation by NP-40 detergent solubilisation followed by immunoblotting revealed a similar trend to that observed by FloIT. Thus, the amount of Fluc^{DM} found in the insoluble

fraction was reduced for both Neuro-2a and NSC-34 cells expressing $HSF1^{WT}$ or $HSF1^{+}$ compared to the $HSF1^{-}$ control (Figure 5.9C). In both cell lines, the amount of $Fluc^{DM}$ observed in the soluble fraction increased slightly upon co-expression of $HSF1^{+}$ and was markedly higher in cells co-expressing $HSF1^{WT}$. Immunoblotting with an anti-HSF1 antibody confirmed the overexpression of the various HSF1 isoforms in these cells following transfection. To test whether overexpression of HSF1 was consistent with activation of the heat shock response and subsequent upregulation of common stress-inducible Hsps, cell lysates were probed for Hsp40, Hsc70 (constitutive Hsp70) and Hsp90 expression. Heat-shocked HeLa cell lysate was used as a positive control for the expression of these Hsps in this experiment (Figure 5.9D). Immunoblotting revealed that Hsp40, Hsc70 and Hsp90 were endogenously expressed in Neuro-2a and NSC-34 cells. Furthermore, the levels of Hsp40 and Hsp90 increased in Neuro-2a and NSC-34 cells transfected to express $HSF1^{+}$ compared to cells expressing $HSF1^{-}$, suggesting that expression of the constitutively active form of HSF1 does result in the activation of stress-inducible chaperones. Interestingly, levels of these Hsps were not substantially increased in cells expressing $HSF1^{WT}$, which suggests that the ability of $HSF1^{WT}$ to inhibit $Fluc^{DM}$ inclusion formation may be independent of its transcriptional activity.

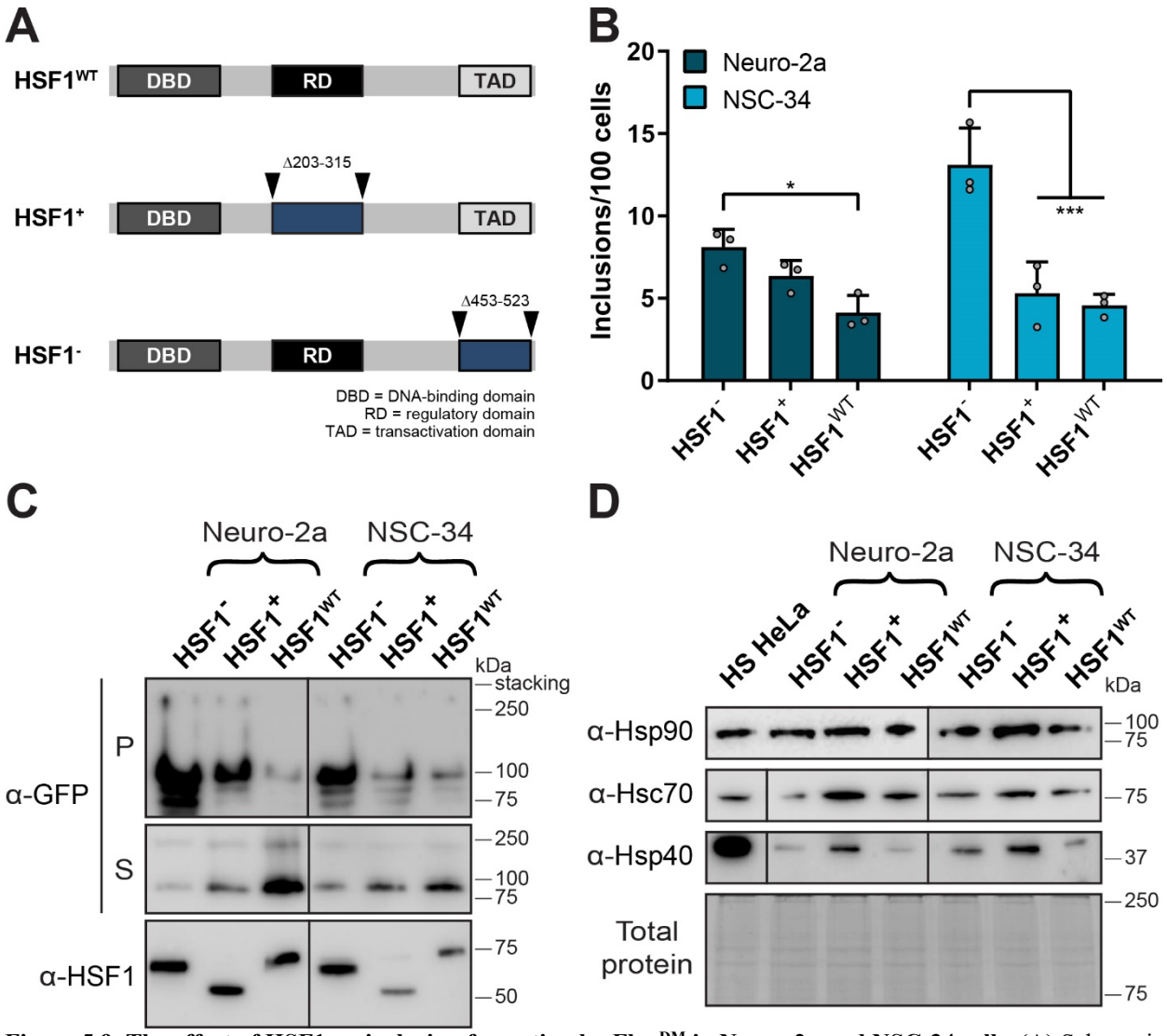

Figure 5.9. The effect of HSF1 on inclusion formation by Fluc^{DM} in Neuro-2a and NSC-34 cells. (A) Schematic overview of plasmids encoding HSF1^{WT} and constitutively active HSF1 (HSF1^{+}) or inactive HSF1 (HSF1^{-}) mutational variants. The DNA binding domain (DBD) was unaltered in all variants, whilst the regulatory domain (RD) (Δ203-315) and the transactivation domain (TAD) (Δ453-523) were deleted in the active and inactive forms of HSF1, respectively. Neuro-2a and NSC-34 cells were transiently co-transfected to express Fluc^{DM}-EGFP and HSF1^{WT}, HSF1^{+} or HSF1^{-}. Cells were analysed 48 h post-transfection by **(B)** FloIT or **(C and D)** NP-40 fractionation and subsequent immunoblotting. Data in (B) are presented as the mean ± S.E.M (n=3) of the number of inclusions per 100 cells. Significant differences between group means were determined using a one-way ANOVA ($P < 0.05$) followed by a Tukey's post-hoc test. Group means determined to be statistically different from each other are indicated ($*P < 0.05$ and $***P < 0.001$). In (C) an anti-GFP antibody was used to detect Fluc^{DM} in the insoluble pellet (P) and soluble (S) fractions and expression of the HSF1 variants in the total protein fraction was detected with an anti-HSF1 antibody. For (D) in the total protein fraction, antibodies against Hsp40, Hsc70 and Hsp90 were used to detect expression of the corresponding Hsps. Total protein was used as a loading control. A heat-shocked (HS; at 42°C for 1 h with 3 h recovery at 37°C) HeLa cell lysate was used as a positive control to probe for expression of Hsps. The blots shown are representative of two experiments.

An interesting observation following the co-expression of the HSF1 variants with Fluc^{DM} was that a decrease in the amount of insoluble protein directly correlated to an increase in the amount of soluble Fluc^{DM} present in lysates from both Neuro-2a and NSC-34 cells (see Figure 5.9C). To further investigate this, the formation of Fluc^{DM} inclusions in cells co-expressing the HSF1

variants was assessed by epifluorescence microscopy. There was little difference in the appearance of the Fluc^{DM} inclusions observed in Neuro-2a (*top*) or NSC-34 (*bottom*) cells expressing either HSF1^{-} (*left*) or HSF1^{+} (*centre*), albeit there appeared to be a slight reduction in the overall number of inclusions in cells expressing HSF1^{+} (Figure 5.10). Thus, the Fluc inclusions formed in these cells appeared as discrete, highly fluorescent puncta. In contrast, in cells expressing HSF1^{WT} (*right*), the majority of the green fluorescence appeared diffuse and was located throughout the cytoplasm and the nucleus. In very few of these cells were punctate Fluc^{DM} inclusions observed. Thus, these results support the findings of the fractionation and immunoblotting and indicate that HSF1 reduces inclusion formation by Fluc^{DM} and maintains the protein in a soluble state.

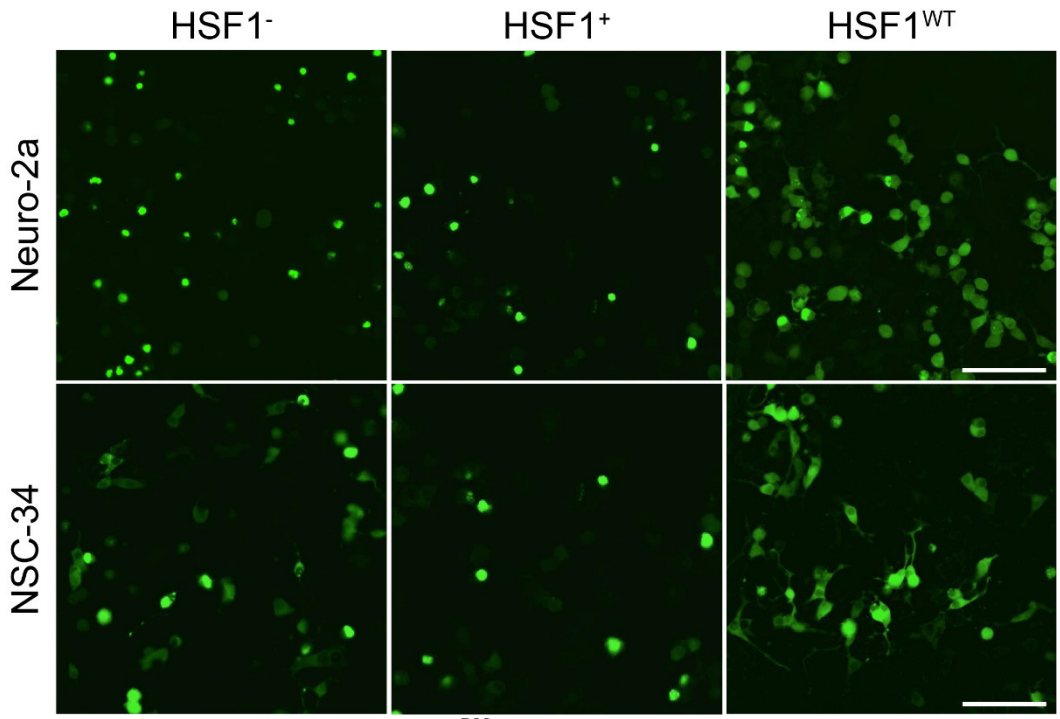

Figure 5.10. The formation of inclusions by Fluc^{DM} in Neuro-2a and NSC-34 cells following overexpression of HSF1, as assessed by epifluorescence microscopy. Neuro-2a and NSC-34 cells were transiently co-transfected to express Fluc^{DM}-EGFP and either an inactive form of HSF1 (HSF1^{-}), a constitutively active HSF1 (HSF1^{+}) or HSF1^{WT} Live cells were analysed 48 h post-transfection by epifluorescence microscopy to examine the formation of inclusions. Images are representative of three experiments and show epifluorescence micrographs of Neuro-2a (*top*) and NSC-34 (*bottom*) cells co-transfected with Fluc^{DM}-EGFP and HSF1^{-} (*left*), HSF1^{+} (*centre*) or HSF1^{WT} (*right*). EGFP fluorescence was detected by excitation at 488 nm. All images were taken using a Leica DMi8 fluorescence microscope and the 20× objective lens. Scale bar represents 100 µm.

5.3.4.2 Degradation by the ubiquitin-proteasome system

To ascertain whether the ubiquitin-proteasome system plays a critical role in preventing the aggregation of $Fluc^{DM}$ into inclusions in Neuro-2a and NSC-34 cells, the $Ub^{[9]}$-mRFP plasmid was co-transfected into cells for the overexpression of ubiquitin, with the aim of upregulating proteasomal activity. Briefly, the translation of the $Ub^{[9]}$-mRFP precursor results in the expression of nine free ubiquitin monomers and one fluorescent mRFP protein (Figure 5.11A) (Salomons et al., 2009). The drug MG132 was used as a proteasome inhibitor in these experiments. Treatment of Neuro-2a and NSC-34 cells with MG132 significantly increased the number of $Fluc^{DM}$ inclusions compared to DMSO-treated cells or cells expressing $Ub^{[9]}$-mRFP; however, for both cell types, expression of $Ub^{[9]}$-mRFP did not change the number of inclusions formed compared to the DMSO-treated controls (Figure 5.11B).

In these cells, the distribution of $Fluc^{DM}$ found in the insoluble fraction mirrored the results obtained by FloIT, whereby increased insoluble $Fluc^{DM}$ was observed in the lysates of cells treated with MG132 (Figure 5.11C). There was a slight reduction (Neuro-2a) or increase (NSC-34) in the amount of insoluble $Fluc^{DM}$ observed following expression of $Ub^{[9]}$-mRFP; however, the amount of soluble $Fluc^{DM}$ did not differ substantially between treatment groups. Inhibition of the proteasome in these experiments was confirmed by an increase in polyubiquitinated species, observed as large, high molecular mass smears by immunoblotting with an anti-ubiquitin antibody in both the soluble and insoluble fractions (Figure 5.11D). However, the amount of free ubiquitin did not appear to change substantially in cells transfected to express $Ub^{[9]}$-mRFP compared to the controls. The relatively small mass of the protein can make transfer onto the blotting membrane difficult, given that smaller proteins need less time to transfer, which can lead to ‘over-transfer’ (Otter et al., 1987, Bolt and Mahoney, 1997, Kurien and Hal Scofield, 2015). Thus, levels of free ubiquitin following expression of $Ub^{[9]}$-mRFP were assessed by immunostaining with a ubiquitin probe followed by confocal microscopy.

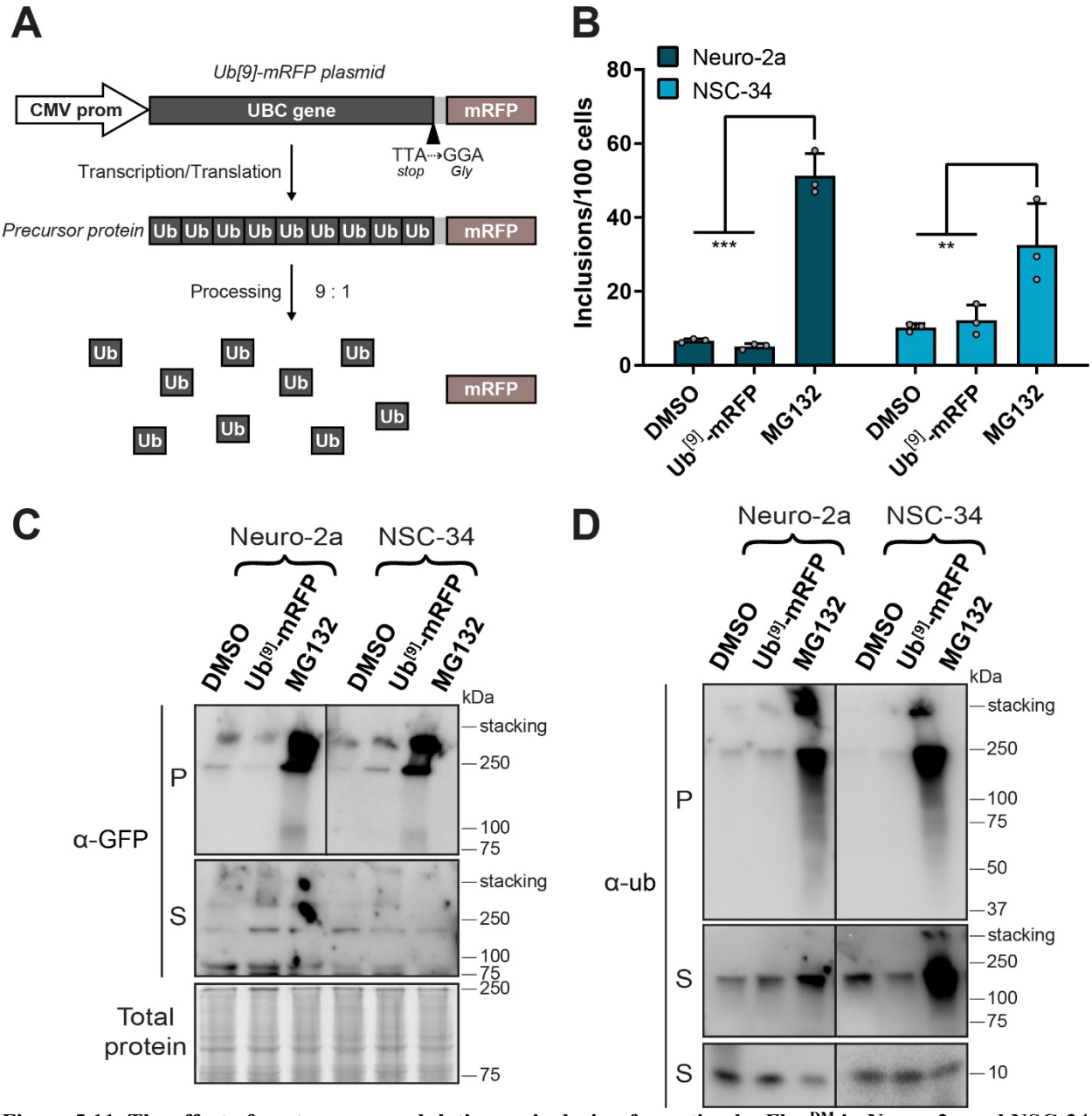

Figure 5.11. The effect of proteasome modulation on inclusion formation by Fluc^{DM} in Neuro-2a and NSC-34 cells. (A) Schematic representation of the plasmid encoding Ub$^{[9]}$-mRFP for the overexpression of ubiquitin. The polyubiquitin precursor (UBC) gene, encoding nine ubiquitin monomers, is in frame with mRFP and downstream of a CMV promoter for mammalian expression. Following transcription and translation, the ubiquitin precursors are rapidly processed by ubiquitin C-terminal hydrolases and the chimeric Ub$^{[9]}$-mRFP is converted into nine ubiquitin monomers and one fluorescent mRFP protein. Neuro-2a and NSC-34 cells were co-transfected to express Fluc^{DM}-EGFP and Ub$^{[9]}$-mRFP or mRFP (as a control) and, 42 h post-transfection, cells co-expressing mRFP were treated with the proteasome inhibitor MG132 (10 µM) or a DMSO as a control. Cells were incubated for a further 6 h and then analysed by **(B)** FloIT or **(C and D)** NP-40 fractionation and subsequent immunoblotting. Data in (B) are presented as the mean ± S.E.M (n=3) of the number of inclusions per 100 cells. Significant differences between group means were determined using a one-way ANOVA ($P < 0.05$) followed by a Tukey's post-hoc test. Group means determined to be statistically different from each other are indicated (**$P < 0.01$ and ***$P < 0.001$). In (C) an anti-GFP antibody was used to detect Fluc^{DM} in the insoluble pellet (P) and soluble (S) fractions and total protein was used as a loading control. In (D) an anti-ubiquitin antibody was used to detect high molecular mass, polyubiquitinated proteins in the insoluble pellet (P) and soluble (S) fractions, and free ubiquitin monomers in the soluble fraction. The blots shown are from a single experiment.

In order to confirm that transfection with the $Ub^{[9]}$-mRFP plasmid results in the overexpression of ubiquitin, the probe tUi-HA, which has previously been shown to bind strongly and specifically to free ubiquitin (Choi et al., 2019, Farrawell et al., 2020) was tested. Neuro-2a and NSC-34 cells were transfected to express $Fluc^{DM}$-EGFP and either $Ub^{[9]}$-mRFP or mRFP alone (as a negative control) and, following immunostaining with the free ubiquitin probe tUi-HA, fixed cells were imaged by confocal microscopy. Neuro-2a cells transfected to express the mRFP control exhibited diffuse expression of the protein (Figure 5.12A; *top*). As expected, the tUi-HA probe for free ubiquitin was detected in all cells at a relatively low level, with increased expression observed in some cells. In the mRFP alone expressing control cells, increased expression of ubiquitin did not correlate with higher levels of mRFP. In contrast, in Neuro-2a cells expressing $Ub^{[9]}$-mRFP, the fluorescence from the mRFP protein directly correlated with increased levels of immunostaining with the tUi-HA probe (Figure 5.12A; *bottom*). Similarly, in NSC-34 cells, expression of mRFP alone was not associated with increased amounts of free ubiquitin (Figure 5.12B; *top*), whereas cells expressing $Ub^{[9]}$-mRFP did contain high levels of immunostaining with the tUi-HA probe (Figure 5.12B; *bottom*). Together, this confirms that expression of $Ub^{[9]}$-mRFP is correlated with increased expression of free ubiquitin in these cells.

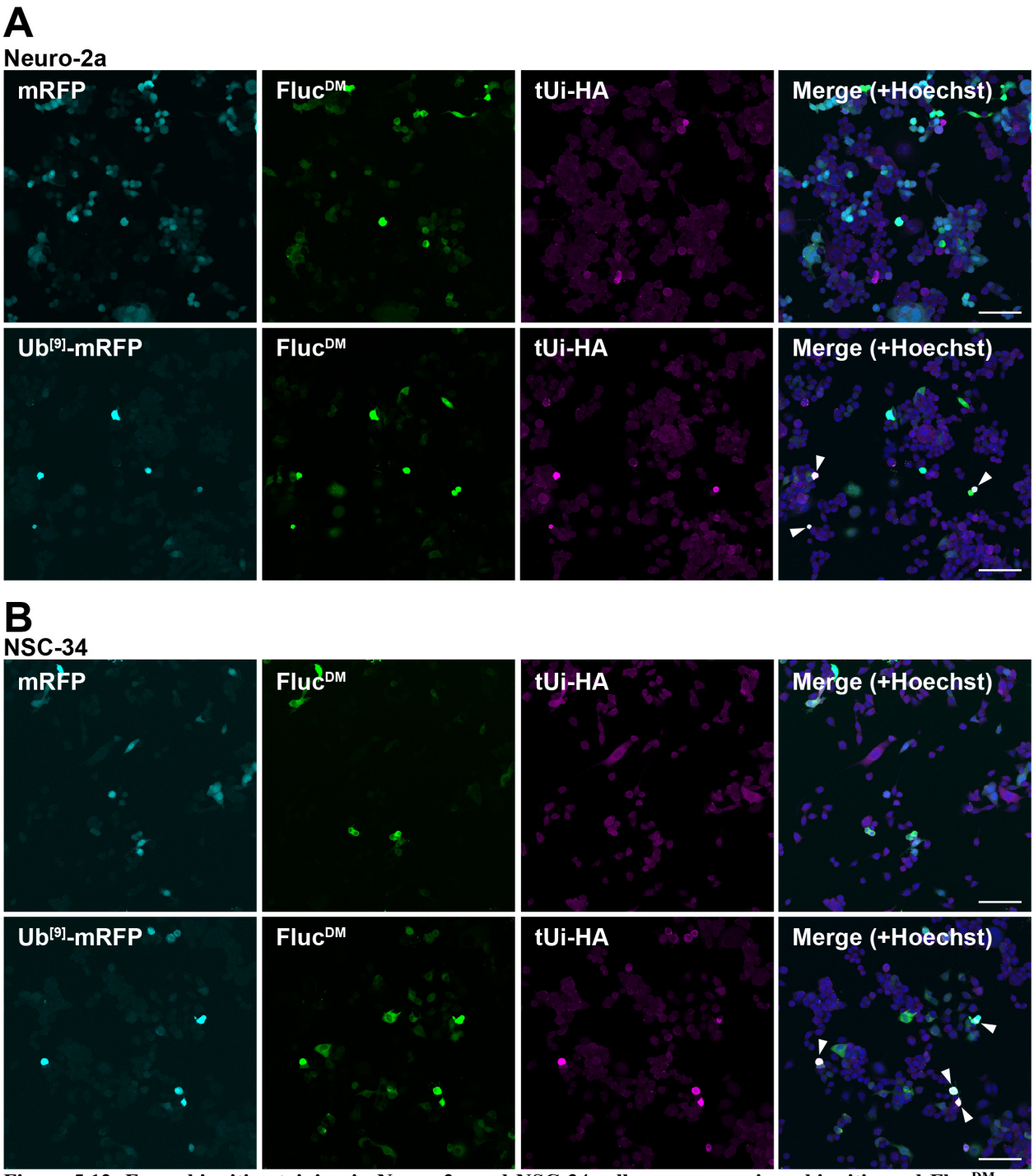

Figure 5.12. Free ubiquitin staining in Neuro-2a and NSC-34 cells overexpressing ubiquitin and Fluc^{DM}, as assessed by confocal microscopy. (A) Neuro-2a and **(B)** NSC-34 cells were co-transfected to express Fluc^{DM}-EGFP and mRFP (*top*) or Ub$^{[9]}$-mRFP (*bottom*) and, 48 h post-transfection, were fixed, permeabilised and analysed following immunostaining by confocal microscopy. Expression of mRFP (*cyan*) and Fluc^{DM}-EGFP (*green*) were detected following excitation at 552 nm and 488 nm, respectively. Expression of the HA-tagged free ubiquitin tUi probe (*magenta*) was excited with a 638 nm laser and nuclei stained with Hoechst 33482 (*blue*) were excited at 405 nm. Images are representative of three experiments and examples of cells containing high levels of ubiquitin (following transfection with Ub$^{[9]}$-mRFP) co-localised with HA-tagged tUi (free ubiquitin probe) are denoted by the arrowheads. All images were taken at 20× magnification using a Leica SP8 confocal microscope. Scale bars represents 100 µm.

5.3.4.3 Autophaghic degradation

To assess the impact of autophagy on the formation of inclusions by $Fluc^{DM}$, Neuro-2a and NSC-34 cells were treated with either rapamycin, a previously identified inducer of autophagy (Ravikumar et al., 2004) or the autophagy inhibitor, bafilomycin A1 (Yoshimori et al., 1991, Yamamoto et al., 1998). As measured by FloIT, treatment of both Neuro-2a and NSC-34 cells with bafilomycin A1 resulted in a significant increase in the number of $Fluc^{DM}$ inclusions formed in cells compared to the DMSO-treated cells (Figure 5.13A). Treatment with rapamycin had no effect on inclusion formation by $Fluc^{DM}$ in either Neuro-2a or NSC-34 cells. Similar results were obtained following NP-40 cell fractionation and immunoblotting of lysates from these cells. Thus, treatment with the autophagy inhibitor bafilomycin A1 increased the amount of $Fluc^{DM}$ found in the insoluble pellet fraction in both Neuro-2a and NSC-34 cells (Figure 5.13B). Interestingly, treatment with rapamycin led to an apparent increase in the amount of insoluble $Fluc^{DM}$ in Neuro-2a cell lysates, but decreased it in NSC-34 cells. Furthermore, the amount of soluble $Fluc^{DM}$ in NSC-34 cells treated with rapamycin increased relative to the DMSO-treated cells. Inhibition of autophagy by bafilomycin A1 was confirmed by the increased expression of SQSTM1/p62 and microtubule-associated protein-light chain 3II (LC3II) (commonly used markers of autophagy). Similarly, conversion of LC3I to LC3II, which is associated with mammalian autophagosome formation (Kabeya et al., 2000), increased following treatment with rapamycin.

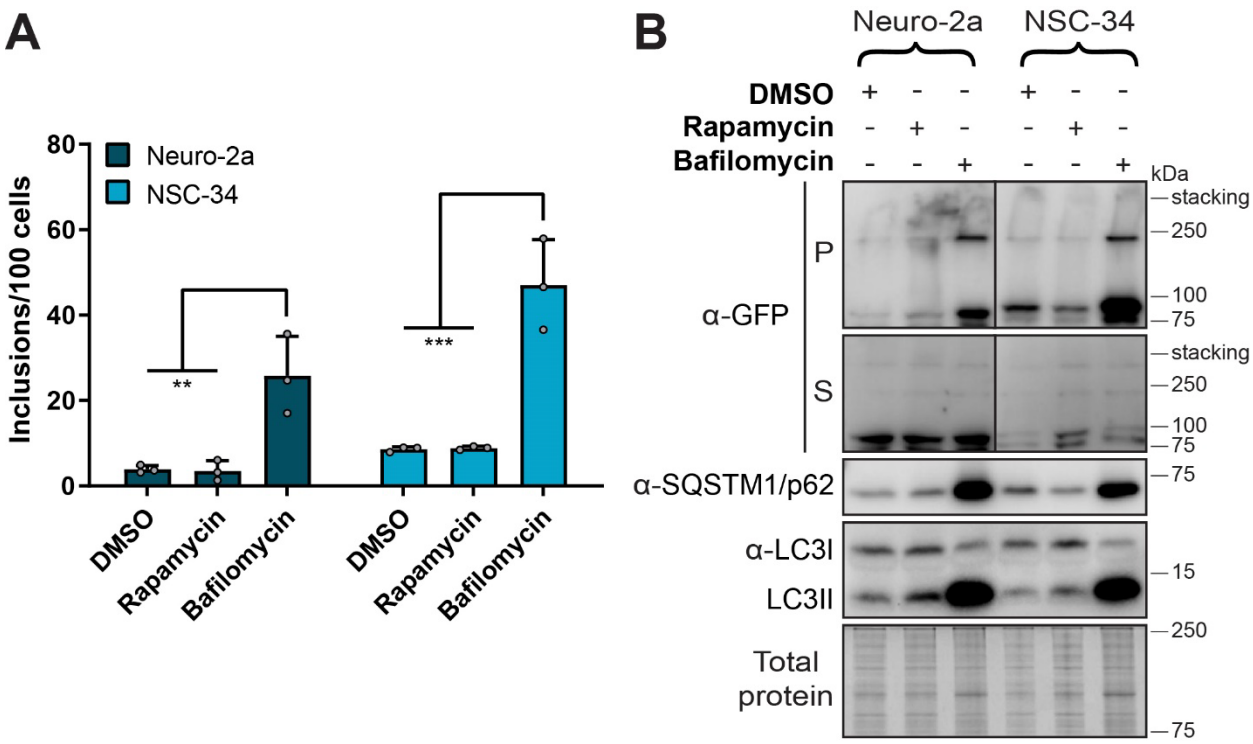

Figure 5.13. The effect of autophagy regulation on inclusion formation by Fluc^{DM} in Neuro-2a and NSC-34 cells. Neuro-2a and NSC-34 cells were transfected to express Fluc^{DM}-EGFP and, 24 h post-transfection, cells were treated with either bafilomycin A1 (1 μM), rapamycin (1 μM) or DMSO as a control. Cells were incubated for a further 16 h and then analysed by **(A)** FloIT or **(B)** NP-40 fractionation and subsequent immunoblotting. Data in (A) are presented as the mean ± S.E.M (n=3) of the number of inclusions per 100 cells. Significant differences between group means were determined using a one-way ANOVA ($P < 0.05$) followed by a Tukey's post-hoc test. Group means determined to be statistically different from each other are indicated (**$P < 0.01$ and ***$P < 0.001$). In (B) an anti-GFP antibody was used to detect Fluc^{DM} in the insoluble pellet (P) and soluble (S) fractions. In the total protein fraction, the expression of SQSTM1/p62 and expression of LC3I/LC3II was detected with an anti-SQSTM1/p62 antibody and an anti-LC3B antibody, respectively. Total protein was used as a loading control. The blots shown are from a single experiment.

5.3.4.4 The ER-stress response

To assess the impact of the ER stress pathway on the capacity of Neuro-2a and NSC-34 cells to prevent inclusion formation by Fluc^{DM}, cells expressing Fluc^{DM} were treated with either azoramide, which has been shown to upregulate ER-resident chaperones for improved ER protein folding (Fu et al., 2015), or thapsigargin, a well-known inducer of ER stress in mammalian cells (Oslowski and Urano, 2011). Following treatment with thapsigargin, the number of inclusions formed by Fluc^{DM} increased in both Neuro-2a and NSC-34 cells compared to the respective DMSO-treated controls, as assessed by FloIT (Figure 5.14A). Treatment with azoramide did not reduce inclusion formation by Fluc^{DM} in either cell line; rather, there was a trend by which the number of inclusions increased relative to the DMSO control, however, this did not reach statistical significance. Similar results were obtained by NP-40 cell fractionation and subsequent

immunoblotting of cell lysates from these samples. Thus, the amount of insoluble $Fluc^{DM}$ increased following treatment with either azoramide or thapsigargin in both Neuro-2a and NSC-34 cells compared to the DMSO-treated control cells (Figure 5.14B). Interestingly, the amount of soluble $Fluc^{DM}$ increased in Neuro-2a cells treated with azoramide, and even more so in cells treated with thapsigargin. Neither of these treatments led to a change in the amount of soluble $Fluc^{DM}$ in NSC-34 cells.

Expression of the major ER-resident chaperone GRP78/BiP (HspA5) confirmed that treatment with thapsigargin induced ER stress. Treatment with azoramide increased the expression of GRP78/BiP relative to the DMSO-treated control in both cells lines, a result which is consistent with previous work (Figure 5.14B) (Fu et al., 2015). Whilst treatment with either azoramide or thapsigargin both resulted in the increased expression of the ER-resident chaperone GRP78/BiP, the mechanistic action of these drugs is distinct. Thapsigargin induces ER stress by inhibiting the ER Ca^{2+}/ATPase, resulting in perturbation of calcium homeostasis in the cell. As a result, unfolded proteins accumulate in the ER and cause ER stress (Oslowski and Urano, 2011), which is often distinguished by the increased expression of GRP78/BiP in response to ER stress. Azoramide treatment is associated with an increase in ER Ca^{2+}/ATPase levels, leading to enhanced protein-folding in the ER and subsequently, increased expression of GRP78/BiP and other ER-resident chaperone proteins, such as DNAJC3, DNAJC10 and HspH4 (Fu et al., 2015). The expression of GRP78/BiP can therefore be used as marker to report on the functional status of the ER as it is involved in both the general folding of proteins and in the maintenance of proteostasis following ER stress.

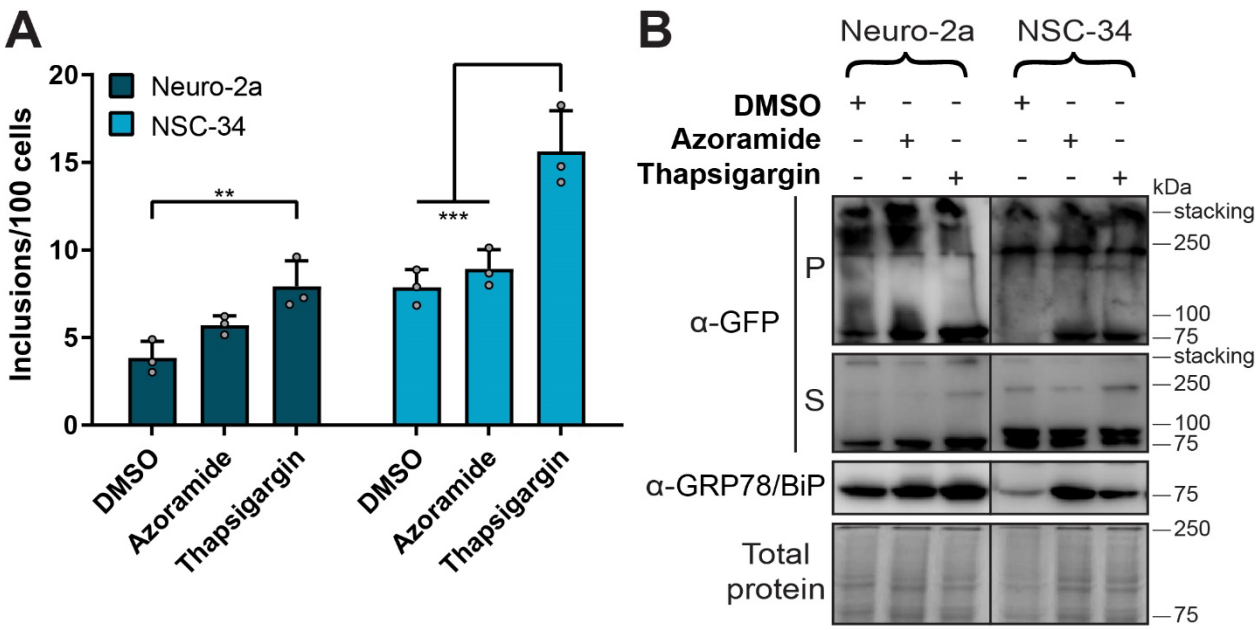

Figure 5.14. The effect of ER stress modulation on inclusion formation by Fluc^{DM} in Neuro-2a and NSC-34 cells. Neuro-2a and NSC-34 cells were transfected to express Fluc^{DM}-EGFP and, 24 h post-transfection, cells were treated with either azoramide (20 µM), thapsigargin (3 µM) or, as a control, an equivalent volume of DMSO. Cells were incubated for a further 16 h and then analysed by **(A)** FloIT or **(B)** NP-40 fractionation and subsequent immunoblotting. Data in (A) are presented as the mean ± S.E.M (n=3) of the number of inclusions per 100 cells. Significant differences between group means were determined using a one-way ANOVA ($P < 0.05$) followed by a Tukey's post-hoc test. Group means determined to be statistically different from each other are indicated (**$P < 0.01$ and ***$P < 0.001$). In (B) an anti-GFP antibody was used to detect Fluc^{DM} in the insoluble pellet (P) and soluble (S) fractions. In the total protein fraction, the expression of the ER-resident chaperone GRP78/BiP was detected with an anti-GRP78/BiP antibody and total protein was used as a loading control. The blots shown are from a single experiment.

5.4 Discussion

As the accumulation of aggregation-prone proteins into inclusions is a pathological hallmark of many diseases, it is critical to understand the precise roles various proteostasis pathways have in preventing this process. Moreover, quantitatively assessing the proteostasis capacity of a cell remains one of the major challenges in the field. The proteostasis capacity defines its ability to prevent protein accumulation and aggregation through the regulation of the protein quality control network. The ability to quantitatively measure the proteostasis capacity of a cell is an important step towards deciphering why some cell types are more susceptible to the formation of inclusions (and cause disease) than others. Furthermore, the deterioration of proteostasis capacity with age is believed to be related to an increase in toxic protein aggregation that is associated with disease (Brehme et al., 2014, Hipp et al., 2014).

In this work, aggregation indices were derived from flow cytometric analyses of cells expressing aggregation-prone protein $Fluc^{DM}$. This was done as a first step towards measuring the proteostasis capacity of cells. Along with real-time fluorescence microscopy, the flow cytometry-derived aggregation indices demonstrate that NSC-34 cells are more susceptible to inclusion formation by $Fluc^{DM}$ than Neuro-2a cells. Thus, the results demonstrate that lower amounts of $Fluc^{DM}$ are required before inclusions start to form in NSC-34 cells compared to Neuro-2a cells. The level of expression of an aggregation-prone protein is known to impact the formation of inclusions, with proteins forming inclusions more readily when expressed at high levels (Arrasate et al., 2004, Ramdzan et al., 2012, Ormsby et al., 2013, Ramdzan et al., 2013, Ciryam et al., 2015). By taking into account the level of $Fluc^{DM}$ expressed in the cell population, the aggregation-indices derived from this work enable comparison between different cell types. Moreover, both the $PulSA_{AI}$ and $FloIT_{AI}$ were in accord with each other and the results obtained when cells expressing similar levels of Fluc were analysed by PulSA. It must be noted that PulSA has a limited capability to detect cells that contain smaller, punctate inclusions, as is the case for many proteins whose

aggregation is associated with disease (e.g. TDP-43 and SOD1 aggregation associated with ALS) (Whiten et al., 2016). For this reason, and since FloIT can enumerate these smaller inclusions in cell lysates, FloIT may be the preferred method to develop this work in the future as it is broadly applicable to most (if not all) model systems of intracellular protein aggregation.

Whilst the results of this study highlight that flow cytometric methods can be used as a medium-to-high-throughput approach to measure the proteostasis capacity of cells, they only provide a snapshot of a cell population at a single point in time. Experiments utilising live cell imaging techniques can provide valuable temporal information on the rate of inclusion formation in cells and whether cells die as a result of the toxicity associated with inclusion formation. In this work, the EGFP-positive cells were tracked over time in order to determine the toxicity of expression of the Fluc constructs as compared to EGFP alone, in a similar manner to that previously described to deduce the cytotoxicity associated with SOD1 ALS-causing mutations in comparison to wild-type SOD1 (McAlary et al., 2016). The results demonstrate that whilst expression of $Fluc^{DM}$ was cytotoxic to both cell lines used in this work, it was most cytotoxic to NSC-34 cells. Moreover, expression of $Fluc^{WT}$ was only cytotoxic to NSC-34 cells: the viability of Neuro-2a cells expressing $Fluc^{WT}$ was similar to that of cells expressing EGFP alone. Taken together with the aggregation-indices derived from the flow cytometry, these results strongly suggest that aggregation-prone $Fluc^{DM}$ more readily forms toxic inclusions in NSC-34 cells compared to Neuro-2a cells.

One potential reason why NSC-34 cells are more susceptible to cytotoxic inclusion formation than Neuro-2a cells is that they are less equipped to deal with protein aggregation as it arises. Previous work has indicated that the global proteomes of Neuro-2a and NSC-34 cells are very similar (Hornburg et al., 2014); however, the types of proteins that readily associate with aggregation-prone proteins as they form inclusions in these cells had never been defined. Differences in the

classes of proteins found within proteinaceous deposits may begin to explain why some cell types can more readily prevent inclusion formation (Bergemalm et al., 2010). Mass spectrometry analysis revealed that the classes of proteins trapped within $Fluc^{DM}$ inclusions in Neuro-2a and NSC-34 cells are near identical. These protein classes include important components of the systems in place that maintain intracellular proteostasis, including chaperones and components of the proteasome.

The most enriched classes of proteins identified in $Fluc^{DM}$ inclusions in both NSC-34 and Neuro-2a cells were those associated with the translational machinery. Indeed, previous work has suggested that disruption of translation is associated with neurodegenerative disorders. For example, Halliday et al. (2017) identified a link between the expression of misfolded forms of prion and tau proteins, and translational repression *in vivo*. Translation-relevant terms were also reported by Kamelgarn et al. (2018) in a gene ontology assessment of the proteins contained within cytoplasmic inclusions formed by the ALS- and frontotemporal dementia-associated fused in sarcoma (FUS) protein. Moreover, in a humanised mouse model of ALS/frontotemporal dementia, the expression of mutant FUS inhibited protein synthesis and led to impaired neuronal synaptic function (López-Erauskin et al., 2018). Furthermore, the unfolded protein response pathway, which mediates the rate of protein synthesis in cells, is over-activated in the brains of patients with neurodegenerative diseases (Jackson et al., 2015, Halliday et al., 2017, Bosco, 2018, López-Erauskin et al., 2018, Zhang et al., 2018) and therefore may be a promising target for pharmacological intervention to alleviate translational repression in neurodegeneration. The identification of translational machinery within $Fluc^{DM}$ inclusions reinforces the notion that the aggregation of proteins into inclusions disrupts protein translation and this is associated with neurodegenerative disease pathogenesis.

Another highly represented class of proteins found within Fluc^{DM} inclusions in both cell lines were chaperones, including members of the Hsp40, Hsp70, Hsp90, Hsp110 families and the chaperonin TriC/CCT. Previous work has demonstrated the presence of chaperone proteins localised within proteinaceous deposits. For example, Hsp70 and Hsp40 were found to be associated with inclusions formed by polyQ-expanded ataxin-1 (Cummings et al., 2001), ataxin-3 (Chai et al., 1999) and huntingtin (Wyttenbach et al., 2000). Intracellular inclusions formed by mutant SOD1 contain αB-crystallin and Hsc70 (Bergemalm et al., 2010). Hsp70 has been identified in protein aggregates extracted from the brains of ALS/frontotemporal dementia patients with TDP-43-positive proteinopathies (Laferrière et al., 2019). Furthermore, Hsp27 and αB-crystallin were detected within neurofibrillary tangles of patients with Alzheimer's disease (Renkawek et al., 1994). It remains to be determined why chaperone proteins are found within inclusions associated with neurodegenerative diseases; however, it is likely due to their roles in maintaining the solubility and function of aggregation-prone proteins. Thus, the presence of chaperones in inclusions may be due to them having an important role in mitigating the toxicity of inclusions (e.g. through disaggregation). Conversely, chaperones may localise to inclusions due to them failing to rescue misfolded proteins from aggregation.

A variety of proteins that play a role in proteostasis were found to be associated with Fluc^{DM} inclusions in both Neuro-2a and NSC-34 cells. These included proteasome components, proteins related to processing in the ER, and chaperones. Thus, whilst there were few differences between Neuro-2a and NSC-34 cells with regard to the classes of proteins that associate with Fluc^{DM} in inclusions formed in these cells, these data highlight the important role that protein quality control pathways of the proteostasis network play in attempting to mitigate cytotoxic protein aggregation. Whilst the major classes of proteins found to be associated with Fluc^{DM} inclusions in Neuro-2a and NSC-34 cells were similar, the exact proteins identified did differ between cell lines. This does prompt the question whether the abundance of proteins and complexes may account for the

differences in proteins identified between these neuronal cell lines. Given this, it is possible that destabilised $Fluc^{DM}$ "seeds" the formation of inclusions which causes other proteins to co-aggregate through a nonselective process; however, this was not experimentally tested in this work. Nonetheless, this prompted further investigation into the impact of the individual protein quality control pathways in preventing $Fluc^{DM}$ inclusion formation in NSC-34 and Neuro-2a cells.

The heat shock response is a stress-inducible pathway that protects cells from conditions that promote protein misfolding. Since HSF1 is the master regulator of the heat shock response in cells (Vihervaara and Sistonen, 2014, Gomez-Pastor et al., 2018), activation of HSF1 has been proposed as a potential therapeutic for the amelioration of protein misfolding diseases (Kampinga and Bergink, 2016). In this work, as assessed by FloIT, $Fluc^{DM}$ inclusion formation was reduced (by ~50%) in Neuro-2a cells by overexpression of $HSF1^{WT}$, and in NSC-34 cells by overexpression of $HSF1^{WT}$ or $HSF1^{+}$. There was a trend by which expression of $HSF1^{+}$ reduced intracellular inclusion formation by $Fluc^{DM}$ in Neuro-2a cells when analysed by FloIT, however, this result was not statistically significant. Immunoblotting revealed a marked reduction in insoluble $Fluc^{DM}$ in these Neuro-2a cells, suggesting that expression of $HSF1^{+}$ does have some capacity to reduce inclusion formation, but to a lesser extent than $HSF1^{WT}$. These data are largely consistent with previous work which demonstrated that inclusions formed by mutant TDP-43 are reduced following overexpression of $HSF1^{WT}$ or $HSF1^{+}$ (Chen et al., 2016, Wang et al., 2017). Expression of $HSF1^{+}$ reduces the intracellular inclusion formation of polyQ-expanded ataxin-1 (Rimoldi et al., 2001) and atrophin-1 (Fujimoto et al., 2005). Furthermore, $HSF1^{WT}$ expression in a SOD1 mouse model of ALS delays disease progression (Lin et al., 2013) and decreases the accumulation of polyQ-expanded androgen receptor in mice, thereby promoting neuronal survival (Kondo et al., 2013).

The $HSF1^{+}$ isoform lacks the regulatory domain and therefore does not need to be released from chaperone-HSF1 complexes to perform its function. It was hypothesised that expression of $HSF1^{+}$ would result in the upregulation of downstream HSF1-target Hsps to a similar or greater extent than $HSF1^{WT}$ expression. This was confirmed in this study; however, $HSF1^{WT}$ was more effective than $HSF1^{+}$ at inhibiting $Fluc^{DM}$ inclusion formation. Roth et al. (2014) reported that a sustained heat shock response can impair the protein folding capacity of cells. This may explain why $HSF1^{+}$ is less effective at inhibiting $Fluc^{DM}$ inclusion formation compared to $HSF1^{WT}$ in Neuro-2a and NSC-34 cells. In addition, upregulation of downstream products of HSF1 activation may be insufficient to prevent inclusion formation of some aggregation-prone proteins in cells (Bersuker et al., 2013). This is supported by the results of this work since expression of $HSF1^{+}$, but not $HSF1^{WT}$, resulted in the increased expression of Hsps such as Hsp40 and Hsp90, however overexpression of $HSF1^{WT}$ was more effective at preventing the formation of inclusions by $Fluc^{DM}$. This suggests that the anti-aggregation capacity of $HSF1^{WT}$ is not solely dependent upon the upregulation of Hsps. Indeed, the increase in soluble $Fluc^{DM}$ observed by immunoblotting and epifluorescence microscopy indicates that $HSF1^{WT}$ expression may have downstream effects on other arms of the proteostasis machinery. For example, HSF1 activation can induce the expression of products known to be responsible for trafficking misfolded proteins for degradation via the ubiquitin-proteasome system or by autophagy (Trinklein et al., 2004, Vihervaara and Sistonen, 2014). Moreover, heat shock can accelerate the rate of endogenous protein degradation by the proteasome in mammalian cells, which is evidenced by an increase in the ubiquitination of cellular proteins and a decrease in the levels of free ubiquitin (Parag et al., 1987). Thus, activation of HSF1 may upregulate downstream products of the heat shock response in Neuro-2a and NSC-34 cells, which help to maintain $Fluc^{DM}$ in a soluble state so that it can be acted upon by the degradation machinery. Overall, the data presented here provide evidence that activation of HSF1 can bolster the capacity of Neuro-2a and NSC-34 cells to prevent protein aggregation. Thus, HSF1 activation may be a therapeutic approach for the treatment of neurodegenerative diseases (Neef et al., 2010,

Neef et al., 2011, Kampinga and Bergink, 2016, Dayalan Naidu and Dinkova-Kostova, 2017, Gomez-Pastor et al., 2018). Future work should aim to elucidate the precise mechanisms by which activation of HSF1 inhibits intracellular inclusion formation.

Previous studies have indicated that the ubiquitin-proteasome system degrades up to 90% of the aberrant, short-lived, denatured, destabilised or damaged nuclear and cytosolic proteins within eukaryotic cells (Rock et al., 1994, Hershko and Ciechanover, 1998, Glickman and Ciechanover, 2002, Luo and Le, 2010). It is also widely accepted that defects in the ability of the proteasome to degrade misfolded or aggregated proteins are linked to various neurodegenerative disorders (Mori et al., 1987, Manetto et al., 1988, Li et al., 2010). The results from this work indicate that inhibition of proteasomal degradation in Neuro-2a or NSC-34 cells expressing $Fluc^{DM}$ leads to a significant increase in the formation of inclusions in these cells. Furthermore, overexpression of free ubiquitin did not have a significant effect on $Fluc^{DM}$ inclusion formation in these cells, at least under the experimental conditions tested in this work. The increase in $Fluc^{DM}$ aggregation in cells following treatment with MG132 suggests that this aggregation-prone protein is degraded by the proteasome, a result that is consistent with the results presented in Chapter 4 of this thesis. While proteasome inhibitors are cheap and readily available, activators of the proteasome are less well described. In this work, overexpression of ubiquitin was chosen as an activator of proteasomal degradation since an increase in free ubiquitin correlates to the accelerated ubiquitination of destabilised proteins for subsequent targeting for degradation by the proteasome (Salomons et al., 2009). However, further work is required to confirm that overexpression of ubiquitin does increase proteasome activity in these cells.

Previous studies have identified that small molecule proteasome activators can enhance proteasomal degradation to inhibit disease-related protein aggregation in cells. For example, Lee et al. (2010) utilised a small molecule inhibitor of ubiquitin-specific protease 14, a proteasome-

associated deubiquitinating enzyme, to promote the degradation of misfolded proteins such as tau and TDP-43 (Lee et al., 2010). Similarly, the overexpression of the cellular proteasome activator 28 was shown to improve cell viability in a polyQ-expanded huntingtin-expressing neuronal cell line (Seo et al., 2007). To test whether enhanced proteasome activity (i.e. using small molecule proteasome activators) can boost the ability of NSC-34 cells to prevent $Fluc^{DM}$ inclusion formation, further studies are required. Upregulation of the ubiquitin-proteasome system through proteasomal activation may offer a novel therapeutic strategy to reduce the accumulation of misfolded proteins in cells that have been exposed to cellular stress or during aging.

In some cases the proteasome is unable to the facilitate degradation of aggregated proteins (Lee and Goldberg, 1998). Induced activation of autophagy via certain drugs (e.g. rapamycin) has been shown to be effective in removing aggregates that are unable to be degraded by the proteasome (Rubinsztein et al., 2012). Moreover, previous work has demonstrated that activation of autophagy can alleviate protein aggregation and its associated toxicity in disease models of Parkinson's disease (Webb et al., 2003), Alzheimer's disease (Haung Yu et al., 2005) and Huntington's disease (Ravikumar et al., 2004, Bjørkøy et al., 2005). These results highlight the important role of autophagy in clearing aggregation-prone proteins, independent of the proteasome. To decipher whether autophagy plays a significant role in the degradation of aggregation-prone $Fluc^{DM}$ in Neuro-2a and NSC-34 cells, cells expressing $Fluc^{DM}$ were treated with the autophagy inhibitor bafilomycin A1 or autophagy activator rapamycin. The results from these experiments show there was no significant effect of rapamycin treatment on inclusion formation in either cell line. However, upon treatment with bafilomycin A1, $Fluc^{DM}$ inclusion formation increased significantly, such that it reached similar levels to that measured following inhibition of the proteasome. These result suggest that autophagy does play a key role in the clearance of aggregation-prone $Fluc^{DM}$ in these cells; however, since rapamycin treatment did not further decrease $Fluc^{DM}$ inclusion formation, this suggests that the autophagic pathway is already maximal

in these cells and so is not able to be further boosted by rapamycin. This is further supported by the results of the immunoblotting assay, which show that the conversion of LC3I to LC3II (i.e. autophagosome formation) is only slightly increased following treatment with rapamycin.

The final protein quality control network investigated in this work was the effect of ER stress, which triggers a dynamic signalling pathway known as the unfolded protein response (Hetz, 2012). The ER is an important component of the cell that helps to ensure correct folding of many newly synthesised secretory and transmembrane proteins. Perturbations in ER homeostasis can result in an accumulation of unfolded proteins in the ER lumen, termed ER stress (Oslowski and Urano, 2011). Ongoing ER stress, owing to mutations in disease-related genes or malfunctions in the secretory pathway, can lead to cell death and, in some cases, neurodegeneration (Ron and Walter, 2007, Hetz and Mollereau, 2014). In this study, treatment of Neuro-2a and NSC-34 cells expressing $Fluc^{DM}$ with thapsigargin significantly increased inclusion formation in cells, as measured by FloIT, thus demonstrating that ER stress can induce cytosolic accumulation of $Fluc^{DM}$ inclusions. Similar to activators of the proteasome, molecules that promote ER protein folding to reduce ER stress are limited. Azoramide is one known small-molecule modulator of the unfolded protein response that has been reported to lead to an increase in the expression of ER-resident chaperones (e.g. HspH4, GRP78/BiP/HspA5, DNAJC3) for improved protein folding in the ER (Fu et al., 2015); however, its efficacy to prevent intracellular inclusion formation had not been previously tested. Whilst treatment with azoramide was found to increase expression of GRP78/BiP, it had no effect on inclusion formation by $Fluc^{DM}$ in Neuro-2a or NSC-34 cells. Although the working concentrations of azoramide used in this research were chosen based upon a previous study (Fu et al., 2015), it may be that the concentrations used were too low or perhaps a 16 h incubation was insufficient to elicit a significant effect on inclusion formation in these cells. Future work should aim to repeat these experiments with a broader range of azoramide

concentrations to determine whether increasing the expression of ER-resident chaperones can decrease the formation of inclusions in the cytoplasm.

The increase in protein aggregation and accumulation of $Fluc^{DM}$ into inclusions following treatment with thapsigargin was much less than what was observed following treatment of cells with MG132. Together these results support previous findings of a link between ER stress and the functionality of the ubiquitin-proteasome system. Menéndez-Benito et al. (2005) proposed a model whereby ER stress reduces the functionality of the ubiquitin-proteasome system, resulting in some accumulation of misfolded proteins in the cell. However, this accumulation normally only represents ~10% of what is observed when the ubiquitin-proteasome system is inhibited (Menéndez-Benito et al., 2005), findings that are supported by the data obtained for Neuro-2a cells in this study. This suggests that when the ER is faced with an excess of ER misfolded proteins, resulting in ER stress, the degradative capacity of the ubiquitin-proteasome system is compromised, leading to an increased imbalance of substrates in the cytosol. When comparing the relative accumulation of misfolded $Fluc^{DM}$ into inclusions following thapsigargin versus MG132 treatment, it is interesting to note that NSC-34 cells are much more sensitive to thapsigargin treatment than Neuro-2a cells (50% of the NSC-34 cells were found to contain inclusions following thapsigargin treatment, compared to 15% of Neuro-2a cells). Therefore, the susceptibility of NSC-34 cells to protein aggregation may be related to the functional status of the ER and the levels of ER client proteins (Tanaka and Matsuda, 2014).

Overall, this work successfully exploited the aggregation-prone nature of $Fluc^{DM}$ to quantitatively ascertain that NSC-34 cells are more susceptible to inclusion formation by destabilised proteins than Neuro-2a cells. Moreover, the methods presented here mark a first step towards generating a proteostasis capacity index that is broadly applicable to many cell types. Whilst the proteins identified within $Fluc^{DM}$-containing proteinaceous deposits in Neuro-2a and NSC-34 cells were

near identical, the major classes included those belonging to the protein quality control network, suggesting that these systems are important in maintaining the solubility of the protein in these cells. Investigation into the major arms of the protein quality control network validated the use of $Fluc^{DM}$ as a biological tool that can be used to study the proteostasis pathways responsible for regulating the aggregation of destabilised proteins into inclusions. By utilising pharmacological and genetic approaches to modulate the proteostasis machinery, the results presented in this chapter suggest that the ubiquitin-proteasome and autophagy pathways are both responsible for the degradation of $Fluc^{DM}$ in Neuro-2a and NSC-34 cells. Furthermore, the functional status of the heat shock response and/or the ER appears to contribute to the increased susceptibility of NSC-34 cells to inclusion formation compared to Neuro-2a cells. Identification of the pathways important in preventing protein aggregation, along with techniques that can be used to assess the susceptibility of cell types to inclusion formation, provides a basis for the development of effective therapies against neurodegenerative diseases.

Chapter 6: Conclusions and future directions

The maintenance of proteostasis is essential for cell and organism survival. Many neurodegenerative conditions are associated with protein aggregation and their incidence increases with age, suggestive of a failure in the ability of cells to effectively maintain proteostasis in response to cellular aging (Carra et al., 2008b, Behl, 2011, Minoia et al., 2014a). Overwhelming evidence demonstrates that molecular chaperones provide protective effects against protein aggregation; that the levels of many molecular chaperones is dramatically up-regulated during times of cellular stress highlights the important role they play in preventing the accumulation of aggregation-prone proteins into inclusions and plaques in the body. More broadly, identification of the proteostasis mechanisms that play key roles in preventing protein aggregation, as well as techniques that can be used to assess the susceptibility of cells to inclusion formation, provides a foundation for the development of effective therapies to treat neurodegenerative disorders. Thus, the basis of the work presented in this thesis was to determine how proteostasis mechanisms, and in particular Hsp molecular chaperones, prevent inclusion formation by aggregation-prone proteins.

6.1 FloIT is a broadly applicable and quantitative method to assess inclusion formation

The previously described flow cytometric technique FloIT (Whiten et al., 2016) was utilised extensively in the work presented in this thesis. In Chapters 3 and 4, FloIT was used to screen various human Hsp isoforms to identify those most effective at suppressing inclusion formation by the aggregation-prone protein $Fluc^{DM}$. Previous to this, Hsp overexpression screens to identify inhibitors of protein aggregation – including the effects of Hsp activity following mutations in crucial domains/residues – have typically relied on using traditional biochemical analyses, such as filter trap assays or fluorescence microscopy to count cells with inclusions (Hageman et al., 2010, Vos et al., 2010, Hageman et al., 2011, Minoia et al., 2014b, Kakkar et al., 2016a, Serlidaki et al., 2020). Whilst the basic principle behind the filter trap assay and FloIT are the same (i.e. analysis of insoluble protein in a cell lysate), FloIT offers several advantages over the filter trap

assay. First, FloIT can be used in a medium-to-high-throughput capacity for rapid non-subjective quantification of inclusions across samples that may differ in transfection efficiency and cell number. Second, FloIT can identify (and enumerate) inclusions that differ in size, granularity and even protein composition, making FloIT broadly applicable to most (if not all) model systems of protein aggregation in cells (Whiten et al., 2016). The work in this thesis describes the first use of FloIT as a quantitative method to screen for the ability of molecular chaperones (and their mutational variants) to prevent protein aggregation in cells. Furthermore, when the results of the FloIT assay were compared to detergent-based cellular fractionation followed by immunoblotting or counts of cells with inclusions, the FloIT data revealed the same (or similar) trends regarding the aggregation state of the protein, suggesting that FloIT can provide the same level of information as these traditional biochemical assays. Future cell-based overexpression screens conducted to assess the effects of Hsp activity on inclusion formation by other aggregation-prone proteins should therefore consider using FloIT due to it being a quantitative and non-subjective approach.

One disadvantage of FloIT is that the aggregation-prone protein under investigation needs to be fluorescently tagged in order to enumerate inclusions within a cell lysate. In addition, since members of the Hsp library screened as part of Chapter 3 were also not fluorescently tagged, differences in the amount of chaperone being expressed between groups was not able to be determined. It is therefore possible that an increase in the expression of individual Hsps could be responsible for differences in the capacity for some Hsps to inhibit the formation of inclusions by $Fluc^{DM}$ more potently than others. As previously reported, the addition of bulky fluorescent tags can significantly perturb the conformation and function of the target protein (Zacharias et al., 2002). One possible way to alleviate this issue is through the use of self-labelling enzymes, such as SNAP (Sun et al., 2011), CLIP (Gautier et al., 2008) or Halo (Los et al., 2008) tags, which are fused in frame with the protein of interest to enable the covalent attachment of small fluorescent

ligands. Ideally, a fluorescent tag to label proteins for cell-based experiments should be small in size, specific, chemically stable and bright, and have minimal perturbation on the folding and function of the target protein. However, it is not always possible to meet all of these criteria and compromises are often made depending on the system under investigation. Overall, the overexpression screen was conducted as part of an initial analysis of many Hsps for their capacity to modulate $Fluc^{DM}$ inclusion formation, with the aim to perform follow up analyses on those found to be the most potent suppressors of $Fluc^{DM}$ aggregation. As part of the work presented in Chapter 4, use of immunoblotting confirmed that the expression of V5-tagged DNAJBs did not differ substantially between groups. Based on these findings it was concluded that variances in the capacity of Hsp family members to inhibit $Fluc^{DM}$ would primarily be due to intrinsic differences in their chaperone activity against this aggregation-prone client protein.

The work presented in Chapter 5 successfully developed FloIT as one method for the derivation of an aggregation index to measure the proteostasis capacity of two neuronal cell lines. The approach undertaken in this work extends upon the previously reported uses of FloIT (Whiten et al., 2016, Zeineddine et al., 2017, San Gil et al., 2020) by taking into account the amount of aggregation-prone protein that is expressed in the transfected cell population. Future experiments should seek to incorporate other cell lines, such as cancer (e.g. HeLa and MCF-7 cells) and human-derived neuronal (e.g. SH-SY5Y cells) cell lines or primary neurons differentiated from human stem cells, in this type of approach as this would help to validate that this method for determining the susceptibility of cell types to inclusion formation is broadly applicable. The eventual development of a system to score or rank the proteostasis capacity of cells based on the propensity of an aggregation-prone protein to form inclusions would be a significant step towards delineating why some cell types are more susceptible to inclusion formation than others. Overall, the different uses of FloIT described in this thesis highlight the power and potential applications of this technique to the field of proteostasis.

6.2 Fluc^{DM} as an aggregation-prone protein to model inclusion formation in cells

Cell-based models are important biological tools that can be used to study protein aggregation in response to cellular stress within the highly dynamic intracellular environment. This work exploited Fluc^{DM} as a structurally destabilised aggregation-prone protein to study the amorphous aggregation of proteins into inclusions in cells. One distinct advantage of using Fluc^{DM} for this work is that it readily forms cytosolic inclusions without the need to apply an unfolding stress (Gupta et al., 2011). It therefore acts as an intracellular proteostasis sensor by reporting on the capacity of cells to maintain the protein in a soluble state. To-date, the majority of cell-based studies conducted to reveal the interaction of Hsps with client proteins have investigated proteins whose aggregation is disease related (Hageman et al., 2010, Hageman et al., 2011, Månsson et al., 2014a, Kakkar et al., 2016a, Serlidaki et al., 2020). However, as these proteins are expressed endogenously in cells, their misfolding and aggregation may be associated with disruptions to functional interactions that normally take place in the cell. Thus, Fluc^{DM} was chosen for this work since the overall aim was to identify generic proteostasis mechanisms in cells that engage with aggregation-prone proteins to prevent their aggregation into inclusions, rather than those that may be specific for certain proteins. The work presented in Chapters 3 and 4 successfully identified generic modulators of protein aggregation that arises as a result the destabilisation of a client protein, highlighting the suitability of Fluc^{DM} as a model protein. Furthermore, this work confirmed that inclusion formation by Fluc^{DM} can be monitored in response to the expression of wild-type or mutational DNAJB variants, thereby facilitating the discovery of key mechanistic details pertaining to how DNAJBs engage with destabilised proteins in cells (Chapter 4). Another advantage of using Fluc^{DM} in this work was that the protein retains residual luciferase activity, and thus it was possible to not only assess the capacity of chaperones to prevent aggregation, but also retain Fluc^{DM} in a folded (functional) state (Chapter 3).

As part of the work described in Chapter 5 of this thesis, proteins that assembled with Fluc^{DM} in inclusions in both Neuro-2a and NSC-34 cells were identified. Many of these proteins were associated with major KEGG pathways related to neurodegenerative diseases, including Alzheimer's disease, Parkinson's disease, Huntington's disease, spinocerebellar ataxia, ALS and prion-related diseases. This again highlights the suitability of Fluc^{DM} as an aggregation-prone protein that can be used to model inclusion formation associated with these neurodegenerative diseases. Furthermore, the results from this work demonstrate that Fluc^{DM} is an extremely effective biosensor that can be used to detect changes in proteostasis capacity following genetic and pharmacological modulation. Finally, this work confirmed that Fluc^{DM} is a suitable protein to compare the proteostasis capacity of different cell types.

Based on the Hsp overexpression screen performed as part of Chapter 3, the capacity of the chaperones tested to prevent Fluc^{DM} inclusion formation was found not to be equivalent. For example, the overexpression of a subset of members of the sHsp family (HspB4 HspB6, HspB7 and HspB9) significantly reduced inclusion formation by Fluc^{DM}, whereas others had no effect (HspB1, HspB5 and HspB8). The ability of specific sHsps to prevent aggregation appears to be dependent upon the client protein (discussed in depth in Chapter 3). Despite this, the capacity of a diverse range of sHsps to inhibit the formation of amorphous (Crippa et al., 2010, Carra et al., 2013, Minoia et al., 2014b) and amyloidogenic (Outeiro et al., 2006, Vos et al., 2010, Cox and Ecroyd, 2017) aggregates in cells suggests that methods aimed at increasing the expression or activity of individual sHsps remains a valid option for the amelioration of protein folding diseases. Further research into the interactions between sHsps and Fluc^{DM} would enhance our understanding of the molecular mechanisms by which sHsps stabilise aggregation-prone proteins in the cell.

The capacity of HspB7 to inhibit the aggregation of polyQ-expanded proteins has prompted further investigation into the mechanism by which it inhibits amyloidogenesis in cells (Vos et al., 2010).

However, the process by which HspB7 inhibits inclusion formation by destabilised proteins has not been clearly defined. As such, using HspB7 as an example, future work could express $Fluc^{DM}$ and V5-tagged HspB7 mutational variants in cells to elucidate whether the anti-aggregation activity of HspB7 is dependent upon the N- and/or C-terminal region, or the serine-rich stretch in the α-crystallin domain. A similar approach has been described previously in which expression of mutational variants of HspB7 with polyQ-expanded huntingtin revealed that the anti-aggregation activity of HspB7 was dependent upon an interaction with the N-terminal domain (Vos et al., 2010) The canonical mechanism of sHsp chaperone activity is believed to involve large polydisperse oligomeric complexes that, via dynamic subunit exchange, bind client proteins, which are then transferred to the Hsp70 machinery for refolding (Basha et al., 2004, Bryantsev et al., 2007). To test whether HspB7 inhibits $Fluc^{DM}$ inclusion formation in cells by forming oligomers, future work could express HspB7 or HspB5 (a canonical sHsp) and separate the cell lysates on sucrose gradients to observe complex formation. To assess whether the capacity of HspB7 to inhibit inclusion formation by $Fluc^{DM}$ is dependent upon interaction with the Hsp70 chaperone machinery, $Fluc^{DM}$ could be co-expressed with HspB7, with or without Bag1. Since Bag1 needs to be in a precise stoichiometric ratio with Hsp70 proteins in order to adequately accelerate the Hsp70 ATPase cycle (Nollen et al., 2000, Gässler et al., 2001, Kampinga and Craig, 2010), if Bag1 overexpression did not significantly affect the capacity of HspB7 to prevent $Fluc^{DM}$ inclusion formation, this would indicate that HspB7 does not require interaction with Hsp70. Finally, co-expression of HspB7 with $Fluc^{DM}$, followed by treatment with proteasomal (e.g. MG132 or bortezomib) or autophagy (e.g. bafilomycin A1 or 3-methyladenine) inhibitors could elucidate whether the anti-aggregation activity of HspB7 is dependent upon proteolytic processing by the degradation machinery.

In line with the findings of the sHsp screen, only certain members of the Hsp70 family (i.e. HspA1A and HspA2) were effective at preventing inclusion formation by $Fluc^{DM}$, whilst

overexpression of the NEFs tested in this study did not inhibit Fluc^{DM} inclusion formation. In addition, all the DNAJBs tested were potent inhibitors of intracellular inclusion formation by Fluc^{DM}. Overall, these data provide evidence that overexpression of specific Hsps may prevent amorphous aggregates from forming in cells. However, this work also highlights that when seeking to target Hsp molecular chaperone action for preventing aggregation associated with disease, not all Hsps are equal and there is a need to identify the Hsps capable of preventing the aggregation of the disease-related protein (Kakkar et al., 2014). The results presented in Chapters 3 and 4 of this thesis highlight those Hsps capable of preventing generic aspects of the amorphous aggregation of proteins into inclusions in cells.

6.3 Proteostasis mechanisms employed by cells to prevent inclusion formation

6.3.1 The mechanism by which DNAJBs prevent the aggregation of Fluc^{DM} into inclusions

A primary aim of this work was to utilise Fluc^{DM} to identify proteostasis mechanisms within the cell that are important in maintaining the solubility of destabilised proteins. In Chapter 3, the DNAJB family of proteins were identified as potent suppressors of Fluc^{DM} inclusion formation. Accordingly, in Chapter 4, the mechanism by which specific members of the DNAJB family, namely DNAJB6 and DNAJB8, prevent the aggregation of Fluc^{DM} into inclusions was investigated. Based on these findings a new model for the chaperone mechanism of these DNAJB proteins is presented below. Previous research has identified that DNAJB6-like proteins inhibit the primary nucleation of β-hairpin structures in amyloid-β and polyQ peptides to prevent mature amyloid fibril formation by participating in intramolecular hydrogen bonding with hydroxyl groups in side chains of S/T residues present in the substrate binding domain (Figure 6.1A) (Hageman et al., 2010, Månsson et al., 2014a, Kakkar et al., 2016b). In contrast, this work identified that DNAJB6 and DNAJB8 bind destabilised proteins, such as Fluc^{DM}, via the conserved TTK-LKS motif in the C-terminal domain, in doing so holding the protein in a soluble,

degradation-competent state. These DNAJBs then interact with Hsp70 to support Hsp70-dependent degradation of the destabilised protein via the proteasome (Figure 6.1B).

The finding that DNAJB6 and DNAJB8 possess two distinct domains for binding substrates, highlights the potential of specifically targeting DNAJB chaperone action in the context of protein aggregation associated with disease. This work suggests that it may be possible to identify small drug-like molecules that target a distinct substrate binding region of DNAJB6 or DNAJB8, thereby modulating their capacity to bind to certain client proteins without perturbing their ability to inhibit other forms of protein aggregation as it arises in the cell. For example, it may be possible to develop molecules that boost the ability of these DNAJBs to prevent amyloid formation without interfering with the capacity of these chaperones to bind to destabilised proteins, such as those that arise as a result of an acute cellular stress.

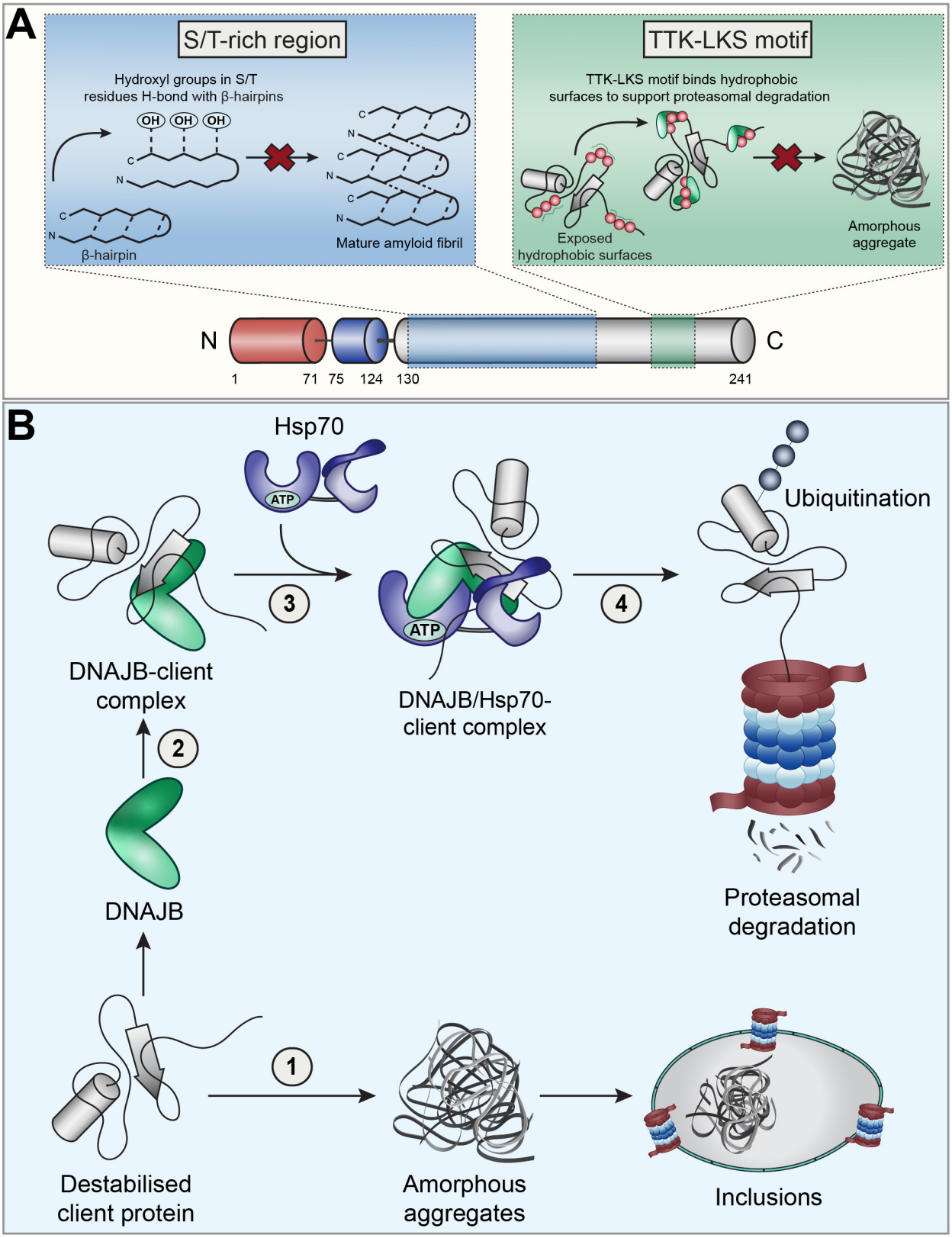

Figure 6.1. The proposed model by which DNAJBs interact with Hsp70 for the handling of destabilised aggregation-prone client proteins in the cell. (A) The hydroxyl groups within the side chains of the S/T-rich region in DNAJB6-like proteins participate in intramolecular hydrogen bonding with β-hairpin structures to prevent their primary nucleation into mature amyloid fibrils. In contrast, DNAJB6-like proteins bind destabilised proteins via the conserved TTK-LKS motif in the C-terminal domain to support Hsp70-dependent degradation via the proteasome. **(B)** (1) Destabilised client proteins can aggregate via a disordered mechanism to form amorphous aggregates which may be sequestered into distinct proteinaceous JUNQ inclusions, previously reported to be associated with proteasomes. (2) Alternatively, DNAJBs can interact with destabilised client proteins to prevent their aggregation. (3) Destabilised client proteins can be held by DNAJBs in a soluble form for delivery to Hsp70 for (4) degradation via the proteasome.

Whilst co-localisation of Fluc^{DM} and DNAJB8 within inclusions was observed as part of the work described in Chapter 4, this technique is limited in its capacity to resolve physical protein-protein interactions. Thus, future work should aim to demonstrate a direct physical interaction between Fluc^{DM} and DNAJB6 or DNAJB8, and examine the effect on DNAJB-Fluc^{DM} binding following mutation of the C-terminal substrate binding domain. A traditional method used to decipher the formation of protein-protein interactions is co-immunoprecipitation; however, these types of experiments are extremely challenging with the DNAJB proteins because the DNAJB-client interactions are generally very weak and transient, and therefore lost during the standard lysis conditions. Another technique for detecting protein-protein interactions that could be performed to confirm interaction between DNAJBs and Fluc^{DM} is biotinylation-based proximity labelling (BioID) in live mammalian cells (Roux et al., 2012). BioID utilises a promiscuous *E.coli* biotin ligase fused to the protein of interest for the selective biotinylation of proteins in proximity to the fusion protein. Following cell lysis and protein denaturation, the biotinylated proteins can be captured by streptavidin affinity purification for subsequent analysis by mass spectrometry or immunoblotting. Thus, by fusing the biotin ligase to DNAJB6 or DNAJB8, client proteins engaged by these chaperones could be identified. Another potential area for future study would be to validate the mechanism by which DNAJB6 or DNAJB8 inhibits Fluc^{DM} aggregation *in vivo*. This could be achieved using a similar approach to that described previously by Hageman et al. (2010), where Fluc^{DM} is expressed in a transgenic *Xenopus laevis* model under the control of a muscle specific promoter. DNAJB6 or DNAJB8, along with variants containing mutations in the J-domain or C-terminal domain, could then be expressed to assess the effects on Fluc^{DM} inclusion formation (Hageman et al., 2010).

6.3.2 Proteostasis mechanisms to prevent destabilised inclusion formation may differ between cell types

Based on the results presented in Chapter 4, DNAJBs facilitate interaction of destabilised client proteins with Hsp70 for their subsequent degradation via the proteasome: autophagy plays little (if any) role in the processing of $Fluc^{DM}$ in HEK293 cells. However, manipulation of the arms of the protein quality control network in Chapter 5 indicated that, in Neuro-2a and NSC-34 cells, the capacity of the proteasome or autophagy to degrade $Fluc^{DM}$ was equal. These data suggest that neurons may not utilise the same cellular pathways to maintain proteostasis in response to inclusion formation by destabilised proteins. The neurodegenerative diseases associated with failures in proteostasis are typically late onset (i.e. middle age or later), depending on whether the disease occurs from sporadic or familial origins. Thus, neurons remain functional for decades; however, in some neuronal cells, age-related declines in proteostasis mechanisms lead to misfolding and aggregation (Balch et al., 2008, Douglas and Dillin, 2010). The ability of neurons to maintain proteostasis throughout many decades of life has been attributed to the protective nature of the chaperone machinery (Smith et al., 2015). Links between mutations in molecular chaperones and familial cases of neurodegenerative disease further demonstrate the importance of molecular chaperones in the maintenance of proteostasis in neurons (Hansen et al., 2002, Irobi et al., 2004, De Mena et al., 2009, Selcen et al., 2009). It would therefore be interesting to determine whether the mechanisms by which chaperones prevent $Fluc^{DM}$ inclusion formation in Neuro-2a and NSC-34 cells is the same as that reported here for HEK293 cells. In addressing this area, future studies could utilise a similar approach to that undertaken in this work, i.e. by overexpressing individual DNAJBs (or H/Q variants) in neuronal cells, combined with the inhibition of degradation pathways. Continued work into assessing which components of the proteostasis network are the most critical with regard to preventing protein aggregation in cells may enable therapeutic targeting of key regulators of this process as a means of treating neurodegenerative diseases.

6.3.3 The effect of the heat shock response on intracellular inclusion formation

A major result of the work presented in this thesis was that overexpression of HSF1 reduced inclusion formation by $Fluc^{DM}$ in both Neuro-2a and NSC-34 cells (Chapter 5). Interestingly, it was found that the mechanism by which $HSF1^{WT}$ overexpression leads to a decrease in inclusion formation by $Fluc^{DM}$ is not dependent upon the upregulation of Hsp levels in the cell. Previous work has demonstrated that HSF1 activation can increase the rate of protein degradation by the proteasome in mammalian cells (Parag et al., 1987, Vihervaara and Sistonen, 2014). Thus, HSF1 overexpression in this work may increase the presentation of destabilised proteins to the ubiquitin-proteasome system for degradation. To test this, future work could utilise immunoblotting to investigate whether $Fluc^{DM}$ is ubiquitinated upon overexpression of HSF1, and therefore most likely intended for proteasomal degradation. Changes in the level of expression of representative proteasomal regulatory subunits (e.g. 20Sα, 20Sβ3, 19S and 11S) could also be detected by immunoblotting. Alternatively, the chymotrypsin-, caspase-, or trypsin-like specific proteasome activities could be measured in lysates from cells overexpressing HSF1 (or not), as described previously (Taylor et al., 2005). Future work to elucidate the mechanism by which HSF1 overexpression inhibits destabilised protein aggregation in cells is important given that modulation of the heat shock response for disease intervention is continuing to be explored as a potential avenue for therapeutic intervention (Gomez-Pastor et al., 2018).

Previous research has established pathological hallmarks of neurodegenerative diseases (i.e. protein aggregation and neuro-inflammation), are poor inducers of the heat shock response in neuronal cells (Nishimura et al., 1991, Krueger et al., 1999, Pavlik and Aneja, 2007, Oza et al., 2008, Yang et al., 2008, San Gil et al., 2020). This suggests that the cause of protein aggregation associated with neurodegenerative diseases may be the inability of neurons to sense and respond to protein destabilisation. It may therefore be beneficial to pharmacologically or genetically upregulate the heat shock response in these vulnerable cell types. Future work could utilise a stable

Neuro-2a cell line that harbours a fluorescent reporter of heat shock response activation, such as that previously described (San Gil et al., 2020), that is co-transfected with $Fluc^{DM}$, to screen compound libraries for the identification of heat shock response-inducing compounds. This method would facilitate the screening of compounds which induce the heat shock response as well as deciphering whether (or not) this is correlated with a decline in inclusion formation in cells.

6.4 Concluding remarks

The work presented in this thesis confirms $Fluc^{DM}$ as a "proteostasis sensor" and model protein that can be used to investigate the ability of the protein quality control network to engage with, and process, destabilised client proteins in cells. Through the use of FloIT, the work in this thesis provides a basis for developing this flow cytometric technique as a standard approach for assessing inclusion formation in cells, measuring the proteostasis capacity of cells, or as a screening tool to identify proteins and compounds capable of preventing protein aggregation associated with a variety of neurodegenerative diseases. For the first time, this work identified that DNAJBs possess at least two distinct substrate binding regions for interacting with client proteins, one involved in the interactions with amyloid-forming proteins and the other involved in binding to destabilised proteins in danger of amorphously aggregating. Thus, this work significantly contributes to our understanding of how DNAJBs interact with client proteins in the cell to prevent their aggregation into inclusions. Overall, this knowledge highlights the potential of targeting molecular chaperones and arms of the protein quality control network for the amelioration of debilitating neurodegenerative diseases associated with protein aggregation.

Chapter 7: References

Abarbanel, J.M., Frisher, S. & Osimani, A. 1986. Primary amyloidosis with peripheral neuropathy and signs of motor neuron disease. *Neurology,* **36,** 1125-1127.

Abu-Farha, M., Cherian, P., Al-Khairi, I., Tiss, A., Khadir, A., Kavalakatt, S., Warsame, S., Dehbi, M., Behbehani, K. & Abubaker, J. 2015. DNAJB3/HSP-40 cochaperone improves insulin signaling and enhances glucose uptake *in vitro* through JNK repression. *Scientific Reports,* **5,** 14448.

Abubaker, J., Tiss, A., Abu-Farha, M., Al-Ghimlas, F., Al-Khairi, I., Baturcam, E., Cherian, P., Elkum, N., Hammad, M., John, J., Kavalakatt, S., Khadir, A., Warsame, S., Dermime, S., Behbehani, K. & Dehbi, M. 2013. DNAJB3/HSP-40 cochaperone is downregulated in obese humans and is restored by physical exercise. *PLoS ONE,* **8,** e69217.

Adachi, H., Katsuno, M., Waza, M., Minamiyama, M., Tanaka, F. & Sobue, G. 2009. Heat shock proteins in neurodegenerative diseases: pathogenic roles and therapeutic implications. *International Journal of Hyperthermia,* **25,** 647-654.

Agarraberes, F.A. & Dice, J.F. 2001. A molecular chaperone complex at the lysosomal membrane is required for protein translocation. *Journal of Cell Science,* **114,** 2491-2499.

Ago, T., Liu, T., Zhai, P., Chen, W., Li, H., Molkentin, J.D., Vatner, S.F. & Sadoshima, J. 2008. A redox-dependent pathway for regulating class II HDACs and cardiac hypertrophy. *Cell,* **133,** 978-993.

Åkerfelt, M., Morimoto, R.I. & Sistonen, L. 2010. Heat shock factors: integrators of cell stress, development and lifespan. *Nature Reviews Molecular Cell Biology,* **11,** 545-555.

Albanèse, V., Yam, A.Y.W., Baughman, J., Parnot, C. & Frydman, J. 2006. Systems analyses reveal two chaperone networks with distinct functions in eukaryotic cells. *Cell,* **124,** 75-88.

Alexandrescu, A.T. 2005. Amyloid accomplices and enforcers. *Protein Science,* **14,** 1-12.

Allan Drummond, D. & Wilke, C.O. 2009. The evolutionary consequences of erroneous protein synthesis. *Nature Reviews Genetics,* **10,** 715-724.

Anckar, J. & Sistonen, L. 2011. Regulation of HSF1 function in the heat stress response: implications in aging and disease. *Annual Review of Biochemistry,* **80,** 1089-1115.

Andersson, H., Baechi, T., Hoechl, M. & Richter, C. 1998. Autofluorescence of living cells. *Journal of Microscopy,* **191,** 1-7.

Andley, U.P., Song, Z., Wawrousek, E.F. & Bassnett, S. 1998. The molecular chaperone αA-crystallin enhances lens epithelial cell growth and resistance to UVA stress. *Journal of Biological Chemistry,* **273,** 31252-31261.

Andréasson, C., Fiaux, J., Rampelt, H., Mayer, M.P. & Bukau, B. 2008. Hsp110 is a nucleotide-activated exchange factor for Hsp70. *Journal of Biological Chemistry,* **283,** 8877-8884.

Anfinsen, C.B. 1973. Principles that govern the folding of protein chains. *Science,* **181,** 223-230.

Antoku, K., Maser, R.S., Scully, W.J., Delach, S.M. & Johnson, D.E. 2001. Isolation of Bcl-2 binding proteins that exhibit homology with BAG-1 and suppressor of death domains protein. *Biochemical and Biophysical Research Communications,* **286,** 1003-1010.

Aquilina, J.A., Shrestha, S., Morris, A.M. & Ecroyd, H. 2013. Structural and functional aspects of hetero-oligomers formed by the small heat shock proteins αB-crystallin and HSP27. *Journal of Biological Chemistry,* **288,** 13602-13609.

Arndt, V., Daniel, C., Nastainczyk, W., Alberti, S. & Höhfeld, J. 2005. BAG-2 acts as an inhibitor of the chaperone-associated ubiquitin ligase CHIP. *Molecular Biology of the Cell,* **16,** 5891-5900.

Arrasate, M., Mitra, S., Schweitzer, E.S., Segal, M.R. & Finkbeiner, S. 2004. Inclusion body formation reduces levels of mutant huntingtin and the risk of neuronal death. *Nature,* **431,** 805-810.

Arrigo, A.P., Virot, S., Chaufour, S., Firdaus, W., Kretz-Remy, C. & Diaz-Latoud, C. 2005. Hsp27 consolidates intracellular redox homeostasis by upholding glutathione in its reduced form and by decreasing iron intracellular levels. *Antioxidants and Redox Signaling,* **7,** 414-424.

Auluck, P.K., Chan, H.Y.E., Trojanowski, J.Q., Lee, V.M.Y. & Bonini, N.M. 2002. Chaperone suppression of α-synuclein toxicity in a *Drosophila* model for Parkinson's disease. *Science,* **295,** 865-868.

Baaklini, I., Wong, M.J.H., Hantouche, C., Patel, Y., Shrier, A. & Young, J.C. 2012. The DNAJA2 substrate release mechanism is essential for chaperone-mediated folding. *Journal of Biological Chemistry,* **287,** 41939-41954.

Bagola, K. & Sommer, T. 2008. Protein quality control: on IPODs and other JUNQ. *Current Biology,* **18,** R1019-R1021.

Bailey, C.K., Andriola, I.F.M., Kampinga, H.H. & Merry, D.E. 2002. Molecular chaperones enhance the degradation of expanded polyglutamine repeat androgen receptor in a cellular model of spinal and bulbar muscular atrophy. *Human Molecular Genetics,* **11,** 515-523.

Balch, W.E., Morimoto, R.I., Dillin, A. & Kelly, J.W. 2008. Adapting proteostasis for disease intervention. *Science,* **319,** 916-919.

Balchin, D., Hayer-Hartl, M. & Hartl, F.U. 2016. *In vivo* aspects of protein folding and quality control. *Science,* **353,** 1-12.

Banci, L., Bertini, I., Durazo, A., Girotto, S., Gralla, E.B., Martinelli, M., Valentine, J.S., Vieru, M. & Whitelegge, J.P. 2007. Metal-free superoxide dismutase forms soluble oligomers under physiological conditions: a possible general mechanism for familial ALS. *Proceedings of the National Academy of Sciences of the United States of America,* **104,** 11263-11267.

Basha, E., Lee, G.J., Demeler, B. & Vierling, E. 2004. Chaperone activity of cytosolic small heat shock proteins from wheat. *European Journal of Biochemistry,* **271,** 1426-1436.

Beckmann, R.P., Mizzen, L.A. & Welch, W.J. 1990. Interaction of Hsp70 with newly synthesized proteins: implications for protein folding and assembly. *Science,* **248,** 850-854.

Behl, C. 2011. BAG3 and friends: co-chaperones in selective autophagy during aging and disease. *Autophagy,* **7,** 795-798.

Behnke, J., Mann, M.J., Scruggs, F.L., Feige, M.J. & Hendershot, L.M. 2016. Members of the Hsp70 family recognize distinct types of sequences to execute ER quality control. *Molecular Cell,* **63,** 739-752.

Bellmann, K., Jäättelä, M., Wissing, D., Burkart, V. & Kolb, H. 1996. Heat shock protein Hsp70 overexpression confers resistance against nitric oxide. *FEBS Letters,* **391,** 185-188.

Ben-Zvi, A., Miller, E.A. & Morimoto, R.I. 2009. Collapse of proteostasis represents an early molecular event in *Caenorhabditis elegan*s aging. *Proceedings of the National Academy of Sciences of the United States of America,* **106,** 14914-14919.

Bergemalm, D., Forsberg, K., Srivastava, V., Graffmo, K.S., Andersen, P.M., Brännström, T., Wingsle, G. & Marklund, S.L. 2010. Superoxide dismutase-1 and other proteins in inclusions from transgenic amyotrophic lateral sclerosis model mice. *Journal of Neurochemistry,* **114,** 408-418.

Bersuker, K., Hipp, M.S., Calamini, B., Morimoto, R.I. & Kopito, R.R. 2013. Heat shock response activation exacerbates inclusion body formation in a cellular model of Huntington disease. *Journal of Biological Chemistry,* **288,** 23633-23638.

Bhagyalaxmi, S.G., Srinivas, P.N.B.S., Barton, K.A., Kumar, K.R., Vidyavathi, M., Petrash, J.M., Bhanuprakash Reddy, G. & Padma, T. 2009. A novel mutation (F71L) in αA-crystallin with defective chaperone-like function associated with age-related cataract. *Biochimica et Biophysica Acta - Molecular Basis of Disease,* **1792,** 974-981.

Bharadwaj, S., Ali, A. & Ovsenek, N. 1999. Multiple components of the HSP90 chaperone complex function in regulation of heat shock factor 1 *in vivo*. *Molecular and Cellular Biology,* **19,** 8033-8041.

Bjørkøy, G., Lamark, T., Brech, A., Outzen, H., Perander, M., Øvervatn, A., Stenmark, H. & Johansen, T. 2005. p62/SQSTM1 forms protein aggregates degraded by autophagy and has a protective effect on huntingtin-induced cell death. *Journal of Cell Biology,* **171,** 603-614.

Blomfield, J. & Farrar, J.F. 1969. The fluorescent properties of maturing arterial elastin. *Cardiovascular Research,* **3,** 161-170.

Blumen, S.C., Astord, S., Robin, V., Vignaud, L., Toumi, N., Cieslik, A., Achiron, A., Carasso, R.L., Gurevich, M., Braverman, I., Blumen, N., Munich, A., Barkats, M. & Viollet, L. 2012. A rare recessive distal hereditary motor neuropathy with HSJ1 chaperone mutation. *Annals of Neurology,* **71,** 509-519.

Bolt, M.W. & Mahoney, P.A. 1997. High-efficiency blotting of proteins of diverse sizes following sodium dodecyl sulfate-polyacrylamide gel electrophoresis. *Analytical Biochemistry,* **247,** 185-192.

Boncoraglio, A., Minoia, M. & Carra, S. 2012. The family of mammalian small heat shock proteins (HSPBs): implications in protein deposit diseases and motor neuropathies. *International Journal of Biochemistry and Cell Biology,* **44,** 1657-1669.

Bonnycastle, L.L.C., Yu, C.E., Hunt, C.R., Trask, B.J., Clancy, K.P., Weber, J.L., Patterson, D. & Schellenberg, G.D. 1994. Cloning, sequencing, and mapping of the human chromosome 14 heat shock protein gene (hspa2). *Genomics,* **23,** 85-93.

Borchelt, D.R., Guarnieri, M., Wong, P.C., Lee, M.K., Slunt, H.S., Xu, Z.S., Sisodia, S.S., Price, D.L. & Cleveland, D.W. 1995. Superoxide dismutase 1 subunits with mutations linked to familial amyotrophic lateral sclerosis do not affect wild-type subunit function. *Journal of Biological Chemistry,* **270,** 3234-3238.

Borrell-Pagès, M., Canals, J.M., Cordelières, F.P., Parker, J.A., Pineda, J.R., Grange, G., Bryson, E.A., Guillermier, M., Hirsch, E., Hantraye, P., Cheetham, M.E., Néri, C., Alberch, J., Brouillet, E., Saudou, F. & Humbert, S. 2006. Cystamine and cysteamine increase brain levels of BDNF in Huntington disease via HSJ1b and transglutaminase. *Journal of Clinical Investigation,* **116,** 1410-1424.

Bosco, D.A. 2018. Translation dysregulation in neurodegenerative disorders. *Proceedings of the National Academy of Sciences of the United States of America,* **115,** 12842-12844.

Brehme, M., Voisine, C., Rolland, T., Wachi, S., Soper, J.H., Zhu, Y., Orton, K., Villella, A., Garza, D., Vidal, M., Ge, H. & Morimoto, R.I. 2014. A chaperome subnetwork safeguards proteostasis in aging and neurodegenerative disease. *Cell Reports,* **9,** 1135-1150.

Briknarová, K., Takayama, S., Homma, S., Baker, K., Cabezas, E., Hoyt, D.W., Li, Z., Satterthwait, A.C. & Ely, K.R. 2002. BAG4/SODD protein contains a short BAG domain. *Journal of Biological Chemistry,* **277,** 31172-31178.

Broadley, S.A. & Hartl, F.U. 2009. The role of molecular chaperones in human misfolding diseases. *FEBS Letters,* **583,** 2647-2653.

Brockwell, D.J. & Radford, S.E. 2007. Intermediates: ubiquitous species on folding energy landscapes? *Current Opinion in Structural Biology,* **17,** 30-37.

Brodsky, J.L. & Schekman, R. 1993. A Sec63p-BiP complex from yeast is required for protein translocation in a reconstituted proteoliposome. *Journal of Cell Biology,* **123,** 1355-1363.

Bryantsev, A.L., Kurchashova, S.Y., Golyshev, S.A., Polyakov, V.Y., Wunderink, H.F., Kanon, B., Budagova, K.R., Kabakov, A.E. & Kampinga, H.H. 2007. Regulation of stress-induced intracellular sorting and chaperone function of Hsp27 (HspB1) in mammalian cells. *Biochemical Journal,* **407,** 407-417.

Bucciantini, M., Giannoni, E., Chiti, F., Baroni, F., Formigli, L., Zurdo, J., Taddei, N., Ramponi, G., Dobson, C.M. & Stefani, M. 2002. Inherent toxicity of aggregates implies a common mechanism for protein misfolding diseases. *Nature,* **416,** 507-511.

Buchberger, A., Schröder, H., Hesterkamp, T., Schönfeld, H.J. & Bukau, B. 1996. Substrate shuttling between the DnaK and GroEL systems indicates a chaperone network promoting protein folding. *Journal of Molecular Biology,* **261,** 328-333.

Bukau, B., Weissman, J. & Horwich, A. 2006. Molecular chaperones and protein quality control. *Cell,* **125,** 443-451.

Carra, S. 2009. The stress-inducible HspB8-Bag3 complex induces the eIF2α kinase pathway: implications for protein quality control and viral factory degradation? *Autophagy,* **5,** 428-429.

Carra, S., Boncoraglio, A., Kanon, B., Brunsting, J.F., Minoia, M., Rana, A., Vos, M.J., Seidel, K., Sibon, O.C.M. & Kampinga, H.H. 2010. Identification of the *Drosophila* ortholog of HSPB8: implication of HSPB8 loss of function in protein folding diseases. *Journal of Biological Chemistry,* **285,** 37811-37822.

Carra, S., Brunsting, J.F., Lambert, H., Landry, J. & Kampinga, H.H. 2009. HspB8 participates in protein quality control by a non-chaperone-like mechanism that requires eIF2α phosphorylation. *Journal of Biological Chemistry,* **284,** 5523-5532.

Carra, S., Rusmini, P., Crippa, V., Giorgetti, E., Boncoraglio, A., Cristofani, R., Naujock, M., Meister, M., Minoia, M., Kampinga, H.H. & Poletti, A. 2013. Different anti-aggregation and pro-degradative functions of the members of the mammalian sHSP family in neurological disorders. *Philosophical Transactions of the Royal Society B: Biological Sciences,* **368,** 1-13.

Carra, S., Seguin, S.J., Lambert, H. & Landry, J. 2008a. HspB8 chaperone activity toward poly(Q)-containing proteins depends on its association with Bag3, a stimulator of macroautophagy. *Journal of Biological Chemistry,* **283,** 1437-1444.

Carra, S., Seguin, S.J. & Landry, J. 2008b. HspB8 and Bag3: a new chaperone complex targeting misfolded proteins to macroautophagy. *Autophagy,* **4,** 237-239.

Carra, S., Sivilotti, M., Zobel, A.T.C., Lambert, H. & Landry, J. 2005. HspB8, a small heat shock protein mutated in human neuromuscular disorders, has *in vivo* chaperone activity in cultured cells. *Human Molecular Genetics,* **14,** 1659-1669.

Cashman, N.R., Durham, H.D., Blusztajn, J.K., Oda, K., Tabira, T., Shaw, I.T., Dahrouge, S. & Antel, J.P. 1992. Neuroblastoma × spinal cord (NSC) hybrid cell lines resemble developing motor neurons. *Developmental Dynamics,* **194,** 209-221.

Cattaneo, E., Rigamonti, D., Goffredo, D., Zuccato, C., Squitieri, F. & Sipione, S. 2001. Loss of normal huntingtin function: new developments in Huntington's disease research. *Trends in Neurosciences,* **24,** 182-188.

Cecchi, C., Baglioni, S., Fiorillo, C., Pensalfini, A., Liguri, G., Nosi, D., Rigacci, S., Bucciantini, M. & Stefani, M. 2005. Insights into the molecular basis of the differing susceptibility of varying cell types to the toxicity of amyloid aggregates. *Journal of Cell Science,* **118,** 3459-3470.

Chacinska, A., Koehler, C.M., Milenkovic, D., Lithgow, T. & Pfanner, N. 2009. Importing mitochondrial proteins: machineries and mechanisms. *Cell,* **138,** 628-644.

Chai, Y., Koppenhafer, S.L., Bonini, N.M. & Paulson, H.L. 1999. Analysis of the role of heat shock protein (Hsp) molecular chaperones in polyglutamine disease. *Journal of Neuroscience,* **19,** 10338-10347.

Chamberlain, A.K., Macphee, C.E., Zurdo, J., Morozova-Roche, L.A., Hill, H.a.O., Dobson, C.M. & Davis, J.J. 2000. Ultrastructural organization of amyloid fibrils by atomic force microscopy. *Biophysical Journal,* **79,** 3282-3293.

Chan, H.Y.E., Warrick, J.M., Gray-Board, G.L., Paulson, H.L. & Bonini, N.M. 2000. Mechanisms of chaperone suppression of polyglutamine disease: selectivity, synergy and modulation of protein solubility in *Drosophila*. *Human Molecular Genetics,* **9,** 2811-2820.

Chapple, J.P. & Cheetham, M.E. 2003. The chaperone environment at the cytoplasmic face of the endoplasmic reticulum can modulate rhodopsin processing and inclusion formation. *Journal of Biological Chemistry,* **278,** 19087-19094.

Chapple, J.P., Van Der Spuy, J., Poopalasundaram, S. & Cheetham, M.E. 2004. Neuronal DnaJ proteins HSJ1a and HSJ1b: a role in linking the Hsp70 chaperone machine to the ubiquitin-proteasome system? *Biochemical Society Transactions,* **32,** 640-642.

Charette, S.J., Lavoie, J.N., Lambert, H. & Landry, J. 2000. Inhibition of Daxx-mediated apoptosis by heat shock protein 27. *Molecular and Cellular Biology,* **20,** 7602-7612.

Cheetham, M.E. & Caplan, A.J. 1998. Structure, function and evolution of DnaJ: conservation and adaptation of chaperone function. *Cell Stress and Chaperones,* **3,** 28-36.

Chen, H.J., Mitchell, J.C., Novoselov, S., Miller, J., Nishimura, A.L., Scotter, E.L., Vance, C.A., Cheetham, M.E. & Shaw, C.E. 2016. The heat shock response plays an important role in TDP-43 clearance: evidence for dysfunction in amyotrophic lateral sclerosis. *Brain,* **139,** 1417-1432.

Chen, M.S., Roti Roti, J. & Laszlo, A. 1999. Hsc40, a new member of the Hsp40 family, exhibits similar expression profile to that of Hsc70 in mammalian cells. *Gene,* **238,** 333-341.

Chen, M.Z., Moily, N.S., Bridgford, J.L., Wood, R.J., Radwan, M., Smith, T.A., Song, Z., Tang, B.Z., Tilley, L., Xu, X., Reid, G.E., Pouladi, M.A., Hong, Y. & Hatters, D.M. 2017. A thiol probe for measuring unfolded protein load and proteostasis in cells. *Nature Communications,* **8,** 474.

Cheung, J.K. & Truskett, T.M. 2005. Coarse-grained strategy for modeling protein stability in concentrated solutions. *Biophysical Journal,* **89,** 2372-2384.

Chiarelli, N., Carini, G., Zoppi, N., Ritelli, M. & Colombi, M. 2019. Molecular insights in the pathogenesis of classical Ehlers-Danlos syndrome from transcriptome-wide expression profiling of patients' skin fibroblasts. *PLoS ONE,* **14,** e0211647.

Chirico, W.J., Waters, M.G. & Blobel, G. 1988. 70K heat shock related proteins stimulate protein translocation into microsomes. *Nature,* **332,** 805-810.

Chiti, F. & Dobson, C.M. 2006. Protein misfolding, functional amyloid, and human disease. *Annual Review of Biochemistry,* **75,** 333-366.

Choi, Y.S., Bollinger, S.A., Prada, L.F., Scavone, F., Yao, T. & Cohen, R.E. 2019. High-affinity free ubiquitin sensors for quantifying ubiquitin homeostasis and deubiquitination. *Nature Methods,* **16,** 771-777.

Chowdary, T.K., Raman, B., Ramakrishna, T. & Rao, C.M. 2004. Mammalian Hsp22 is a heat-inducible small heat-shock protein with chaperone-like activity. *Biochemical Journal,* **381,** 379-387.

Ciryam, P., Kundra, R., Morimoto, R.I., Dobson, C.M. & Vendruscolo, M. 2015. Supersaturation is a major driving force for protein aggregation in neurodegenerative diseases. *Trends in Pharmacological Sciences,* **36,** 72-77.

Cox, D. & Ecroyd, H. 2017. The small heat shock proteins αB-crystallin (HSPB5) and Hsp27 (HSPB1) inhibit the intracellular aggregation of α-synuclein. *Cell Stress and Chaperones,* **22,** 589-600.

Cox, D., Selig, E., Griffin, M.D.W., Carver, J.A. & Ecroyd, H. 2016. Small heat-shock proteins prevent α-synuclein aggregation via transient interactions and their efficacy is affected by the rate of aggregation. *Journal of Biological Chemistry,* **291,** 22618-22629.

Craig, E.A. 2018. Hsp70 at the membrane: driving protein translocation. *BMC Biology,* **16,** 11.

Crippa, V., D'agostino, V.G., Cristofani, R., Rusmini, P., Cicardi, M.E., Messi, E., Loffredo, R., Pancher, M., Piccolella, M., Galbiati, M., Meroni, M., Cereda, C., Carra, S., Provenzani, A. & Poletti, A. 2016. Transcriptional induction of the heat shock protein B8 mediates the clearance of misfolded proteins responsible for motor neuron diseases. *Scientific Reports,* **6,** 22827.

Crippa, V., Sau, D., Rusmini, P., Boncoraglio, A., Onesto, E., Bolzoni, E., Galbiati, M., Fontana, E., Marino, M., Carra, S., Bendotti, C., De Biasi, S. & Poletti, A. 2010. The small heat shock protein B8 (HspB8) promotes autophagic removal of misfolded proteins involved in amyotrophic lateral sclerosis (ALS). *Human Molecular Genetics,* **19,** 3440-3456.

Croft, D., Mundo, A.F., Haw, R., Milacic, M., Weiser, J., Wu, G., Caudy, M., Garapati, P., Gillespie, M., Kamdar, M.R., Jassal, B., Jupe, S., Matthews, L., May, B., Palatnik, S., Rothfels, K., Shamovsky, V., Song, H., Williams, M., Birney, E., Hermjakob, H., Stein, L. & D'eustachio, P. 2014. The Reactome pathway knowledgebase. *Nucleic Acids Research,* **42,** D472-D477.

Cummings, C.J., Sun, Y., Opal, P., Antalffy, B., Mestril, R., Orr, H.T., Dillmann, W.H. & Zoghbi, H.Y. 2001. Over-expression of inducible HSP70 chaperone suppresses neuropathology and improves motor function in SCA1 mice. *Human Molecular Genetics,* **10,** 1511-1518.

Daugaard, M., Kirkegaard-Sørensen, T., Ostenfeld, M.S., Aaboe, M., Høyer-Hansen, M., Ørntoft, T.F., Rohde, M. & Jäättelä, M. 2007a. Lens epithelium-derived growth factor is an Hsp70-2 regulated guardian of lysosomal stability in human cancer. *Cancer Research,* **67,** 2559-2567.

Daugaard, M., Rohde, M. & Jäättelä, M. 2007b. The heat shock protein 70 family: highly homologous proteins with overlapping and distinct functions. *FEBS Letters,* **581,** 3702-3710.

Dayalan Naidu, S. & Dinkova-Kostova, A.T. 2017. Regulation of the mammalian heat shock factor 1. *FEBS Journal,* **284,** 1606-1627.

De Mena, L., Coto, E., Sánchez-Ferrero, E., Ribacoba, R., Guisasola, L.M., Salvador, C., Blázquez, M. & Alvarez, V. 2009. Mutational screening of the mortalin gene (HSPA9) in Parkinson's disease. *Journal of Neural Transmission,* **116,** 1289-1293.

De Wit, N.J.W., Verschuure, P., Kappé, G., King, S.M., De Jong, W.W., Van Muijen, G.N.P. & Boelens, W.C. 2004. Testis-specific human small heat shock protein HSPB9 is a cancer/testis antigen, and potentially interacts with the dynein subunit TCTEL1. *European Journal of Cell Biology,* **83,** 337-345.

Demand, J., Alberti, S., Patterson, C. & Höhfeld, J. 2001. Cooperation of a ubiquitin domain protein and an E3 ubiquitin ligase during chaperone/proteasome coupling. *Current Biology,* **11,** 1569-1577.

Deshaies, R.J., Koch, B.D., Werner-Washburne, M., Craig, E.A. & Schekman, R. 1988. A subfamily of stress proteins facilitates translocation of secretory and mitochondrial precursor polypeptides. *Nature,* **332,** 800-805.

Dikic, I. 2017. Proteasomal and autophagic degradation systems. *Annual Review of Biochemistry,* **86,** 193-224.

Dix, D.J., Allen, J.W., Collins, B.W., Mori, C., Nakamura, N., Poorman-Allen, P., Goulding, E.H. & Eddy, E.M. 1996. Targeted gene disruption of Hsp70-2 results in failed meiosis, germ cell apoptosis, and male infertility. *Proceedings of the National Academy of Sciences of the United States of America,* **93,** 3264-3268.

Dix, D.J., Allen, J.W., Collins, B.W., Poorman-Allen, P., Mori, C., Blizard, D.R., Brown, P.R., Goulding, E.H., Strong, B.D. & Eddy, E.M. 1997. HSP70-2 is required for desynapsis of synaptonemal complexes during meiotic prophase in juvenile and adult mouse spermatocytes. *Development,* **124,** 4595-4603.

Dobson, C.M. 2003. Protein folding and misfolding. *Nature,* **426,** 884-890.

Dobson, C.M. 2004. Experimental investigation of protein folding and misfolding. *Methods,* **34,** 4-14.

Dong, M., Bridges, J.P., Apsley, K., Xu, Y. & Weaver, T.E. 2008. ERdj4 and ERdj5 are required for endoplasmic reticulum-associated protein degradation of misfolded surfactant protein C. *Molecular Biology of the Cell,* **19,** 2620-2630.

Doong, H., Price, J., Kim, Y.S., Gasbarre, C., Probst, J., Liotta, L.A., Blanchette, J., Rizzo, K. & Kohn, E. 2000. CAIR-1/BAG-3 forms an EGF-regulated ternary complex with phospholipase C-γ and Hsp70/Hsc70. *Oncogene,* **19,** 4385-4395.

Doong, H., Vrailas, A. & Kohn, E.C. 2002. What's in the 'BAG'? - a functional domain analysis of the BAG-family proteins. *Cancer Letters,* **188,** 25-32.

Douglas, P.M. & Dillin, A. 2010. Protein homeostasis and aging in neurodegeneration. *Journal of Cell Biology,* **190,** 719-729.

Dragovic, Z., Broadley, S.A., Shomura, Y., Bracher, A. & Hartl, F.U. 2006. Molecular chaperones of the Hsp110 family act as nucleotide exchange factors of Hsp70s. *EMBO Journal,* **25,** 2519-2528.

Dreiza, C.M., Brophy, C.M., Komalavilas, P., Furnish, E.J., Joshi, L., Pallero, M.A., Murphy-Ullrich, J.E., Von Rechenberg, M., Ho, Y.S.J., Richardson, B., Xu, N., Zhen, Y., Peltier, J.M. & Panitch, A. 2005. Transducible heat shock protein 20 (HSP20) phosphopeptide alters cytoskeletal dynamics. *FASEB Journal,* **19,** 261-263.

Duffy, P.E. & Tennyson, V.M. 1965. Phase and electron microscopic observations of Lewy bodies and melanin granules in the substantia nigra and locus caeruleus in Parkinson's disease. *Journal of Neuropathology and Experimental Neurology,* **24,** 398-414.

Ebbinghaus, S., Dhar, A., Mcdonald, J.D. & Gruebele, M. 2010. Protein folding stability and dynamics imaged in a living cell. *Nature Methods,* **7,** 319-323.

Ecroyd, H. & Carver, J.A. 2008. Unraveling the mysteries of protein folding and misfolding. *IUBMB Life,* **60,** 769-774.

Ecroyd, H., Meehan, S., Horwitz, J., Aquilina, J.A., Benesch, J.L.P., Robinson, C.V., Macphee, C.E. & Carver, J.A. 2007. Mimicking phosphorylation of αB-crystallin affects its chaperone activity. *Biochemical Journal,* **401,** 129-141.

Ellis, R.J. & Minton, A.P. 2006. Protein aggregation in crowded environments. *Biological Chemistry,* **387,** 485-497.

Eroglu, B., Moskophidis, D. & Mivechi, N.F. 2010. Loss of Hsp110 leads to age-dependent tau hyperphosphorylation and early accumulation of insoluble amyloid β. *Molecular and Cellular Biology,* **30,** 4626-4643.

Esser, C., Alberti, S. & Höhfeld, J. 2004. Cooperation of molecular chaperones with the ubiquitin/proteasome system. *Biochimica et Biophysica Acta,* **1695,** 171-188.

Evans, C.G., Wisén, S. & Gestwicki, J.E. 2006. Heat shock proteins 70 and 90 inhibit early stages of amyloid β-(1-42) aggregation *in vitro*. *Journal of Biological Chemistry,* **281,** 33182-33191.

Eyles, S.J. & Gierasch, L.M. 2010. Nature's molecular sponges: small heat shock proteins grow into their chaperone roles. *Proceedings of the National Academy of Sciences of the United States of America,* **107,** 2727-2728.

Fan, C.Y., Ren, H.Y., Lee, P., Caplan, A.J. & Cyr, D.M. 2005. The type I Hsp40 zinc finger-like region is required for Hsp70 to capture non-native polypeptides from Ydj. *Journal of Biological Chemistry,* **280,** 695-702.

Fan, G.C., Chu, G., Mitton, B., Song, Q., Yuan, Q. & Kranias, E.G. 2004. Small heat-shock protein Hsp20 phosphorylation inhibits β-agonist-induced cardiac apoptosis. *Circulation Research,* **94,** 1474-1482.

Fares, M., Li, Y., Liu, Y., Miao, K., Gao, Z., Zhai, Y. & Zhang, X. 2018. A molecular rotor-based halo-tag ligand enables a fluorogenic proteome stress sensor to detect protein misfolding in mildly stressed proteome. *Bioconjugate Chemistry,* **29,** 215-224.

Farrawell, N.E., Mcalary, L., Lum, J.S., Chisholm, C.G., Warraich, S.T., Blair, I.P., Vine, K.L., Saunders, D.N. & Yerbury, J.J. 2020. Ubiquitin homeostasis is disrupted in TDP-43 and FUS cell models of ALS. *iScience,* **23,** 101700.

Fayazi, Z., Ghosh, S., Marion, S., Bao, X., Shero, M. & Kazemi-Esfarjani, P. 2006. A *Drosophila* ortholog of the human MRJ modulates polyglutamine toxicity and aggregation. *Neurobiology of Disease,* **24,** 226-244.

Feder, M.E. & Hofmann, G.E. 1999. Heat-shock proteins, molecular chaperones, and the stress response: evolutionary and ecological physiology. *Annual Review of Physiology,* **61,** 243-282.

Fink, A.L. 1998. Protein aggregation: folding aggregates, inclusion bodies and amyloid. *Folding and Design,* **3,** R9-R23.

Fink, A.L., Calciano, L.J., Goto, Y., Kurotsu, T. & Falleros, D.R. 1994. Classification of acid denaturation of proteins: intermediates and unfolded states. *Biochemistry,* **33,** 12504-12511.

Finkbeiner, S., Cuervo, A.M., Morimoto, R.I. & Muchowski, P.J. 2006. Disease-modifying pathways in neurodegeneration. *Journal of Neuroscience,* **26,** 10349-10357.

Fontaine, J.M., Rest, J.S., Welsh, M.J. & Benndorf, R. 2003. The sperm outer dense fiber protein is the 10th member of the superfamily of mammalian small stress proteins. *Cell Stress and Chaperones,* **8,** 62-69.

Forloni, G., Angeretti, N., Chiesa, R., Monzani, E., Salmona, M., Bugiani, O. & Tagliavini, F. 1993. Neurotoxicity of a prion protein fragment. *Nature,* **362,** 543-546.

Frydman, J., Nimmesgern, E., Ohtsuka, K. & Hartl, F.U. 1994. Folding of nascent polypeptide chains in a high molecular mass assembly with molecular chaperones. *Nature,* **370,** 111-117.

Fu, S., Yalcin, A., Lee, G.Y., Li, P., Fan, J., Arruda, A.P., Pers, B.M., Yilmaz, M., Eguchi, K. & Hotamisligil, G.S. 2015. Phenotypic assays identify azoramide as a small-molecule modulator of the unfolded protein response with antidiabetic activity. *Science Translational Medicine,* **7,** 292ra298.

Fuchs, M., Poirier, D.J., Seguin, S.J., Lambert, H., Carra, S., Charette, S.J. & Landry, J. 2010. Identification of the key structural motifs involved in HspB8/HspB6-Bag3 interaction. *Biochemical Journal,* **425,** 245-255.

Fujimoto, D., Akiba, K.Y. & Nakamura, N. 1977. Isolation and characterization of a fluorescent material in bovine achilles tendon collagen. *Biochemical and Biophysical Research Communications,* **76,** 1124-1129.

Fujimoto, M., Takaki, E., Hayashi, T., Kitaura, Y., Tanaka, Y., Inouye, S. & Nakai, A. 2005. Active HSF1 significantly suppresses polyglutamine aggregate formation in cellular and mouse models. *Journal of Biological Chemistry,* **280,** 34908-34916.

Gamerdinger, M., Carra, S. & Behl, C. 2011. Emerging roles of molecular chaperones and co-chaperones in selective autophagy: focus on BAG proteins. *Journal of Molecular Medicine,* **89,** 1175-1182.

Gamerdinger, M., Hajieva, P., Kaya, A.M., Wolfrum, U., Hartl, F.U. & Behl, C. 2009. Protein quality control during aging involves recruitment of the macroautophagy pathway by BAG3. *EMBO Journal,* **28,** 889-901.

Gao, X.C., Zhou, C.J., Zhou, Z.R., Zhang, Y.H., Zheng, X.M., Song, A.X. & Hu, H.Y. 2011. Co-chaperone HSJ1a dually regulates the proteasomal degradation of ataxin-3. *PLoS ONE,* **6,** e19763.

Garrido, C., Paul, C., Seigneuric, R. & Kampinga, H.H. 2012. The small heat shock proteins family: the long forgotten chaperones. *International Journal of Biochemistry and Cell Biology,* **44,** 1588-1592.

Gässler, C.S., Wiederkehr, T., Brehmer, D., Bukau, B. & Mayer, M.P. 2001. Bag-1M accelerates nucleotide release for human Hsc70 and Hsp70 and can act concentration-dependent as positive and negative cofactor. *Journal of Biological Chemistry,* **276,** 32538-32544.

Gautier, A., Juillerat, A., Heinis, C., Corrêa Jr, I.R., Kindermann, M., Beaufils, F. & Johnsson, K. 2008. An engineered protein tag for multiprotein labeling in living cells. *Chemistry and Biology,* **15,** 128-136.

Ghosh, J.G., Shenoy Jr, A.K. & Clark, J.I. 2006. N- and C-terminal motifs in human αB crystallin play an important role in the recognition, selection, and solubilization of substrates. *Biochemistry,* **45,** 13847-13854.

Gidalevitz, T., Ben-Zvi, A., Ho, K.H., Brignull, H.R. & Morimoto, R.I. 2006. Progressive disruption of cellular protein folding in models of polyglutamine diseases. *Science,* **311,** 1471-1474.

Gidalevitz, T., Kikis, E.A. & Morimoto, R.I. 2010. A cellular perspective on conformational disease: the role of genetic background and proteostasis networks. *Current Opinion in Structural Biology,* **20,** 23-32.

Gillis, J., Schipper-Krom, S., Juenemann, K., Gruber, A., Coolen, S., Van Den Nieuwendijk, R., Van Veen, H., Overkleeft, H., Goedhart, J., Kampinga, H.H. & Reits, E.A. 2013. The DNAJB6 and DNAJB8 protein chaperones prevent intracellular aggregation of polyglutamine peptides. *Journal of Biological Chemistry,* **288,** 17225-17237.

Glickman, M.H. & Ciechanover, A. 2002. The ubiquitin-proteasome proteolytic pathway: destruction for the sake of construction. *Physiological Reviews,* **82,** 373-428.

Golenhofen, N., Perng, M.D., Quinlan, R.A. & Drenckhahn, D. 2000. Comparison of the small heat shock proteins αb-crystallin, MKBP, HSP25, HSP20, and cvHSP in heart and skeletal muscle. *Histochemistry and Cell Biology,* **122,** 415-425.

Gomez-Pastor, R., Burchfiel, E.T. & Thiele, D.J. 2018. Regulation of heat shock transcription factors and their roles in physiology and disease. *Nature Reviews Molecular Cell Biology,* **19,** 4-19.

Gómez, A.V., Galleguillos, D., Maass, J.C., Battaglioli, E., Kukuljan, M. & Andrés, M.E. 2008. CoREST represses the heat hock response mediated by HSF1. *Molecular Cell,* **31,** 222-231.

Govin, J., Caron, C., Escoffier, E., Ferro, M., Kuhn, L., Rousseaux, S., Eddy, E.M., Garin, J. & Khochbin, S. 2006. Post-meiotic shifts in HSPA2/HSP70.2 chaperone activity during mouse spermatogenesis. *Journal of Biological Chemistry,* **281,** 37888-37892.

Greenwald, J. & Riek, R. 2010. Biology of amyloid: structure, function, and regulation. *Structure,* **18,** 1244-1260.

Gribaldo, S., Lumia, V., Creti, R., Conway De Macario, E., Sanangelantoni, A. & Cammarano, P. 1999. Discontinuous occurrence of the hsp70 (dnaK) gene among Archaea and sequence features of HSP70 suggest a novel outlook on phylogenies inferred from this protein. *Journal of Bacteriology,* **181,** 434-443.

Guo, Y., Guettouche, T., Fenna, M., Boellmann, F., Pratt, W.B., Toft, D.O., Smith, D.F. & Voellmy, R. 2001. Evidence for a mechanism of repression of heat shock factor 1 transcriptional activity by a multichaperone complex. *Journal of Biological Chemistry,* **276,** 45791-45799.

Gupta, R., Kasturi, P., Bracher, A., Loew, C., Zheng, M., Villella, A., Garza, D., Hartl, F.U. & Raychaudhuri, S. 2011. Firefly luciferase mutants as sensors of proteome stress. *Nature Methods,* **8,** 879-884.

Haass, C. & Selkoe, D.J. 2007. Soluble protein oligomers in neurodegeneration: lessons from the Alzheimer's amyloid β-peptide. *Nature Reviews Molecular Cell Biology,* **8,** 101-112.

Hafizur, R.M., Yano, M., Gotoh, T., Mori, M. & Terada, K. 2004. Modulation of chaperone activities of Hsp70 and Hsp70-2 by a mammalian DnaJ/Hsp40 homolog, DjA4. *Journal of Biochemistry,* **135,** 193-200.

Hageman, J. & Kampinga, H.H. 2009. Computational analysis of the human HSPH/HSPA/DNAJ family and cloning of a human HSPH/HSPA/DNAJ expression library. *Cell Stress and Chaperones,* **14,** 1-21.

Hageman, J., Rujano, M.A., Van Waarde, M.a.W.H., Kakkar, V., Dirks, R.P., Govorukhina, N., Oosterveld-Hut, H.M.J., Lubsen, N.H. & Kampinga, H.H. 2010. A DNAJB chaperone subfamily with HDAC-dependent activities suppresses toxic protein aggregation. *Molecular Cell,* **37,** 355-369.

Hageman, J., Van Waarde, M.a.W.H., Zylicz, A., Walerych, D. & Kampinga, H.H. 2011. The diverse members of the mammalian HSP70 machine show distinct chaperone-like activities. *Biochemical Journal,* **435,** 127-142.

Hageman, J., Vos, M.J., Van Waarde, M.a.W.H. & Kampinga, H.H. 2007. Comparison of intra-organellar chaperone capacity for dealing with stress-induced protein unfolding. *Journal of Biological Chemistry,* **282,** 34334-34345.

Halliday, M., Radford, H., Zents, K.a.M., Molloy, C., Moreno, J.A., Verity, N.C., Smith, E., Ortori, C.A., Barrett, D.A., Bushell, M. & Mallucci, G.R. 2017. Repurposed drugs targeting eIF2α-P-mediated translational repression prevent neurodegeneration in mice. *Brain,* **140,** 1768-1783.

Hanai, R. & Mashima, K. 2003. Characterization of two isoforms of a human DnaJ homologue, HSJ2. *Molecular Biology Reports,* **30,** 149-153.

Hansen, J.J., Dürr, A., Cournu-Rebeix, I., Georgopoulos, C., Ang, D., Nielsen, M.N., Davoine, C.S., Brice, A., Fontaine, B., Gregersen, N. & Bross, P. 2002. Hereditary spastic paraplegia SPG13 is associated with a mutation in the gene encoding the mitochondrial chaperonin Hsp60. *American Journal of Human Genetics,* **70,** 1328-1332.

Hardy, J. & Selkoe, D.J. 2002. The amyloid hypothesis of Alzheimer's disease: progress and problems on the road to therapeutics. *Science,* **297,** 353-356.

Harms, M.B., Sommerville, R.B., Allred, P., Bell, S., Ma, D., Cooper, P., Lopate, G., Pestronk, A., Weihl, C.C. & Baloh, R.H. 2012. Exome sequencing reveals DNAJB6 mutations in dominantly-inherited myopathy. *Annals of Neurology,* **71,** 407-416.

Harper, J.D. & Lansbury Jr, P.T. 1997. Models of amyloid seeding in Alzheimer's disease and scrapie: mechanistic truths and physiological consequences of the time-dependent solubility of amyloid proteins. *Annual Review of Biochemistry,* **66,** 385-407.

Hartl, F.U. 1996. Molecular chaperones in cellular protein folding. *Nature,* **381,** 571-580.

Hartl, F.U., Bracher, A. & Hayer-Hartl, M. 2011. Molecular chaperones in protein folding and proteostasis. *Nature,* **475,** 324-332.

Hartl, F.U. & Hayer-Hartl, M. 2002. Molecular chaperones in the cytosol: from nascent chain to folded protein. *Science,* **295,** 1852-1858.

Hartl, F.U. & Hayer-Hartl, M. 2009. Converging concepts of protein folding *in vitro* and *in vivo*. *Nature Structural and Molecular Biology,* **16,** 574-581.

Haslbeck, M., Franzmann, T., Weinfurtner, D. & Buchner, J. 2005. Some like it hot: the structure and function of small heat-shock proteins. *Nature Structural and Molecular Biology,* **12,** 842-846.

Haung Yu, W., Cuervo, A.M., Kumar, A., Peterhoff, C.M., Schmidt, S.D., Lee, J.H., Mohan, P.S., Mercken, M., Farmery, M.R., Tjernberg, L.O., Jiang, Y., Duff, K., Uchiyama, Y., Näslund, J., Mathews, P.M., Cataldo, A.M. & Nixon, R.A. 2005. Macroautophagy - A novel β-amyloid peptide-generating pathway activated in Alzheimer's disease. *Journal of Cell Biology,* **171,** 87-98.

Held, T., Barakat, A.Z., Mohamed, B.A., Paprotta, I., Meinhardt, A., Engel, W. & Adham, I.M. 2011. Heat-shock protein HSPA4 is required for progression of spermatogenesis. *Reproduction,* **142,** 133-144.

Held, T., Paprotta, I., Khulan, J., Hemmerlein, B., Binder, L., Wolf, S., Schubert, S., Meinhardt, A., Engel, W. & Adham, I.M. 2006. Hspa4l-deficient mice display increased incidence of male infertility and hydronephrosis development. *Molecular and Cellular Biology,* **26,** 8099-8108.

Hershko, A. & Ciechanover, A. 1998. The ubiquitin system. *Annual Review of Biochemistry,* **67,** 425-479.

Hetz, C. 2012. The unfolded protein response: controlling cell fate decisions under ER stress and beyond. *Nature Reviews Molecular Cell Biology,* **13,** 89-102.

Hetz, C. 2021. Adapting the proteostasis capacity to sustain brain healthspan. *Cell,* **184,** in press.

Hetz, C. & Mollereau, B. 2014. Disturbance of endoplasmic reticulum proteostasis in neurodegenerative diseases. *Nature Reviews Neuroscience,* **15,** 233-249.

Hetz, C., Zhang, K. & Kaufman, R.J. 2020. Mechanisms, regulation and functions of the unfolded protein response. *Nature Reviews Molecular Cell Biology,* **21,** 421-438.

Heyrovská, N., Frydman, J., Höhfeld, J. & Hartl, F.U. 1998. Directionality of polypeptide transfer in the mitochondrial pathway of chaperone-mediated protein folding. *Biological Chemistry,* **379,** 301-309.

Hideyuki, M., Takayoshi, K., Hozumi, T., Dai, H., Tokichi, M. & Chikako, T. 1993. Isolation and characterization of SSE1 and SSE2, new members of the yeast HSP70 multigene family. *Gene,* **132,** 57-66.

Hilton, G.R., Lioe, H., Stengel, F., Baldwin, A.J. & Benesch, J.P. 2013. Small heat-shock proteins: paramedics of the cell. *Topics in Current Chemistry,* **328,** 69-98.

Hipp, M.S., Kasturi, P. & Hartl, F.U. 2019. The proteostasis network and its decline in ageing. *Nature Reviews Molecular Cell Biology,* **20,** 421-435.

Hipp, M.S., Park, S.H. & Hartl, F.U. 2014. Proteostasis impairment in protein-misfolding and -aggregation diseases. *Trends in Cell Biology,* **24,** 506-514.

Hornburg, D., Drepper, C., Butter, F., Meissner, F., Sendtner, M. & Mann, M. 2014. Deep proteomic evaluation of primary and cell line motoneuron disease models delineates major differences in neuronal characteristics. *Molecular and Cellular Proteomics,* **13,** 3410-3420.

Hou, H., Zhang, Y., Huang, Y., Yi, Q., Lv, L., Zhang, T., Chen, D., Hao, Q. & Shi, Q. 2012. Inhibitors of phosphatidylinositol 3′-kinases promote mitotic cell death in HeLa cells. *PLoS ONE,* **7,** e35665.

Howarth, J.L., Kelly, S., Keasey, M.P., Glover, C.P.J., Lee, Y.B., Mitrophanous, K., Chapple, J.P., Gallo, J.M., Cheetham, M.E. & Uney, J.B. 2007. Hsp40 molecules that target to the ubiquitin-proteasome system decrease inclusion formation in models of polyglutamine disease. *Molecular Therapy,* **15,** 1100-1105.

Huang, P., Gautschi, M., Walter, W., Rospert, S. & Craig, E.A. 2005. The Hsp70 Ssz1 modulates the function of the ribosome-associated J-protein Zuol. *Nature Structural and Molecular Biology,* **12,** 497-504.

Huang, Y., Arora, K., Mun, K.S., Yang, F., Moon, C.S., Yarlagadda, S., Jegga, A., Weaver, T. & Naren, A.P. 2019. Targeting DNAJB9, a novel ER luminal co-chaperone, to rescue ΔF508-CFTR. *Scientific Reports,* **9,** 9808.

Hussein, R.M., Hashem, R.M. & Rashed, L.A. 2015. Evaluation of the amyloid beta-GFP fusion protein as a model of amyloid beta peptides-mediated aggregation: a study of DNAJB6 chaperone. *Frontiers in Molecular Neuroscience,* **8,** 40.

Hutt, D.M., Powers, E.T. & Balch, W.E. 2009. The proteostasis boundary in misfolding diseases of membrane traffic. *FEBS Letters,* **583,** 2639-2646.

Iqbal, K., Liu, F., Gong, C.X., Del Alonso, A.C. & Grundke-Iqbal, I. 2009. Mechanisms of tau-induced neurodegeneration. *Acta Neuropathologica,* **118,** 53-69.

Irobi, J., Van Impe, K., Seeman, P., Jordanova, A., Dierick, I., Verpoorten, N., Michalik, A., De Vriendt, E., Jacobs, A., Van Gerwen, V., Vennekens, K., Mazanec, R., Tournev, I., Hilton-Jones, D., Talbot, K., Kremensky, I., Van Den Bosch, L., Robberecht, W., Vandekerckhove, J., Van Broeckhoven, C., Gettemans, J., De Jonghe, P. & Timmerman, V. 2004. Hot-spot residue in small heat-shock protein 22 causes distal motor neuropathy. *Nature Genetics,* **36,** 597-601.

Ishii, T., Haga, S., Yagishita, S. & Tateishi, J. 1984. The presence of complements in amyloid plaques of Creutzfeldt-Jakob disease and Gerstmann-Straussler-Scheinker disease. *Applied Pathology,* **2,** 370-379.

Islamovic, E., Duncan, A., Bers, D.M., Gerthoffer, W.T. & Mestril, R. 2007. Importance of small heat shock protein 20 (hsp20) C-terminal extension in cardioprotection. *Journal of Molecular and Cellular Cardiology,* **42,** 862-869.

Ito, H., Kamei, K., Iwamoto, I., Inaguma, Y., Nohara, D. & Kato, K. 2001. Phosphorylation-induced change of the oligomerization state of αB-crystallin. *Journal of Biological Chemistry,* **276,** 5346-5352.

Iwaki, T., Iwaki, A., Tateishi, J. & Goldman, J.E. 1994. Sense and antisense modification of glial αB-crystallin production results in alterations of stress fiber formation and thermoresistance. *Journal of Cell Biology,* **125,** 1385-1393.

Jäättelä, M. & Wissing, D. 1993. Heat-shock proteins protect cells from monocyte cytotoxicity: possible mechanism of self-protection. *Journal of Experimental Medicine,* **177,** 231-236.

Jackson, K.L., Dayton, R.D., Orchard, E.A., Ju, S., Ringe, D., Petsko, G.A., Maquat, L.E. & Klein, R.L. 2015. Preservation of forelimb function by UPF1 gene therapy in a rat model of TDP-43-induced motor paralysis. *Gene Therapy,* **22,** 20-28.

Jakob, U., Gaestel, M., Engel, K. & Buchner, J. 1993. Small heat shock proteins are molecular chaperones. *Journal of Biological Chemistry,* **268,** 1517-1520.

James, P., Pfund, C. & Craig, E.A. 1997. Functional specificity among Hsp70 molecular chaperones. *Science,* **275,** 387-389.

Jana, N.R., Tanaka, M., Wang, G.H. & Nukina, N. 2000. Polyglutamine length-dependent interaction of Hsp40 and Hsp70 family chaperones with truncated N-terminal huntingtin: their role in suppression of aggregation and cellular toxicity. *Human Molecular Genetics,* **9,** 2009-2018.

Janus, C., Pearson, J., Mclaurin, J., Mathews, P.M., Jiang, Y., Schmidt, S.D., Chishti, M.A., Horne, P., Heslin, D., French, J., Mount, H.T.J., Nixon, R.A., Mercken, M., Bergeron, C., Fraser, P.E., St George-Hyslop, P. & Westaway, D. 2000. Aβ peptide immunization reduces behavioural impairment and plaques in a model of Alzheimer's disease. *Nature,* **408,** 979-982.

Jiang, Y., Woronicz, J.D., Liu, W. & Goeddel, D.V. 1999. Prevention of constitutive TNF receptor 1 signaling by silencer of death domains. *Science,* **283,** 543-546.

Jin, J.K., Whittaker, R., Glassy, M.S., Barlow, S.B., Gottlieb, R.A. & Glembotski, C.C. 2008. Localization of phosphorylated αB-crystallin to heart mitochondria during ischemia-reperfusion. *American Journal of Physiology - Heart and Circulatory Physiology,* **294,** H337-H344.

Johansen, T. & Lamark, T. 2011. Selective autophagy mediated by autophagic adapter proteins. *Autophagy,* **7,** 279-296.

Johnston, C.L., Marzano, N.R., Paudel, B.P., Wright, G., Benesch, J.L.P., Van Oijen, A.M. & Ecroyd, H. 2021. Single-molecule fluorescence-based approach reveals novel mechanistic insights into human small heat shock protein chaperone function. *Journal of Biological Chemistry,* **296,** 15419.

Johnston, J.A., Ward, C.L. & Kopito, R.R. 1998. Aggresomes: a cellular response to misfolded proteins. *Journal of Cell Biology,* **143,** 1883-1898.

Kabeya, Y., Mizushima, N., Ueno, T., Yamamoto, A., Kirisako, T., Noda, T., Kominami, E., Ohsumi, Y. & Yoshimori, T. 2000. LC3, a mammalian homologue of yeast Apg8p, is localized in autophagosome membranes after processing. *EMBO Journal,* **19,** 5720-5728.

Kaganovich, D., Kopito, R. & Frydman, J. 2008. Misfolded proteins partition between two distinct quality control compartments. *Nature,* **454,** 1088-1095.

Kakkar, V., Kuiper, E.F.E., Pandey, A., Braakman, I. & Kampinga, H.H. 2016a. Versatile members of the DNAJ family show Hsp70 dependent anti-aggregation activity on RING1 mutant parkin C289G. *Scientific Reports,* **6,** 34830.

Kakkar, V., Månsson, C., De Mattos, E.P., Bergink, S., Van Der Zwaag, M., Van Waarde, M.a.W.H., Kloosterhuis, N.J., Melki, R., Van Cruchten, R.T.P., Al-Karadaghi, S., Arosio, P., Dobson, C.M., Knowles, T.P.J., Bates, G.P., Van Deursen, J.M., Linse, S., Van De Sluis, B., Emanuelsson, C. & Kampinga, H.H. 2016b. The S/T-rich motif in the DNAJB6 chaperone delays polyglutamine aggregation and the onset of disease in a mouse model. *Molecular Cell,* **62,** 272-283.

Kakkar, V., Meister-Broekema, M., Minoia, M., Carra, S. & Kampinga, H.H. 2014. Barcoding heat shock proteins to human diseases: looking beyond the heat shock response. *Disease Models and Mechanisms,* **7,** 421-434.

Kalia, L.V., Kalia, S.K., Chau, H., Lozano, A.M., Hyman, B.T. & Mclean, P.J. 2011. Ubiquitinylation of α-synuclein by carboxyl terminus Hsp70-interacting protein (CHIP) is regulated by Bcl-2-associated athanogene 5 (BAG5). *PLoS ONE,* **6,** e14695.

Kamelgarn, M., Chen, J., Kuang, L., Jin, H., Kasarskis, E.J. & Zhu, H. 2018. ALS mutations of FUS suppress protein translation and disrupt the regulation of nonsense-mediated decay. *Proceedings of the National Academy of Sciences of the United States of America,* **115,** E11904-E11913.

Kampinga, H.H., Andreasson, C., Barducci, A., Cheetham, M.E., Cyr, D., Emanuelsson, C., Genevaux, P., Gestwicki, J.E., Goloubinoff, P., Huerta-Cepas, J., Kirstein, J., Liberek, K., Mayer, M.P., Nagata, K., Nillegoda, N.B., Pulido, P., Ramos, C., De Los Rios, P., Rospert, S., Rosenzweig, R., Sahi, C., Taipale, M., Tomiczek, B., Ushioda, R., Young, J.C., Zimmermann, R., Zylicz, A., Zylicz, M., Craig, E.A. & Marszalek, J. 2019. Function, evolution, and structure of J-domain proteins. *Cell Stress and Chaperones,* **24,** 7-15.

Kampinga, H.H. & Bergink, S. 2016. Heat shock proteins as potential targets for protective strategies in neurodegeneration. *The Lancet Neurology,* **14,** 749-759.

Kampinga, H.H. & Craig, E.A. 2010. The HSP70 chaperone machinery: J proteins as drivers of functional specificity. *Nature Reviews Molecular Cell Biology,* **11,** 579-592.

Kampinga, H.H. & Garrido, C. 2012. HSPBs: small proteins with big implications in human disease. *International Journal of Biochemistry and Cell Biology,* **44,** 1706-1710.

Kampinga, H.H., Hageman, J., Vos, M.J., Kubota, H., Tanguay, R.M., Bruford, E.A., Cheetham, M.E., Chen, B. & Hightower, L.E. 2009. Guidelines for the nomenclature of the human heat shock proteins. *Cell Stress and Chaperones,* **14,** 105-111.

Kandasamy, G. & Andréasson, C. 2018. Hsp70-Hsp110 chaperones deliver ubiquitin-dependent and -independent substrates to the 26S proteasome for proteolysis in yeast. *Journal of Cell Science,* **131,** jcs210948.

Kappé, G., Franck, E., Verschuure, P., Boelens, W.C., Leunissen, J.a.M. & De Jong, W.W. 2003. The human genome encodes 10 α-crystallin-related small heat shock proteins: HspB1-10. *Cell Stress and Chaperones,* **8,** 53-61.

Karamanos, T.K., Tugarinov, V. & Clore, G.M. 2019. Unraveling the structure and dynamics of the human DNAJB6b chaperone by NMR reveals insights into Hsp40-mediated proteostasis. *Proceedings of the National Academy of Sciences of the United States of America,* **116,** 21529-21538.

Kato, S., Hayashi, H., Nakashima, K., Nanba, E., Kato, M., Hirano, A., Nakano, I., Asayama, K. & Ohama, E. 1997. Pathological characterization of astrocytic hyaline inclusions in familial amyotrophic lateral sclerosis. *American Journal of Pathology,* **151,** 611-620.

Kaushik, S. & Cuervo, A.M. 2015. Proteostasis and aging. *Nature Medicine,* **21,** 1406-1415.

Kawahara, T., Yanagi, H., Yura, T. & Mori, K. 1997. Endoplasmic reticulum stress-induced mRNA splicing permits synthesis of transcription factor Hac1p/Ern4p that activates the unfolded protein response. *Molecular Biology of the Cell,* **8,** 1845-1862.

Kazemi-Esfarjani, P. & Benzer, S. 2000. Genetic suppression of polyglutamine toxicity in *Drosophila*. *Science,* **287,** 1837-1840.

Ke, L., Meijering, R.a.M., Hoogstra-Berends, F., Mackovicova, K., Vos, M.J., Van Gelder, I.C., Henning, R.H., Kampinga, H.H. & Brundel, B.J.J.M. 2011. HSPB1, HSPB6, HSPB7 and HSPB8 protect against rhoA GTPase-induced remodeling in tachypaced atrial myocytes. *PLoS ONE,* **6,** e20395.

Kettern, N., Dreiseidler, M., Tawo, R. & Höhfeld, J. 2010. Chaperone-assisted degradation: multiple paths to destruction. *Biological Chemistry,* **391,** 481-489.

Khurana, R., Gillespie, J.R., Talapatra, A., Minert, L.J., Ionescu-Zanetti, C., Millett, I. & Fink, A.L. 2001. Partially folded intermediates as critical precursors of light chain amyloid fibrils and amorphous aggregates. *Biochemistry,* **40,** 3525-3535.

Kidd, M. 1963. Paired helical filaments in electron microscopy of Alzheimer's disease. *Nature,* **197,** 192-193.

Kimura, A., Ogata, K., Altan, B., Yokobori, T., Ide, M., Mochiki, E., Toyomasu, Y., Kogure, N., Yanoma, T., Suzuki, M., Bai, T., Oyama, T. & Kuwano, H. 2016. Nuclear heat shock protein 110 expression is associated with poor prognosis and chemotherapy resistance in gastric cancer. *Oncotarget,* **7,** 18415-18423.

Kirstein, J., Strahl, H., Molière, N., Hamoen, L.W. & Turgay, K. 2008. Localization of general and regulatory proteolysis in Bacillus subtilis cells. *Molecular Microbiology,* **70,** 682-694.

Klaips, C.L., Jayaraj, G.G. & Hartl, F.U. 2018. Pathways of cellular proteostasis in aging and disease. *Journal of Cell Biology,* **217,** 51-63.

Klionsky, D.J. & Emr, S.D. 2000. Autophagy as a regulated pathway of cellular degradation. *Science,* **290,** 1717-1721.

Klucken, J., Shin, Y., Masliah, E., Hyman, B.T. & Mclean, P.J. 2004. Hsp70 reduces α-synuclein aggregation and toxicity. *Journal of Biological Chemistry,* **279,** 25497-25502.

Knee, D.A., Froesch, B.A., Nuber, U., Takayama, S. & Reed, J.C. 2001. Structure-function analysis of Bag1 proteins: effects on androgen receptor transcriptional activity. *Journal of Biological Chemistry,* **276,** 12718-12724.

Kobayashi, Y., Kume, A., Li, M., Doyu, M., Hata, M., Ohtsuka, K. & Sobue, G. 2000. Chaperones Hsp70 and Hsp40 suppress aggregate formation and apoptosis in cultured neuronal cells expressing truncated androgen receptor protein with expanded polyglutamine tract. *Journal of Biological Chemistry,* **275,** 8772-8778.

Komatsu, M., Waguri, S., Chiba, T., Murata, S., Iwata, J.I., Tanida, I., Ueno, T., Koike, M., Uchiyama, Y., Kominami, E. & Tanaka, K. 2006. Loss of autophagy in the central nervous system causes neurodegeneration in mice. *Nature,* **441,** 880-884.

Kondo, N., Katsuno, M., Adachi, H., Minamiyama, M., Doi, H., Matsumoto, S., Miyazaki, Y., Iida, M., Tohnai, G., Nakatsuji, H., Ishigaki, S., Fujioka, Y., Watanabe, H., Tanaka, F., Nakai, A. & Sobue, G. 2013. Heat shock factor-1 influences pathological lesion distribution of polyglutamine-induced neurodegeneration. *Nature Communications,* **4,** 1405.

Kopito, R.R. 2000. Aggresomes, inclusion bodies and protein aggregation. *Trends in Cell Biology,* **10,** 524-530.

Kota, P., Summers, D.W., Ren, H.Y., Cyr, D.M. & Dokholyan, N.V. 2009. Identification of a consensus motif in substrates bound by a type I Hsp40. *Proceedings of the National Academy of Sciences of the United States of America,* **106,** 11073-11078.

Krief, S., Faivre, J.F., Robert, P., Le Douarin, B., Brument-Larignon, N., Lefrère, I., Bouzyk, M.M., Anderson, K.M., Greller, L.D., Tobin, F.L., Souchet, M. & Bril, A. 1999. Identification and characterization of cvHsp. A novel human small stress protein selectively expressed in cardiovascular and insulin-sensitive tissues. *Journal of Biological Chemistry,* **274,** 36592-36600.

Kroemer, G. & Jäättelä, M. 2005. Lysosomes and autophagy in cell death control. *Nature Reviews Cancer,* **5,** 886-897.

Krueger, A.M.R., Armstrong, J.N., Plumier, J.C., Robertson, H.A. & Currie, R.W. 1999. Cell specific expression of Hsp70 in neurons and glia of the rat hippocampus after hyperthermia and kainic acid-induced seizure activity. *Molecular Brain Research,* **71,** 265-278.

Kubota, H., Kitamura, A. & Nagata, K. 2011. Analyzing the aggregation of polyglutamine-expansion proteins and its modulation by molecular chaperones. *Methods,* **53,** 267-274.

Kulig, M. & Ecroyd, H. 2012. The small heat-shock protein αB-crystallin uses different mechanisms of chaperone action to prevent the amorphous versus fibrillar aggregation of α-lactalbumin. *Biochemical Journal,* **448,** 343-352.

Kuo, Y., Ren, S., Lao, U., Edgar, B.A. & Wang, T. 2013. Suppression of polyglutamine protein toxicity by co-expression of a heat-shock protein 40 and a heat-shock protein 110. *Cell Death and Disease,* **4,** e833.

Kurien, B.T. & Hal Scofield, R. 2015. Western blotting: an introduction. *Methods in Molecular Biology,* **1312,** 17-30.

Kwak, H.J., Jun, C.D., Pae, H.O., Yoo, J.C., Park, Y.C., Choi, B.M., Na, Y.G., Park, R.K., Chung, H.T., Chung, H.Y., Park, W.Y. & Seo, J.S. 1998. The role of inducible 70-kDa heat shock protein in cell cycle control, differentiation, and apoptotic cell death of the human myeloid leukemic HL- 60 cells. *Cellular Immunology,* **187,** 1-12.

Labbadia, J. & Morimoto, R.I. 2015. The biology of proteostasis in aging and disease. *Annual Review of Biochemistry,* **84,** 435-464.

Labbadia, J., Novoselov, S.S., Bett, J.S., Weiss, A., Paganetti, P., Bates, G.P. & Cheetham, M.E. 2012. Suppression of protein aggregation by chaperone modification of high molecular weight complexes. *Brain,* **135,** 1180-1186.

Laemmli, U.K. 1970. Cleavage of structural proteins during the assembly of the head of bacteriophage T4. *Nature,* **227,** 680-685.

Laferrière, F., Maniecka, Z., Pérez-Berlanga, M., Hruska-Plochan, M., Gilhespy, L., Hock, E.M., Wagner, U., Afroz, T., Boersema, P.J., Barmettler, G., Foti, S.C., Asi, Y.T., Isaacs, A.M., Al-Amoudi, A., Lewis, A., Stahlberg, H., Ravits, J., De Giorgi, F., Ichas, F., Bezard, E., Picotti, P., Lashley, T. & Polymenidou, M. 2019. TDP-43 extracted from frontotemporal lobar degeneration subject brains displays distinct aggregate assemblies and neurotoxic effects reflecting disease progression rates. *Nature Neuroscience,* **22,** 65-77.

Lai, C.W., Oteros, J.H., Hendershots, L.M. & Snapp, E. 2012. ERdj4 protein is a soluble endoplasmic reticulum (ER) DnaJ family protein that interacts with ER-associated degradation machinery. *Journal of Biological Chemistry,* **287,** 7969-7978.

Lai, Z., Colón, W. & Kelly, J.W. 1996. The acid-mediated denaturation pathway of transthyretin yields a conformational intermediate that can self-assemble into amyloid. *Biochemistry,* **35,** 6470-6482.

Lang-Rollin, I., Rideout, H. & Stefanis, L. 2003. Ubiquitinated inclusions and neuronal cell death. *Histology and Histopathology,* **18,** 509-517.

Langer, T., Lu, C., Echols, H., Flanagan, J., Hayer, M.K. & Hartl, F.U. 1992. Successive action of DnaK, DnaJ and GroEL along the pathway of chaperone-mediated protein folding. *Nature,* **356,** 683-689.

Lavoie, J.N., Hickey, E., Weber, L.A. & Landry, J. 1993. Modulation of actin-microfilament dynamics and fluid phase pinocytosis by phosphorylation of heat shock protein 27. *Journal of Biological Chemistry,* **268,** 24210-24214.

Lavoie, J.N., Lambert, H., Hickey, E., Weber, L.A. & Landry, J. 1995. Modulation of cellular thermoresistance and actin filament stability accompanies phosphorylation-induced changes in the oligomeric structure of heat shock protein 27. *Molecular and Cellular Biology,* **15,** 505-516.

Lee, A.S. 2005. The ER chaperone and signaling regulator GRP78/BiP as a monitor of endoplasmic reticulum stress. *Methods,* **35,** 373-381.

Lee, B.H., Lee, M.J., Park, S., Oh, D.C., Elsasser, S., Chen, P.C., Gartner, C., Dimova, N., Hanna, J., Gygi, S.P., Wilson, S.M., King, R.W. & Finley, D. 2010. Enhancement of proteasome activity by a small-molecule inhibitor of USP14. *Nature,* **467,** 179-184.

Lee, D.H. & Goldberg, A.L. 1998. Proteasome inhibitors: valuable new tools for cell biologists. *Trends in Cell Biology,* **8,** 397-403.

Lee, G.J. & Vierling, E. 2000. A small heat shock protein cooperates with heat shock protein 70 systems to reactivate a heat-denatured protein. *Plant Physiology,* **122,** 189-197.

Lee, S., Carson, K., Rice-Ficht, A. & Good, T. 2006. Small heat shock proteins differentially affect Aβ aggregation and toxicity. *Biochemical and Biophysical Research Communications,* **347,** 527-533.

Leist, M. & Jäättelä, M. 2001. Four deaths and a funeral: from caspases to alternative mechanisms. *Nature Reviews Molecular Cell Biology,* **2,** 589-598.

Li, G.C., Li, L., Liu, Y.K., Mak, J.Y., Chen, L. & Lee, W.M.F. 1991. Thermal response of rat fibroblasts stably transfected with the human 70-kDa heat shock protein-encoding gene. *Proceedings of the National Academy of Sciences of the United States of America,* **88,** 1681-1685.

Li, X., Wang, C.E., Huang, S., Xu, X., Li, X.J., Li, H. & Li, S. 2010. Inhibiting the ubiquitin-proteasome system leads to preferential accumulation of toxic N-terminal mutant huntingtin fragments. *Human Molecular Genetics,* **19,** 2445-2455.

Lilienbaum, A. 2013. Relationship between the proteasomal system and autophagy. *International Journal of Biochemistry and Molecular Biology,* **4,** 1-26.

Lim, J. & Yue, Z. 2015. Neuronal aggregates: formation, clearance, and spreading. *Developmental Cell,* **32,** 491-501.

Lin, P.Y., Simon, S.M., Koh, W.K., Folorunso, O., Umbaugh, C.S. & Pierce, A. 2013. Heat shock factor 1 over-expression protects against exposure of hydrophobic residues on mutant SOD1 and early mortality in a mouse model of amyotrophic lateral sclerosis. *Molecular Neurodegeneration,* **8,** 43.

Lin, Z., Madan, D. & Rye, H.S. 2008. GroEL stimulates protein folding through forced unfolding. *Nature Structural and Molecular Biology,* **15,** 303-311.

Lindquist, S. 1986. The heat-shock response. *Annual Review of Biochemistry,* **55,** 1151-1191.

Lindquist, S. & Craig, E.A. 1988. The heat-shock proteins. *Annual Review of Genetics,* **22,** 631-677.

Linke, K., Wolfram, T., Bussemer, J. & Jakob, U. 2003. The roles of the two zinc binding sites in DnaJ. *Journal of Biological Chemistry,* **278,** 44457-44466.

Liu, K., Tedeschi, A., Park, K.K. & He, Z. 2011. Neuronal intrinsic mechanisms of axon regeneration. *Annual Review of Neuroscience,* **34,** 131-152.

Liu, W.J., Ye, L., Huang, W.F., Guo, L.J., Xu, Z.G., Wu, H.L., Yang, C. & Liu, H.F. 2016. p62 links the autophagy pathway and the ubiqutin-proteasome system upon ubiquitinated protein degradation. *Cellular and Molecular Biology Letters,* **21,** 29.

Liu, Y., Zhang, X., Chen, W., Tan, Y.L. & Kelly, J.W. 2015. Fluorescence turn-on folding sensor to monitor proteome stress in live cells. *Journal of the American Chemical Society,* **137,** 11303-11311.

Loo, D.T., Copani, A., Pike, C.J., Whittemore, E.R., Walencewicz, A.J. & Cotman, C.W. 1993. Apoptosis is induced by β-amyloid in cultured central nervous system neurons. *Proceedings of the National Academy of Sciences of the United States of America,* **90,** 7951-7955.

López-Erauskin, J., Tadokoro, T., Baughn, M.W., Myers, B., Mcalonis-Downes, M., Chillon-Marinas, C., Asiaban, J.N., Artates, J., Bui, A.T., Vetto, A.P., Lee, S.K., Le, A.V., Sun, Y., Jambeau, M., Boubaker, J., Swing, D., Qiu, J., Hicks, G.G., Ouyang, Z., Fu, X.D., Tessarollo, L., Ling, S.C., Parone, P.A., Shaw, C.E., Marsala, M., Lagier-Tourenne, C., Cleveland, D.W. & Da Cruz, S. 2018. ALS/FTD-linked mutation in FUS suppresses intra-axonal protein synthesis and drives disease without nuclear loss-of-function of FUS. *Neuron,* **100,** 816-830.

Los, G.V., Encell, L.P., Mcdougall, M.G., Hartzell, D.D., Karassina, N., Zimprich, C., Wood, M.G., Learish, R., Ohana, R.F., Urh, M., Simpson, D., Mendez, J., Zimmerman, K., Otto, P., Vidugiris, G., Zhu, J., Darzins, A., Klaubert, D.H., Bulleit, R.F. & Wood, K.V. 2008. HaloTag: a novel protein labeling technology for cell imaging and protein analysis. *ACS Chemical Biology,* **3,** 373-382.

Lu, Z. & Cyr, D.M. 1998. The conserved carboxyl terminus and zinc finger-like domain of the co-chaperone Ydj1 assist Hsp70 in protein folding. *Journal of Biological Chemistry,* **273,** 5970-5978.

Lunkes, A. & Mandel, J.L. 1998. A cellular model that recapitulates major pathogenic steps of Huntington's disease. *Human Molecular Genetics,* **7,** 1355-1361.

Luo, G.R. & Le, W.D. 2010. Collective roles of molecular chaperones in protein degradation pathways associated with neurodegenerative diseases. *Current Pharmaceutical Biotechnology,* **11,** 180-187.

Mackay, D.S., Andley, U.P. & Shiels, A. 2003. Cell death triggered by a novel mutation in the alphaA-crystallin gene underlies autosomal dominant cataract linked to chromosome 21q. *European Journal of Human Genetics,* **11,** 784-793.

Malhotra, J.D. & Kaufman, R.J. 2007. The endoplasmic reticulum and the unfolded protein response. *Seminars in Cell and Developmental Biology,* **18,** 716-731.

Manetto, V., Perry, G., Tabaton, M., Mulvihill, P., Fried, V.A., Smith, H.T., Gambetti, P. & Autilio-Gambetti, L. 1988. Ubiquitin is associated with abnormal cytoplasmic filaments

characteristic of neurodegenerative diseases. *Proceedings of the National Academy of Sciences of the United States of America,* **85,** 4501-4505.

Månsson, C., Arosio, P., Hussein, R., Kampinga, H.H., Hashem, R.M., Boelens, W.C., Dobson, C.M., Knowles, T.P.J., Linse, S. & Emanuelsson, C. 2014a. Interaction of the molecular chaperone DNAJB6 with growing amyloid-beta 42 (Aβ42) aggregates leads to sub-stoichiometric inhibition of amyloid formation. *Journal of Biological Chemistry,* **289,** 31066-31076.

Månsson, C., Kakkar, V., Monsellier, E., Sourigues, Y., Härmark, J., Kampinga, H.H., Melki, R. & Emanuelsson, C. 2014b. DNAJB6 is a peptide-binding chaperone which can suppress amyloid fibrillation of polyglutamine peptides at substoichiometric molar ratios. *Cell Stress and Chaperones,* **19,** 227-239.

Månsson, C., Van Cruchten, R.T.P., Weininger, U., Yang, X., Cukalevski, R., Arosio, P., Dobson, C.M., Knowles, T., Akke, M., Linse, S. & Emanuelsson, C. 2018. Conserved S/T residues of the human chaperone DNAJB6 are required for effective inhibition of Aβ42 amyloid fibril formation. *Biochemistry,* **57,** 4891-4892.

Matlack, K.E.S., Plath, K., Misselwitz, B. & Rapoport, T.A. 1997. Protein transport by purified yeast sec complex and Kar2p without membranes. *Science,* **277,** 938-941.

Matsumori, M., Itoh, H., Toyoshima, I., Komatsuda, A., Sawada, K.I., Fukuda, J., Tanaka, T., Okubo, A., Kinouchi, H., Mizoi, K., Hama, T., Suzuki, A., Hamada, F., Otaka, M., Shoji, Y. & Takada, G. 2002. Characterization of the 105-kDa molecular chaperone. Identification, biochemical properties, and localization. *European Journal of Biochemistry,* **269,** 5632-5641.

Mattson, M.P. 2000. Apoptosis in neurodegenerative disorders. *Nature Reviews Molecular Cell Biology,* **1,** 120-129.

Matus, S., Glimcher, L.H. & Hetz, C. 2011. Protein folding stress in neurodegenerative diseases: a glimpse into the ER. *Current Opinion in Cell Biology,* **23,** 239-252.

Mcalary, L., Aquilina, J.A. & Yerbury, J.J. 2016. Susceptibility of mutant SOD1 to form a destabilized monomer predicts cellular aggregation and toxicity but not *in vitro* aggregation propensity. *Frontiers in Neuroscience,* **10,** 1-16.

Mcgeer, P.L. & Mcgeer, E.G. 1995. The inflammatory response system of brain: implications for therapy of Alzheimer and other neurodegenerative diseases. *Brain Research Reviews,* **21,** 195-218.

Mcgeer, P.L., Schulzer, M. & Mcgeer, E.G. 1996. Arthritis and anti-inflammatory agents as possible protective factors for Alzheimer's disease: a review of 17 epidemiologic studies. *Neurology,* **47,** 425-432.

Mclean, P.J., Kawamata, H., Shariff, S., Hewett, J., Sharma, N., Ueda, K., Breakefield, X.O. & Hyman, B.T. 2002. TorsinA and heat shock proteins act as molecular chaperones: suppression of α-synuclein aggregation. *Journal of Neurochemistry,* **83,** 846-854.

Menéndez-Benito, V., Verhoef, L.G.G.C., Masucci, M.G. & Dantuma, N.P. 2005. Endoplasmic reticulum stress compromises the ubiquitin-proteasome system. *Human Molecular Genetics,* **14,** 2787-2799.

Mestril, R., Chi, S.H., Sayen, M.R., O'reilly, K. & Dillmann, W.H. 1994. Expression of inducible stress protein 70 in rat heart myogenic cells confers protection against simulated ischemia-induced injury. *Journal of Clinical Investigation,* **93,** 759-767.

Michels, A.A., Kanon, B., Konings, A.W.T., Ohtsuka, K., Bensaude, O. & Kampinga, H.H. 1997. Hsp70 and Hsp40 chaperone activities in the cytoplasm and the nucleus of mammalian cells. *Journal of Biological Chemistry,* **272,** 33283-33289.

Michels, A.A., Nguyen, V.T., Konings, A.W.T., Kampinga, H.H. & Bensaude, O. 1995. Thermostability of a nuclear-targeted luciferase expressed in mammalian cells: destabilizing influence of the intranuclear microenvironment. *European Journal of Biochemistry,* **234,** 382-389.

Miller, J., Arrasate, M., Brooks, E., Libeu, C.P., Legleiter, J., Hatters, D., Curtis, J., Cheung, K., Krishnan, P., Mitra, S., Widjaja, K., Shaby, B.A., Lotz, G.P., Newhouse, Y., Mitchell, E.J., Osmand, A., Gray, M., Thulasiramin, V., Saudou, F., Segal, M., Yang, X.W., Masliah, E., Thompson, L.M., Muchowski, P.J., Weisgraber, K.H. & Finkbeiner, S. 2011. Identifying polyglutamine protein species in situ that best predict neurodegeneration. *Nature Chemical Biology,* **7,** 925-934.

Milner, C.M. & Duncan Campbell, R. 1990. Structure and expression of the three MHC-linked HSP70 genes. *Immunogenetics,* **32,** 242-251.

Minoia, M., Boncoraglio, A., Vinet, J., Morelli, F.F., Brunsting, J.F., Poletti, A., Krom, S., Reits, E., Kampinga, H.H. & Carra, S. 2014a. BAG3 induces the sequestration of proteasomal clients into cytoplasmic puncta. *Autophagy,* **10,** 1603-1621.

Minoia, M., Grit, C. & Kampinga, H.H. 2014b. HSPA1A-independent suppression of PARK2 C289G protein aggregation by human small heat shock proteins. *Molecular and Cellular Biology,* **34,** 3570-3578.

Morgan, D., Diamond, D.M., Gottschall, P.E., Ugen, K.E., Dickey, C., Hardy, J., Duff, K., Jantzen, P., Dicarlo, G., Wilcock, D., Connor, K., Hatcher, J., Hope, C., Gordon, M. & Arendash, G.W. 2000. Aβ peptide vaccination prevents memory loss in an animal model of Alzheimer's disease. *Nature,* **408,** 982-985.

Morgan, J.R., Jiang, J., Oliphint, P.A., Jin, S., Gimenez, L.E., Busch, D.J., Foldes, A.E., Zhuo, Y., Sousa, R. & Lafer, E.M. 2013. A role for an Hsp70 nucleotide exchange factor in the regulation of synaptic vesicle endocytosis. *Journal of Neuroscience,* **33,** 8009-8021.

Mori, H., Kondo, J. & Ihara, Y. 1987. Ubiquitin is a component of paired helical filaments in Alzheimer's disease. *Science,* **235,** 1641-1644.

Morimoto, R.I. 2008. Proteotoxic stress and inducible chaperone networks in neurodegenerative disease and aging. *Genes and Development,* **22,** 1427-1438.

Morimoto, R.I. 2011. The heat shock response: systems biology of proteotoxic stress in aging and disease. *Cold Spring Harbor Symposia on Quantitative Biology,* **76,** 91-99.

Morrison, L.E., Hoover, H.E., Thuerauf, D.J. & Glembotski, C.C. 2003. Mimicking phosphorylation of αB-crystallin on serine-59 is necessary and sufficient to provide maximal protection of cardiac myocytes from apoptosis. *Circulation Research,* **92,** 203-211.

Morrow, G., Heikkila, J.J. & Tanguay, R.M. 2006. Differences in the chaperone-like activities of the four main small heat shock proteins of *Drosophila melanogaster*. *Cell Stress and Chaperones,* **11,** 51-60.

Mosser, D.D., Caron, A.W., Bourget, L., Meriin, A.B., Sherman, M.Y., Morimoto, R.I. & Massie, B. 2000. The chaperone function of Hsp70 is required for protection against stress-induced apoptosis. *Molecular and Cellular Biology,* **20,** 7146-7159.

Muchowski, P.J., Schaffar, G., Sittler, A., Wanker, E.E., Hayer-Hartl, M.K. & Hartl, F.U. 2000. Hsp70 and Hsp40 chaperones can inhibit self-assembly of polyglutamine proteins into amyloid-like fibrils. *Proceedings of the National Academy of Sciences of the United States of America,* **97,** 7841-7846.

Munro, S. & Pelham, H.R.B. 1987. A C-terminal signal prevents secretion of luminal ER proteins. *Cell,* **48,** 899-907.

Myeku, N. & Figueiredo-Pereira, M.E. 2011. Dynamics of the degradation of ubiquitinated proteins by proteasomes and autophagy: association with sequestosome 1/p62. *Journal of Biological Chemistry,* **286,** 22426-22440.

Myers, J.K. & Pace, C.N. 1996. Hydrogen bonding stabilizes globular proteins. *Biophysical Journal,* **71,** 2033-2039.

Mymrikov, E.V., Daake, M., Richter, B., Haslbeck, M. & Buchner, J. 2017. The chaperone activity and substrate spectrum of human small heat shock proteins. *Journal of Biological Chemistry,* **292,** 672-684.

Nagy, M., Fenton, W.A., Li, D., Furtak, K. & Horwich, A.L. 2016. Extended survival of misfolded G85R SOD1-linked ALS mice by transgenic expression of chaperone Hsp110. *Proceedings of the National Academy of Sciences of the United States of America,* **113,** 5424-5428.

Nakagawa, M., Tsujimoto, N., Nakagawa, H., Iwaki, T., Fukumaki, Y. & Iwaki, A. 2001. Association of HSPB2, a member of the small heat shock protein family, with mitochondria. *Experimental Cell Research,* **271,** 161-168.

Nassif, N.D., Cambray, S.E. & Kraut, D.A. 2014. Slipping up: partial substrate degradation by ATP-dependent proteases. *IUBMB Life,* **66,** 309-317.

Naylor, L.H. 1999. Reporter gene technology: the future looks bright. *Biochemical Pharmacology,* **58,** 749-757.

Neef, D.W., Jaeger, A.M., Gomez-Pastor, R., Willmund, F., Frydman, J. & Thiele, D.J. 2014. A direct regulatory interaction between chaperonin TRiC and stress-responsive transcription factor HSF1. *Cell Reports,* **9,** 955-966.

Neef, D.W., Jaeger, A.M. & Thiele, D.J. 2011. Heat shock transcription factor 1 as a therapeutic target in neurodegenerative diseases. *Nature Reviews Drug Discovery,* **10,** 930-944.

Neef, D.W., Turski, M.L. & Thiele, D.J. 2010. Modulation of heat shock transcription factor 1 as a therapeutic target for small molecule intervention in neurodegenerative disease. *PLoS Biology,* **8,** e1000291.

Neumann, M., Sampathu, D.M., Kwong, L.K., Truax, A.C., Micsenyi, M.C., Chou, T.T., Bruce, J., Schuck, T., Grossman, M., Clark, C.M., Mccluskey, L.F., Miller, B.L., Masliah, E., Mackenzie, I.R., Feldman, H., Feiden, W., Kretzschmar, H.A., Trojanowski, J.Q. & Lee, V.M.Y. 2006. Ubiquitinated TDP-43 in frontotemporal lobar degeneration and amyotrophic lateral sclerosis. *Science,* **314,** 130-133.

Nicholl, I.D. & Quinlan, R.A. 1994. Chaperone activity of α-crystallins modulates intermediate filament assembly. *EMBO Journal,* **13,** 945-953.

Nillegoda, N.B., Kirstein, J., Szlachcic, A., Berynskyy, M., Stank, A., Stengel, F., Arnsburg, K., Gao, X., Scior, A., Aebersold, R., Guilbride, D.L., Wade, R.C., Morimoto, R.I., Mayer, M.P. & Bukau, B. 2015. Crucial HSP70 co-chaperone complex unlocks metazoan protein disaggregation. *Nature,* **524,** 247-251.

Nillegoda, N.B., Stank, A., Malinverni, D., Alberts, N., Szlachcic, A., Barducci, A., De Los Rios, P., Wade, R.C. & Bukau, B. 2017. Evolution of an intricate J-protein network driving protein disaggregation in eukaryotes. *eLife,* **6,** e24560.

Nishimura, R.N., Dwyer, B.E., Clegg, K., Cole, R. & De Vellis, J. 1991. Comparison of the heat shock response in cultured cortical neurons and astrocytes. *Molecular Brain Research,* **9,** 39-45.

Nishizawa, S., Hirohashi, Y., Torigoe, T., Takahashi, A., Tamura, Y., Mori, T., Kanaseki, T., Kamiguchi, K., Asanuma, H., Morita, R., Sokolovskaya, A., Matsuzaki, J., Yamada, R., Fujii, R., Kampinga, H.H., Kondo, T., Hasegawa, T., Hara, I. & Sato, N. 2012. Hsp DNAJB8 controls tumor-initiating ability in renal cancer stem-like cells. *Cancer Research,* **72,** 2844-2854.

Nixon, B., Bromfield, E.G., Dun, M.D., Redgrove, K.A., Mclaughlin, E.A. & Aitken, R.J. 2015. The role of the molecular chaperone heat shock protein A2 (HSPA2) in regulating human sperm-egg recognition. *Asian Journal of Andrology,* **17,** 568-573.

Noh, S.J., Jeong, W.J., Rho, J.H., Shin, D.M., Ahn, H.B., Park, W.C., Rho, S.H., Soung, Y.H., Kim, T.H., Park, B.S. & Yoo, Y.H. 2008. Sensitization of RPE cells by αB-crystallin siRNA to SAHA-induced stage 1 apoptosis through abolishing the association of αB-crystallin with HDAC1 in SC35 speckles. *Investigative Ophthalmology and Visual Science,* **49,** 4753-4759.

Nollen, E.a.A., Brunsting, J.F., Roelofsen, H., Weber, L.A. & Kampinga, H.H. 1999. *In vivo* chaperone activity of heat shock protein 70 and thermotolerance. *Molecular and Cellular Biology,* **19,** 2069-2079.

Nollen, E.a.A., Brunsting, J.F., Song, J., Kampinga, H.H. & Morimoto, R.I. 2000. Bag1 functions *in vivo* as a negative regulator of Hsp70 chaperone activity. *Molecular and Cellular Biology,* **20,** 1083-1088.

Noonan, E.J., Place, R.F., Rasoulpour, R.J., Giardina, C. & Hightower, L.E. 2007. Cell number-dependent regulation of Hsp70B′ expression: evidence of an extracellular regulator. *Journal of Cellular Physiology,* **210,** 201-211.

Novoselov, S.S., Mustill, W.J., Gray, A.L., Dick, J.R., Kanuga, N., Kalmar, B., Greensmith, L. & Cheetham, M.E. 2013. Molecular chaperone mediated late-stage neuroprotection in the SOD1G93A mouse model of amyotrophic lateral sclerosis. *PLoS ONE,* **8,** e73944.

Nylandsted, J., Gyrd-Hansen, M., Danielewicz, A., Fehrenbacher, N., Lademann, U., Høyer-Hansen, M., Weber, E., Multhoff, G., Rohde, M. & Jäättelä, M. 2004. Heat shock protein 70 promotes cell survival by inhibiting lysosomal membrane permeabilization. *Journal of Experimental Medicine,* **200,** 425-435.

Oh, H.J., Easton, D., Murawski, M., Kaneko, Y. & Subjeck, J.R. 1999. The chaperoning activity of Hsp110: identification of functional domains by use of targeted deletions. *Journal of Biological Chemistry,* **274,** 15712-15718.

Ojha, J., Masilamoni, G., Dunlap, D., Udoff, R.A. & Cashikar, A.G. 2011. Sequestration of toxic oligomers by HspB1 as a cytoprotective mechanism. *Molecular and Cellular Biology,* **31,** 3146-3157.

Oka, O.B.V., Pringle, M.A., Schopp, I.M., Braakman, I. & Bulleid, N.J. 2013. ERdj5 is the ER reductase that catalyzes the removal of non-native disulfides and correct folding of the LDL receptor. *Molecular Cell,* **50,** 793-804.

Oka, S.I., Ago, T., Kitazono, T., Zablocki, D. & Sadoshima, J. 2009. The role of redox modulation of class II histone deacetylases in mediating pathological cardiac hypertrophy. *Journal of Molecular Medicine,* **87,** 785-791.

Olzscha, H., Schermann, S.M., Woerner, A.C., Pinkert, S., Hecht, M.H., Tartaglia, G.G., Vendruscolo, M., Hayer-Hartl, M., Hartl, F.U. & Vabulas, R.M. 2011. Amyloid-like aggregates sequester numerous metastable proteins with essential cellular functions. *Cell,* **144,** 67-78.

Ormsby, A.R., Ramdzan, Y.M., Mok, Y.F., Jovanoski, K.D. & Hatters, D.M. 2013. A platform to view huntingtin exon 1 aggregation flux in the cell reveals divergent influences from chaperones hsp40 and hsp70. *Journal of Biological Chemistry,* **288,** 37192-37203.

Oshita, S.E., Chen, F., Kwan, T., Yehiely, F. & Cryns, V.L. 2010. The small heat shock protein HspB2 is a novel anti-apoptotic protein that inhibits apical caspase activation in the extrinsic apoptotic pathway. *Breast Cancer Research and Treatment,* **124,** 307-315.

Oslowski, C.M. & Urano, F. 2011. Measuring ER stress and the unfolded protein response using mammalian tissue culture system. *Methods in Enzymology,* **490,** 71-92.

Otter, T., King, S.M. & Witman, G.B. 1987. A two-step procedure for efficient electrotransfer of both high-molecular-weight (>400,000) and low-molecular-weight (<20,000) proteins. *Analytical Biochemistry,* **162,** 370-377.

Outeiro, T.F., Klucken, J., Strathearn, K.E., Liu, F., Nguyen, P., Rochet, J.C., Hyman, B.T. & Mclean, P.J. 2006. Small heat shock proteins protect against α-synuclein-induced toxicity and aggregation. *Biochemical and Biophysical Research Communications,* **351,** 631-638.

Oza, J., Yang, J., Chen, K.Y. & Liu, A.Y.C. 2008. Changes in the regulation of heat shock gene expression in neuronal cell differentiation. *Cell Stress and Chaperones,* **13,** 73-84.

Pandey, P., Farber, R., Nakazawa, A., Kumar, S., Bharti, A., Nalin, C., Weichselbaum, R., Kufe, D. & Kharbanda, S. 2000. Hsp27 functions as a negative regulator of cytochrome c-dependent activation of procaspase-3. *Oncogene,* **19,** 1975-1981.

Papp, E., Nardai, G., Soti, C. & Csermely, P. 2003. Molecular chaperones, stress proteins and redox homeostasis. *BioFactors,* **17,** 249-257.

Parag, H.A., Raboy, B. & Kulka, R.G. 1987. Effect of heat shock on protein degradation in mammalian cells: involvement of the ubiquitin system. *EMBO Journal,* **6,** 55-61.

Parsian, A.J., Sheren, J.E., Tao, T.Y., Goswami, P.C., Malyapa, R., Van Rheeden, R., Watson, M.S. & Hunt, C.R. 2000. The human Hsp70B gene at the HSPA7 locus of chromosome 1 is transcribed but non-functional. *Biochimica et Biophysica Acta,* **1494,** 201-205.

Pavlik, A. & Aneja, I.S. 2007. Cerebral neurons and glial cell types inducing heat shock protein Hsp70 following heat stress in the rat. *Progress in Brain Research,* **162,** 417-431.

Pemberton, S., Madiona, K., Pieri, L., Kabani, M., Bousset, L. & Melki, R. 2011. Hsc70 protein interaction with soluble and fibrillar α-synuclein. *Journal of Biological Chemistry,* **286,** 34690-34699.

Perales-Calvo, J., Muga, A. & Moro, F. 2010. Role of DnaJ G/F-rich domain in conformational recognition and binding of protein substrates. *Journal of Biological Chemistry,* **285,** 34231-34239.

Peyrin, J.M., Lasmézas, C.I., Haïk, S., Tagliavini, F., Salmona, M., Williams, A., Richie, D., Deslys, J.P. & Dormont, D. 1999. Microglial cells respond to amyloidogenic PrP peptide by the production of inflammatory cytokines. *Neuroreport,* **10,** 723-729.

Polier, S., Dragovic, Z., Hartl, F.U. & Bracher, A. 2008. Structural basis for the cooperation of Hsp70 and Hsp110 chaperones in protein folding. *Cell,* **133,** 1068-1079.

Polier, S., Hartl, F.U. & Bracher, A. 2010. Interaction of the Hsp110 molecular chaperones from S. cerevisiae with substrate protein. *Journal of Molecular Biology,* **401,** 696-707.

Powers, E.T., Morimoto, R.I., Dillin, A., Kelly, J.W. & Balch, W.E. 2009. Biological and chemical approaches to diseases of proteostasis deficiency. *Annual Review of Biochemistry,* **78,** 959-991.

Priya, S., Sharma, S.K. & Goloubinoff, P. 2013. Molecular chaperones as enzymes that catalytically unfold misfolded polypeptides. *FEBS Letters,* **587,** 1981-1987.

Proctor, C.J. & Lorimer, I.a.J. 2011. Modelling the role of the Hsp70/Hsp90 system in the maintenance of protein homeostasis. *PLoS ONE,* **6,** e22038.

Prudencio, M., Hart, P.J., Borchelt, D.R. & Andersen, P.M. 2009. Variation in aggregation propensities among ALS-associated variants of SOD1: correlation to human disease. *Human Molecular Genetics,* **18,** 3217-3226.

Qian, J., Ren, X., Wang, X., Zhang, P., Jones, W.K., Molkentin, J.D., Fan, G.C. & Kranias, E.G. 2009. Blockade of Hsp20 phosphorylation exacerbates cardiac ischemia/reperfusion injury by suppressed autophagy and increased cell death. *Circulation Research,* **105,** 1223-1231.

Quintas, A., Vaz, D.C., Cardoso, I., Saraiva, M.J.M. & Brito, R.M.M. 2001. Tetramer dissociation and monomer partial unfolding precedes protofibril formation in amyloidogenic transthyretin variants. *Journal of Biological Chemistry,* **276,** 27207-27213.

Ramdzan, Y.M., Polling, S., Chia, C.P.Z., Ng, I.H.W., Ormsby, A.R., Croft, N.P., Purcell, A.W., Bogoyevitch, M.A., Ng, D.C.H., Gleeson, P.A. & Hatters, D.M. 2012. Tracking protein aggregation and mislocalization in cells with flow cytometry. *Nature Methods,* **9,** 467-470.

Ramdzan, Y.M., Trubetskov, M.M., Ormsby, A.R., Newcombe, E.A., Sui, X., Tobin, M.J., Bongiovanni, M.N., Gras, S.L., Dewson, G., Miller, J.M.L., Finkbeiner, S., Moily, N.S., Niclis, J., Parish, C.L., Purcell, A.W., Baker, M.J., Wilce, J.A., Waris, S., Stojanovski, D., Böcking, T., Ang, C.S., Ascher, D.B., Reid, G.E. & Hatters, D.M. 2017. Huntingtin inclusions trigger cellular quiescence, deactivate apoptosis, and lead to delayed necrosis. *Cell Reports,* **19,** 919-927.

Ramdzan, Y.M., Wood, R. & Hatters, D.M. 2013. Pulse shape analysis (PulSA) to track protein translocalization in cells by flow cytometry: applications for polyglutamine aggregation. *Methods in Molecular Biology,* **1017,** 85-93.

Rampelt, H., Kirstein-Miles, J., Nillegoda, N.B., Chi, K., Scholz, S.R., Morimoto, R.I. & Bukau, B. 2012. Metazoan Hsp70 machines use Hsp110 to power protein disaggregation. *EMBO Journal,* **31,** 4221-4235.

Rapoport, I., Boll, W., Yu, A., Böcking, T. & Kirchhausen, T. 2008. A motif in the clathrin heavy chain required for the Hsc70/auxilin uncoating reaction. *Molecular Biology of the Cell,* **19,** 405-413.

Rauch, J.N. & Gestwicki, J.E. 2014. Binding of human nucleotide exchange factors to heat shock protein 70 (Hsp70) generates functionally distinct complexes *in vitro*. *Journal of Biological Chemistry,* **289,** 1402-1414.

Raudvere, U., Kolberg, L., Kuzmin, I., Arak, T., Adler, P., Peterson, H. & Vilo, J. 2019. g: Profiler: a web server for functional enrichment analysis and conversions of gene lists (2019 update). *Nucleic Acids Research,* **47,** W191-W198.

Ravikumar, B., Vacher, C., Berger, Z., Davies, J.E., Luo, S., Oroz, L.G., Scaravilli, F., Easton, D.F., Duden, R., O'kane, C.J. & Rubinsztein, D.C. 2004. Inhibition of mTOR induces autophagy and reduces toxicity of polyglutamine expansions in fly and mouse models of Huntington disease. *Nature Genetics,* **36,** 585-595.

Raviol, H., Sadlish, H., Rodriguez, F., Mayer, M.P. & Bukau, B. 2006. Chaperone network in the yeast cytosol: Hsp110 is revealed as an Hsp70 nucleotide exchange factor. *EMBO Journal,* **25,** 2510-2518.

Reaume, A.G., Elliott, J.L., Hoffman, E.K., Kowall, N.W., Ferrante, R.J., Siwek, D.F., Wilcox, H.M., Flood, D.G., Beal, M.F., Brown Jr, R.H., Scott, R.W. & Snider, W.D. 1996. Motor neurons in Cu/Zn superoxide dismutase-deficient mice develop normally but exhibit enhanced cell death after axonal injury. *Nature Genetics,* **13,** 43-47.

Redinbaugh, M.G. & Turley, R.B. 1986. Adaptation of the bicinchoninic acid protein assay for use with microtiter plates and sucrose gradient fractions. *Analytical Biochemistry,* **153,** 267-271.

Renkawek, K., Bosman, G.I.C.G.M. & De Jong, W.W. 1994. Expression of small heat-shock protein Hsp27 in reactive gliosis in Alzheimer disease and other types of dementia. *Acta Neuropathologica,* **87,** 511-519.

Richter-Landsberg, C. & Goldbaum, O. 2003. Stress proteins in neural cells: functional roles in health and disease. *Cellular and Molecular Life Sciences,* **60,** 337-349.

Richter, K., Haslbeck, M. & Buchner, J. 2010. The heat shock response: life on the verge of death. *Molecular Cell,* **40,** 253-266.

Rimoldi, M., Servadio, A. & Zimarino, V. 2001. Analysis of heat shock transcription factor for suppression of polyglutamine toxicity. *Brain Research Bulletin,* **56,** 353-362.

Ritossa, F. 1962. A new puffing pattern induced by temperature shock and DNP in *Drosophila*. *Experientia,* **18,** 571-573.

Rock, K.L., Gramm, C., Rothstein, L., Clark, K., Stein, R., Dick, L., Hwang, D. & Goldberg, A.L. 1994. Inhibitors of the proteasome block the degradation of most cell proteins and the generation of peptides presented on MHC class I molecules. *Cell,* **78,** 761-771.

Rohde, M., Daugaard, M., Jensen, M.H., Helin, K., Nylandsted, J. & Jäättelä, M. 2005. Members of the heat-shock protein 70 family promote cancer cell growth by distinct mechanisms. *Genes and Development,* **19,** 570-582.

Ron, D. & Walter, P. 2007. Signal integration in the endoplasmic reticulum unfolded protein response. *Nature Reviews Molecular Cell Biology,* **8,** 519-529.

Rose, J.M., Novoselov, S.S., Robinson, P.A. & Cheetham, M.E. 2011. Molecular chaperone-mediated rescue of mitophagy by a Parkin RING1 domain mutant. *Human Molecular Genetics,* **20,** 16-27.

Rosenzweig, R., Nillegoda, N.B., Mayer, M.P. & Bukau, B. 2019. The Hsp70 chaperone network. *Nature Reviews Molecular Cell Biology,* **20,** 665-680.

Roth, D.M. & Balch, W.E. 2011. Modeling general proteostasis: proteome balance in health and disease. *Current Opinion in Cell Biology,* **23,** 126-134.

Roth, D.M., Hutt, D.M., Tong, J., Bouchecareilh, M., Wang, N., Seeley, T., Dekkers, J.F., Beekman, J.M., Garza, D., Drew, L., Masliah, E., Morimoto, R.I. & Balch, W.E. 2014.

Modulation of the maladaptive stress response to manage diseases of protein folding. *PLoS Biology,* **12,** e1001998.

Roux, K.J., Kim, D.I., Raida, M. & Burke, B. 2012. A promiscuous biotin ligase fusion protein identifies proximal and interacting proteins in mammalian cells. *Journal of Cell Biology,* **196,** 801-810.

Rubinsztein, D.C. 2006. The roles of intracellular protein-degradation pathways in neurodegeneration. *Nature,* **443,** 780-786.

Rubinsztein, D.C., Codogno, P. & Levine, B. 2012. Autophagy modulation as a potential therapeutic target for diverse diseases. *Nature Reviews Drug Discovery,* **11,** 709-730.

Rutkowski, D.T. & Kaufman, R.J. 2007. That which does not kill me makes me stronger: adapting to chronic ER stress. *Trends in Biochemical Sciences,* **32,** 469-476.

Sahi, C., Lee, T., Inada, M., Pleiss, J.A. & Craig, E.A. 2010. Cwc23, an essential J protein critical for pre-mRNA splicing with a dispensable J domain. *Molecular and Cellular Biology,* **30,** 33-42.

Salomons, F.A., Menéndez-Benito, V., Böttcher, C., Mccray, B.A., Taylor, J.P. & Dantuma, N.P. 2009. Selective accumulation of aggregation-prone proteasome substrates in response to proteotoxic stress. *Molecular and Cellular Biology,* **29,** 1774-1785.

San Gil, R., Berg, T. & Ecroyd, H. 2017. Using bicistronic constructs to evaluate the chaperone activities of heat shock proteins in cells. *Scientific Reports,* **7,** 2387.

San Gil, R., Cox, D., Mcalary, L., Berg, T., Walker, A.K., Yerbury, J.J., Ooi, L. & Ecroyd, H. 2020. Neurodegenerative disease-associated protein aggregates are poor inducers of the heat shock response in neuronal cells. *Journal of Cell Science,* **133,** jcs243709.

Sarparanta, J., Jonson, P.H., Golzio, C., Sandell, S., Luque, H., Screen, M., Mcdonald, K., Stajich, J.M., Mahjneh, I., Vihola, A., Raheem, O., Penttilä, S., Lehtinen, S., Huovinen, S., Palmio, J., Tasca, G., Ricci, E., Hackman, P., Hauser, M., Katsanis, N. & Udd, B. 2012. Mutations affecting the cytoplasmic functions of the co-chaperone DNAJB6 cause limb-girdle muscular dystrophy. *Nature Genetics,* **44,** 450-455.

Saxena, S. & Caroni, P. 2011. Selective neuronal vulnerability in neurodegenerative diseases: from stressor thresholds to degeneration. *Neuron,* **71,** 35-48.

Schenk, D. 2002. Amyloid-β immunotherapy for Alzheimer's disease: the end of the beginning. *Nature Reviews Neuroscience,* **3,** 824-828.

Schenk, D., Barbour, R., Dunn, W., Gordon, G., Grajeda, H., Guldo, T., Hu, K., Huang, J., Johnson-Wood, K., Khan, K., Kholodenko, D., Lee, M., Liao, Z., Lieberburg, I., Motter, R., Mutter, L., Soriano, F., Shopp, G., Vasquez, N., Vandevert, C., Walker, S., Wogulis, M., Yednock, T., Games, D. & Seubert, P. 1999. Immunization with amyloid-β attenuates Alzheimer disease-like pathology in the PDAPP mouse. *Nature,* **400,** 173-177.

Schnell, D.J. & Hebert, D.N. 2003. Protein translocons: multifunctional mediators of protein translocation across membranes. *Cell,* **112,** 491-505.

Schröder, H., Langer, T., Hartl, F.U. & Bukau, B. 1993. DnaK, DnaJ and GrpE form a cellular chaperone machinery capable of repairing heat-induced protein damage. *EMBO Journal,* **12,** 4137-4144.

Schubert, U., Antón, L.C., Gibbs, J., Norbury, C.C., Yewdell, J.W. & Bennink, J.R. 2000. Rapid degradation of a large fraction of newly synthesized proteins by proteasomes. *Nature,* **404,** 770-774.

Schuermann, J.P., Jiang, J., Cuellar, J., Llorca, O., Wang, L., Gimenez, L.E., Jin, S., Taylor, A.B., Demeler, B., Morano, K.A., Hart, P.J., Valpuesta, J.M., Lafer, E.M. & Sousa, R. 2008. Structure of the Hsp110:Hsc70 nucleotide exchange machine. *Molecular Cell,* **31,** 232-243.

Scior, A., Buntru, A., Arnsburg, K., Ast, A., Iburg, M., Juenemann, K., Pigazzini, M.L., Mlody, B., Puchkov, D., Priller, J., Wanker, E.E., Prigione, A. & Kirstein, J. 2018. Complete suppression of Htt fibrilization and disaggregation of Htt fibrils by a trimeric chaperone complex. *EMBO Journal,* **37,** 282-299.

Scotter, E.L., Chen, H.J. & Shaw, C.E. 2015. TDP-43 proteinopathy and ALS: insights into disease mechanisms and therapeutic targets. *Neurotherapeutics,* **12,** 352-363.

Sebastian, R.M. & Shoulders, M.D. 2020. Chemical biology framework to illuminate proteostasis. *Annual Review of Biochemistry,* **89,** 529-555.

Seglen, P.O. & Gordon, P.B. 1982. 3-methyladenine: specific inhibitor of autophagic/lysosomal protein degradation in isolated rat hepatocytes. *Proceedings of the National Academy of Sciences of the United States of America,* **79,** 1889-1892.

Selcen, D., Muntoni, F., Burton, B.K., Pegoraro, E., Sewry, C., Bite, A.V. & Engel, A.G. 2009. Mutation in BAG3 causes severe dominant childhood muscular dystrophy. *Annals of Neurology,* **65,** 83-89.

Selkoe, D.J. 2004. Cell biology of protein misfolding: the examples of Alzheimer's and Parkinson's diseases. *Nature Cell Biology,* **6,** 1054-1061.

Seo, H., Sonntag, K.C., Kim, W., Cattaneo, E. & Isacson, O. 2007. Proteasome activator enhances survival of Huntington's disease neuronal model cells. *PLoS ONE,* **2,** e238.

Serlidaki, D., Van Waarde, M.a.W.H., Rohland, L., Wentink, A.S., Dekker, S.L., Kamphuis, M.J., Boertien, J.M., Brunsting, J.F., Nillegoda, N.B., Bukau, B., Mayer, M.P., Kampinga, H.H. & Bergink, S. 2020. Functional diversity between HSP70 paralogs caused by variable interactions with specific co-chaperones. *Journal of Biological Chemistry,* **295,** 7301-7316.

Shaner, L., Sousa, R. & Morano, K.A. 2006. Characterization of Hsp70 binding and nucleotide exchange by the yeast Hsp110 chaperone Sse1. *Biochemistry,* **45,** 15075-15084.

Shannon, P., Markiel, A., Ozier, O., Baliga, N.S., Wang, J.T., Ramage, D., Amin, N., Schwikowski, B. & Ideker, T. 2003. Cytoscape: a software environment for integrated models of biomolecular interaction networks. *Genome Research,* **13,** 2498-2504.

Shea, J.E. & Brooks, C.L. 2001. From folding theories to folding proteins: a review and assessment of simulation studies of protein folding and unfolding. *Annual Review of Physical Chemistry,* **52,** 499-535.

Shemetov, A.A. & Gusev, N.B. 2011. Biochemical characterization of small heat shock protein HspB8 (Hsp22)-Bag3 interaction. *Archives of Biochemistry and Biophysics,* **513,** 1-9.

Sherman, M.Y. & Goldberg, A.L. 2001. Cellular defenses against unfolded proteins: a cell biologist thinks about neurodegenerative diseases. *Neuron,* **29,** 15-32.

Shevchenko, A., Tomas, H., Havliš, J., Olsen, J.V. & Mann, M. 2007. In-gel digestion for mass spectrometric characterization of proteins and proteomes. *Nature Protocols,* **1,** 2856-2860.

Shi, Y., Mosser, D.D. & Morimoto, R.I. 1998. Molecular chaperones as HSF1-specific transcriptional repressors. *Genes and Development,* **12,** 654-666.

Shiber, A., Breuer, W. & Ravid, T. 2014. Flow cytometric quantification and characterization of intracellular protein aggregates in yeast. *Prion,* **8,** 276-284.

Shorter, J. 2011. The mammalian disaggregase machinery: Hsp110 synergizes with Hsp70 and Hsp40 to catalyze protein disaggregation and reactivation in a cell-free system. *PLoS ONE,* **6,** e26319.

Smith, H.L., Li, W. & Cheetham, M.E. 2015. Molecular chaperones and neuronal proteostasis. *Seminars in Cell and Developmental Biology,* **40,** 142-152.

Smith, M.L., Gourdon, D., Little, W.C., Kubow, K.E., Eguiluz, R.A., Luna-Morris, S. & Vogel, V. 2007. Force-induced unfolding of fibronectin in the extracellular matrix of living cells. *PLoS Biology,* **5,** 2243-2254.

Söderberg, C.a.G., Månsson, C., Bernfur, K., Rutsdottir, G., Härmark, J., Rajan, S., Al-Karadaghi, S., Rasmussen, M., Höjrup, P., Hebert, H. & Emanuelsson, C. 2018. Structural modelling of the DNAJB6 oligomeric chaperone shows a peptide-binding cleft lined with conserved S/T-residues at the dimer interface. *Scientific Reports,* **8,** 5199.

Son, W.Y., Han, C.T., Hwang, S.H., Lee, J.H., Kim, S. & Kim, Y.C. 2000. Repression of hspA2 messenger RNA in human testes with abnormal spermatogenesis. *Fertility and Sterility,* **73,** 1138-1144.

Soto, C. 2003. Unfolding the role of protein misfolding in neurodegenerative diseases. *Nature Reviews Neuroscience,* **4,** 49-60.

Soto, C. & Pritzkow, S. 2018. Protein misfolding, aggregation, and conformational strains in neurodegenerative diseases. *Nature Neuroscience,* **21,** 1332-1340.

Spiess, C., Beil, A. & Ehrmann, M. 1999. A temperature-dependent switch from chaperone to protease in a widely conserved heat shock protein. *Cell,* **97,** 339-347.

Stathopulos, P.B., Rumfeldt, J.a.O., Scholz, G.A., Irani, R.A., Frey, H.E., Hallewell, R.A., Lepock, J.R. & Meiering, E.M. 2003. Cu/Zn superoxide dismutase mutants associated with amyotrophic lateral sclerosis show enhanced formation of aggregates *in vitro*. *Proceedings of the National Academy of Sciences of the United States of America,* **100,** 7021-7026.

Stefani, M. 2008. Protein folding and misfolding on surfaces. *International Journal of Molecular Sciences,* **9,** 2515-2542.

Stranks, S.D., Ecroyd, H., Van Sluyter, S., Waters, E.J., Carver, J.A. & Von Smekal, L. 2009. Model for amorphous aggregation processes. *Physical Review E,* **80,** 1-13.

Sugiyama, Y., Suzuki, A., Kishikawa, M., Akutsu, R., Hirose, T., Waye, M.M.Y., Tsui, S.K.W., Yoshida, S. & Ohno, S. 2000. Muscle develops a specific form of small heat shock protein complex composed of MKBP/HSPB2 and HSPB3 during myogenic differentiation. *Journal of Biological Chemistry,* **275,** 1095-1104.

Sun, X., Zhang, A., Baker, B., Sun, L., Howard, A., Buswell, J., Maurel, D., Masharina, A., Johnsson, K., Noren, C.J., Xu, M.Q. & Corrêa Jr, I.R. 2011. Development of SNAP-tag fluorogenic probes for wash-free fluorescence imaging. *ChemBioChem,* **12,** 2217-2226.

Suzuki, A., Sugiyama, Y., Hayashi, Y., Nyu-I, N., Yoshida, M., Nonaka, I., Ishiura, S.I., Arahata, K. & Ohno, S. 1998. MKBP, a novel member of the small heat shock protein family, binds and activates the myotonic dystrophy protein kinase. *Journal of Cell Biology,* **140,** 1113-1124.

Szklarczyk, D., Morris, J.H., Cook, H., Kuhn, M., Wyder, S., Simonovic, M., Santos, A., Doncheva, N.T., Roth, A., Bork, P., Jensen, L.J. & Von Mering, C. 2017. The STRING database in 2017: quality-controlled protein-protein association networks, made broadly accessible. *Nucleic Acids Research,* **45,** D362-D368.

Takada, H., Chen, N.J., Mirtsos, C., Suzuki, S., Suzuki, N., Wakeham, A., Mak, T.W. & Yeh, W.C. 2003. Role of SODD in regulation of tumor necrosis factor responses. *Molecular and Cellular Biology,* **23,** 4026-4033.

Takahashi, H., Furukawa, T., Yano, T., Sato, N., Takizawa, J., Kurasaki, T., Abe, T., Narita, M., Masuko, M., Koyama, S., Toba, K., Takahashi, M. & Aizawa, Y. 2007. Identification of an overexpressed gene, HSPA4L, the product of which can provoke prevalent humoral immune responses in leukemia patients. *Experimental Hematology,* **35,** 1091-1099.

Takayama, S., Bimston, D.N., Matsuzawa, S.I., Freeman, B.C., Aime-Sempe, C., Xie, Z., Morimoto, R.I. & Reed, J.C. 1997. BAG-1 modulates the chaperone activity of Hsp70/Hsc70. *EMBO Journal,* **16,** 4887-4896.

Takayama, S., Krajewski, S., Krajewska, M., Kitada, S., Zapata, J.M., Kochel, K., Knee, D., Scudiero, D., Tudor, G., Miller, G.J., Miyashita, T., Yamada, M. & Reed, J.C. 1998. Expression and location of Hsp70/Hsc-binding anti-apoptotic protein BAG-1 and its variants in normal tissues and tumor cell lines. *Cancer Research,* **58,** 3116-3131.

Takayama, S. & Reed, J.C. 2001. Molecular chaperone targeting and regulation by BAG family proteins. *Nature Cell Biology,* **3,** E237-E241.

Takeuchi, H., Kobayashi, Y., Yoshihara, T., Niwa, J.I., Doyu, M., Ohtsuka, K. & Sobue, G. 2002. Hsp70 and Hsp40 improve neurite outgrowth and suppress intracytoplasmic aggregate formation in cultured neuronal cells expressing mutant SOD1. *Brain Research,* **949,** 11-22.

Tanaka, K. & Matsuda, N. 2014. Proteostasis and neurodegeneration: the roles of proteasomal degradation and autophagy. *Biochimica et Biophysica Acta,* **1843,** 197-204.

Tanaka, M., Kim, Y.M., Lee, G., Junn, E., Iwatsubo, T. & Mouradian, M.M. 2004. Aggresomes formed by α-synuclein and synphilin-1 are cytoprotective. *Journal of Biological Chemistry,* **279,** 4625-4631.

Taylor, D.M., Kabashi, E., Agar, J.N., Minotti, S. & Durham, H.D. 2005. Proteasome activity or expression is not altered by activation of the heat shock transcription factor Hsf1 in cultured fibroblasts or myoblasts. *Cell Stress and Chaperones,* **10,** 230-241.

Taylor, D.M., Tradewell, M.L., Minotti, S. & Durham, H.D. 2007. Characterizing the role of Hsp90 in production of heat shock proteins in motor neurons reveals a suppressive effect of wild-type Hsf1. *Cell Stress and Chaperones,* **12,** 151-162.

Taylor, R.C. & Dillin, A. 2011. Aging as an event of proteostasis collapse. *Cold Spring Harbor Perspectives in Biology,* **3,** 1-17.

Thiruvalluvan, A., De Mattos, E.P., Brunsting, J.F., Bakels, R., Serlidaki, D., Barazzuol, L., Conforti, P., Fatima, A., Koyuncu, S., Cattaneo, E., Vilchez, D., Bergink, S., Boddeke, E.H.W.G., Copray, S. & Kampinga, H.H. 2020. DNAJB6, a key factor in neuronal sensitivity to amyloidogenesis. *Molecular Cell,* **78,** 346-358.

Thress, K., Song, J., Morimoto, R.I. & Kornbluth, S. 2001. Reversible inhibition of Hsp70 chaperone function by Scythe and Reaper. *EMBO Journal,* **20,** 1033-1041.

Ticozzi, N., Ratti, A. & Silani, V. 2010. Protein aggregation and defective RNA metabolism as mechanisms for motor neuron damage. *CNS and Neurological Disorders Drug Targets,* **9,** 285-296.

Tittelmeier, J., Sandhof, C.A., Ries, H.M., Druffel-Augustin, S., Mogk, A., Bukau, B. & Nussbaum-Krammer, C. 2020. The HSP110/HSP70 disaggregation system generates spreading-competent toxic α-synuclein species. *EMBO Journal,* **39,** e103954.

Tóth, M.E., Gombos, I. & Sántha, M. 2015. Heat shock proteins and their role in human diseases. *Acta Biologica Szegediensis,* **59,** 121-141.

Towbin, H., Staehelin, T. & Gordon, J. 1979. Electrophoretic transfer of proteins from polyacrylamide gels to nitrocellulose sheets: procedure and some applications. *Proceedings of the National Academy of Sciences of the United States of America,* **76,** 4350-4354.

Treweek, T.M., Meehan, S., Ecroyd, H. & Carver, J.A. 2015. Small heat-shock proteins: important players in regulating cellular proteostasis. *Cellular and Molecular Life Sciences,* **72,** 429-451.

Trinklein, N.D., Murray, J.I., Hartman, S.J., Botstein, D. & Myers, R.M. 2004. The role of heat shock transcription factor 1 in the genome-wide regulation of the mammalian heat shock response. *Molecular Biology of the Cell,* **15,** 1254-1261.

Tsai, J. & Douglas, M.G. 1996. A conserved HPD sequence of the J-domain is necessary for YDJ1 stimulation of Hsp70 ATPase activity at a site distinct from substrate binding. *Journal of Biological Chemistry,* **271,** 9347-9354.

Tsukamoto, Y., Kuwabara, K., Hirota, S., Kawano, K., Yoshikawa, K., Ozawa, K., Kobayashi, T., Yanagi, H., Stern, D.M., Tohyama, M., Kitamura, Y. & Ogawa, S. 1998. Expression of the 150-kd oxygen-regulated protein in human breast cancer. *Laboratory Investigation,* **78,** 699-706.

Turner, B.J. & Talbot, K. 2008. Transgenics, toxicity and therapeutics in rodent models of mutant SOD1-mediated familial ALS. *Progress in Neurobiology,* **85,** 94-134.

Tyedmers, J., Mogk, A. & Bukau, B. 2010. Cellular strategies for controlling protein aggregation. *Nature Reviews Molecular Cell Biology,* **11,** 777-788.

Udan-Johns, M., Bengoechea, R., Bell, S., Shao, J., Diamond, M.I., True, H.L., Weihl, C.C. & Baloh, B.H. 2014. Prion-like nuclear aggregation of TDP-43 during heat shock is regulated by HSP40/70 chaperones. *Human Molecular Genetics,* **23,** 157-170.

Ungewickell, E., Ungewickell, H., Holstein, S.E.H., Lindner, R., Prasad, K., Barouch, W., Martini, B., Greene, L.E. & Eisenberg, E. 1995. Role of auxilin in uncoating clathrin-coated vesicles. *Nature,* **378,** 632-635.

Ushioda, R., Miyamoto, A., Inoue, M., Watanabe, S., Okumura, M., Maegawa, K.I., Uegaki, K., Fujii, S., Fukuda, Y., Umitsu, M., Takagi, J., Inaba, K., Mikoshiba, K. & Nagata, K. 2016. Redox-assisted regulation of Ca^{2+} homeostasis in the endoplasmic reticulum by disulfide reductase ERdj5. *Proceedings of the National Academy of Sciences of the United States of America,* **113,** E6055-E6063.

Uversky, V.N. & Ptitsyn, O.B. 1994. "Partly folded state", a new equilibrium state of protein molecules: four-state guanidinium chloride-induced unfolding of β-lactamase at low temperature. *Biochemistry,* **33,** 2782-2791.

Van Den Berg, B., Ellis, R.J. & Dobson, C.M. 1999. Effects of macromolecular crowding on protein folding and aggregation. *EMBO Journal,* **18,** 6927-6933.

Van Rijk, A.F., Stege, G.J.J., Bennink, E.J., May, A. & Bloemendal, H. 2003. Nuclear staining for the small heat shock protein αB-crystallin colocalizes with splicing factor SC35. *European Journal of Cell Biology,* **82,** 361-368.

Vihervaara, A. & Sistonen, L. 2014. HSF1 at a glance. *Journal of Cell Science,* **127,** 261-266.

Vos, M.J., Hageman, J., Carra, S. & Kampinga, H.H. 2008. Structural and functional diversities between members of the human HSPB, HSPH, HSPA, and DNAJ chaperone families. *Biochemistry,* **47,** 7001-7011.

Vos, M.J., Kanon, B. & Kampinga, H.H. 2009. HSPB7 is a SC35 speckle resident small heat shock protein. *Biochimica et Biophysica Acta - Molecular Cell Research,* **1793,** 1343-1353.

Vos, M.J., Zijlstra, M.P., Kanon, B., Van Waarde-Verhagen, M.a.W.H., Brunt, E.R.P., Oosterveld-Hut, H.M.J., Carra, S., Sibon, O.C.M. & Kampinga, H.H. 2010. HSPB7 is the most potent polyQ aggregation suppressor within the HSPB family of molecular chaperones. *Human Molecular Genetics,* **19,** 4677-4693.

Walsh, D.M., Klyubin, I., Fadeeva, J.V., Cullen, W.K., Anwyl, R., Wolfe, M.S., Rowan, M.J. & Selkoe, D.J. 2002. Naturally secreted oligomers of amyloid β protein potently inhibit hippocampal long-term potentiation *in vivo*. *Nature,* **416,** 535-539.

Wang, H.G., Takayama, S., Rapp, U.R. & Reed, J.C. 1996. Bcl-2 interacting protein, BAG-1, binds to and activates the kinase Raf-1. *Proceedings of the National Academy of Sciences of the United States of America,* **93,** 7063-7068.

Wang, J., Farr, G.W., Zeiss, C.J., Rodriguez-Gil, D.J., Wilson, J.H., Furtak, K., Rutkowski, D.T., Kaufman, R.J., Ruse, C.I., Yates Iii, J.R., Perrin, S., Feany, M.B. & Horwich, A.L. 2009. Progressive aggregation despite chaperone associations of a mutant SOD1-YFP in transgenic mice that develop ALS. *Proceedings of the National Academy of Sciences of the United States of America,* **106,** 1392-1397.

Wang, P., Wander, C.M., Yuan, C.X., Bereman, M.S. & Cohen, T.J. 2017. Acetylation-induced TDP-43 pathology is suppressed by an HSF1-dependent chaperone program. *Nature Communications,* **8,** 82.

Wang, W., Nema, S. & Teagarden, D. 2010. Protein aggregation - pathways and influencing factors. *International Journal of Pharmaceutics,* **390,** 89-99.

Warrick, J.M., Chan, H.Y.E., Gray-Board, G.L., Chai, Y., Paulson, H.L. & Bonini, N.M. 1999. Suppression of polyglutamine-mediated neurodegeneration in *Drosophila* by the molecular chaperone HSP70. *Nature Genetics,* **23,** 425-428.

Watson, E.D., Geary-Joo, C., Hughes, M. & Cross, J.C. 2007. The Mrj co-chaperone mediates keratin turnover and prevents the formation of toxic inclusion bodies in trophoblast cells of the placenta. *Development,* **134,** 1809-1817.

Watson, E.D., Mattar, P., Schuurmans, C. & Cross, J.C. 2009. Neural stem cell self-renewal requires the Mrj co-chaperone. *Developmental Dynamics,* **238,** 2564-2574.

Webb, J.L., Ravikumar, B., Atkins, J., Skepper, J.N. & Rubinsztein, D.C. 2003. α-synuclein is degraded by both autophagy and the proteasome. *Journal of Biological Chemistry,* **278,** 25009-25013.

Westermark, P., Benson, M.D., Buxbaum, J.N., Cohen, A.S., Frangione, B., Ikeda, S.I., Masters, C.L., Merlini, G., Saraiva, M.J. & Sipe, J.D. 2005. Amyloid: toward terminology

clarification: report from the nomenclature committee of the international society of amyloidosis. *Amyloid,* **12,** 1-4.

Westhoff, B., Chapple, J.P., Van Der Spuy, J., Höhfeld, J. & Cheetham, M.E. 2005. HSJ1 is a neuronal shuttling factor for the sorting of chaperone clients to the proteasome. *Current Biology,* **15,** 1058-1064.

Wexler, N.S., Young, A.B., Tanzi, R.E., Travers, H., Starosta-Rubinstein, S., Penney, J.B., Snodgrass, S.R., Shoulson, I., Gomez, F., Arroyo, M.a.R., Penchaszadeh, G.K., Moreno, H., Gibbons, K., Faryniarz, A., Hobbs, W., Anderson, M.A., Bonilla, E., Conneally, P.M. & Gusella, J.F. 1987. Homozygotes for Huntington's disease. *Nature,* **326,** 194-197.

Whiten, D.R., San Gil, R., Mcalary, L., Yerbury, J.J., Ecroyd, H. & Wilson, M.R. 2016. Rapid flow cytometric measurement of protein inclusions and nuclear trafficking. *Scientific Reports,* **6,** 31138.

Wigley, C.W., Fabunmi, R.P., Lee, M.G., Marino, C.R., Muallem, S., Demartino, G.N. & Thomas, P.J. 1999. Dynamic association of proteasomal machinery with the centrosome. *Journal of Cell Biology,* **145,** 481-490.

Wilhelmus, M.M.M., Boelens, W.C., Otte-Höller, I., Kamps, B., De Waal, R.M.W. & Verbeek, M.M. 2006. Small heat shock proteins inhibit amyloid-β protein aggregation and cerebrovascular amyloid-β protein toxicity. *Brain Research,* **1089,** 67-78.

Wils, H., Kleinberger, G., Janssens, J., Pereson, S., Joris, G., Cuijt, I., Smits, V., Ceuterick-De Groote, C., Van Broeckhoven, C. & Kumar-Singh, S. 2010. TDP-43 transgenic mice develop spastic paralysis and neuronal inclusions characteristic of ALS and frontotemporal lobar degeneration. *Proceedings of the National Academy of Sciences of the United States of America,* **107,** 3858-3863.

Winkler, J., Tyedmers, J., Bukau, B. & Mogk, A. 2012. Hsp70 targets Hsp100 chaperones to substrates for protein disaggregation and prion fragmentation. *Journal of Cell Biology,* **198,** 387-404.

Wisniewska, M., Karlberg, T., Lehtiö, L., Johansson, I., Kotenyova, T., Moche, M. & Schüler, H. 2010. Crystal structures of the ATPase domains of four human Hsp70 isoforms: HSPA1L/Hsp70-hom, HSPA2/Hsp70-2, HSPA6/Hsp70B', and HSPA5/BiP/GRP78. *PLoS ONE,* **5,** e8625.

Wissing, D. & Jäättelä, M. 1996. HSP27 and HSP70 increase the survival of WEHI-S cells exposed to hyperthermia. *International Journal of Hyperthermia,* **12,** 125-138.

Wood, R.J., Ormsby, A.R., Radwan, M., Cox, D., Sharma, A., Vöpel, T., Ebbinghaus, S., Oliveberg, M., Reid, G.E., Dickson, A. & Hatters, D.M. 2018. A biosensor-based framework to measure latent proteostasis capacity. *Nature Communications,* **9,** 287.

Wyatt, A.R., Yerbury, J.J., Ecroyd, H. & Wilson, M.R. 2013. Extracellular chaperones and proteostasis. *Annual Review of Biochemistry,* **82,** 295-322.

Wyss-Coray, T. & Mucke, L. 2002. Inflammation in neurodegenerative disease - a double-edged sword. *Neuron,* **35,** 419-432.

Wyttenbach, A., Carmichael, J., Swartz, J., Furlong, R.A., Narain, Y., Rankin, J. & Rubinsztein, D.C. 2000. Effects of heat shock, heat shock protein 40 (HDJ-2), and proteasome inhibition on protein aggregation in cellular models of Huntington's disease. *Proceedings of the National Academy of Sciences of the United States of America,* **97,** 2898-2903.

Wyttenbach, A., Sauvageot, O., Carmichael, J., Diaz-Latoud, C., Arrigo, A.P. & Rubinsztein, D.C. 2002. Heat shock protein 27 prevents cellular polyglutamine toxicity and suppresses the increase of reactive oxygen species caused by huntingtin. *Human Molecular Genetics,* **11,** 1137-1151.

Xu, P., Duong, D.M., Seyfried, N.T., Cheng, D., Xie, Y., Robert, J., Rush, J., Hochstrasser, M., Finley, D. & Peng, J. 2009. Quantitative proteomics reveals the function of unconventional ubiquitin chains in proteasomal degradation. *Cell,* **137,** 133-145.

Xu, Y.F., Gendron, T.F., Zhang, Y.J., Lin, W.L., D'alton, S., Sheng, H., Casey, M.C., Tong, J., Knight, J., Yu, X., Rademakers, R., Boylan, K., Hutton, M., Mcgowan, E., Dickson, D.W.,

Lewis, J. & Petrucelli, L. 2010. Wild-type human TDP-43 expression causes TDP-43 phosphorylation, mitochondrial aggregation, motor deficits, and early mortality in transgenic mice. *Journal of Neuroscience,* **30,** 10851-10859.

Yamamoto, A., Tagawa, Y., Yoshimori, T., Moriyama, Y., Masaki, R. & Tashiro, Y. 1998. Bafilomycin A1 prevents maturation of autophagic vacuoles by inhibiting fusion between autophagosomes and lysosomes in rat hepatoma cell line, H-4-II-E cells. *Cell Structure and Function,* **23,** 33-42.

Yamashita, H., Kawamata, J., Okawa, K., Kanki, R., Nakamizo, T., Hatayama, T., Yamanaka, K., Takahashi, R. & Shimohama, S. 2007. Heat-shock protein 105 interacts with and suppresses aggregation of mutant Cu/Zn superoxide dismutase: clues to a possible strategy for treating ALS. *Journal of Neurochemistry,* **102,** 1497-1505.

Yang, J., Oza, J., Bridges, K., Chen, K.Y. & Liu, A.Y.C. 2008. Neural differentiation and the attenuated heat shock response. *Brain Research,* **1203,** 39-50.

Yates, S.L., Burgess, L.H., Kocsis-Angle, J., Antal, J.M., Dority, M.D., Embury, P.B., Piotrkowski, A.M. & Brunden, K.R. 2000. Amyloid β and amylin fibrils induce increases in proinflammatory cytokine and chemokine production by THP-1 cells and murine microglia. *Journal of Neurochemistry,* **74,** 1017-1025.

Yerbury, J.J., Gower, D., Vanags, L., Roberts, K., Lee, J.A. & Ecroyd, H. 2013. The small heat shock proteins αb-crystallin and Hsp27 suppress SOD1 aggregation *in vitro*. *Cell Stress and Chaperones,* **18,** 251-257.

Yerbury, J.J., Ooi, L., Dillin, A., Saunders, D.N., Hatters, D.M., Beart, P.M., Cashman, N.R., Wilson, M.R. & Ecroyd, H. 2016. Walking the tightrope: proteostasis and neurodegenerative disease. *Journal of Neurochemistry,* **137,** 489-505.

Yoshimori, T., Yamamoto, A., Moriyama, Y., Futai, M. & Tashiro, Y. 1991. Bafilomycin A1, a specific inhibitor of vacuolar-type H^+-ATPase, inhibits acidification and protein degradation in lysosomes of cultured cells. *Journal of Biological Chemistry,* **266,** 17707-17712.

Yu, N., Kakunda, M., Pham, V., Lill, J.R., Du, P., Wongchenko, M., Yan, Y., Firestein, R. & Huang, X. 2015. HSP105 recruits protein phosphatase 2A to dephosphorylate ß-catenin. *Molecular and Cellular Biology,* **35,** 1390-1400.

Zacharias, D.A., Violin, J.D., Newton, A.C. & Tsien, R.Y. 2002. Partitioning of lipid-modified monomeric GFPs into membrane microdomains of live cells. *Science,* **296,** 913-916.

Zappasodi, R., Ruggiero, G., Guarnotta, C., Tortoreto, M., Tringali, C., Cavanè, A., Cabras, A.D., Castagnoli, L., Venerando, B., Zaffaroni, N., Gianni, A.M., De Braud, F., Tripodo, C., Pupa, S.M. & Di Nicola, M. 2015. HSPH1 inhibition downregulates Bcl-6 and c-Myc and hampers the growth of human aggressive B-cell non-Hodgkin lymphoma. *Blood,* **125,** 1768-1771.

Zarouchlioti, C., Parfitt, D.A., Li, W., Gittings, L.M. & Cheetham, M.E. 2018. DNAJ proteins in neurodegeneration: essential and protective factors. *Philosophical Transactions of the Royal Society B: Biological Sciences,* **373,** 1738.

Zeineddine, R., Whiten, D.R., Farrawell, N.E., Mcalary, L., Hanspal, M.A., Kumita, J.R., Wilson, M.R. & Yerbury, J.J. 2017. Flow cytometric measurement of the cellular propagation of TDP-43 aggregation. *Prion,* **11,** 195-204.

Zeiner, M., Gebauer, M. & Gehring, U. 1997. Mammalian protein RAP46: an interaction partner and modulator of 70 kDa heat shock proteins. *EMBO Journal,* **16,** 5483-5490.

Zhang, S., Greening, D.W. & Hong, Y. 2021. Recent advances in bioanalytical methods to measure proteome stability in cells. *Analyst,* **146,** 2097-2109.

Zhang, Y.J., Gendron, T.F., Ebbert, M.T.W., O'raw, A.D., Yue, M., Jansen-West, K., Zhang, X., Prudencio, M., Chew, J., Cook, C.N., Daughrity, L.M., Tong, J., Song, Y., Pickles, S.R., Castanedes-Casey, M., Kurti, A., Rademakers, R., Oskarsson, B., Dickson, D.W., Hu, W., Gitler, A.D., Fryer, J.D. & Petrucelli, L. 2018. Poly(GR) impairs protein translation and

stress granule dynamics in C9orf72-associated frontotemporal dementia and amyotrophic lateral sclerosis. *Nature Medicine,* **24,** 1136-1142.

Zheng, X., Krakowiak, J., Patel, N., Beyzavi, A., Ezike, J., Khalil, A.S. & Pincus, D. 2016. Dynamic control of Hsf1 during heat shock by a chaperone switch and phosphorylation. *eLife,* **5,** 1-26.

Zhu, D., Dix, D.J. & Eddy, E.M. 1997. HSP70-2 is required for CDC2 kinase activity in meiosis I of mouse spermatocytes. *Development,* **124,** 3007-3014.

Zhu, Y.H., Ma, T.M. & Wang, X. 2005. Gene transfer of heat-shock protein 20 protects against ischemia/reperfusion injury in rat hearts. *Acta Pharmacologica Sinica,* **26,** 1193-1200.

Zoghbi, H.Y. & Orr, H.T. 2000. Glutamine repeats and neurodegeneration. *Annual Review of Neuroscience,* **23,** 217-247.

Zuo, D., Subjeck, J. & Wang, X.Y. 2016. Unfolding the role of large heat shock proteins: new insights and therapeutic implications. *Frontiers in Immunology,* **7,** 75.

Zuo, J., Baler, R., Dahl, G. & Voellmy, R. 1994. Activation of the DNA-binding ability of human heat shock transcription factor 1 may involve the transition from an intramolecular to an intermolecular triple-stranded coiled-coil structure. *Molecular and Cellular Biology,* **14,** 7557-7568.

Zuo, J., Rungger, D. & Voellmy, R. 1995. Multiple layers of regulation of human heat shock transcription factor 1. *Molecular and Cellular Biology,* **15,** 4319-4330.

Chapter 8: Appendices

Appendix I

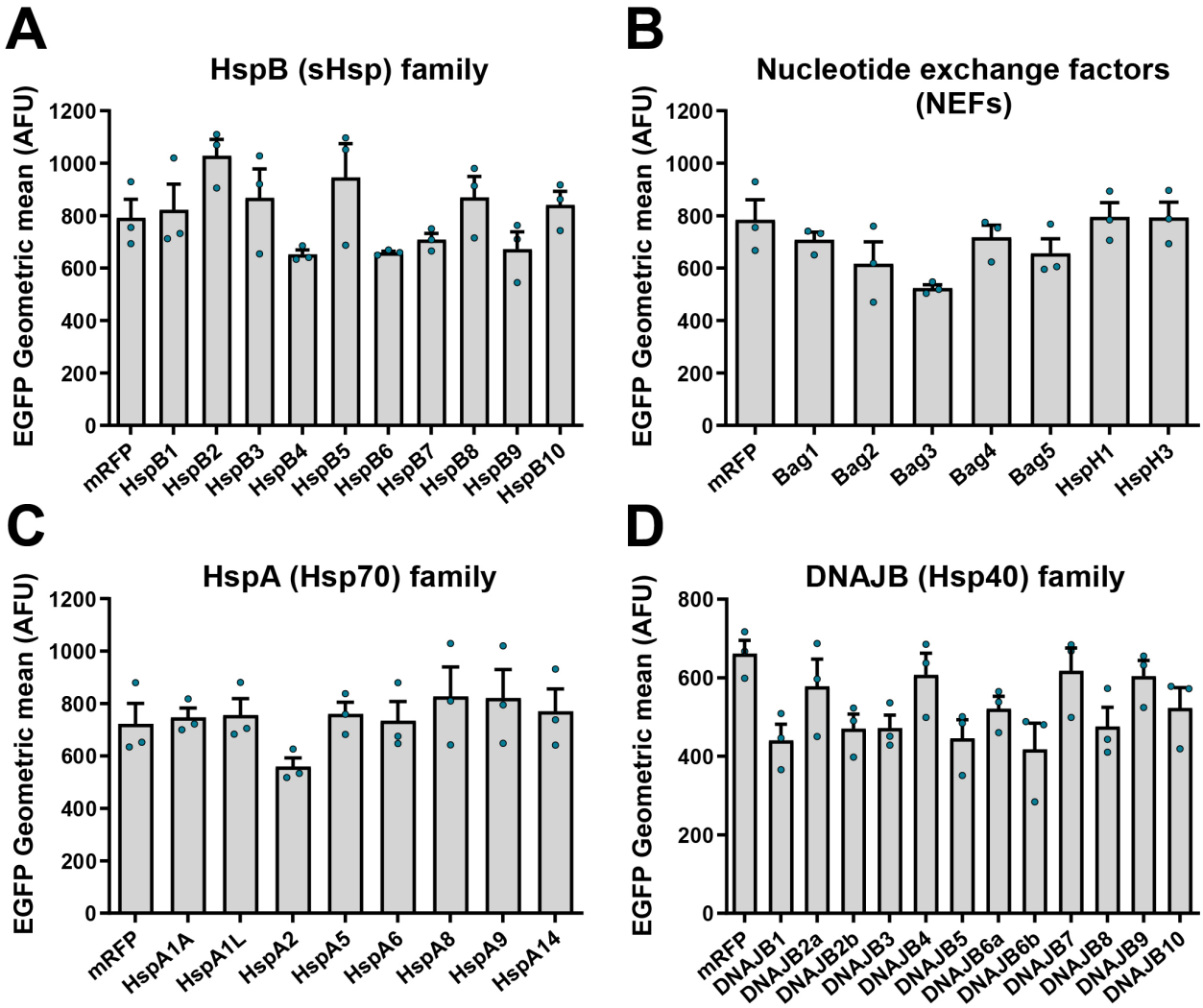

Figure 8.1. The amount of Fluc^{DM}-EGFP expressed in cells following co-transfection with a Hsp in the overexpression screen. Flp-In T-Rex HEK293 cells were co-transfected with V5-tagged members of the **(A)** HspB, **(B)** nucleotide exchange factor (NEF), **(C)** HspA or **(D)** DNAJB family or mRFP (as a negative control) and Fluc^{DM}-EGFP and analysed 48 h post-transfection by quantitative flow cytometry. Data are the mean ± S.E.M (n=3) of the EGFP geometric mean (arbitrary fluorescence units; AFU) of live, transfected cells co-expressing Fluc^{DM}-EGFP and a HspB, NEF, HspA or DNAJB member (or mRFP as a negative control), as measured by flow cytometry. Significant differences between group means were tested using a one-way ANOVA but no statistically significant differences were found ($P > 0.05$ in all cases).

Appendix II

Table 8.1. Proteins found in Fluc^{DM} inclusions in Neuro-2a and NSC-34 cells following proteomic mass spectrometry. The lists of proteins identified in Neuro-2a and NSC-34 cells represent only those with an abundance ≥ 2-fold higher than proteins identified in the corresponding untransfected control, and which appeared in all three biological replicates of each sample. Proteins are sorted by name in alphabetical order and corresponding UniProt accession numbers are provided.

Neuro-2a		***NSC-34***	
UniProt accession #	***Description***	***UniProt accession #***	***Description***
Q9CQV8-1	14-3-3 protein beta/alpha	*P62259*	14-3-3 protein epsilon
P62259	14-3-3 protein epsilon	*P68254-1*	14-3-3 protein theta
P61982	14-3-3 protein gamma	*P63101*	14-3-3 protein zeta/delta
P63101	14-3-3 protein zeta/delta	*Q8VDM4*	26S proteasome non-ATPase regulatory subunit 2
Q8VI94	2'-5'-oligoadenylate synthase-like protein 1	*P62334*	26S proteasome regulatory subunit 10B
Q9WVJ2	26S proteasome non-ATPase regulatory subunit 13	*P62192*	26S proteasome regulatory subunit 4
Q8VDM4	26S proteasome non-ATPase regulatory subunit 2	*O88685*	26S proteasome regulatory subunit 6A
P14685	26S proteasome non-ATPase regulatory subunit 3	*P54775*	26S proteasome regulatory subunit 6B
P62334	26S proteasome regulatory subunit 10B	*P46471*	26S proteasome regulatory subunit 7
P62192	26S proteasome regulatory subunit 4	*P62196*	26S proteasome regulatory subunit 8
O88685	26S proteasome regulatory subunit 6A	*Q8VE22*	28S ribosomal protein S23, mitochondrial
P54775	26S proteasome regulatory subunit 6B	*Q99N87*	28S ribosomal protein S5, mitochondrial
P46471	26S proteasome regulatory subunit 7	*Q80X85*	28S ribosomal protein S7, mitochondrial
P62196	26S proteasome regulatory subunit 8	*Q9D7N3*	28S ribosomal protein S9, mitochondrial
Q9CQE3	28S ribosomal protein S17, mitochondrial	*Q9CQF0*	39S ribosomal protein L11, mitochondrial
Q8VE22	28S ribosomal protein S23, mitochondrial	*Q9CPR5*	39S ribosomal protein L15, mitochondrial
Q80ZS3	28S ribosomal protein S26, mitochondrial	*Q99N95*	39S ribosomal protein L3, mitochondrial
Q9ER88-1	28S ribosomal protein S29, mitochondrial	*Q8K2M0*	39S ribosomal protein L38, mitochondrial
Q80X85	28S ribosomal protein S7, mitochondrial	*Q9Z2Q5*	39S ribosomal protein L40, mitochondrial
Q9D7N3	28S ribosomal protein S9, mitochondrial	*Q9CQN7*	39S ribosomal protein L41, mitochondrial
Q9CPR5	39S ribosomal protein L15, mitochondrial	*Q9EQI8*	39S ribosomal protein L46, mitochondrial
Q9CQL5	39S ribosomal protein L18, mitochondrial	*Q8K2Y7*	39S ribosomal protein L47, mitochondrial
Q9D1N9	39S ribosomal protein L21, mitochondrial	*Q9D1H8*	39S ribosomal protein L53, mitochondrial
Q9D1B9	39S ribosomal protein L28, mitochondrial	*P63325*	40S ribosomal protein S10
Q921S7	39S ribosomal protein L37, mitochondrial	*P62301*	40S ribosomal protein S13
Q9Z2Q5	39S ribosomal protein L40, mitochondrial	*P62843*	40S ribosomal protein S15

Q9CQN7	39S ribosomal protein L41, mitochondrial	*P63276*	40S ribosomal protein S17
Q8K2Y7	39S ribosomal protein L47, mitochondrial	*P62270*	40S ribosomal protein S18
P63325	40S ribosomal protein S10	*Q9CZX8*	40S ribosomal protein S19
P62301	40S ribosomal protein S13	*P62849-1*	40S ribosomal protein S24
P62843	40S ribosomal protein S15	*P62858*	40S ribosomal protein S28
P63276	40S ribosomal protein S17	*P62862*	40S ribosomal protein S30
Q9CZX8	40S ribosomal protein S19	*P62082*	40S ribosomal protein S7
P62267	40S ribosomal protein S23	*P14206*	40S ribosomal protein SA
P62849-1	40S ribosomal protein S24	*P10852*	4F2 cell-surface antigen heavy chain
P62852	40S ribosomal protein S25	*Q5EG47*	5'-AMP-activated protein kinase catalytic subunit alpha-1
P62858	40S ribosomal protein S28	*P47955*	60S acidic ribosomal protein P1
P62862	40S ribosomal protein S30	*P35979*	60S ribosomal protein L12
P62242	40S ribosomal protein S8	*P67984*	60S ribosomal protein L22
Q6ZWN5	40S ribosomal protein S9	*P62751*	60S ribosomal protein l23a
P14206	40S ribosomal protein SA	*P61255*	60S ribosomal protein L26
P10852	4F2 cell-surface antigen heavy chain	*P61358*	60S ribosomal protein L27
Q9JLJ2	4-trimethylaminobutyraldehyde dehydrogenase	*P62900*	60S ribosomal protein L31
Q5EG47	5'-AMP-activated protein kinase catalytic subunit alpha-1	*Q6ZWV7*	60S ribosomal protein L35
Q9CR57	60S ribosomal protein L14	*P47964*	60S ribosomal protein L36
P62717	60S ribosomal protein l18a	*P47962*	60S ribosomal protein L5
P62751	60S ribosomal protein l23a	*P12970*	60S ribosomal protein l7a
P61358	60S ribosomal protein L27	*Q9CQ60*	6-phosphogluconolactonase
P14115	60S ribosomal protein l27a	*Q8QZT1*	Acetyl-CoA acetyltransferase, mitochondrial
P62889	60S ribosomal protein L30	*Q9EST5-1*	Acidic leucine-rich nuclear phosphoprotein 32 family member B
P62911	60S ribosomal protein L32	*Q99KI0*	Aconitate hydratase, mitochondrial
P47964	60S ribosomal protein L36	*P60710*	Actin, cytoplasmic 1
P47962	60S ribosomal protein L5	*Q9JM76*	Actin-related protein 2/3 complex subunit 3
P12970	60S ribosomal protein l7a	*Q9D8Z1*	Activating signal cointegrator 1 complex subunit 1
Q9DCD0	6-phosphogluconate dehydrogenase, decarboxylating	*P08030*	Adenine phosphoribosyltransferase
Q9CQ60	6-phosphogluconolactonase	*P50247*	Adenosylhomocysteinase
Q8QZT1	Acetyl-CoA acetyltransferase, mitochondrial	*P54822*	Adenylosuccinate lyase
Q9EST5-1	Acidic leucine-rich nuclear phosphoprotein 32 family member B	*P46664*	Adenylosuccinate synthetase isozyme 2
Q99KI0	Aconitate hydratase, mitochondrial	*P61205*	ADP-ribosylation factor 3
Q9Z2N8	Actin-like protein 6A	*Q9JKX6*	ADP-sugar pyrophosphatase
Q9WV32	Actin-related protein 2/3 complex subunit 1B	*O08715*	A-kinase anchor protein 1, mitochondrial
Q9CVB6	Actin-related protein 2/3 complex subunit 2	*Q8BGQ7*	Alanine-tRNA ligase, cytoplasmic
P59999	Actin-related protein 2/3 complex subunit 4	*P47738*	Aldehyde dehydrogenase, mitochondrial
Q8BK64	Activator of 90 kDa heat shock protein ATPase homolog 1	*Q8C0I1*	Alkyldihydroxyacetonephosphate synthase, peroxisomal

Q8C6B9	Active regulator of SIRT1	*P17182*	Alpha-enolase
P08030	Adenine phosphoribosyltransferase	*Q6PAM1*	Alpha-taxilin
P50247	Adenosylhomocysteinase	*Q91X58*	AN1-type zinc finger protein 2B
Q9R0Y5-1	Adenylate kinase isoenzyme 1	*Q8K298*	Anillin
P54822	Adenylosuccinate lyase	*P07356*	Annexin A2
P46664	Adenylosuccinate synthetase isozyme 2	*Q9Z0X1*	Apoptosis-inducing factor 1, mitochondrial
P48962	ADP/ATP translocase 1	*Q80WC7-1*	Arf-GAP domain and FG repeat-containing protein 2
P51881	ADP/ATP translocase 2	*Q9QWY8*	Arf-GAP with SH3 domain, ANK repeat and PH domain-containing protein 1
P61205	ADP-ribosylation factor 3	*Q91YI0*	Argininosuccinate lyase
Q9CQW2	ADP-ribosylation factor-like protein 8B	*Q8BP47*	Asparagine-tRNA ligase, cytoplasmic
Q9CZS1	Aldehyde dehydrogenase X, mitochondrial	*Q03265*	ATP synthase subunit alpha, mitochondrial
P47738	Aldehyde dehydrogenase, mitochondrial	*P56480*	ATP synthase subunit beta, mitochondrial
Q8C0I1	Alkyldihydroxyacetonephosphate synthase, peroxisomal	*Q9DB20*	ATP synthase subunit O, mitochondrial
P61164	Alpha-centractin	*Q8K268*	ATP-binding cassette sub-family F member 3
P17182	Alpha-enolase	*Q8BH59*	Calcium-binding mitochondrial carrier protein Aralar1
Q8R010	Aminoacyl tRNA synthase complex-interacting multifunctional protein 2	*Q8BK63-1*	Casein kinase I isoform alpha
Q9JKC8	Ap-3 complex subunit mu-1	*P67871*	Casein kinase II subunit beta
O35841	Apoptosis inhibitor 5	*P30999-1*	Catenin delta-1
Q9Z0X1	Apoptosis-inducing factor 1, mitochondrial	*P60766-2*	Cell division control protein 42 homolog
Q80WC7-1	Arf-GAP domain and FG repeat-containing protein 2	*Q08288*	Cell growth-regulating nucleolar protein
Q9D0I9	Arginine-tRNA ligase, cytoplasmic	*Q9Z1Q5*	Chloride intracellular channel protein 1
Q9Z2A5	Arginyl-tRNA-protein transferase 1	*Q9QYB1*	Chloride intracellular channel protein 4
Q8BP47	Asparagine-tRNA ligase, cytoplasmic	*Q9CY57*	Chromatin target of PRMT1 protein
Q922B2	Aspartate-tRNA ligase, cytoplasmic	*Q6NVF9*	Cleavage and polyadenylation specificity factor subunit 6
Q9Z2W0	Aspartyl aminopeptidase	*Q8BTV2*	Cleavage and polyadenylation specificity factor subunit 7
Q03265	ATP synthase subunit alpha, mitochondrial	*P11440*	Cyclin-dependent kinase 1
P56480	ATP synthase subunit beta, mitochondrial	*P30285*	Cyclin-dependent kinase 4
P56135	ATP synthase subunit f, mitochondrial	*Q03147*	Cyclin-dependent kinase 7
Q9CPQ8	ATP synthase subunit g, mitochondrial	*P97315*	Cysteine and glycine-rich protein 1
Q9DB20	ATP synthase subunit O, mitochondrial	*Q9DCT8*	Cysteine-rich protein 2
P61222	ATP-binding cassette sub-family E member 1	*Q9CZ13*	Cytochrome b-c1 complex subunit 1, mitochondrial
Q8K268	ATP-binding cassette sub-family F member 3	*Q9DB77*	Cytochrome b-c1 complex subunit 2, mitochondrial
Q91V92	ATP-citrate synthase	*P00405*	Cytochrome c oxidase subunit 2
Q9CZ42-1	ATP-dependent (S)-NAD(P)H-hydrate dehydratase	*P19536*	Cytochrome c oxidase subunit 5B, mitochondrial
P12382	ATP-dependent 6-phosphofructokinase, liver type	*Q9D0M3*	Cytochrome c1, heme protein, mitochondrial

Q61655	ATP-dependent RNA helicase DDX19A	*Q61753*	D-3-phosphoglycerate dehydrogenase
O88967	ATP-dependent zinc metalloprotease YME1L1	*Q9JII5*	DAZ-associated protein 1
Q9Z2H5-1	Band 4.1-like protein 1	*Q80XN0*	D-beta-hydroxybutyrate dehydrogenase, mitochondrial
P18155	Bifunctional methylenetetrahydrofolate dehydrogenase/cyclohydrolase, mitochondrial	*Q99L04*	Dehydrogenase/reductase SDR family member 1
Q9CWJ9	Bifunctional purine biosynthesis protein PurH	*Q99J47*	Dehydrogenase/reductase SDR family member 7B
Q8BHX3-1	Borealin	*Q9Z110-1*	Delta-1-pyrroline-5-carboxylate synthase
Q9CXW3	Calcyclin-binding protein	*Q8BHC4*	Dephospho-CoA kinase domain-containing protein
Q60865	Caprin-1	*O54908*	Dickkopf-related protein 1
P67871	Casein kinase II subunit beta	*O08749*	Dihydrolipoyl dehydrogenase, mitochondrial
P60766-2	Cell division control protein 42 homolog	*Q8BMF4*	Dihydrolipoyllysine-residue acetyltransferase component of pyruvate dehydrogenase complex, mitochondrial
Q9QYB1	Chloride intracellular channel protein 4	*Q9D2G2-1*	Dihydrolipoyllysine-residue succinyltransferase component of 2-oxoglutarate dehydrogenase complex, mitochondrial
Q9CY57	Chromatin target of PRMT1 protein	*O08553*	Dihydropyrimidinase-related protein 2
P23198	Chromobox protein homolog 3	*Q9EQF6*	Dihydropyrimidinase-related protein 5
Q99KN9-1	Clathrin interactor 1	*Q8BWT5*	Disco-interacting protein 2 homolog A
Q8BQZ5-1	Cleavage and polyadenylation specificity factor subunit 4	*P37913*	DNA ligase 1
Q6NVF9	Cleavage and polyadenylation specificity factor subunit 6	*Q9EQ28*	DNA polymerase delta subunit 3
Q99LC2	Cleavage stimulation factor subunit 1	*P97310*	DNA replication licensing factor mcm2
O89079	Coatomer subunit epsilon	*P25206*	DNA replication licensing factor mcm3
P11440	Cyclin-dependent kinase 1	*P49717*	DNA replication licensing factor MCM4
P97315	Cysteine and glycine-rich protein 1	*Q61881*	DNA replication licensing factor MCM7
P63254	Cysteine-rich protein 1	*P52432*	DNA-directed RNA polymerases I and III subunit RPAC1
Q9DCT8	Cysteine-rich protein 2	*P63037*	DnaJ homolog subfamily A member 1
Q9CZ13	Cytochrome b-c1 complex subunit 1, mitochondrial	*Q9QYJ0*	DnaJ homolog subfamily A member 2
Q9DB77	Cytochrome b-c1 complex subunit 2, mitochondrial	*Q99M87-1*	DnaJ homolog subfamily A member 3, mitochondrial
P00405	Cytochrome c oxidase subunit 2	*Q99KV1*	DnaJ homolog subfamily B member 11
Q62425	Cytochrome c oxidase subunit NDUFA4	*Q9QYI4*	DnaJ homolog subfamily B member 12
Q3U308	Cytoplasmic tRNA 2-thiolation protein 2	*O54946-1*	DnaJ homolog subfamily B member 6
Q9R060	Cytosolic Fe-S cluster assembly factor nubp1	*Q5U458*	DnaJ homolog subfamily C member 11
Q9JII5	DAZ-associated protein 1	*O70152*	Dolichol-phosphate mannosyltransferase subunit 1
Q80XN0	D-beta-hydroxybutyrate dehydrogenase, mitochondrial	*Q91YQ5*	Dolichyl-diphosphooligosaccharide-protein glycosyltransferase subunit 1
Q99J47	Dehydrogenase/reductase SDR family member 7B	*Q9QXS6*	Drebrin

Q9QXB9	Developmentally-regulated GTP-binding protein 2	*Q62418*	Drebrin-like protein
O08749	Dihydrolipoyl dehydrogenase, mitochondrial	*P63168*	Dynein light chain 1, cytoplasmic
Q9D2G2-1	Dihydrolipoyllysine-residue succinyltransferase component of 2-oxoglutarate dehydrogenase complex, mitochondrial	*Q8VDF2*	E3 ubiquitin-protein ligase UHRF1
O08553	Dihydropyrimidinase-related protein 2	*Q99LC5*	Electron transfer flavoprotein subunit alpha, mitochondrial
Q62188	Dihydropyrimidinase-related protein 3	*P10126*	Elongation factor 1-alpha 1
P25206	DNA replication licensing factor mcm3	*P62631*	Elongation factor 1-alpha 2
Q61881	DNA replication licensing factor MCM7	*P58252*	Elongation factor 2
Q76KJ5	DNA-directed RNA polymerase I subunit RPA34	*Q8K0D5*	Elongation factor G, mitochondrial
Q80UW8	DNA-directed RNA polymerases I, II, and III subunit RPABC1	*O08579*	Emerin
P63037	DnaJ homolog subfamily A member 1	*P84089*	Enhancer of rudimentary homolog
Q99M87-1	DnaJ homolog subfamily A member 3, mitochondrial	*P42125*	Enoyl-CoA delta isomerase 1, mitochondrial
Q99KV1	DnaJ homolog subfamily B member 11	*Q9D379*	Epoxide hydrolase 1
Q91WN1	DnaJ homolog subfamily C member 9	*O70378*	ER membrane protein complex subunit 8
O70152	Dolichol-phosphate mannosyltransferase subunit 1	*Q91X78*	Erlin-1
Q9QXS6	Drebrin	*Q8BFZ9*	Erlin-2
Q62418	Drebrin-like protein	*P60843*	Eukaryotic initiation factor 4A-I
Q9D7X3	Dual specificity protein phosphatase 3	*Q91VC3*	Eukaryotic initiation factor 4A-III
Q8K1M6-1	Dynamin-1-like protein	*Q8BWY3*	Eukaryotic peptide chain release factor subunit 1
P63168	Dynein light chain 1, cytoplasmic	*Q8JZQ9*	Eukaryotic translation initiation factor 3 subunit B
Q6ZPJ3	E2 ubiquitin-conjugating enzyme UBE2O	*O70194*	Eukaryotic translation initiation factor 3 subunit D
Q3U319	E3 ubiquitin-protein ligase BRE1B	*Q9DCH4*	Eukaryotic translation initiation factor 3 subunit F
Q3UIR3-1	E3 ubiquitin-protein ligase DTX3L	*Q91WK2*	Eukaryotic translation initiation factor 3 subunit H
P46935	E3 ubiquitin-protein ligase NEDD4	*Q9QZD9*	Eukaryotic translation initiation factor 3 subunit I
Q61701-1	ELAV-like protein 4	*P63073*	Eukaryotic translation initiation factor 4E
Q99LC5	Electron transfer flavoprotein subunit alpha, mitochondrial	*Q8BIW1*	Exopolyphosphatase PRUNE1
Q9DCW4	Electron transfer flavoprotein subunit beta	*Q921I9*	Exosome complex component Rrp41
P10126	Elongation factor 1-alpha 1	*Q3U7R1*	Extended synaptotagmin-1
P62631	Elongation factor 1-alpha 2	*P47754*	F-actin-capping protein subunit alpha-2
Q9D8N0	Elongation factor 1-gamma	*P47757-1*	F-actin-capping protein subunit beta
P58252	Elongation factor 2	*Q920E5*	Farnesyl pyrophosphate synthase
Q8K0D5	Elongation factor G, mitochondrial	*P49945*	Ferritin light chain 2
P84089	Enhancer of rudimentary homolog	*Q80X90*	Filamin-B
P42125	Enoyl-CoA delta isomerase 1, mitochondrial	*P42128*	Forkhead box protein K1
Q8C7X2	ER membrane protein complex subunit 1	*Q9WVR4*	Fragile X mental retardation syndrome-related protein 2

O70378	ER membrane protein complex subunit 8	*P05064*	Fructose-bisphosphate aldolase A
P60843	Eukaryotic initiation factor 4A-I	*P97807-1*	Fumarate hydratase, mitochondrial
Q8R050	Eukaryotic peptide chain release factor GTP-binding subunit ERF3A	*P25322*	G1/S-specific cyclin-D1
Q8BWY3	Eukaryotic peptide chain release factor subunit 1	*P16045*	Galectin-1
Q8BJW6-1	Eukaryotic translation initiation factor 2A	*Q9D0D5*	General transcription factor IIE subunit 1
Q8JZQ9	Eukaryotic translation initiation factor 3 subunit B	*Q00612*	Glucose-6-phosphate 1-dehydrogenase X
Q9DCH4	Eukaryotic translation initiation factor 3 subunit F	*O09172*	Glutamate-cysteine ligase regulatory subunit
Q9Z1D1	Eukaryotic translation initiation factor 3 subunit G	*P19157*	Glutathione S-transferase P 1
Q9QZD9	Eukaryotic translation initiation factor 3 subunit I	*P16858*	Glyceraldehyde-3-phosphate dehydrogenase
Q6NZJ6	Eukaryotic translation initiation factor 4 gamma 1	*Q9CZD3*	Glycine-tRNA ligase
Q8VBV3	Exosome complex component Rrp4	*Q9WV60*	Glycogen synthase kinase-3 beta
Q921I9	Exosome complex component Rrp41	*O70310*	Glycylpeptide N-tetradecanoyltransferase 1
P56960	Exosome component 10	*Q3THK7*	GMP synthase [glutamine-hydrolyzing]
P47754	F-actin-capping protein subunit alpha-2	*Q61543*	Golgi apparatus protein 1
P47757-1	F-actin-capping protein subunit beta	*P62827*	GTP-binding nuclear protein RAN
Q91WJ8	Far upstream element-binding protein 1	*O08582*	GTP-binding protein 1
Q3U0V1	Far upstream element-binding protein 2	*Q921J2*	GTP-binding protein Rheb
Q61553	Fascin	*P62880*	Guanine nucleotide-binding protein G(I)/G(S)/G(T) subunit beta-2
P05064	Fructose-bisphosphate aldolase A	*P27601*	Guanine nucleotide-binding protein subunit alpha-13
P97807-1	Fumarate hydratase, mitochondrial	*Q9CQS2*	H/ACA ribonucleoprotein complex subunit 3
Q9R0N0	Galactokinase	*Q99M31-1*	Heat shock 70 kDa protein 14
P16045	Galectin-1	*Q61316*	Heat shock 70 kDa protein 4
P58854	Gamma-tubulin complex component 3	*P07901*	Heat shock protein HSP 90-alpha
Q9Z1Z0-1	General vesicular transport factor p115	*P11499*	Heat shock protein HSP 90-beta
Q00612	Glucose-6-phosphate 1-dehydrogenase X	*Q99020*	Heterogeneous nuclear ribonucleoprotein A/B
O09172	Glutamate-cysteine ligase regulatory subunit	*Q9CX86*	Heterogeneous nuclear ribonucleoprotein A0
P19157	Glutathione S-transferase P 1	*P49312-1*	Heterogeneous nuclear ribonucleoprotein A1
P16858	Glyceraldehyde-3-phosphate dehydrogenase	*Q8BG05*	Heterogeneous nuclear ribonucleoprotein A3
Q9CZD3	Glycine-tRNA ligase	*Q9Z130*	Heterogeneous nuclear ribonucleoprotein D-like
Q9WV60	Glycogen synthase kinase-3 beta	*P70333*	Heterogeneous nuclear ribonucleoprotein H2
Q8C5Q4	G-rich sequence factor 1	*P61979*	Heterogeneous nuclear ribonucleoprotein K
P62827	GTP-binding nuclear protein RAN	*O88569*	Heterogeneous nuclear ribonucleoproteins A2/B1
Q921J2	GTP-binding protein Rheb	*P17710-1*	Hexokinase-1
Q9CQC9	GTP-binding protein SAR1b	*P70349*	Histidine triad nucleotide-binding protein 1

P63094	Guanine nucleotide-binding protein G(s) subunit alpha isoforms short	*P10922*	Histone H1.0
Q9CY66-1	H/ACA ribonucleoprotein complex subunit 1	*P43277*	Histone H1.3
Q9CQS2	H/ACA ribonucleoprotein complex subunit 3	*P43274*	Histone H1.4
P01900	H-2 class I histocompatibility antigen, D-D alpha chain	*P43276*	Histone H1.5
Q99M31-1	Heat shock 70 kDa protein 14	*Q64523*	Histone H2A type 2-C
Q61316	Heat shock 70 kDa protein 4	*Q8BFU2*	Histone H2A type 3
Q61699	Heat shock protein 105 kDa	*Q3THW5*	Histone H2A.V
Q9CQN1	Heat shock protein 75 kDa, mitochondrial	*Q64475*	Histone H2B type 1-B
P07901	Heat shock protein HSP 90-alpha	*Q64524*	Histone H2B type 2-E
P11499	Heat shock protein HSP 90-beta	*P62806*	Histone H4
Q99LI8	Hepatocyte growth factor-regulated tyrosine kinase substrate	*Q61081*	Hsp90 co-chaperone Cdc37
Q99020	Heterogeneous nuclear ribonucleoprotein A/B	*Q8JZK9*	Hydroxymethylglutaryl-CoA synthase, cytoplasmic
Q9CX86	Heterogeneous nuclear ribonucleoprotein A0	*Q9JLZ6*	Hypermethylated in cancer 2 protein
P49312-1	Heterogeneous nuclear ribonucleoprotein A1	*Q9JKR6*	Hypoxia up-regulated protein 1
Q8BG05	Heterogeneous nuclear ribonucleoprotein A3	*Q9D819*	Inorganic pyrophosphatase
Q60668-1	Heterogeneous nuclear ribonucleoprotein D0	*Q9CXY6*	Interleukin enhancer-binding factor 2
Q9Z130	Heterogeneous nuclear ribonucleoprotein D-like	*O88844*	Isocitrate dehydrogenase [NADP] cytoplasmic
P70333	Heterogeneous nuclear ribonucleoprotein H2	*P54071*	Isocitrate dehydrogenase [NADP], mitochondrial
Q921F4-1	Heterogeneous nuclear ribonucleoprotein L-like	*P52480-2*	Isoform M1 of pyruvate kinase PKM
Q7TMK9	Heterogeneous nuclear ribonucleoprotein Q	*P28738*	Kinesin heavy chain isoform 5C
Q00PI9	Heterogeneous nuclear ribonucleoprotein U-like protein 2	*Q9Z1R2*	Large proline-rich protein BAG6
O88569	Heterogeneous nuclear ribonucleoproteins A2/B1	*Q924L1*	LETM1 domain-containing protein 1
P70349	Histidine triad nucleotide-binding protein 1	*Q922Q8*	Leucine-rich repeat-containing protein 59
Q8BY71	Histone acetyltransferase type B catalytic subunit	*P24527*	Leukotriene A-4 hydrolase
P10922	Histone H1.0	*Q99M04*	Lipoyl synthase, mitochondrial
P43275	Histone H1.1	*P06151*	L-lactate dehydrogenase A chain
P43277	Histone H1.3	*Q9QUJ7-1*	Long-chain-fatty-acid-CoA ligase 4
P43274	Histone H1.4	*Q8JZR0*	Long-chain-fatty-acid-CoA ligase 5
P43276	Histone H1.5	*P34884*	Macrophage Migration inhibitory factor
Q64523	Histone H2A type 2-C	*P28667*	MARCKS-related protein
Q8BFU2	Histone H2A type 3	*Q91ZV0*	Melanoma inhibitory activity protein 2
Q3THW5	Histone H2A.V	*Q80UU9*	Membrane-associated progesterone receptor component 2
P27661	Histone H2AX	*O08663*	Methionine aminopeptidase 2
Q9D2U9	Histone H2B type 3-A	*Q3ULD5*	Methylcrotonoyl-CoA carboxylase beta chain, mitochondrial
P62806	Histone H4	*Q99J09*	Methylosome protein 50

Q9WVG6-1	Histone-arginine methyltransferase CARM1	*Q8CAQ8-1*	MICOS complex subunit Mic60
Q99P31	Hsp70-binding protein 1	*Q8K009*	Mitochondrial 10-formyltetrahydrofolate dehydrogenase
Q61081	Hsp90 co-chaperone Cdc37	*Q9CR62*	Mitochondrial 2-oxoglutarate/malate carrier protein
Q8JZK9	Hydroxymethylglutaryl-CoA synthase, cytoplasmic	*Q9WVA3*	Mitotic checkpoint protein BUB3
P00493	Hypoxanthine-guanine phosphoribosyltransferase	*Q9D2Y4-1*	Mixed lineage kinase domain-like protein
Q9JKR6	Hypoxia up-regulated protein 1	*Q9DCG9*	Multifunctional methyltransferase subunit TRM112-like protein
Q8VI75	Importin-4	*Q99KX1*	Myeloid leukaemia factor 2
Q91YE6	Importin-9	*Q60605*	Myosin light polypeptide 6
Q9D819	Inorganic pyrophosphatase	*P97434-1*	Myosin phosphatase Rho-interacting protein
P24547	Inosine-5'-monophosphate dehydrogenase 2	*Q9DBH0*	NEDD4-like E3 ubiquitin-protein ligase WWP2
Q8K3X4	Interferon regulatory factor 2-binding protein-like	*Q91YD9*	Neural Wiskott-Aldrich syndrome protein
Q9CXY6	Interleukin enhancer-binding factor 2	*P08551*	Neurofilament light polypeptide
Q9Z0R6-1	Intersectin-2	*P08553*	Neurofilament medium polypeptide
P70404	Isocitrate dehydrogenase [NAD] subunit gamma 1, mitochondrial	*P06837*	Neuromodulin
O88844	Isocitrate dehydrogenase [NADP] cytoplasmic	*Q8BHN3*	Neutral alpha-glucosidase AB
P54071	Isocitrate dehydrogenase [NADP], mitochondrial	*Q99KQ4*	Nicotinamide phosphoribosyltransferase
Q7M6Y3-5	Isoform 5 of Phosphatidylinositol-binding clathrin assembly protein	*Q6GQT9*	Nodal modulator 1
P15331-3	Isoform 5b of Peripherin	*Q99K48*	Non-POU domain-containing octamer-binding protein
P52480-2	Isoform M1 of Pyruvate kinase PKM	*Q9CPT5*	Nucleolar protein 16
Q9Z127	Large neutral amino acids transporter small subunit 1	*P25976-1*	Nucleolar transcription factor 1
Q9CRC8	Leucine-rich repeat-containing protein 40	*Q8R4R6*	Nucleoporin NUP53
Q922Q8	Leucine-rich repeat-containing protein 59	*P28656*	Nucleosome assembly protein 1-like 1
P24527	Leukotriene A-4 hydrolase	*D3YYU8*	Obscurin-like protein 1
P06151	L-lactate dehydrogenase A chain	*Q78XF5*	Oligosaccharyltransferase complex subunit OSTC
Q9QUJ7-1	Long-chain-fatty-acid-CoA ligase 4	*A2AR02*	Peptidyl-prolyl cis-trans isomerase g
Q5SUF2-1	Luc7-like protein 3	*P35700*	Peroxiredoxin-1
Q91ZV0	Melanoma inhibitory activity protein 2	*Q61171*	Peroxiredoxin-2
Q80UU9	Membrane-associated progesterone receptor component 2	*O08807*	Peroxiredoxin-4
Q07646-1	Mesoderm-specific transcript protein	*O08709*	Peroxiredoxin-6
O08663	Methionine aminopeptidase 2	*P83870*	PHD finger-like domain-containing protein 5A
Q8CAQ8-1	MICOS complex subunit Mic60	*P09411*	Phosphoglycerate kinase 1
Q791T5-1	Mitochondrial carrier homolog 1	*Q9Z2M7*	Phosphomannomutase 2
Q791V5	Mitochondrial carrier homolog 2	*Q922V4*	Pleiotropic regulator 1
Q9WTQ8	Mitochondrial import inner membrane translocase subunit tim23	*P57722-1*	Poly(RC)-binding protein 3
Q9CWX4	Mitochondrial RNA pseudouridine synthase RPUSD4	*Q3UEB3-1*	Poly(U)-binding-splicing factor PUF60

Q9CXT8	Mitochondrial-processing peptidase subunit beta	*P29341*	Polyadenylate-binding protein 1
Q9WVA3	Mitotic checkpoint protein BUB3	*Q8BG81*	Polymerase delta-interacting protein 3
Q9D2Y4-1	Mixed lineage kinase domain-like protein	*P17225*	Polypyrimidine tract-binding protein 1
P10404	MLV-related proviral Env polyprotein	*Q9D824-1*	Pre-mRNA 3'-end-processing factor FIP1
Q3V3R1	Monofunctional C1-tetrahydrofolate synthase, mitochondrial	*Q99KP6-1*	Pre-mRNA-processing factor 19
Q8BUN5	Mothers against decapentaplegic homolog 3	*Q9D287*	Pre-mRNA-splicing factor spf27
Q8C570	mRNA export factor	*Q9CWX9*	Probable ATP-dependent RNA helicase DDX47
Q9DCL9	Multifunctional protein ADE2	*P54823*	Probable ATP-dependent RNA helicase DDX6
Q8C181	Muscleblind-like protein 2	*P62962*	Profilin-1
Q60605	Myosin light polypeptide 6	*Q9JJV2-1*	Profilin-2
Q3THE2	Myosin regulatory light chain 12B	*P67778*	Prohibitin
Q9CQZ5	NADH dehydrogenase [ubiquinone] 1 alpha subcomplex subunit 6	*O35129*	Prohibitin-2
Q9DC69	NADH dehydrogenase [ubiquinone] 1 alpha subcomplex subunit 9, mitochondrial	*P17918*	Proliferating cell nuclear antigen
Q9CQC7	NADH dehydrogenase [ubiquinone] 1 beta subcomplex subunit 4	*Q9QUR6*	Prolyl endopeptidase
Q9DCT2	NADH dehydrogenase [ubiquinone] iron-sulfur protein 3, mitochondrial	*Q9JKV1*	Proteasomal ubiquitin receptor ADRM1
P61082	NEDD8-conjugating enzyme Ubc12	*Q8BHL8*	Proteasome inhibitor PI31 subunit
Q91YD9	Neural Wiskott-Aldrich syndrome protein	*Q8CIG8*	Protein arginine N-methyltransferase 5
P06837	Neuromodulin	*Q6PGH1*	Protein BUD31 homolog
Q9D0T1	NHP2-like protein 1	*Q80VD1*	Protein fam98b
Q99KQ4	Nicotinamide phosphoribosyltransferase	*P97376*	Protein FRG1
Q99K48	Non-POU domain-containing octamer-binding protein	*Q91VH6*	Protein MEMO1
Q99P88	Nuclear pore complex protein nup155	*Q2YDW2-1*	Protein misato homolog 1
Q9JIH2	Nuclear pore complex protein Nup50	*O55125*	Protein nipsnap homolog 1
Q6PFD9	Nuclear pore complex protein Nup98-Nup96	*Q8BVQ5*	Protein phosphatase methylesterase 1
Q63850	Nuclear pore glycoprotein p62	*Q01405*	Protein transport protein Sec23A
Q9CPT5	Nucleolar protein 16	*Q9D662*	Protein transport protein Sec23B
Q8VCB1	Nucleoporin ndc1	*Q3UPL0*	Protein transport protein Sec31A
Q6ZQH8	Nucleoporin NUP188 homolog	*Q9CQS8*	Protein transport protein Sec61 subunit beta
Q8R4R6	Nucleoporin NUP53	*Q80U58-1*	Pumilio homolog 2
Q8R2U0-1	Nucleoporin Seh1	*Q9CYI4-1*	Putative RNA-binding protein Luc7-like 1
P97346	Nucleoredoxin	*Q05920*	Pyruvate carboxylase, mitochondrial
Q01768	Nucleoside diphosphate kinase b	*Q9D051*	Pyruvate dehydrogenase E1 component subunit beta, mitochondrial
P28656	Nucleosome assembly protein 1-like 1	*P52480*	Pyruvate kinase PKM
Q6PIP5	Nudc domain-containing protein 1	*Q61598*	Rab GDP dissociation inhibitor beta
Q78XF5	Oligosaccharyltransferase complex subunit OSTC	*Q9CT10*	Ran-binding protein 3
Q8R326	Paraspeckle component 1	*P34022*	Ran-specific GTPase-activating protein

Q8CI51	PDZ and LIM domain protein 5	*P97855*	Ras GTPase-activating protein-binding protein 1
P24369	Peptidyl-prolyl cis-trans isomerase B	*P63001*	Ras-related C3 botulinum toxin substrate 1
Q8BU03	Periodic tryptophan protein 2 homolog	*Q91V41*	Ras-related protein Rab-14
P35700	Peroxiredoxin-1	*Q9D1G1*	Ras-related protein Rab-1B
Q61171	Peroxiredoxin-2	*P62823*	Ras-related protein Rab-3C
O08709	Peroxiredoxin-6	*P61021*	Ras-related protein Rab-5B
P09411	Phosphoglycerate kinase 1	*P35278*	Ras-related protein Rab-5C
Q9D0M1	Phosphoribosyl pyrophosphate synthase-associated protein 1	*P35279*	Ras-related protein Rab-6A
Q5SUR0	Phosphoribosylformylglycinamidine synthase	*Q62193*	Replication protein A 32 kDa subunit
Q61206	Platelet-activating factor acetylhydrolase IB subunit beta	*P70336-1*	Rho-associated protein kinase 2
Q61205	Platelet-activating factor acetylhydrolase IB subunit gamma	*Q62159*	Rho-related GTP-binding protein Rhoc
Q3UEB3-1	Poly(U)-binding-splicing factor PUF60	*P84096*	Rho-related GTP-binding protein Rhog
P17225	Polypyrimidine tract-binding protein 1	*Q8BVY0*	Ribosomal L1 domain-containing protein 1
Q91Z31	Polypyrimidine tract-binding protein 2	*Q9CYH6*	Ribosome biogenesis regulatory protein homolog
Q8BHD7	Polypyrimidine tract-binding protein 3	*Q7TND5*	Ribosome production factor 1
Q9D824-1	Pre-mRNA 3'-end-processing factor FIP1	*Q91VM5*	RNA binding motif protein, X-linked-like-1
Q99KP6-1	Pre-mRNA-processing factor 19	*Q8R4X3*	RNA-binding protein 12
Q9D287	Pre-mRNA-splicing factor spf27	*B2RY56*	RNA-binding protein 25
Q91VN6	Probable ATP-dependent RNA helicase DDX41	*O89086*	RNA-binding protein 3
P54823	Probable ATP-dependent RNA helicase DDX6	*Q8VH51-1*	RNA-binding protein 39
Q9D903	Probable rRNA-processing protein EBP2	*Q61545*	RNA-binding protein EWS
Q9WU78	Programmed cell death 6-interacting protein	*P56959*	RNA-binding protein FUS
P67778	Prohibitin	*Q9CPS7*	RNA-binding protein pno1
O35129	Prohibitin-2	*Q99M28*	RNA-binding protein with serine-rich domain 1
Q60716	Prolyl 4-hydroxylase subunit alpha-2	*P60122*	Ruvb-like 1
Q9QUR6	Prolyl endopeptidase	*Q9WTM5*	Ruvb-like 2
Q9JKV1	Proteasomal ubiquitin receptor ADRM1	*O35609*	Secretory carrier-associated membrane protein 3
Q9JK23	Proteasome assembly chaperone 1	*Q8C650-1*	Septin-10
Q8BHL8	Proteasome inhibitor PI31 subunit	*Q9Z2Q6*	Septin-5
Q9QUM9	Proteasome subunit alpha type-6	*Q80UG5-1*	Septin-9
P54923	Protein ADP-ribosylarginine hydrolase	*P50431*	Serine hydroxymethyltransferase, cytosolic
Q9JIF0-1	Protein arginine N-methyltransferase 1	*Q6PDM2*	Serine/arginine-rich splicing factor 1
Q6PGH1	Protein BUD31 homolog	*Q9R0U0-1*	Serine/arginine-rich splicing factor 10
Q9CZT6	Protein CMSS1	*P84104-1*	Serine/arginine-rich splicing factor 3
A2ADY9	Protein DDI1 homolog 2	*Q8VE97*	Serine/arginine-rich splicing factor 4
P27773	Protein disulfide-isomerase A3	*O35326*	Serine/arginine-rich splicing factor 5
Q922R8	Protein disulfide-isomerase A6	*Q9D0B0*	Serine/arginine-rich splicing factor 9

Q9D0F3	Protein ERGIC-53	*P62715*	Serine/threonine-protein phosphatase 2A catalytic subunit beta isoform
Q3TJZ6	Protein FAM98A	*P62137*	Serine/threonine-protein phosphatase PP1-alpha catalytic subunit
Q80VD1	Protein fam98b	*Q9Z1Z2*	Serine-threonine kinase receptor-associated protein
Q9D945	Protein LLP homolog	*P26638*	Serine-tRNA ligase, cytoplasmic
Q91VH6	Protein MEMO1	*Q99MR6-1*	Serrate RNA effector molecule homolog
O55125	Protein nipsnap homolog 1	*P07724*	Serum albumin
Q8BK67	Protein RCC2	*Q07417*	Short-chain specific acyl-CoA dehydrogenase, mitochondrial
Q9Z1M8	Protein red	*P62315*	Small nuclear ribonucleoprotein Sm D1
Q9D662	Protein transport protein Sec23B	*P62320*	Small nuclear ribonucleoprotein Sm D3
Q3U2P1	Protein transport protein Sec24A	*P27048*	Small nuclear ribonucleoprotein-associated protein B
Q9CYI4-1	Putative RNA-binding protein Luc7-like 1	*Q3UMC0*	Spermatogenesis-associated protein 5
P35486	Pyruvate dehydrogenase E1 component subunit alpha, somatic form, mitochondrial	*Q64674*	Spermidine synthase
Q9D051	Pyruvate dehydrogenase E1 component subunit beta, mitochondrial	*Q64213*	Splicing factor 1
P52480	Pyruvate kinase PKM	*Q8K4Z5*	Splicing factor 3A subunit 1
Q61598	Rab GDP dissociation inhibitor beta	*P26369*	Splicing factor U2AF 65 kDa subunit
P46061	Ran GTPase-activating protein 1	*Q8VIJ6*	Splicing factor, proline- and glutamine-rich
Q9CT10	Ran-binding protein 3	*Q9JLI8-1*	Squamous cell carcinoma antigen recognized by T-cells 3
P34022	Ran-specific GTPase-activating protein	*Q60598*	Src substrate cortactin
P97855	Ras GTPase-activating protein-binding protein 1	*O54988-1*	STE20-like serine/threonine-protein kinase
P97379-1	Ras GTPase-activating protein-binding protein 2	*Q9WUD1*	STIP1 homology and U box-containing protein 1
Q91V41	Ras-related protein Rab-14	*Q9WUM5*	Succinate-CoA ligase [ADP/GDP-forming] subunit alpha, mitochondrial
Q9D1G1	Ras-related protein Rab-1B	*Q9D0K2*	Succinyl-CoA:3-ketoacid coenzyme A transferase 1, mitochondrial
P62823	Ras-related protein Rab-3C	*Q80TB8*	Synaptic vesicle membrane protein VAT-1 homolog-like
Q9CQD1	Ras-related protein Rab-5A	*P11983*	T-complex protein 1 subunit alpha
P35278	Ras-related protein Rab-5C	*P80318*	T-complex protein 1 subunit gamma
Q9R0M6	Ras-related protein Rab-9A	*P42932*	T-complex protein 1 subunit theta
Q9QYF1	Retinol dehydrogenase 11	*P80317*	T-complex protein 1 subunit zeta
Q61210	Rho guanine nucleotide exchange factor 1	*Q91W90*	Thioredoxin domain-containing protein 5
P70336-1	Rho-associated protein kinase 2	*P20108*	Thioredoxin-dependent peroxide reductase, mitochondrial
P84096	Rho-related GTP-binding protein Rhog	*O08583-1*	THO complex subunit 4
O88796	Ribonuclease P protein subunit p30	*Q9QZ06*	Toll-interacting protein
P07742	Ribonucleoside-diphosphate reductase large subunit	*Q8VI33*	Transcription initiation factor TFIID subunit 9
Q8BVY0	Ribosomal L1 domain-containing protein 1	*O35295*	Transcriptional activator protein Pur-beta
Q9JJF3	Ribosomal oxygenase 1	*Q9R099*	Transducin beta-like protein 2
Q8BK35	Ribosome biogenesis protein NOP53	*Q6PFR5*	Transformer-2 protein homolog alpha

Q9JJA4	Ribosome biogenesis protein WDR12	*P62996-1*	Transformer-2 protein homolog beta
Q9CYH6	Ribosome biogenesis regulatory protein homolog	*Q01853*	Transitional endoplasmic reticulum ATPase
Q9D7H3	RNA 3'-terminal phosphate cyclase	*P40142*	Transketolase
Q91VM5	RNA binding motif protein, X-linked-like-1	*Q99LD9*	Translation initiation factor eif-2B subunit beta
Q8BP71-1	RNA binding protein fox-1 homolog 2	*Q9DAM7*	Transmembrane protein 263
Q8R4X3	RNA-binding protein 12	*Q64737*	Trifunctional purine biosynthetic protein adenosine-3
O89086	RNA-binding protein 3	*P17751*	Triosephosphate isomerase
Q8VH51-1	RNA-binding protein 39	*Q64514-1*	Tripeptidyl-peptidase 2
Q61545	RNA-binding protein EWS	*Q99LF4*	tRNA-splicing ligase Rtcb homolog
P56959	RNA-binding protein FUS	*P32921*	Tryptophan-tRNA ligase, cytoplasmic
Q61474	RNA-binding protein Musashi homolog 1	*Q9ERD7*	Tubulin beta-3 chain
Q8BW10	RNA-binding protein NOB1	*P99024*	Tubulin beta-5 chain
P60122	Ruvb-like 1	*Q921Y2*	U3 small nucleolar ribonucleoprotein protein IMP3
Q9WTM5	Ruvb-like 2	*Q810V0*	U3 small nucleolar ribonucleoprotein protein Mpp10
Q80SW1	S-adenosylhomocysteine hydrolase-like protein 1	*Q8VCY6*	U3 small nucleolar RNA-associated protein 6 homolog
Q8BRF7	Sec1 family domain-containing protein 1	*Q922U1*	U4/U6 small nuclear ribonucleoprotein Prp3
Q6NZC7	SEC23-interacting protein	*Q9DAW6*	U4/U6 small nuclear ribonucleoprotein Prp4
Q8C1B7	Septin-11	*Q91Z49*	UAP56-interacting factor
Q9Z2Q6	Septin-5	*Q3V0C5-1*	Ubiquitin carboxyl-terminal hydrolase 48
O55131	Septin-7	*P56399*	Ubiquitin carboxyl-terminal hydrolase 5
Q6PDM2	Serine/arginine-rich splicing factor 1	*P58321*	Ubiquitin carboxyl-terminal hydrolase isozyme L4
Q9R0U0-1	Serine/arginine-rich splicing factor 10	*Q80X50*	Ubiquitin-associated protein 2-like
Q62093	Serine/arginine-rich splicing factor 2	*P61089*	Ubiquitin-conjugating enzyme E2 N
P84104-1	Serine/arginine-rich splicing factor 3	*Q02053*	Ubiquitin-like modifier-activating enzyme 1
Q9D0B0	Serine/arginine-rich splicing factor 9	*Q922Y1*	UBX domain-containing protein 1
Q80X41	Serine/threonine-protein kinase VRK1	*Q9DBP5*	UMP-CMP kinase
P62715	Serine/threonine-protein phosphatase 2A catalytic subunit beta isoform	*P40336*	Vacuolar protein sorting-associated protein 26A
P63328	Serine/threonine-protein phosphatase 2B catalytic subunit alpha isoform	*Q9QZ88*	Vacuolar protein sorting-associated protein 29
P26638	Serine-tRNA ligase, cytoplasmic	*Q91XD6*	Vacuolar protein-sorting-associated protein 36
Q07417	Short-chain specific acyl-CoA dehydrogenase, mitochondrial	*O08547*	Vesicle-trafficking protein SEC22b
P16254	Signal recognition particle 14 kDa protein	*P20152*	Vimentin
Q9DBG7	Signal recognition particle receptor subunit alpha	*P63082*	V-type proton ATPase 16 kDa proteolipid subunit
P47758	Signal recognition particle receptor subunit beta	*P50516-1*	V-type proton ATPase catalytic subunit A
P42225	Signal transducer and activator of transcription 1	*Q9Z1G3*	V-type proton ATPase subunit C 1
P42227	Signal transducer and activator of transcription 3	*P51863*	V-type proton ATPase subunit d 1

P62315	Small nuclear ribonucleoprotein Sm D1	*P50518*	V-type proton ATPase subunit E 1
P62320	Small nuclear ribonucleoprotein Sm d3	*Q8BVE3*	V-type proton ATPase subunit H
P27048	Small nuclear ribonucleoprotein-associated protein B	*Q6P1B1*	Xaa-Pro aminopeptidase 1
Q9CQ65	S-methyl-5'-thioadenosine phosphorylase	*Q91YT7*	YTH domain-containing family protein 2
Q8BGH2	Sorting and assembly machinery component 50 homolog	*Q9DB42*	Zinc finger protein 593
Q64674	Spermidine synthase	*Q31125*	Zinc transporter SLC39A7
Q64213	Splicing factor 1		
Q8K4Z5	Splicing factor 3A subunit 1		
Q921M3-1	Splicing factor 3B subunit 3		
Q8JZX4	Splicing factor 45		
P26369	Splicing factor U2AF 65 kDa subunit		
Q8VIJ6	Splicing factor, proline- and glutamine-rich		
Q99JB2	Stomatin-like protein 2, mitochondrial		
Q60864	Stress-induced-phosphoprotein 1		
Q9WUM5	Succinate-CoA ligase [ADP/GDP-forming] subunit alpha, mitochondrial		
Q9Z2I8	Succinate-CoA ligase [GDP-forming] subunit beta, mitochondrial		
Q9D0K2	Succinyl-CoA:3-ketoacid coenzyme A transferase 1, mitochondrial		
Q64332	Synapsin-2		
Q62465	Synaptic vesicle membrane protein VAT-1 homolog		
Q8R191	Synaptogyrin-3		
Q9CXF4	TBC1 domain family member 15		
P11983	T-complex protein 1 subunit alpha		
P42932	T-complex protein 1 subunit theta		
P80317	T-complex protein 1 subunit zeta		
Q91W90	Thioredoxin domain-containing protein 5		
Q8CDN6	Thioredoxin-like protein 1		
O08583-1	THO complex subunit 4		
Q9D0R2	Threonine-tRNA ligase, cytoplasmic		
P39447	Tight junction protein ZO-1		
Q9QZ06	Toll-interacting protein		
Q8CGF7-1	Transcription elongation regulator 1		
Q8VI33	Transcription initiation factor TFIID subunit 9		
P42669	Transcriptional activator protein Pur-alpha		
Q8C4J7	Transducin beta-like protein 3		
Q80YV3	Transformation/transcription domain-associated protein		
Q6PFR5	Transformer-2 protein homolog alpha		
P62996-1	Transformer-2 protein homolog beta		
Q9QUI0	Transforming protein RhoA		
Q01853	Transitional endoplasmic reticulum ATPase		

P40142	Transketolase		
Q61749-1	Translation initiation factor eif-2B subunit delta		
Q62186	Translocon-associated protein subunit delta		
Q9CR67	Transmembrane protein 33		
Q8BI84-1	Transport and Golgi organization protein 1 homolog		
Q8BFY9	Transportin-1		
Q8BKI2	Trinucleotide repeat-containing gene 6B protein		
Q64514-1	Tripeptidyl-peptidase 2		
P32921	Tryptophan-tRNA ligase, cytoplasmic		
P68369	Tubulin alpha-1A chain		
P68368	Tubulin alpha-4A chain		
P99024	Tubulin beta-5 chain		
Q9D1E6	Tubulin-folding cofactor B		
Q61187	Tumor susceptibility gene 101 protein		
P57784	U2 small nuclear ribonucleoprotein A'		
Q921Y2	U3 small nucleolar ribonucleoprotein protein IMP3		
Q810V0	U3 small nucleolar ribonucleoprotein protein Mpp10		
Q9DAW6	U4/U6 small nuclear ribonucleoprotein Prp4		
Q91Z49	UAP56-interacting factor		
Q9JMA1	Ubiquitin carboxyl-terminal hydrolase 14		
Q8BY87-1	Ubiquitin carboxyl-terminal hydrolase 47		
P56399	Ubiquitin carboxyl-terminal hydrolase 5		
Q9R0P9	Ubiquitin carboxyl-terminal hydrolase isozyme L1		
Q7TQI3	Ubiquitin thioesterase otub1		
P68037	Ubiquitin-conjugating enzyme E2 L3		
Q9CZY3	Ubiquitin-conjugating enzyme E2 variant 1		
Q922Y1	UBX domain-containing protein 1		
Q9DBP5	UMP-CMP kinase		
Q9CXL3	Uncharacterized protein c7orf50 homolog		
Q9CQE8	UPF0568 protein c14orf166 homolog		
Q9QZ88	Vacuolar protein sorting-associated protein 29		
Q9EQH3	Vacuolar protein sorting-associated protein 35		
Q9Z1Q9	Valine-tRNA ligase		
Q9WV55	Vesicle-associated membrane protein-associated protein A		
P46460	Vesicle-fusing ATPase		
P20152	Vimentin		
Q60930	Voltage-dependent anion-selective channel protein 2		

Q60931	Voltage-dependent anion-selective channel protein 3		
Q9Z1G4	V-type proton ATPase 116 kDa subunit a isoform 1		
P50516-1	V-type proton ATPase catalytic subunit A		
P62814	V-type proton ATPase subunit B, brain isoform		
Q9Z1G3	V-type proton ATPase subunit C 1		
P50518	V-type proton ATPase subunit E 1		
Q3UMB9	WASH complex subunit 4		
Q9Z0H1	WD repeat-containing protein 46		
Q8VCG3	WD repeat-containing protein 74		
Q8BFQ4	WD repeat-containing protein 82		
Q8BH43	Wiskott-Aldrich syndrome protein family member 2		
Q6P1B1	Xaa-Pro aminopeptidase 1		
Q31125	Zinc transporter SLC39A7		